PSU-IRL-SCI-444

Classification Numbers 1.5.1

THE PENNSYLVANIA STATE UNIVERSITY

IONOSPHERIC RESEARCH

Scientific Report 444

ROCKET-BORNE TIME-OF-FLIGHT MASS SPECTROMETRY

by

Robert F. Reiter

August 1976

The research reported in this document has been supported by The National Science Foundation under Grant No. GA 33446X2.

IONOSPHERE RESEARCH LABORATORY

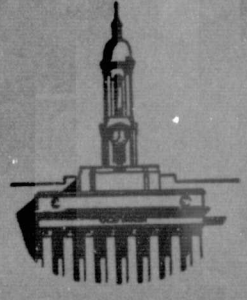

University Park, Pennsylvania

SECURITY CLASSIFICATION OF THIS PAGE *(When Data Entered)*

REPORT DOCUMENTATION PAGE		READ INSTRUCTIONS BEFORE COMPLETING FORM
1. REPORT NUMBER 444	2. GOVT ACCESSION NO.	3. RECIPIENT'S CATALOG NUMBER
4. TITLE *(and Subtitle)* Rocket-Borne Time-of-Flight Mass Spectrometry		5. TYPE OF REPORT & PERIOD COVERED Scientific Report 6. PERFORMING ORG. REPORT NUMBER PSU-IRL-SCI-444
7. AUTHOR*(s)* Robert F. Reiter		8. CONTRACT OR GRANT NUMBER*(s)* NGR 39-009-032
9. PERFORMING ORGANIZATION NAME AND ADDRESS The Ionosphere Research Laboratory 318 Electrical Engineering East Building University Park, Pennsylvania 16802		10. PROGRAM ELEMENT, PROJECT, TASK AREA & WORK UNIT NUMBERS
11. CONTROLLING OFFICE NAME AND ADDRESS		12. REPORT DATE August 1976 13. NUMBER OF PAGES 237
14. MONITORING AGENCY NAME & ADDRESS*(if different from Controlling Office)* The National Science Foundation 1800 G Street, N.W. Washington, D.C. 20550		15. SECURITY CLASS. *(of this report)* NONE 15a. DECLASSIFICATION/DOWNGRADING SCHEDULE
16. DISTRIBUTION STATEMENT *(of this Report)*		
17. DISTRIBUTION STATEMENT *(of the abstract entered in Block 20, if different from Report)* Supporting Agencies		
18. SUPPLEMENTARY NOTES		
19. KEY WORDS *(Continue on reverse side if necessary and identify by block number)* D-Region		

20. ABSTRACT *(Continue on reverse side if necessary and identify by block number)*

Theoretical and numerical analyses are made of planar, cylindrical and spherical-electrode two-field time-of-flight mass spectrometers in order to optimize their operating conditions. A resolving power enhancement method is introduced which can improve the resolving power of these instruments by a factor of 7.5. A numerical analysis of potential barrier gating in time-of-flight mass spectrometers is also made.

Experimental studies of a miniature cylindrical-electrode time-of-flight mass spectrometer and of a miniature hemispherical-electrode time-

DD FORM 1 JAN 73 1473 EDITION OF 1 NOV 65 IS OBSOLETE
S/N 0102-014-6601 |

SECURITY CLASSIFICATION OF THIS PAGE *(When Data Entered)*

of-flight mass spectrometer are presented. The extremely high sensitivity of these instruments and their ability to operate at D-region pressures with an open source make them ideal instruments for D-region ion composition measurements.

The design, testing and successful launch of a sounding rocket experiment package carrying a cylindrical electrode time-of-flight mass spectrometer are discussed. The mass spectrometer data indicate that essentially 100 per cent of the positive electric charge on positive ions is carried by ions with mass-to-charge ratios greater than 500 below an altitude of 92 km. These heavy charge carriers were present at altitudes up to about 100 km.

PSU-IRL-SCI-444
Classification Numbers 1.5.1

Scientific Report 444

Rocket-Borne Time-of-Flight Mass Spectrometry

by

Robert F. Reiter

August 1976

The research reported in this document has been supported by The National Aeronautics and Space Administration under Grant No. NGR 39-009-0032

Submitted by:

B. R. F. Kendall, Professor
of Physics

Approved by:

J. S. Nisbet, Director
Ionosphere Research Laboratory

Ionosphere Research Laboratory

The Pennsylvania State University

University Park, Pennsylvania 16802

ACKNOWLEDGEMENTS

The guidance and encouragement of my adviser, Professor Bruce R. F. Kendall is greatly appreciated. I would also like to thank Mr. John O. Weeks for his help. The assistance of various personnel of the NASA Wallops Station is gratefully acknowledged.

This work was supported by NASA Grant NGR 39-009-032.

TABLE OF CONTENTS

LIST OF TABLES

LIST OF FIGURES

ABSTRACT

Theoretical and numerical analyses are made of planar, cylindrical and spherical-electrode two-field time-of-flight mass spectrometers in order to optimize their operating conditions. A resolving power enhancement method is introduced which can improve the resolving power of these instruments by a factor of 7.5. A numerical analysis of potential barrier gating in time-of-flight mass spectrometers is also made.

Experimental studies of a miniature cylindrical-electrode time-of-flight mass spectrometer and of a miniature hemispherical-electrode time-of-flight mass spectrometer are presented. The extremely high sensitivity of these instruments and their ability to operate at D-region pressures with an open source make them ideal instruments for D-region ion composition measurements.

The design, testing and successful launch of a sounding rocket experiment package carrying a cylindrical electrode time-of-flight mass spectrometer are discussed. The mass spectrometer data indicate that essentially 100 per cent of the positive electric charge on positive ions is carried by ions with mass-to-charge ratios greater than 500 below an altitude of 92 km. These heavy charge carriers were present at altitudes up to about 100 km.

CHAPTER I

INTRODUCTION

1.1 The Ionosphere

The study of the weakly ionized plasma enveloping the entire earth and extending from about 50 km to about 1000 km in altitude was stimulated by two primary reasons. The first was to discover its effects on radio waves, while the second was to discover its effects on the geomagnetic field. Although there were earlier proposals relating to the existence of this plasma, the first significant papers were written by Kennelly (1902) and Heaviside (1902). These researchers explained the success of Marconi's radio experiment (in 1901) by postulating the existence of a conducting layer at a high altitude. The use of the name "ionosphere" for the ionized plasma surrounding the earth was proposed by Watson-Watt (1929) and has become the commonly used term.

The beginnings of the modern theory of the ionosphere were with the works of Hulbert (1928) and Chapman (1931a, b). Since the description by Chapman (1931a, b) of an ionospheric layer, the division of the ionosphere has commonly been into layers. However, the boundaries between these layers have usually been regions of large electron density gradients. These layers are known as the D, E and F-regions (and sometimes the C-region). The D-region is roughly the region below 90 km. The region from about 90 km to between 140 km and 180 km is known as the E-region. The F-region

(usually divided into the F_1 and F_2-regions) extends from 140-180 km to about 300 km. Above 300 km is usually referred to as the topside. The C-region is sometimes used to describe the region from 50 km to 60 km.

With the definite proof of the existence of the ionosphere obtained in the early portion of this century, theorists have attempted to construct ionospheric models. These attempts continue to the present day. The data needed as inputs, for modeling, include temperatures (ionic, neutral and electron), the pressure, the chemical composition (neutral and ionic), reaction rates and solar radiation information. This thesis will discuss the use of time-of-flight mass spectrometers for the measurement of the positive ion composition of the D-region and E-region of the ionosphere.

1.2 Mass Spectrometry in the Ionosphere

The mass spectrometer has become an established and sensitive tool for use in the quantitative analysis of complex mixtures of gases. It is natural, therefore, to apply mass spectrometry to the measurement of neutral and ionic species in the earth's atmosphere. Of special interest, in this thesis, is the study of the ionic species of the earth's atmosphere. The first measurements of ionospheric composition were made using the radio frequency mass spectrometer developed by Bennett (1950). These early measurements were made in the E and F-regions of the ionosphere by Townsend (1952), Johnson and Meadows (1955) and Johnson and Heppner (1955). Although the quantitative results of these measurements are in doubt, they did indicate that the principal ions present in the altitude range of 100 km to 200 km were O^+ (16), NO^+ (30) and O_2^+ (32).

Since these measurements, numerous experimenters, using a variety of mass spectrometers, have entered this field. These experimenters include Boyd and Morris (1955), Boyd (1959, 1960), Boyd et al., (1974), Sayers (1959), Hoffman (1967, 1969, 1970), Hoffman et al., (1973), Istomin (1962), Istomin and Pokhunkov (1963), Bowen et al., (1964), Taylor et al., (1965, 1968), Raitt et al., (1965, 1973), Taylor and Brinton (1961), Young et al., (1967), Goldberg and Aikin (1973), Aikin and Goldberg (1973), Smith et al., (1967), Zhlood'ko et al., (1974), Brinton et al., (1973), Arnold et al., (1969), Goldberg (1975) and Krankowsky et al., (1972c).

A subject of great interest, since the middle 1960's, has been the ionic composition of the D-region. The discovery of hydrated ions of the form $H_3O^+ \cdot (H_2O)_n$ by Narcisi and Bailey (1965) stimulated a great amount of debate. However, the presence of these ions is generally accepted today. The type of ions in the D-region have a great affect on VLF radio wave propagation and knowledge of these ions is crucial for reliable communication using VLF radio wave propagation. Experimental measurements in this region are made extremely difficult by the high ambient pressure and the small ion concentrations. The higher pressures mean a smaller mean free path than the dimensions of the instruments used for measurements. The small ion concentrations result in small ion currents, 10^{-10} amps or less, and introduce problems of current detection. The workers in this field have, for the most part, used quadrupole mass filters which sample through an orifice, typically 1 mm in diameter,

and are differentially pumped by cryopumps or ion pumps. This method allows the use of electron multiplier detectors for ion current detection. Some of the researchers who are working in, or have worked in, D-region ion composition measurements are Narcisi and Bailey (1965), Goldberg and Blumle (1970), Narcisi (1966, 1967, 1969, 1970, 1973), Narcisi et al., (1967, 1969a, b, 1971, 1972a, b, c), Narcisi and Roth (1970), Goldberg and Aikin (1971), Arnold et al., (1969, 1971, 1974), Krankowsky et al., (1972a, b), Johannessen and Krankowsky (1972, 1974), Johannessen et al., (1972) and Arnold and Krankowsky (1974). All these researchers used the quadrupole mass filter introduced by Paul and Raether (1955). Recently, a differentially pumped magnetic sector mass spectrometer was flown by Zbinden et al., (1975) and measured D and E-region positive ion composition.

Negative ions in the D-region have also been subject to study by a number of experimenters. These include Johnson and Heppner (1956), Narcisi (1969, 1973), Arnold et al., (1971), Narcisi et al., (1971, 1972a, b) and Krankowsky et al., (1972a).

1.3 Time-of-Flight Mass Spectrometry

The instruments which are the subject of this thesis are time-of-flight mass spectrometers. The original studies of time-of-flight mass spectrometers were carried out more or less simultaneously by Stephens (1946) and Cameron and Eggers (1948). Further investigations were done by Keller (1949), Takekoshi et al., (1951), Glenn (1952), Wolff and Stephens (1953), Ionov and Mamyrin (1953) and Katzenstein and Friedland (1955).

In 1955, Wiley and McLaren introduced the two-field time-of-flight mass spectrometer. This instrument used two acceleration regions in the ion source. This produced significantly improved resolving power compared to earlier time-of-flight mass spectrometers. The mass spectrometer of Wiley and McLaren (1955) and the earlier time-of-flight mass spectrometers used planar electrodes.

Sayers (1959) and MacKenzie (1964) developed time-of-flight mass spectrometers which used a cylindrical geometry. These instruments were designed for use in ion composition measurements in the E-region of the ionosphere. They did not use the two-field source of Wiley and McLaren (1955) and with a flight path length of 12 cm, had a resolving power of only 3. A successful sounding rocket flight showed the presence of NO^+ (30) and O_2^+ (32). Work was also done on a cylindrical-geometry time-of-flight mass spectrometer by Lincoln (1957). He used a modified vacuum tube with an ion flight path of 5.6 cm and observed a resolving power of about 1.

Diem (1967) reported a time-of-flight mass spectrometer combining the cylindrical geometry of MacKenzie (1964) and the two-field acceleration source of Wiley and McLaren (1955). This instrument had a drift region length of about 4 cm and had a resolving power of 5. These early results were extended by Zabielski (1970), Zabielski, Diem and Kendall (1970), Stein (1974) and Kendall and Reiter (1975). In 1970, Zabielski described a time-of-flight mass spectrometer using a spherical geometry and the two-field source of

Wiley and McLaren (1955). The theory of this instrument was subsequently described, in more detail, by Zabielski, Stein and Kendall (1972/1973) and Stein (1974). Experimental studies of this instrument were reported by Reiter and Kendall (1974). The laboratory version of this instrument had an ion drift length of about 4 cm and a resolving power of 13.

1.4 Statement of the Problem

The principal objective of this thesis is the study of the application of miniature time-of-flight mass spectrometers (TOFMS) with planar, cylindrical and spherical geometries to D-region and E-region ionosphere composition measurements on sounding rockets. The use of time-of-flight mass spectrometers for ionosphere research has been attempted on few occasions in the past (see MacKenzie (1964) and Zabielski (1970)). Since the introduction of the quadrupole mass filter, there has been little use of other types of mass spectrometers for lower E-region and D region ion composition measurements. The development of the miniature time-of-flight mass spectrometers to be discussed in this thesis is to provide an alternate type of mass spectrometer for ion composition measurements in the lower ionosphere.

The first step in accomplishing the principal objective is the theoretical and numerical study of time-of-flight mass spectrometers with planar, cylindrical and spherical geometries in an attempt to optimize their resolving power and sensitivity. The second step is the numerical study of gating in time-of-flight mass spectrometers

in order to understand the effects of gating on resolving power, sensitivity and mass discrimination. The third step is the experimental study of cylindrical and hemispherical-electrode time-of-flight mass spectrometer operation and their suitability for D-region ion composition measurements. The fourth step is the description of the construction and testing of a sounding rocket experiment package carrying a cylindrical-electrode time-of-flight mass spectrometer. The fifth step is a description of the sounding rocket flight and the data reduction procedure for the mass spectrometer data. This step includes a discussion of the calculation of detached shock wave parameters and the effects, on the mass spectrometer data, of sampling through a detached shock wave. The last step is a description of the results of the mass spectrometer measurements, their implications, and a comparison of the results to those of previous researchers.

CHAPTER II

TWO-FIELD TIME-OF-FLIGHT MASS SPECTROMETER THEORY AND NUMERICAL STUDIES

2.1 Introduction

This chapter will develop the mathematical basis for study of the operating conditions of two-field time-of-flight mass spectrometers with planar, cylindrical and spherical geometries. This will be done by first introducing the definitions and the necessary background in order to understand the terms and the previous work on two-field time-of-flight mass spectrometers. This will be followed by a detailed analysis of the time-of-flight for the three geometries. Computer studies of two-field time-of-flight mass spectrometers will be made. In addition, the theory and numerical studies of a possible resolving power enhancement method will be presented at the end of the chapter.

2.2 Definitions

Time-of-flight mass spectrometers can usually be classified as constant energy or constant momentum devices. Constant energy time-of-flight mass spectrometers give the same energy to ions with different mass-to-charge ratios. Constant momentum time-of-flight mass spectrometers give the same momentum to ions with different mass-to-charge ratios. The spectrometers considered in this thesis are all constant energy devices.

In constant energy time-of-flight mass spectrometers, the resolving power is given by $R = t/2\Delta t$ where t is the ion flight

time and Δt is the spread in the time-of-flight of the ions of a given mass. In this thesis, Δt will always signify the full width at half height of any mass peak under study. The resolving power is often equated with resolution in recent studies of mass spectrometers. This is not really correct and this thesis will only use the definition of resolving power given above.

Two important focusing principles, which will be referred to often in this chapter and in the rest of this thesis, are space focusing and velocity focusing. The definitions of space focusing and velocity focusing applied to time-of-flight mass spectrometry are different from the definitions of these terms which are applied to the rest of the mass spectrometry. In this thesis, space focusing occurs if ions of a given mass-to-charge ratio, produced at the same time at different places in the source region with the same velocity, are focused so that they reach the collector at nearly the same time. Velocity focusing occurs, again in this thesis, if ions of a given mass-to-charge ratio, produced at the same time and same place with slightly different velocities, are focused so that they reach the collector at nearly the same time. If perfect velocity focusing and perfect space focusing occur simultaneously, the result is perfect double time focusing.

In order to properly analyze and understand the operation of two-field time-of-flight mass spectrometers with planar, cylindrical and spherical geometries, it will be necessary to derive analytical expressions for the time-of-flight for each geometry. The theory for the planar geometry two-field time-of-

flight mass spectrometer was first worked out by Wiley and McLaren (1955). This work was extended by Stein (1974). A series solution for the cylindrical geometry was derived by Diem (1967) and extended by Zabielski (1970) and Zabielski, Diem and Kendall (1970). A series solution for the spherical geometry was derived by Zabielski (1970) and extended by Zabielski, Stein and Kendall (1972/1973). Closed form solutions for both the cylindrical and spherical geometries were derived by Stein (1974). The expressions presented in this thesis for the time-of-flight for all three geometries will follow those of Stein very closely.

2.3 Linear Constant Energy Time-of-Flight Equation

Consider an ion of mass m, charge q, starting at a point x_i, and with initial velocity v_i. When this ion is placed in an electrostatic field E(x), corresponding to a potential V(x), the equation of motion can be written as

$$\frac{1}{2} m v_i^2 + q V(x_i) = \frac{1}{2} m v^2 + q V(x) \qquad (2.1)$$

In this expression, v is the ion velocity at any point x, and $V(x_i)$ is the potential at the ion's starting point. The time-of-flight equation follows from equation (2.1) by substituting $\frac{dx}{dt} = v$ and integrating both sides of the equation after rearranging terms. This gives

$$t = \pm \left(\frac{m}{2q} \right)^{1/2} \int_{x_i}^{x} \frac{dx'}{\left[\frac{m v_i^2}{2q} + V(x_i) - V(x') \right]^{1/2}} \qquad (2.2)$$

where x is the final position of the ion and the sign is to be chosen to insure an increasing t. The denominator under the integral is always positive so the (+) sign is chosen if $dx' > 0$ and the (-) sign if $dx' < 0$. Equation (2.2) defines the time-of-flight of an ion moving in a straight line.

Reflection points in an ion's path, for an ion with initial velocity in the opposite direction of the electrostatic field, can be calculated from equation (2.1). Since v = 0 at the reflection point

$$V(x_m) = V(x_i) + \frac{mv_i^2}{2q} \tag{2.3}$$

and if the expression for V(x) is known, a solution for x_m can be calculated.

2.4 Two-Field Time-of-Flight Mass Spectrometers; Definitions

The theory of time-of-flight mass spectrometers presented in this chapter deals with idealized mass spectrometers. This ideal two-field time-of-flight mass spectrometer (referred to hereafter as TOFMS) has four electrodes which are planar, (see Figure (2.1)), concentric cylinders (see Figure (2.2)), or concentric spheres (see Figure (2.3)). The outer or left-hand electrode, designated electrode 1, with applied voltage V_1, and radius r_1, is either solid or a grid. The next two electrodes, labeled electrodes 2 and 3, have voltages V_2 and V_3 and radii r_2 and r_3 and need to be essentially transparent to ions. The right-hand or inner electrode, the collector,

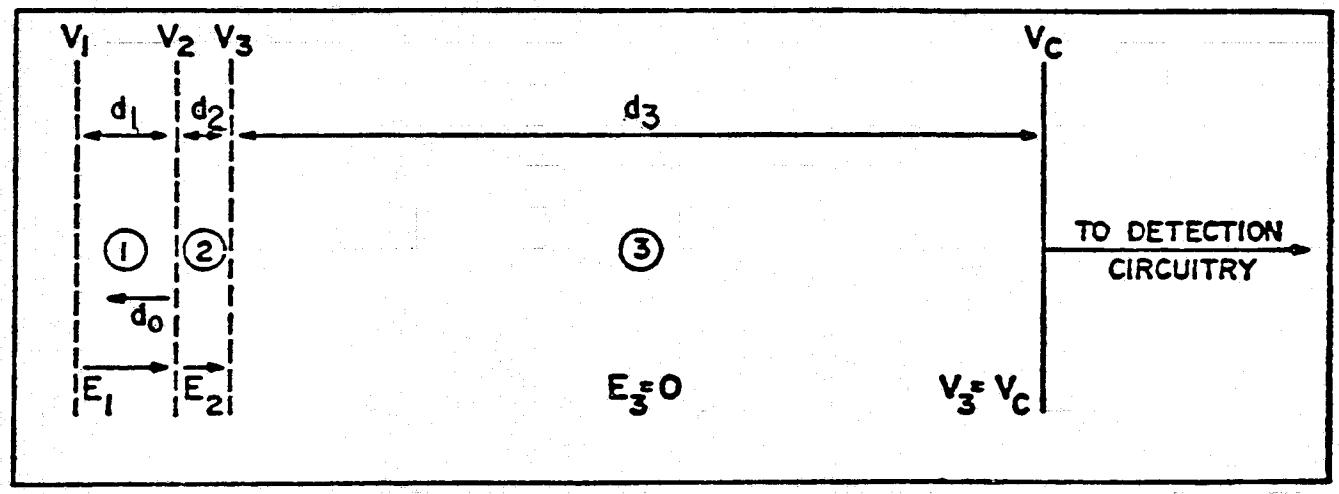

Figure 2.1 Side View of Linear Time-of-Flight Mass Spectrometer of Wiley and McLaren (1955). (Reference: Zabielski (1970)).

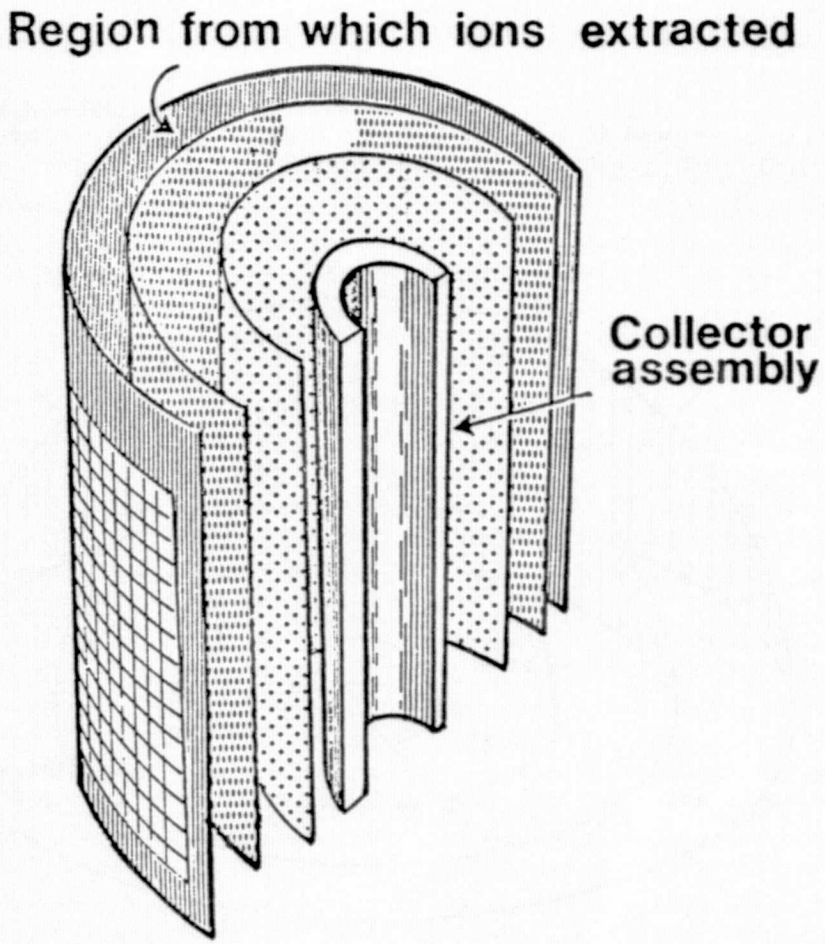

Figure 2.2 Practical Layout of a Cylindrical-Electrode Time-Flight Mass Spectrometer Electrode Structure. (Reference: Zabielski, Diem and Kendall (1970)).

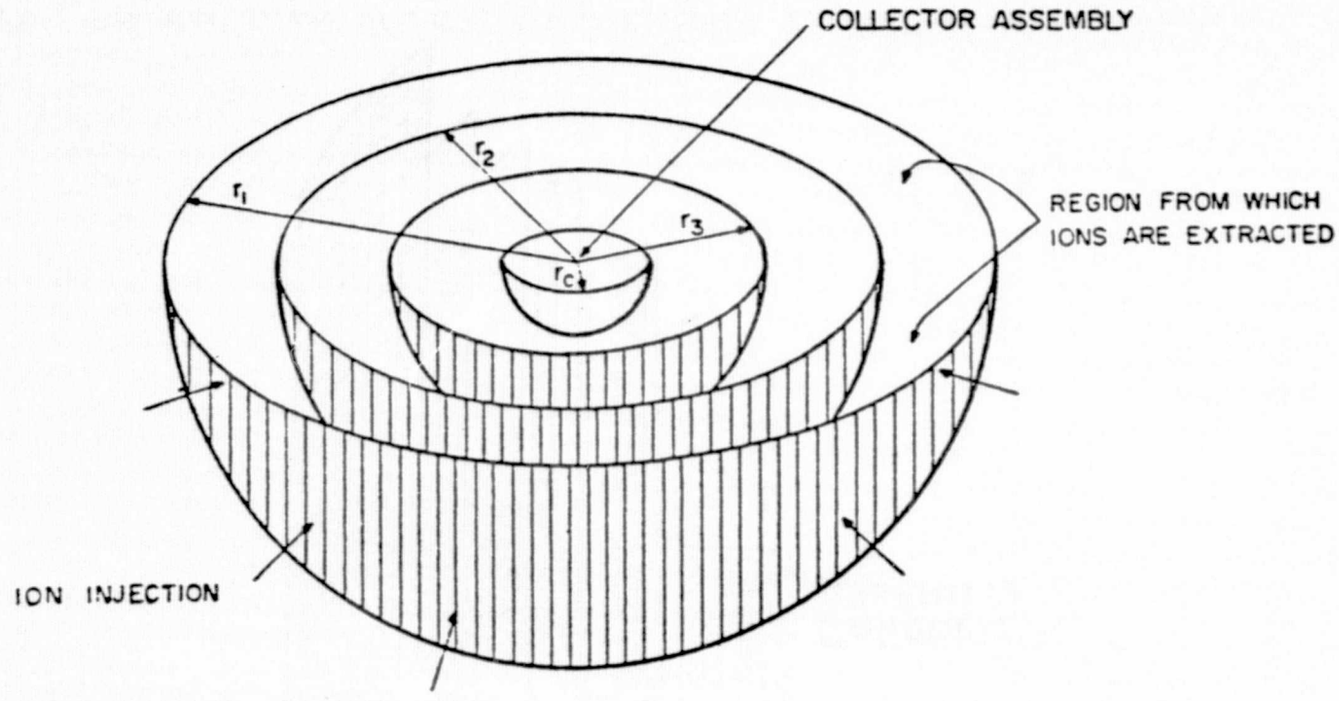

Figure 2.3 Practical Layout of a Spherical-Electrode Time-of-Flight Mass Spectrometer Electrode Structure. (Reference: Zabielski, Stein and Kendall (1972/1973)).

has voltage V_c and radius r_c. These four electrodes bound three regions (designated 1, 2 and 3) and are defined as the source, acceleration and drift regions. The widths of these regions are d_1, d_2 and d_3.

Ions are formed or drawn into the source region when it is field-free ($V_1 = V_2$). The electric field in the source region, E, is then turned on. For positive ions in the TOFMS considered in this thesis, this is usually done by pulsing V_1 more positive (so that $V_1 > V_2$) until all the ions have left the source region. The ion initial position is x_i or r_i and the initial ion velocity is v_i.

In the planar geometry the time-of-flight is independent of initial velocities parallel to the grids. However, in the cylindrical and spherical geometries, non-radial initial ion velocities will affect the time-of-flight. In order to slightly simplify the theory, and because the non-radial velocities will be small in most applications, only radial initial velocities will be considered.

The ions arrive at grid 2 in time t_1, unless the ions have an initial velocity away from the collector large enough so that the ions pass through or strike grid 1, and are lost. When the ions enter the acceleration region, they are influenced by a new electric field E_2 (where $V_2 > V_3$ for positive ions). The time for the ions to traverse the acceleration region is t_2. The ions then pass through grid 3 and enter the field-free drift region. The time for the ions to pass through the drift region is t_3. The total time-of-flight can now be written as

$$t = t_1 + t_2 + t_3 \qquad (2.4)$$

A more general expression for the total time-of-flight should include the turn around time for ions initially travelling away from the collector. If the turn around time is defined as t_t, then we can redefine the time-of-flight for the source region as

$$t_1 = t_1' + \frac{1}{2} t_t \pm \frac{1}{2} t_t \tag{2.5}$$

where t_1' is now the time-of-flight in the source region for ion with initial velocity toward the collector. This now redefines the total time-of-flight as

$$t = t_1' + \frac{1}{2} t_t \pm \frac{1}{2} t_t + t_2 + t_3 \tag{2.6}$$

where the (+) sign represents an initial velocity away from the collector and the (-) sign represents an initial velocity toward the collector.

2.5 Planar Two-Field TOFMS

The electric field E between planar electrodes is a constant (assuming no time variation of the potentials on the electrodes). Therefore, the potential is $V(x) = C_1 x + C_2$, where C_1 and C_2 are defined by the boundary conditions. For two planes, j and k, separated by a distance d, and set at potentials V_j and V_k, the potential between the planes is

$$V(x) = \frac{(V_j - V_k)}{d} x + V_k \tag{2.7}$$

(see Figure (2.4)). The time-of-flight can now be calculated for any initial position x_i, between j and k planes, to any final position x, for any initial velocity v_i, from the time-of-flight equation (equation (2.2)).

For an initial velocity toward the collector, the time-of-flight is

$$t = \pm \left(\frac{m}{2q}\right)^{1/2} \int_{x_i}^{x} \frac{dx'}{\left[\frac{mv_i^2}{2q} + \frac{(V_j - V_k)}{d}(x_i - x')\right]^{1/2}} \tag{2.8}$$

Since $x < x_i$, dx' will be less than 0 and the (-) sign should be used so that $t > 0$. Solving the integral in equation (2.8) gives

$$t = -\left(\frac{m}{2q}\right)^{1/2} \left(\frac{-2d}{(V_j - V_k)}\right) \left[\frac{mv_i^2}{2q} + \frac{(V_j - V_k)}{d}(x_i - x')\right]^{1/2} \Bigg|_{x_i}^{x} \tag{2.9}$$

Evaluating this expression at the limits reduces it to

$$t = \left(\frac{m}{2q}\right)^{1/2} \left(\frac{2d}{(V_j - V_k)}\right) \left[\left\{\frac{(V_j - V_k)}{d}(x_i - x) + \frac{mv_i^2}{2q}\right\}^{1/2} - \left\{\frac{mv_i^2}{2q}\right\}^{1/2}\right] \tag{2.10}$$

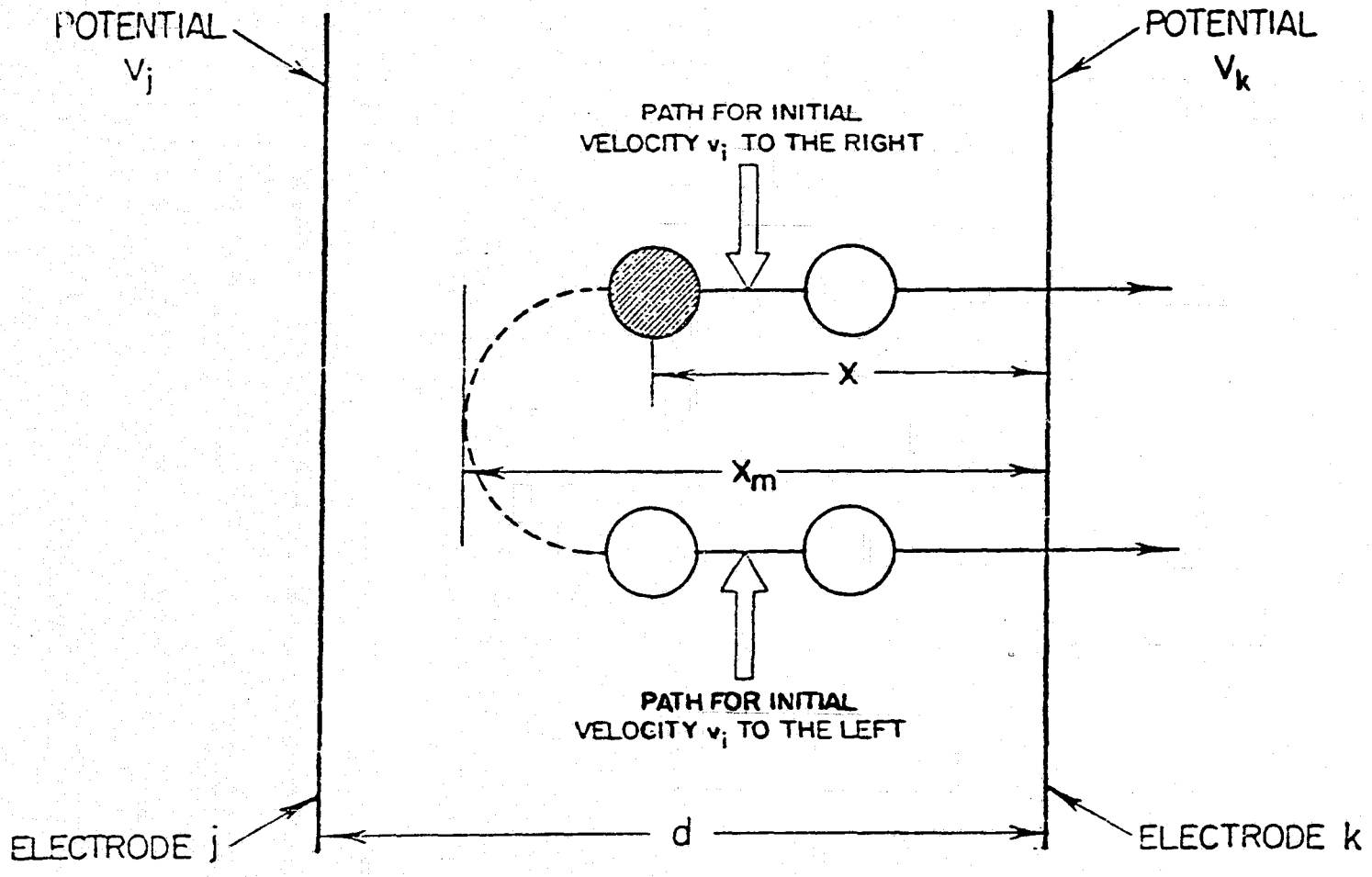

Figure 2.4 Generalized Region Bounded by Planar Electrodes j and k. For Clarity the Cases of Ions Initially Directed to the Left and Right are Indicated with a Separation of Ion Paths. (Reference: Stein (1974)).

The turn around time for an ion with an initial velocity away from the collector must be included. Substituting the appropriate potentials into equation (2.3) produces

$$\frac{(V_j - V_k)}{d} x_m + V_k = \frac{mv_i^2}{2q} + \frac{(V_j - V_k)}{d} x_i + V_k \qquad (2.11)$$

which reduces to

$$x_m = x_i + \left(\frac{mv_i^2}{2q} \right) \frac{d}{(V_j - V_k)} \qquad (2.12)$$

Notice that if $x_m > x_j$, the ion is lost. The turn around time will be just twice the time for the ion to travel from x_m to x_i. Substituting for x_m into equation (2.10) and multiplying by 2 gives the turn around time as

$$t_t = 2 \left(\frac{m}{2q} \right)^{1/2} \left(\frac{2d}{(V_j - V_k)} \right) \left(\frac{mv_i^2}{2q} \right)^{1/2} \qquad (2.13)$$

The time-of-flight can now be calculated for all three regions in the planar TOFMS. In the source region we substitute $d = d_1$, $v_i = v_o$, $x_i - x = d_0$ and $\frac{(V_j - V_k)}{d} = \frac{(V_1 - V_2)}{d_1}$ into equations (2.10) and (2.13).

Then using equation (2.5), the time-of-flight for the source region is

$$t_1 = \left(\frac{m}{2q}\right)^{1/2} \left(\frac{2d_1}{(V_1 - V_2)}\right) \left[\left\{ \frac{(V_1 - V_2)}{d_1} d_o + \frac{mv_o^2}{2q} \right\}^{1/2} \pm \left\{ \frac{mv_o^2}{2q} \right\}^{1/2} \right] \tag{2.14}$$

In the acceleration region $(x_i - x) = d = d_2$, $(V_j - V_k)/d = (V_2 - V_3)/d_2$ and

$$v_i^2 = v_o^2 + \frac{2q}{m} (V_i - V_2) \tag{2.15}$$

Substituting $V_i = (V_1 - V_2)\frac{d_o}{d_1} + V_2$ into equation (2.15) gives

$$v_i^2 = v_o^2 + \frac{2q}{m} \frac{d_o}{d_1} (V_1 - V_2) = \gamma^2 \tag{2.16}$$

When equation (2.16) and the other parameters for the acceleration region are substituted into equation (2.10), the time-of-flight for the acceleration region is given by

$$t_2 = \left(\frac{m}{2q}\right)^{1/2} \left(\frac{2d_2}{(V_2 - V_3)}\right) \left[\left\{ V_2 - V_3 + \frac{m\gamma^2}{2q} \right\}^{1/2} - \left\{ \frac{m\gamma^2}{2q} \right\}^{1/2} \right] \tag{2.17}$$

As the ions traverse the drift region, their velocities will be constant and the equation of motion is

$$qV_3 + \frac{1}{2} mv_d^2 = qV_i + \frac{1}{2} mv_o^2 \tag{2.18}$$

Solving for the drift region velocity gives

$$v_d = \left(\frac{2q}{m}\right)^{1/2} \left\{V_i - V_3 + \frac{mv_o^2}{2q}\right\}^{1/2} \qquad (2.19)$$

where V_i is the potential at the ion starting position. Since v_d is constant through the field-free drift region, the time-of-flight is given by d_3/v_d or

$$t_3 = \left(\frac{m}{2q}\right)^{1/2} \frac{d_3}{\left\{V_i - V_3 + \frac{mv_o^2}{2q}\right\}^{1/2}} \qquad (2.20)$$

Because the drift region is field-free, the same expression for t_3, with the appropriate expression for V_i, can be used for all three geometries to be discussed here. Substituting the proper expression for V_i into equation (2.20) gives

$$t_3 = \left(\frac{m}{2q}\right)^{1/2} \frac{d_3}{\left\{(V_1 - V_2)\frac{d_o}{d_1} + V_2 - V_3 + \frac{mv_o^2}{2q}\right\}^{1/2}} \qquad (2.21)$$

Combining the expressions for the time-of-flight in the three regions gives the total time-of-flight for a planar two-field TOFMS

$$t = \left(\frac{m}{2q}\right)^{1/2}\left\{\left\{\frac{2d_1}{(V_1 - V_2)}\right\}\left[\left\{\frac{(V_1 - V_2)}{d_1} d_o + \frac{mv_o^2}{2q}\right\}^{1/2} \pm \left\{\frac{mv_o^2}{2q}\right\}^{1/2}\right]\right.$$

$$+ \frac{2d_2}{(V_2 - V_3)}\left[\left\{V_2 - V_3 + \frac{m\gamma^2}{2q}\right\}^{1/2} - \left\{\frac{m\gamma^2}{2q}\right\}^{1/2}\right]$$

$$\left. + \frac{d_3}{\left\{(V_1 - V_2)\frac{d_o}{d_1} + V_2 - V_3 + \frac{mv_o^2}{2q}\right\}^{1/2}}\right\} \qquad (2.22)$$

The (+) sign is for an initial velocity away from the collector, while the (-) sign is for an initial velocity toward the collector.

Equation (2.22) reduces to the expressions for the time-of-flight calculated by Wiley and McLaren (1955) and given by their equations (2a), (2b) and (2c). It is necessary to substitute $d_0 = s_0$, $d_1 = s$, $d_2 = d$, $d_3 = D$, $U_0 = \frac{mv_0^2}{2}$, $\frac{(V_1 - V_2)}{d_1} = E_s$, $\frac{(V_2 - V_3)}{d_2} = E_d$ and $U = U_0 + qsE_s + qdE_d$ into equation (2.22) and rearrange the terms. It is also necessary to change the units kg, m, V and sec into amu, cm, eV and μsec, respectively, in order to produce the multiplicative factor of 1.02 used in Wiley and McLaren (1955). Equation (2.22) also reduces to the result presented in equation (1) in Pavlenko et al., (1968) if the erroneous symbol s is corrected to s_0 in Pavlenko's equation (1).

2.6 Cylindrical Two-Field TOFMS

Between two concentric cylinders, the electric field E(r) is proportional to $\frac{1}{r}$. Therefore, the potential is $V(r) = C_1 \ln r + C_2$, where C_1 and C_2 are determined by the boundary conditions. For two concentric cylinders, labelled j and k, with potentials V_j and V_k and radii r_j and r_k, the potential between cylinders is given by

$$V(r) = \frac{(V_j - V_k)}{\ln (r_j/r_k)} \ln (r/r_j) + V_j \qquad (2.23)$$

(see Figure (2.5)).

For an initial velocity toward the collector (inward in the spectrometer considered here) the time-of-flight equation for the cylindrical-geometry mass spectrometer can be derived by substituting the potential given by equation (2.23) into the time-of-flight equation (2.2) and using r instead of x. This gives

$$t = \pm \left(\frac{m}{2q}\right)^{1/2} \int_{r_i}^{r} \frac{dr'}{\left\{\frac{mv_i^2}{2q} + \frac{(V_j - V_k)}{\ln(r_j/r_k)} \ln(r_i/r')\right\}^{1/2}} \qquad (2.24)$$

Since $r < r_0$, dr' will be less than 0 and the (-) sign is chosen so that $t > 0$. If we define

$$C_{jk} = \left\{\frac{mv_i^2}{2q}\right\} \frac{\ln (r_j/r_k)}{(V_j - V_k)} \qquad (2.25)$$

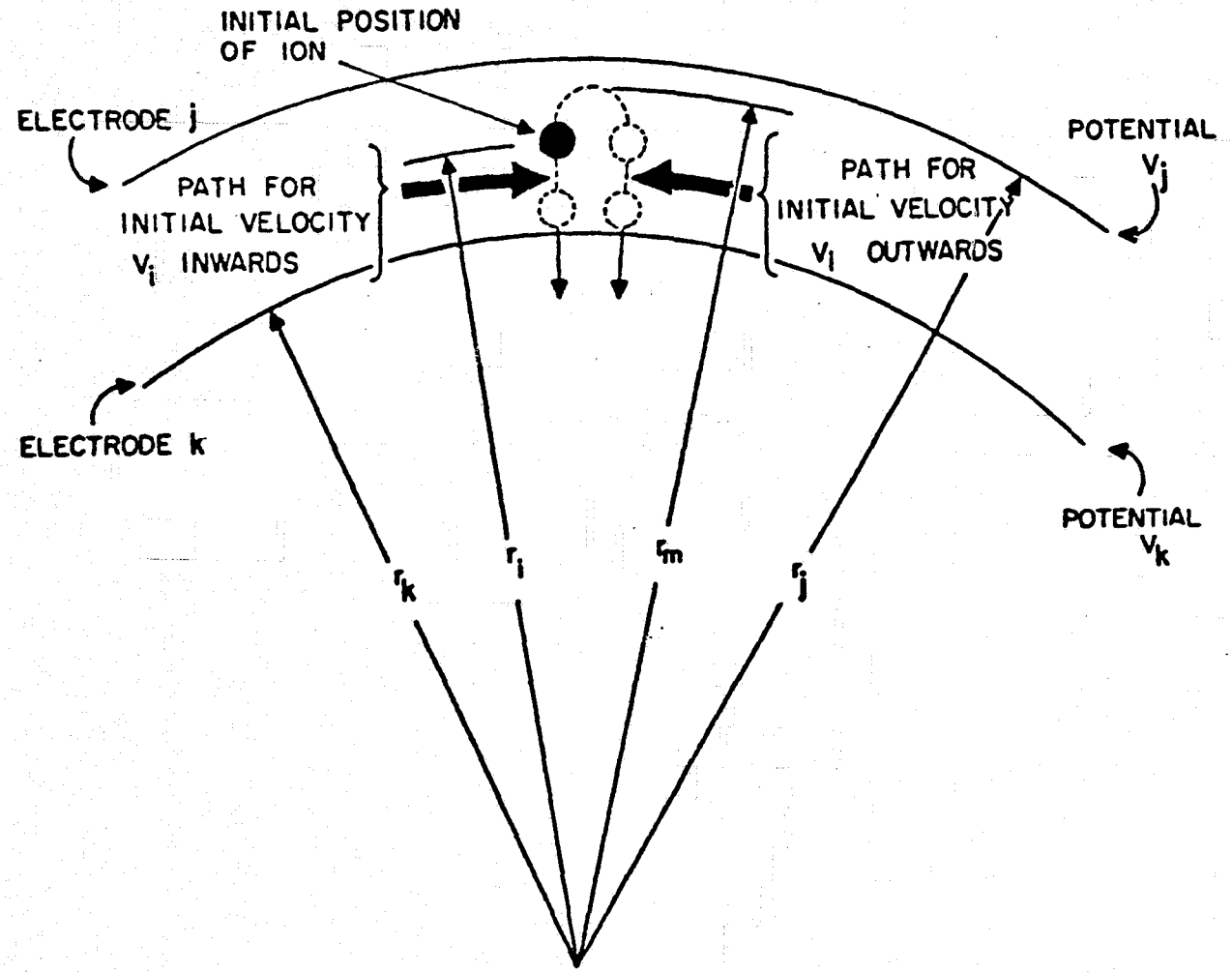

Figure 2.5 Generalized Region Bounded by Cylindrical Electrodes j and k. For Clarity, the Cases of Inward Directed and Outward Directed Initial Velocities are Indicated with Slightly Separate Ion Paths. (Reference: Zabielski, Stein and Kendall (1972/1973)).

and

$$P = \left\{\ln (r_i/r') + C_{jk}\right\}^{1/2} \tag{2.26}$$

then

$$r' = r_i\, e^{-(P^2 - C_{jk})} \tag{2.27}$$

and

$$dr' = -2r_i P\, e^{-(P^2 - C_{jk})}\, dP \tag{2.28}$$

Substituting equations (2.25), (2.26), (2.27) and (2.28) into (2.24) and rearranging terms produces

$$t = -\left(\frac{m}{2q}\right)^{1/2} \int_{C_{jk}^{1/2}}^{\{\ln (r_i/r) + C_{jk}\}^{1/2}} \frac{-2r_i\, P\, e^{-(P^2 - C_{jk})}\, dP}{P\left\{\dfrac{(V_j - V_k)}{\ln(r_j/r_k)}\right\}^{1/2}} \tag{2.29}$$

Taking the constants out of the integral reduces equation (2.29) to

$$t = \left(\frac{m}{2q}\right)^{1/2} 2r_i \left\{\frac{\ln (r_j/r_k)}{(V_j - V_k)}\right\}^{1/2} e^{C_{jk}} \int_{C_{jk}^{1/2}}^{\{\ln(r_i/r)+C_{jk}\}^{1/2}} e^{-P^2}\, dP \tag{2.30}$$

We can write

$$\int_B^A e^{-P^2} dP = \int_o^A e^{-P^2} dP - \int_o^B e^{-P^2} dP = \frac{\sqrt{\pi}}{2} (\text{erf}\, A - \text{erf}\, B) \tag{2.31}$$

where

$$\text{erf}\, A = \frac{2}{\sqrt{\pi}} \int_o^A e^{-y^2} dy \tag{2.31a}$$

Equation (2.30) can now be written as

$$t = \left(\frac{m}{2q} \right)^{1/2} r_i \left\{ \frac{\pi \ln (r_j/r_k)}{(V_j - V_k)} \right\}^{1/2} e^{C_{jk}} \left\{ \text{erf} \left[(\ln (r_i/r) + C_{jk})^{1/2} \right] - \text{erf} \left[C_{jk}^{1/2} \right] \right\} \tag{2.32}$$

The time-of-flight for each region of the mass spectrometer can now be derived. For an initial ion velocity toward the collector in the source region we substitute $r_i = r_o$, $V_j = V_1$, $V_k = V_2$, $r_j = r_1$, $v_i = v_o$ and $r_k = r_2$ into equation (2.32) giving

$$t'_1 = \left(\frac{m}{2q} \right)^{1/2} r_o \left\{ \frac{\pi \ln (r_1/r_2)}{(V_1 - V_2)} \right\}^{1/2} e^{C_{12}} \left\{ \text{erf} \left[(\ln (r_o/r) + C_{12})^{1/2} \right] - \text{erf} \left[C_{12}^{1/2} \right] \right\} \tag{2.33}$$

where

$$C_{12} = \frac{mv_o^2}{2q} \quad \frac{\ln (r_1/r_2)}{(V_1 - V_2)} \tag{2.34}$$

When the ion has an initial outward velocity, the turn around time can be calculated after calculating the turn around radius, r_m. Substituting the appropriate potentials into equation (2.3) gives

$$\frac{(V_j - V_k)}{\ln (r_j/r_k)} \ln (r_m/r_j) + V_j = \frac{mv_i^2}{2q} + \frac{(V_j - V_k)}{\ln(r_j/r_k)} \ln(r_i/r_j) + V_j \tag{2.35}$$

This yields

$$r_m = r_i e^{C_{jk}} \tag{2.36}$$

Note that if $r_m > r_j$ the ion is lost. From equation (2.32) we can solve for the time for an ion to travel from r_m to the initial position r_i by substituting $r = r_i$, $r_i = r_m$ and $v_i = 0$. The turn around time will be exactly twice this time or

$$t_t = \left(\frac{m}{2q} \right)^{1/2} 2r_m \left\{ \frac{\pi \ln(r_j/r_k)}{(V_j - V_k)} \right\}^{1/2} \text{erf} \left[\{\ln(r_m/r_i)\}^{1/2} \right] \tag{2.37}$$

Now substituting for r_m from equation (2.36) gives

$$t_t = \left(\frac{m}{2q} \right)^{1/2} 2r_i \left\{ \frac{\pi \ln (r_j/r_k)}{(V_j - V_k)} \right\}^{1/2} e^{C_{jk}} \text{erf} \left[C_{jk}^{1/2} \right] \tag{2.38}$$

Making the same substitutions used in the derivation of equation (2.33) produces

$$t_t = \left(\frac{m}{2q}\right)^{1/2} 2r_o \left\{\frac{\pi \ln(r_1/r_2)}{(V_1 - V_2)}\right\}^{1/2} e^{C_{12}} \operatorname{erf}\left[C_{12}^{1/2}\right] \tag{2.39}$$

Combining equations (2.33) and (2.39) into equation (2.5) gives an expression for the time-of-flight in the source region

$$t_1 = \left(\frac{m}{2q}\right)^{1/2} r_o \left\{\frac{\pi \ln(r_1/r_2)}{(V_1 - V_2)}\right\}^{1/2} e^{C_{12}} \left\{\operatorname{erf}\left[(\ln(r_o/r_2) + C_{12}\right]^{1/2}\right] \pm \operatorname{erf}\left[C_{12}^{1/2}\right]\right\} \tag{2.40}$$

In the acceleration region region we substitute $r_j = r_i = r_2$, $r = r_k = r_3$, $V_j = V_2$ and $V_k = V_3$ into equation (2.32) along with the initial velocity. The initial velocity for the acceleration region can be calculated from equation (2.1) by making the appropriate substitutions. This gives

$$\frac{1}{2} mv_o^2 + \frac{q(V_1 - V_2)}{\ln(r_1/r_2)} \ln(r_o/r_1) + qV_1 = \frac{1}{2} mv_i^2 + qV_2 \tag{2.41}$$

where v_i is the velocity in question. Solving for v_i^2 gives

$$v_i^2 = \frac{2q}{m} \frac{(V_1 - V_2) \ln(r_o/r_2)}{\ln(r_1/r_2)} + v_o^2 = \beta^2 \tag{2.42}$$

Now the time-of-flight for the acceleration region is given by

$$t_2 = \left(\frac{m}{2q}\right)^{1/2} r_2 \left\{\frac{\pi \ln(r_2/r_3)}{(V_2 - V_3)}\right\}^{1/2} e^{C_{23}} \left\{\text{erf}\left[(\ln(r_2/r_3) + C_{23})^{1/2}\right] - \text{erf}\left[C_{23}^{1/2}\right]\right\} \tag{2.43}$$

where

$$C_{23} = \left(\frac{m\beta^2}{2q}\right) \frac{\ln(r_2/r_3)}{(V_2 - V_3)} \tag{2.44}$$

In the drift region we substitute $d_3 = r_3 - r_c$ into equation (2.20). This gives the time-of-flight for region 3 as

$$t_3 = \left(\frac{m}{2q}\right)^{1/2} \frac{r_3 - r_c}{\left\{V_i - V_3 + \frac{mv_o^2}{2q}\right\}^{1/2}} \tag{2.45}$$

Now combining equations (2.40), (2.43) and (2.45) gives the total time-of-flight for a cylindrical two-field TOFMS as

$$t = \left(\frac{m}{2q}\right)^{1/2} \left\{r_o \left\{\frac{\pi \ln(r_1/r_2)}{(V_1 - V_2)}\right\}^{1/2} e^{C_{12}} \left\{\text{erf}\left[(\ln(r_o/r_2) + C_{12})^{1/2}\right] \pm \text{erf}\left[C_{12}^{1/2}\right]\right\} + r_2 \left\{\frac{\pi \ln(r_2/r_3)}{(V_2 - V_3)}\right\}^{1/2} e^{C_{23}} \left\{\text{erf}\left[(\ln(r_2/r_3) + C_{23})^{1/2}\right] - \text{erf}\left[C_{23}^{1/2}\right]\right\}$$

$$+ \frac{r_3 - r_c}{\left\{V_i - V_3 + \frac{mv_o^2}{2q}\right\}^{1/2}} \Bigg\} \qquad (2.46)$$

The (+) sign corresponds to an initial ion velocity away from the collector while the (-) sign corresponds to an initial ion velocity toward the collector.

Expanding the error function terms of equation (2.46) in Maclaurin series and making the substitutions $r_0 = r_s$, $v_0 = v_s$, $C_{12} = A_{12}$, $V_i = V_s$ and $C_{23} = A_{23}$ produces an expression for the time-of-flight in a cylindrical TOFMS which is identical to the expression obtained by combining equations (11), (12), (15) and (16) in Zabielski, Diem and Kendall (1970), according to equation (2.6) in this thesis. Equation (2.46) is also identical to equation (2.5.26) in Stein (1974) if the substitutions $r_0 = r_s$, $v_0 = v_s$, $C_{12} = A_{12}$, $C_{23} = A_{23}$ and $V_i = V_s$ are made.

2.7 Spherical Two-Field TOFMS

When two concentric spheres, labelled j and k, with radii r_j and r_k, are set at potentials V_j and V_k, the potential between the spheres is $V(r) = C_1/r + C_2$ where C_1 and C_2 are defined by the boundary conditions. Solving for C_1 and C_2 yields

$$V(r) = \frac{-k_{jk}}{r} + \frac{(r_j V_j - r_k V_k)}{(r_j - r_k)} \qquad (2.47)$$

with

$$k_{jk} = \frac{r_j r_k (V_j - V_k)}{(r_j - r_k)} \qquad (2.48)$$

This potential produces an electric field E(r) proportional to $\frac{1}{r^2}$ (see Figure (2.6)).

The time-of-flight can now be calculated for any initial position r_i, between the j and k spheres, to any final position $r(r < r_i)$ for an inward velocity. Substituting equation (2.47) into equation (2.2) and using the variable r instead of x produces

$$t = \pm \left(\frac{m}{2q}\right)^{1/2} \int_{r_i}^{r} \frac{dr'}{\left\{\frac{mv_i^2}{2q} + k_{jk}\left(\frac{1}{r'} - \frac{1}{r_i}\right)\right\}^{1/2}} \tag{2.49}$$

Since $r < r_i$, dr' will be less than 0 and the (-) sign is chosen to give an increasing t. Multiply the numerator and denominator of equation (2.49) by $r'^{1/2}$. After rearranging terms, this yields

$$t = - \left(\frac{m}{2q}\right)^{1/2} \int_{r_i}^{r} \frac{r'^{1/2}\, dr'}{\left\{k_{jk} + \left[\frac{mv_i^2}{2q} - \frac{k_{jk}}{r_i}\right] r'\right\}^{1/2}} \tag{2.50}$$

Now dividing numerator and denominator by

$$\left[\frac{k_{jk}}{r_i} - \frac{mv_i^2}{2q}\right]^{1/2}$$

and defining

$$\alpha_{jk} = \frac{r_i\, k_{jk}}{k_{jk} - r_i\left(\frac{mv_i^2}{2q}\right)}, \tag{2.51}$$

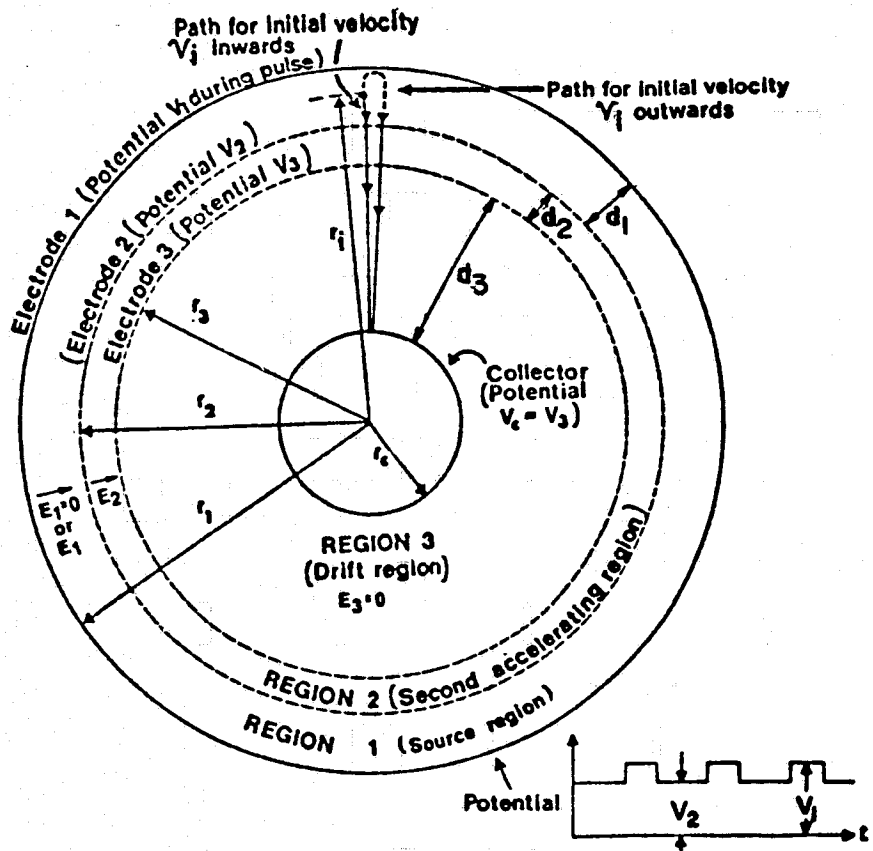

Figure 2.6 Cross Section of Spherical Time-of-Flight Mass Spectrometer with Two Accelerating Regions and a Single Drift Region. Ions are Initially in Region 1, the Source Region. (Reference: Zabielski, Stein and Kendall (1972/1973)).

give t as

$$t = - \left(\frac{m}{2q}\right)^{1/2} \left(\frac{\alpha_{jk}}{k_{jk}}\right)^{1/2} \int_{r_i}^{r} \frac{r'^{1/2}\, dr'}{(\alpha_{jk} - r')^{1/2}} \qquad (2.52)$$

It is now necessary to show that $\alpha_{jk} > 0$ and $\alpha_{jk} - r > 0$ in order to solve the integral in equation (2.52). Let us calculate the maximum radius for an ion with an initial velocity away from the collector. Substituting the proper potentials into equation (2.3) results in

$$\left[\frac{-k_{jk}}{r_m} + \frac{r_j V_j - r_k V_k}{(r_j - r_k)}\right] = \frac{mv_i^2}{2q} + \left[\frac{-k_{jk}}{r_i} + \frac{r_j V_j - r_k V_k}{(r_j - r_k)}\right] \qquad (2.53)$$

Solving for r_m yields $r_m = \alpha_{jk}$ (2.54)

Therefore, $\alpha_{jk} > 0$, and since $r_m \geq r_i$, then $\alpha_{jk} - r > 0$. With the substitution of $r' = x^2$ into equation (2.52) we get

$$t = - \left(\frac{m}{2q}\right)^{1/2} \left(\frac{\alpha_{jk}}{k_{jk}}\right)^{1/2} \int_{r_i}^{r} \frac{2x^2\, dx}{(\alpha_{jk} - x^2)^{1/2}} \qquad (2.55)$$

Since $\alpha_{jk} > 0$ and $\alpha_{jk} - x^2 > 0$, this integral can be evaluated as

$$t = -\left(\frac{m}{2q}\right)^{1/2}\left(\frac{\alpha_{jk}}{k_{jk}}\right)^{1/2}\left\{-x(\alpha_{jk}-x^2)^{1/2} + \alpha_{jk}\sin^{-1}\left\{\frac{x}{\alpha_{jk}^{1/2}}\right\}\right\}\Bigg|_{r_i^{1/2}}^{r^{1/2}} \tag{2.56}$$

where only the principal values for $\sin^{-1}$ are to be used. Evaluating the limits of equation (2.56) yields

$$t = \left(\frac{m}{2q}\right)^{1/2}\left(\frac{\alpha_{jk}}{k_{jk}}\right)^{1/2}\left\{r^{1/2}(\alpha_{jk}-r)^{1/2} - r_i^{1/2}(\alpha_{jk}-r_i)^{1/2} - \alpha_{jk}\left[\sin^{-1}\left\{\left(\frac{r}{\alpha_{jk}}\right)^{1/2}\right\} - \sin^{-1}\left\{\left(\frac{r_i}{\alpha_{jk}}\right)^{1/2}\right\}\right]\right\} \tag{2.57}$$

The time spent in the source region for an ion initially moving toward the collector can be calculated by substituting $v_i = v_0$, $r_i = r_0$, $V_j = V_1$, $V_k = V_2$, $r_j = r_1$ and $r = r_k = r_2$ into equation (2.57). This yields

$$t_1' = \left(\frac{m}{2q}\right)^{1/2}\left(\frac{\alpha_{12}}{k_{12}}\right)^{1/2}\left\{r_2^{1/2}(\alpha_{12}-r_2)^{1/2} - r_o^{1/2}(\alpha_{12}-r_o)^{1/2} - \alpha_{12}\left[\sin^{-1}\left\{\left(\frac{r_2}{\alpha_{12}}\right)^{1/2}\right\} - \sin^{-1}\left\{\left(\frac{r_o}{\alpha_{12}}\right)^{1/2}\right\}\right]\right\} \tag{2.58}$$

The turn around time for ions initially moving away from the collector in the source region can be calculated by substituting $k_{jk} = k_{12}$, $V_j = V_1$, $V_k = V_2$, $r_j = r_1$, $r_k = r_2$, $r_i = r_m = \alpha_{12}$, $r = r_0$, $\alpha_{jk} = \alpha_{12}$ and $v_i = 0$ into equation (2.57) and multiplying by 2. This yields

$$t_t = 2 \left(\frac{m}{2q}\right)^{1/2} \left(\frac{\alpha_{12}}{k_{12}}\right)^{1/2} \left\{ r_o^{1/2} (\alpha_{12} - r_o)^{1/2} - \alpha_{12} \cdot \left[\sin^{-1} \left\{ \left(\frac{r_o}{\alpha_{12}}\right)^{1/2} \right\} - \frac{\pi}{2} \right] \right\} \tag{2.59}$$

Combining equations (2.58) and (2.59) according to equation (2.5) gives the total time-of-flight in the source region as

$$t_1 = \left(\frac{m}{2q}\right)^{1/2} \left(\frac{\alpha_{12}}{k_{12}}\right)^{1/2} \left\{ r_2^{1/2} (\alpha_{12} - r_2)^{1/2} - \alpha_{12} \cdot \left[\sin^{-1} \left\{ \left(\frac{r_2}{\alpha_{12}}\right)^{1/2} \right\} - \frac{\pi}{2} \right] \pm \left(r_o^{1/2} (\alpha_{12} - r_o)^{1/2} - \alpha_{12} \cdot \left[\sin^{-1} \left\{ \left(\frac{r_o}{\alpha_{12}}\right)^{1/2} \right\} - \frac{\pi}{2} \right] \right) \right\} \tag{2.60}$$

The initial velocity of an ion as it enters the acceleration region is given by v_i where v_i is defined by

$$\frac{mv_o^2}{2q} + V_i = \frac{mv_i^2}{2q} + V_2 \qquad (2.61)$$

and where

$$V_i = \frac{-k_{12}}{r_o} + \frac{V_1 r_1 - V_2 r_2}{r_1 - r_2} \qquad (2.62)$$

Solving for v_i^2 yields

$$v_i^2 = \frac{2q}{m} (V_i - V_2) + v_o^2 = \Delta^2 \qquad (2.63)$$

In the acceleration region we substitute $r_j = r_i = r_2$, $r_k = r = r_3$, $\alpha_{jk} = \alpha_{23}$, $k_{jk} = k_{23}$, $V_j = V_2$, $V_k = V_3$ and $v_i = \Delta$ into equation (2.57) to calculate the time-of-flight. This yields

$$t_2 = \left(\frac{m}{2q}\right)^{1/2} \left(\frac{\alpha_{23}}{k_{23}}\right)^{1/2} \left\{ r_3^{1/2} (\alpha_{23} - r_3)^{1/2} - r_2^{1/2} (\alpha_{23} - r_2)^{1/2} \right.$$

$$\left. - \alpha_{23} \left[\sin^{-1} \left\{ \left(\frac{r_3}{\alpha_{23}} \right)^{1/2} \right\} - \sin^{-1} \left\{ \left(\frac{r_2}{\alpha_{23}} \right)^{1/2} \right\} \right] \right\} \qquad (2.64)$$

To calculate the time-of-flight for the drift region, we substitute $d_3 = r_3 - r_c$ into equation (2.20) yielding

$$t_3 = \left(\frac{m}{2q}\right)^{1/2} \frac{r_3 - r_c}{\left\{ V_i - V_3 + \frac{mv_o^2}{2q} \right\}^{1/2}} \qquad (2.65)$$

Combining equations (2.60), (2.64) and (2.65) gives the total time-of-flight as

$$t = \left(\frac{m}{2q}\right)^{1/2} \left\{ \left(\frac{\alpha_{12}}{k_{12}}\right)^{1/2} \left[r_2^{1/2} (\alpha_{12} - r_2)^{1/2} - \alpha_{12} \right. \right.$$

$$\left\{ \sin^{-1} \left[\left(\frac{r_2}{\alpha_{12}}\right)^{1/2} \right] - \frac{\pi}{2} \right\}$$

$$\pm \left[r_o^{1/2} (\alpha_{12} - r_o)^{1/2} - \alpha_{12} \left\{ \sin^{-1} \left[\left(\frac{r_o}{\alpha_{12}}\right)^{1/2} \right] - \frac{\pi}{2} \right\} \right] \Bigg]$$

$$+ \left(\frac{\alpha_{23}}{k_{23}}\right)^{1/2} \left[r_3^{1/2} (\alpha_{23} - r_3)^{1/2} - r_2^{1/2} (\alpha_{23} - r_2)^{1/2} - \alpha_{23} \right.$$

$$\left\{ \sin^{-1} \left[\left(\frac{r_3}{\alpha_{23}}\right)^{1/2} \right] - \sin^{-1} \left[\left(\frac{r_2}{\alpha_{23}}\right)^{1/2} \right] \right\} \Bigg]$$

$$\left. + \frac{r_3 - r_c}{\left\{ V_i - V_3 + \frac{mv_o^2}{2q} \right\}^{1/2}} \right\} \qquad (2.66)$$

where

$$k_{12} = \frac{r_1 r_2 (V_2 - V_3)}{r_1 - r_2} \qquad (2.67)$$

$$k_{23} = \frac{r_2 r_3 (V_2 - V_3)}{r_2 - r_3} \qquad (2.68)$$

$$\alpha_{12} = \frac{r_o k_{12}}{k_{12} - r_o\left(\frac{mv_o^2}{2q}\right)} \tag{2.69}$$

and

$$\alpha_{23} = \frac{r_2 k_{23}}{k_{23} - r_2\left(\frac{m\Delta^2}{2q}\right)} \tag{2.70}$$

The (+) sign represents an initial ion velocity away from the collector and the (-) sign represents an initial ion velocity toward the collector.

Equation (2.66) can be shown to be identical with equations (12), (13), (18) and (19) of Zabielski, Stein and Kendall (1972/1973) combined, using equation (2.6) in this thesis. The substitutions of $r_0 = r_s$, $v_0 = v_s$, $\Delta^2 = \phi^2$, $\frac{k_{12}}{\alpha_{12}} = \frac{\gamma_{12}}{r_s}$ and $\frac{k_{23}}{\alpha_{23}} = \frac{\gamma_{23}}{r_2}$ into equation (2.66) are necessary. When the $\sin^{-1}$ terms are expanded into Maclaurin series and $(\alpha_{12} - r_2)^{1/2}$, $(\alpha_{12} - r_0)^{1/2}$, $(\alpha_{23} - r_3)^{1/2}$ and $(\alpha_{23} - r_2)^{1/2}$ are expanded into binomial series, a simple rearrangement of terms will show equation (2.66) is identical with the results of Zabielski, Stein and Kendall (1972/1973).

Equation (2.66) is also identical with equation (2.6.27) in Stein (1974), with the substitutions of $r_0 = r_s$, $v_0 = v_s$, $V_i = V_s$ and $\Delta^2 = \phi^2$ into equation (2.66).

2.8 Numerical Studies; Two-Field TOFMS

The most convenient method of studying the effect of various operating voltages and grid spacings on the ion flight time

characteristics of TOF mass spectrometers is to use computer simulation. Computer programs were developed by myself using the time-of-flight equations derived earlier in this chapter. These programs calculated ion flight time as a function of ion starting position in the source region, ion initial energy (velocity), electrode spacings, operating voltages and ion mass for planar, cylindrical and spherical-electrode TOFMS.

Numerical studies using computer simulation have been reported by Zabielski (1970), Zabielski, Diem and Kendall (1970), Zabielski, Stein and Kendall (1972/1973) and Stein (1974). Zabielski (1970) discussed time-of-flight versus starting position for all three geometries when there was zero initial ion velocity and near to the optimum space focusing operating conditions. The effects of initial velocities, initial energy spreads, operating voltages which produce better velocity focusing characteristics and varying electrode spacings were, for the most part, ignored. Zabielski, Diem and Kendall (1970) and Zabielski, Stein and Kendall (1972/1973) discussed only optimum space focusing operating conditions for zero initial ion velocities for the cylindrical and spherical geometries, respectively. Stein (1974) concentrated on optimum space focusing characteristics with zero ion initial velocities. However, he did study the effects of varying electrode spacings and discussed the effects of initial ion velocities and initial energy spreads on the flight time characteristics.

One striking characteristic of the results presented by the above authors is the lack of significant variation in the time-of-flight

versus starting position curves between the three TOFMS geometries. Obviously, the radius of curvature of the electrodes for the cylindrical and spherical geometries studies was not small enough, in relation to the interelectrode spacings, to produce a significant variation in the source and acceleration region electric fields as compared with a planar geometry.

In order to fill in the gaps left by previous researchers, this section will concentrate on the effects of initial ion velocities, initial energy spreads, velocity focusing characteristics and exaggerating the cylindrical and spherical geometry effects on flight time characteristics.

Figure (2.7) shows the space focusing characteristics of the planar, cylindrical and spherical geometries for near the optimum space focusing voltage ratio (the voltage ratio is defined as $R = (V_1 - V_3)/(V_2 - V_3)$). This Figure is presented for comparison with the Figures which will follow. The time scale of Figure (2.7) is greatly expanded to bring out the characteristics. An excellent discussion of these curves and the resulting peak shapes can be found in Stein (1974). It must be emphasized that no initial velocity spread has been considered in producing the curves in Figure (2.7). The effect of an initial velocity spread on resolving power is significant. For example, the space focusing resolving power for $R = 1.64$ in a spherical-electrode TOFMS, taken from Figure (2.7), is 1450. However, the actual resolving power for this type of instrument in the laboratory is about 10 due to the initial velocity spread.

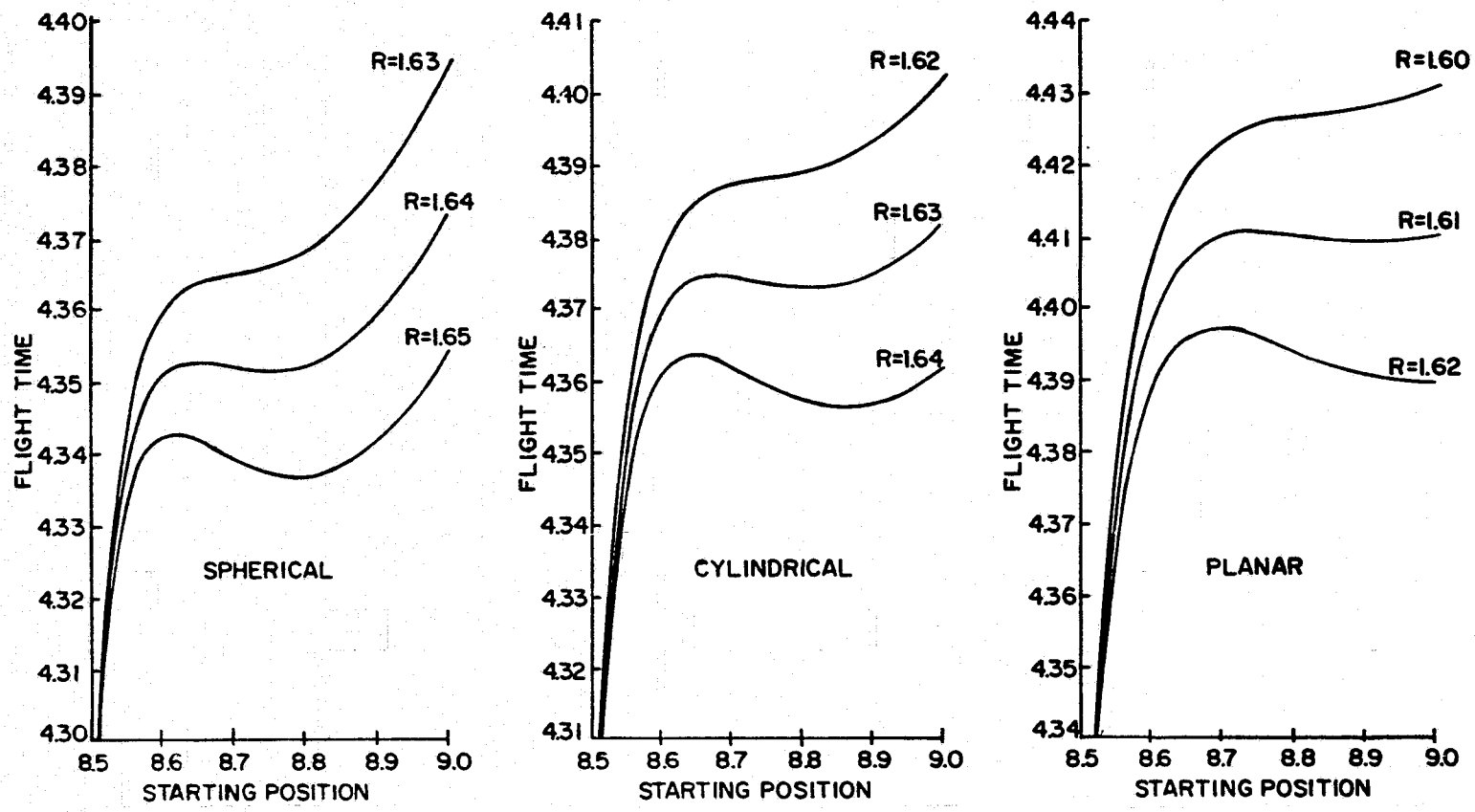

Figure 2.7 Computer Generated Space Focusing Characteristics of Planar, Cylindrical and Spherical Time-of-Flight Mass Spectrometers Having $r_1 = 9.00$, $r_2 = 8.50$, $r_3 = 8.50$ and $r_c = 4.60$ Units. A Normalized Time Scale is Plotted Vertically, Initial Ion Position Horizontally. Initial Velocity Assumed Zero. The Voltage Ratio is Defined by $R = (V_1 - V_3)/(V_2 - V_3)$. (Reference: Zabielski, Stein and Kendall (1972/1973)).

Figure (2.8) illustrates the space focusing curves for high voltage ratios with an initial ion energy of 4 eV in a cylindrical-electrode TOFMS. The bars represent an energy spread of ± 1 eV around the ion initial energy. As the voltage ratio increases, the poorer space focusing characteristic can be easily seen. Also notice the decreasing spread in the flight times due to the initial energy spread. Figure (2.9) illustrates the space focusing characteristics for a spherical-electrode TOFMS for the same conditions as were used in Figure (2.8).

Figure (2.10) represents the changes in the flight time spread for a cylindrical-electrode TOFMS due to a 2 eV initial energy spread as the voltage ratio is increased. This Figure is derived from the time spread bars of Figure (2.8). These curves can be said to represent the velocity focusing characteristics of the cylindrical TOFMS. Perfect velocity focusing would be represented by a straight line at zero time spread. These curves suggest that an extremely high voltage ratio or an extremely long drift region length would be required for perfect velocity focusing. This conclusion confirms the suggestion made by Stein (1974) and by Sanzone (1970). Figure (2.11) represents the velocity focusing characteristics for a spherical TOFMS taken from Figure (2.9).

A comparison of Figure (2.8) to Figure (2.9) and Figure (2.10) to Figure (2.11) illustrates, again, the similarity of the space and velocity focusing characteristics for the cylindrical and spherical geometries. The differences in the curves are minimal for the

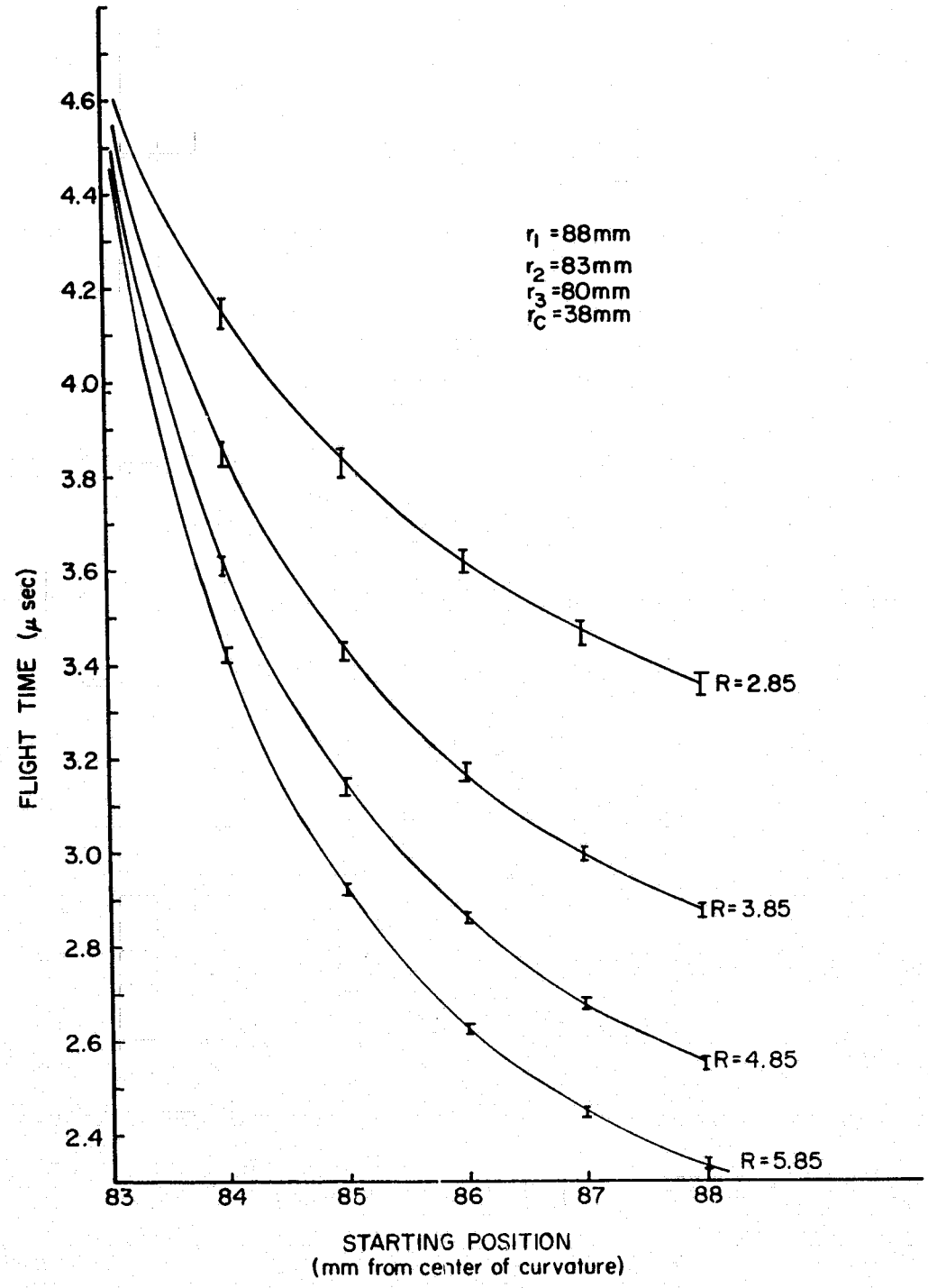

Figure 2.8 Computer Generated Space Focusing Characteristics for a Cylindrical-Electrode TOFMS Having r_1 = 88 mm, r_2 = 83 mm, r_3 = 80 mm, r_c = 38 mm, an Ion Mass of 133 amu, and an Initial Ion Energy of 4 eV (Directed Toward the Collector). The Bars Represent an Initial Energy Spread of ± 1 eV.

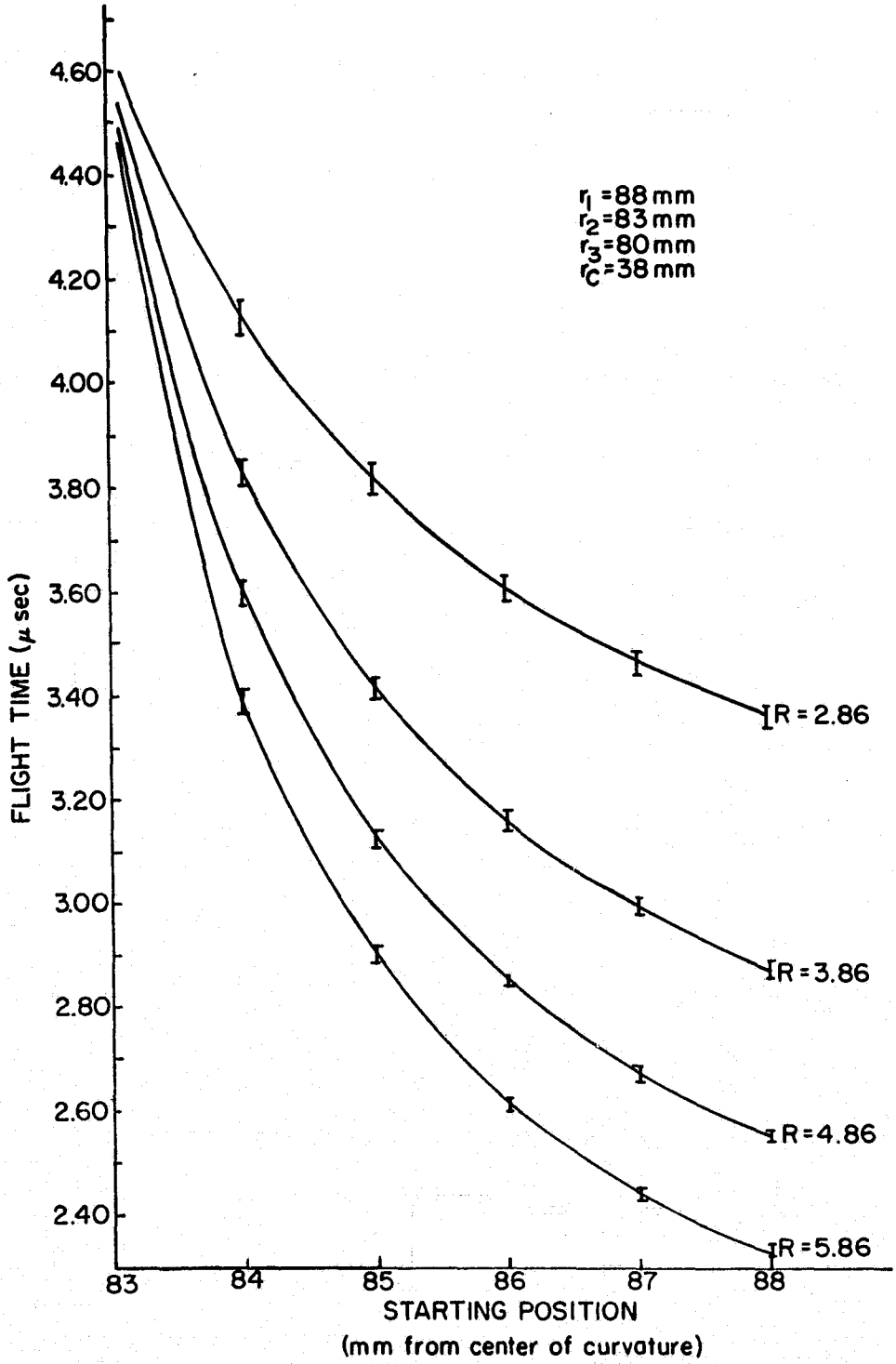

Figure 2.9 Computer Generated Space Focusing Characteristics of a Spherical-Electrode TOFMS Having r_1 = 88 mm, r_2 = 83 mm, r_3 = 80 mm, r_c = 38 mm, an Ion Mass of 133 amu, and an Initial Ion Energy of 4 eV (Directed Toward the Collector). The Bars Represent an Initial Ion Energy Spread of ± 1 eV.

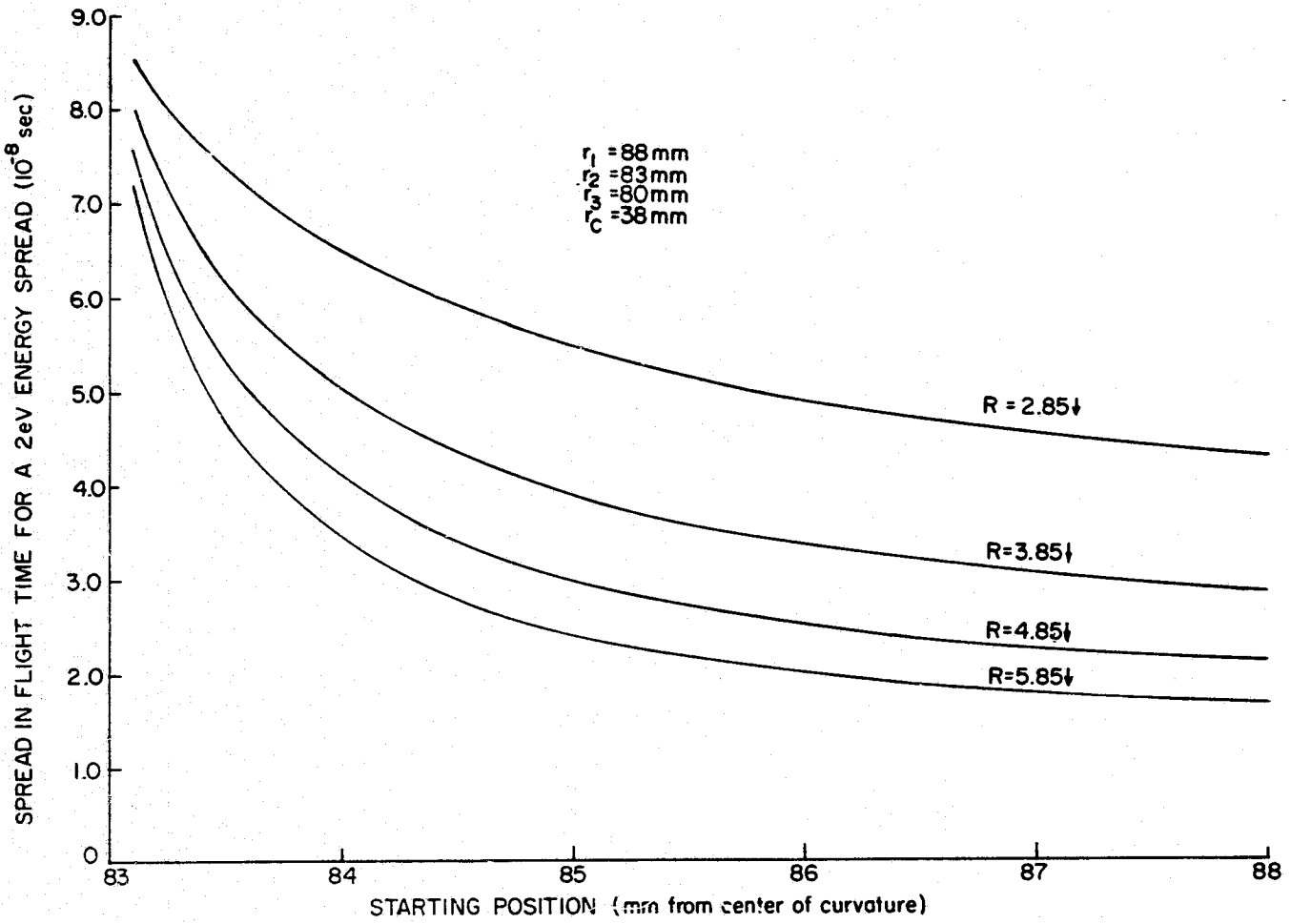

Figure 2.10 Computer Generated Velocity Focusing Characteristics for a Cylindrical-Electrode TOFMS Having r_1 = 88 mm, r_2 = 83 mm, r_3 = 80 mm, r_c = 88 mm, an Ion Mass of 133 amu, and an Initial Ion Energy of 4 eV (Directed Toward the Collector). The Flight Time Spread was Derived from Figure 2.8 for an Initial Ion Energy Spread of ± 1 eV.

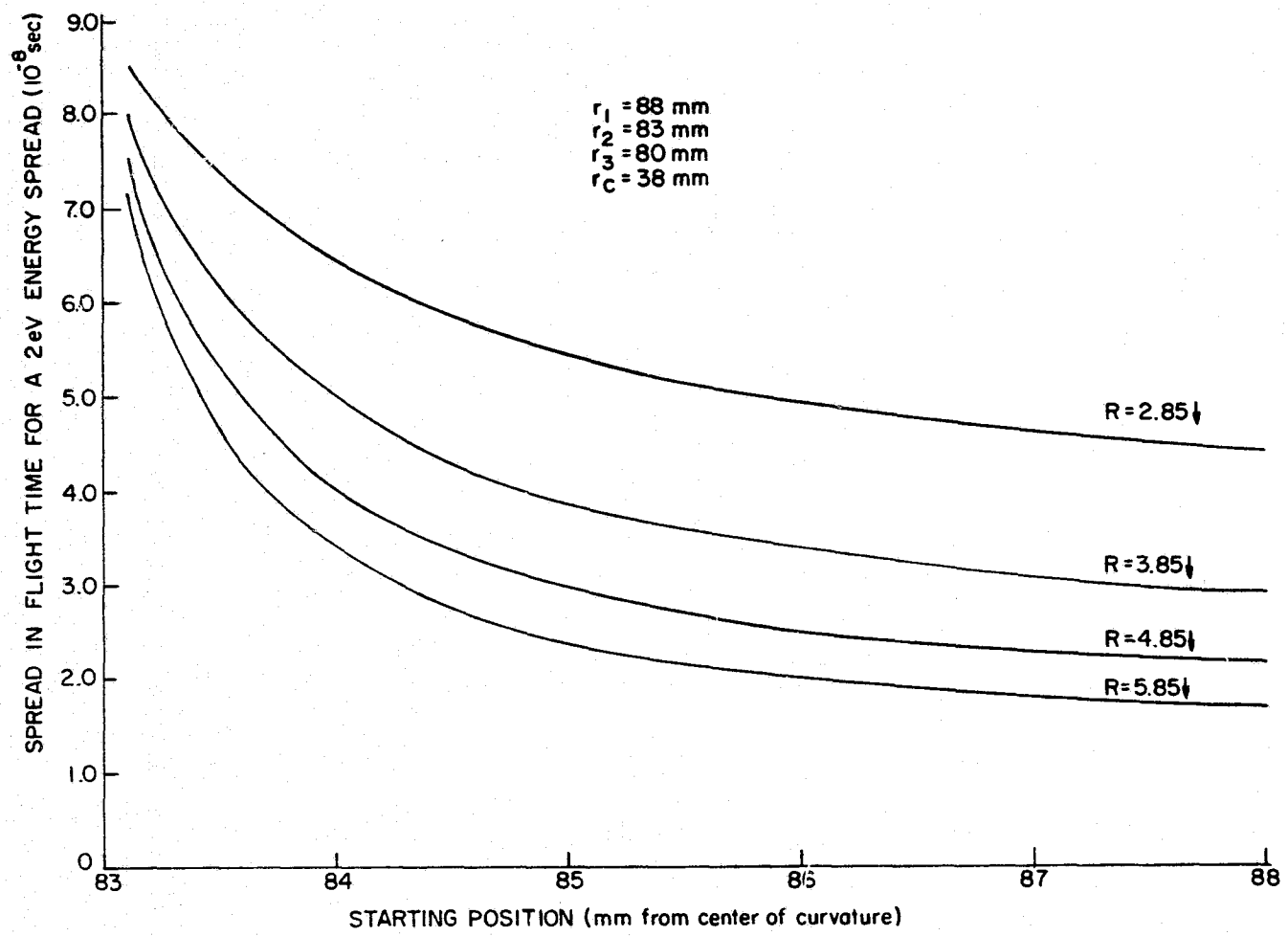

Figure 2.11 Computer Generated Velocity Focusing Characteristics for a Spherical-Electrode TOFMS Having r_1 = 88 mm, r_2 = 83 mm, r_3 = 80 mm, r_c = 38 mm, an Ion Mass of 133 amu, and an Initial Ion Energy of 4 eV (Directed Toward the Collector). The Flight Time Spread was Derived from Figure 2.9 for an Initial Ion Energy Spread of ± 1 eV.

electrode spacings and electrode radii being considered. For simplicity and convenience, I will concentrate on the cylindrical geometry for the remaining Figures in this section.

Figure (2.12) shows the effects of changing the initial ion velocity when a low voltage ratio was used. It also illustrates the time spread (bars) due to a 2 eV initial energy spread for a low voltage ratio. The initial ion velocity was not constant across the source region in the calculation of these curves since V_2 was held constant while V_0 was varied. V_0 was the voltage applied to electrode 1 when the buncher pulse was off. In the usual operation of the two-field TOFMS considered in this thesis $V_0 = V_2$ and the source region is field free, but in these cases, the source region was operated with an electric field when the buncher pulse is off. The ion initial velocity was then dependent on the ion distance from r_2. Varying the ion initial velocity distribution as a function of the position in the source had two important effects. First, changing the ion initial velocity distribution from initial velocities which increased as the ions approach electrode 2 to a distribution in which initial velocities decreased as the ions approach electrode 2 is equivalent to increasing the voltage ratio. Second, the time spread due to the initial energy spread decreases as the initial ion energy is increased. This decrease in the flight time spread occurs because the ion initial energy spread becomes a smaller fraction of the ion initial energy as the initial velocity is increased. This Figure illustrates clearly the reason for reported poor resolving power at near the optimum

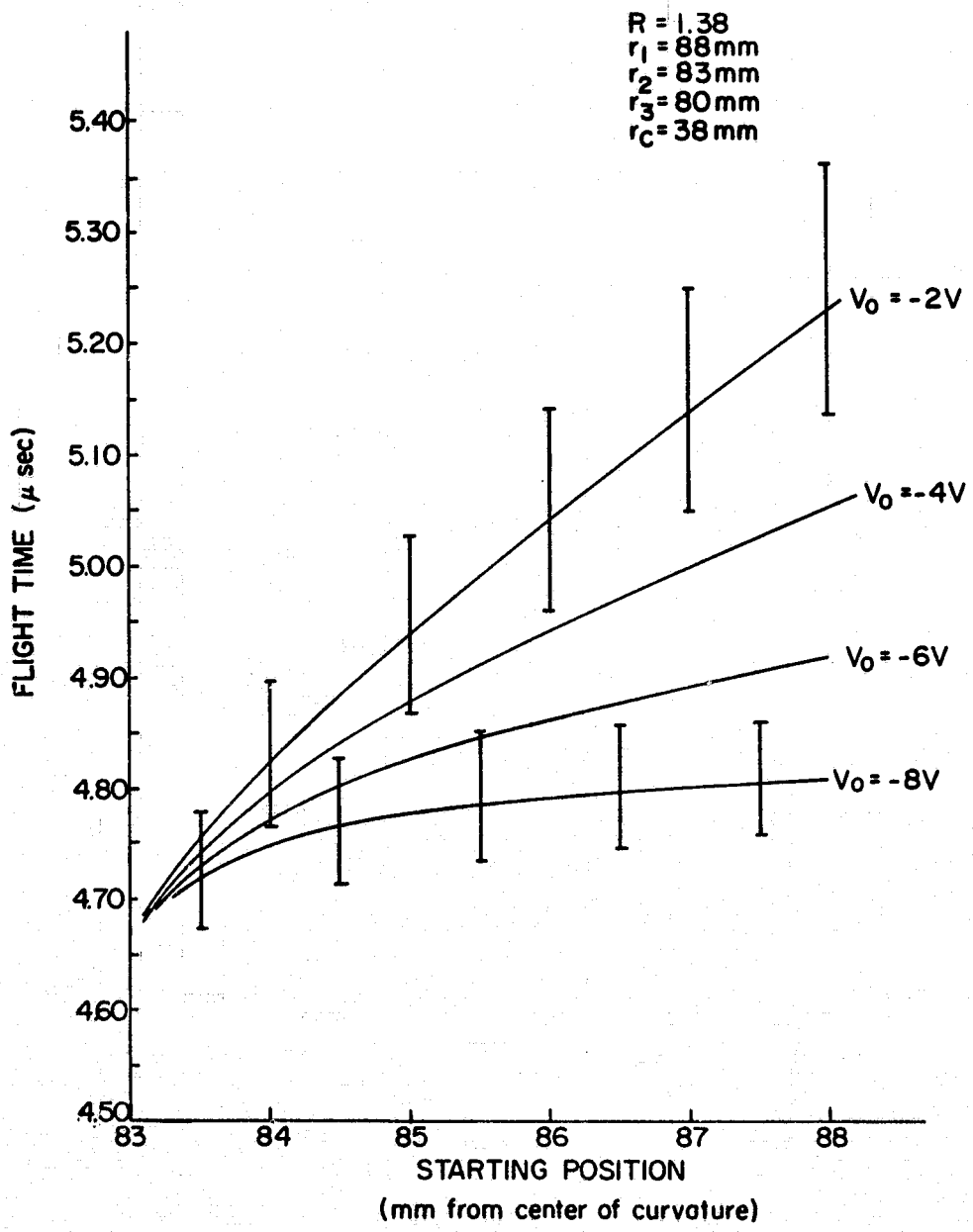

Figure 2.12 Computer Generated Space Focusing Characteristics for a Cylindrical-Electrode TOFMS Having r_1 = 88 mm, r_2 = 83 mm, r_3 = 80 mm, r_c = 38 mm, R = 1.38, and an Ion Mass of 133 amu, While V_0 was Varied. The Bars Represent an Initial Ion Energy Spread of ± 1 eV.

space focusing voltage ratio. The flight time spread, due to an initial ion energy spread (2 eV in this example), is significantly larger than the time spread due to the different ion starting positions (see the curve for $V_0 = -8$ V).

Figure (2.13) shows the effect of varying the collector radius while holding the source and acceleration regions at a constant radius of curvature for R = 1.56. This varies the drift region length. Variation of the drift region length was studied by Stein (1974) to deduce the effect of grid waviness. He looked at only very small variations in the drift region length (less than 1 mm) and concluded that this had very little effect on the shape of the space focusing curves. The effects of larger variations in the drift region length are more pronounced and are very similar to changing the voltage ratio. The curve for $r_c = 38$ mm in Figure (2.13) is very similar to the curve for the cylindrical TOFMS in Figure (2.7). However, when r_c is moved to 58 mm (from the center of curvature), the resulting curve is very similar to the curves in Figure (2.12) for low voltage ratios. The bars in Figure (2.13) again represent the flight time spread due to an initial energy spread of 2 eV (all the remaining Figures in this section will use bars to indicate the flight time spread due to an initial energy spread of 2 eV). The ion initial energy in this Figure and the remaining Figures in this section was 4 eV for all starting positions in the source region. Notice the decrease in the flight time spread in Figure (2.13) due to the initial energy spread as compared with the lower voltage ratio curves in Figure (2.12)

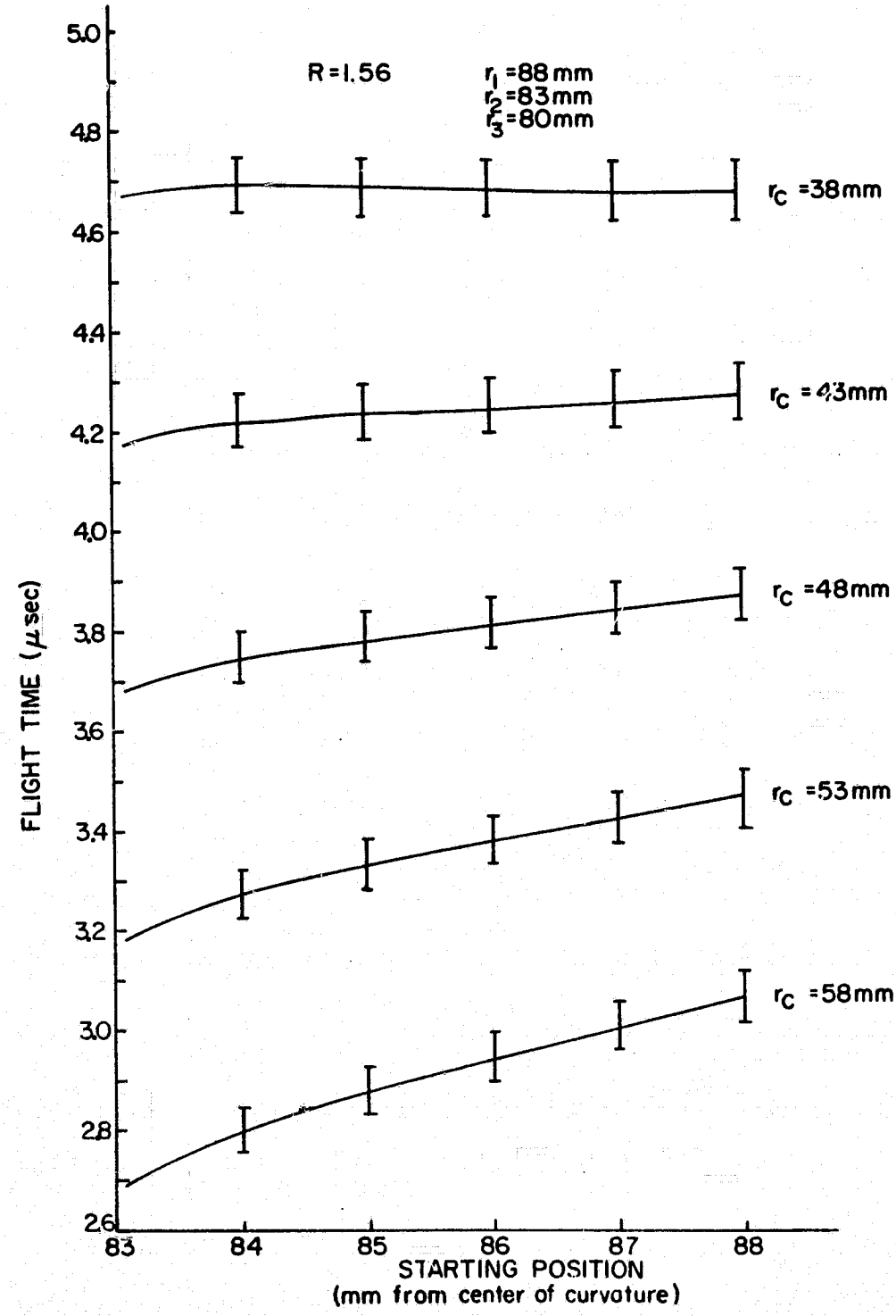

Figure 2.13 Computer Generated Space Focusing Characteristics for a Cylindrical-Electrode TOFMS Having r_1 = 88 mm, r_2 = 83 mm, r_3 = 80 mm, R = 1.56, an Ion Mass of 133 amu, and an Ion Initial Energy of 4 eV (Directed Toward the Collector). While r_c was Varied. The Bars Represent an Initial Ion Energy Spread of ± 1 eV.

Figures (2.14), (2.15) and (2.16) show the flight time curves for voltage ratios of 2.10, 2.56 and 3.06, respectively, while the drift region length is varied as in Figure (2.13). Two important observations can be made from these Figures. The first is the equivalence of decreasing the drift region length to decreasing the voltage ratio, as far as the space focusing characteristics are concerned, without significant variation of the velocity focusing characteristics. The second is the steadily decreasing flight time spread due to the initial energy spread as the voltage ratio increases.

Figures (2.17), (2.18), (2.19) and (2.20) represent the computer derived flight time curves for voltage ratios of 1.5, 2.0, 2.56 and 3.0, respectively, for grid radii which are greatly reduced from those used in Figures (2.13) through (2.16). The source and acceleration region grid spacings are the same as Figures (2.13) through (2.16), but the radii of curvature are greatly reduced. It was thought that these grid radii would emphasize the effect of the cylindrical electrodes on the source and acceleration region electric fields. However, close examination of Figures (2.17) through (2.20) reveals no significant differences from Figures (2.13) through (2.16). Evidently, the electric field between cylindrical electrodes spaced as in Figures (2.13) through (2.20) does not vary significantly from the electric field for similarly spaced planar electrodes. In fact, subsequent calculations showed that a significant variation (greater than 10 per cent) from the electric field between planar electrodes 5 mm apart does not occur until the radii of curvature for similarly

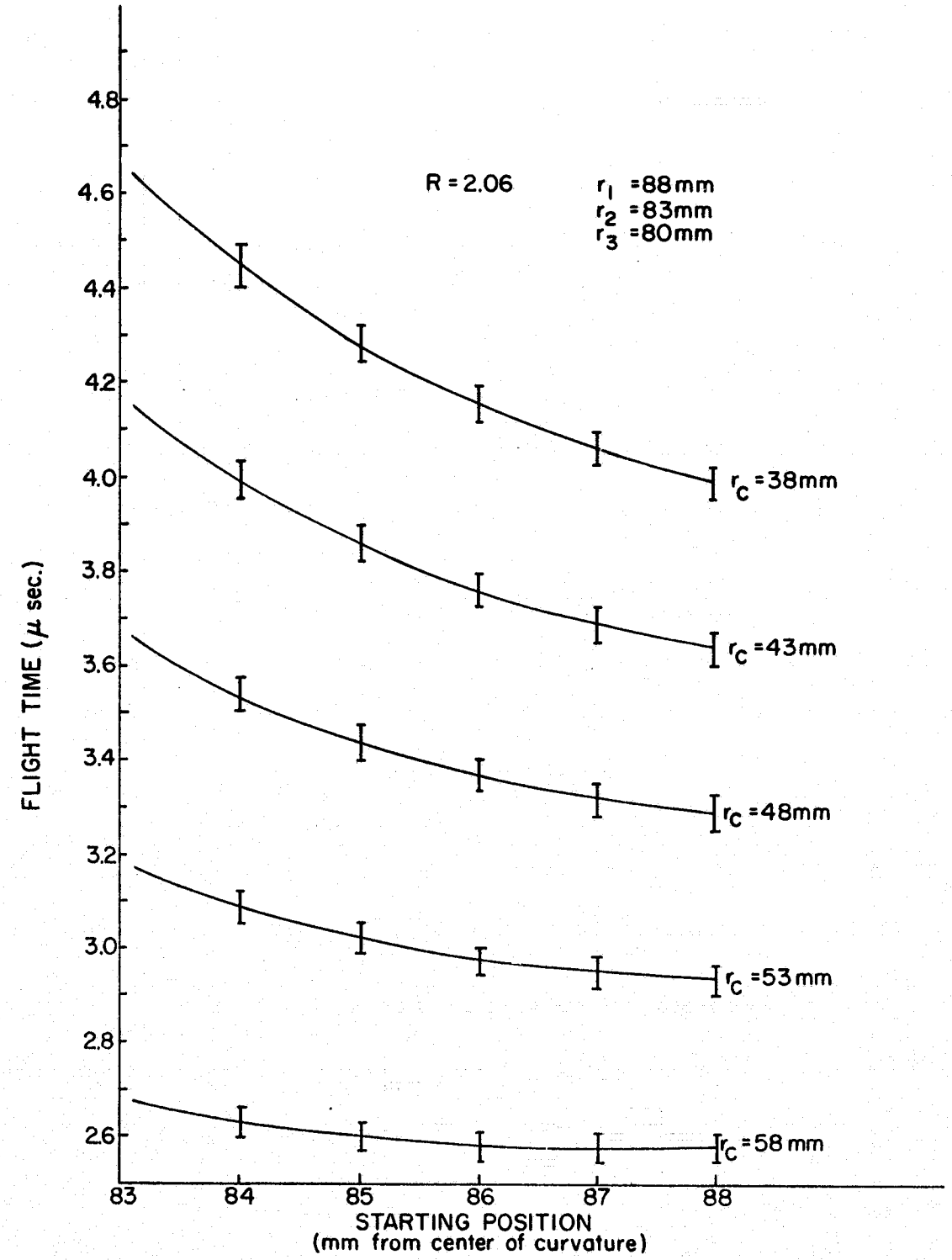

Figure 2.14 Computer Generated Space Focusing Characteristics for a Cylindrical-Electrode TOFMS Having r_1 = 88 mm, r_2 = 83 mm, r_3 = 80 mm, R = 2.06, an Ion Mass of 133 amu, and an Ion Initial Energy of 4 eV (Directed Toward the Collector), While r_c was Varied. The Bars Represent an Initial Ion Energy Spread of ± 1 eV.

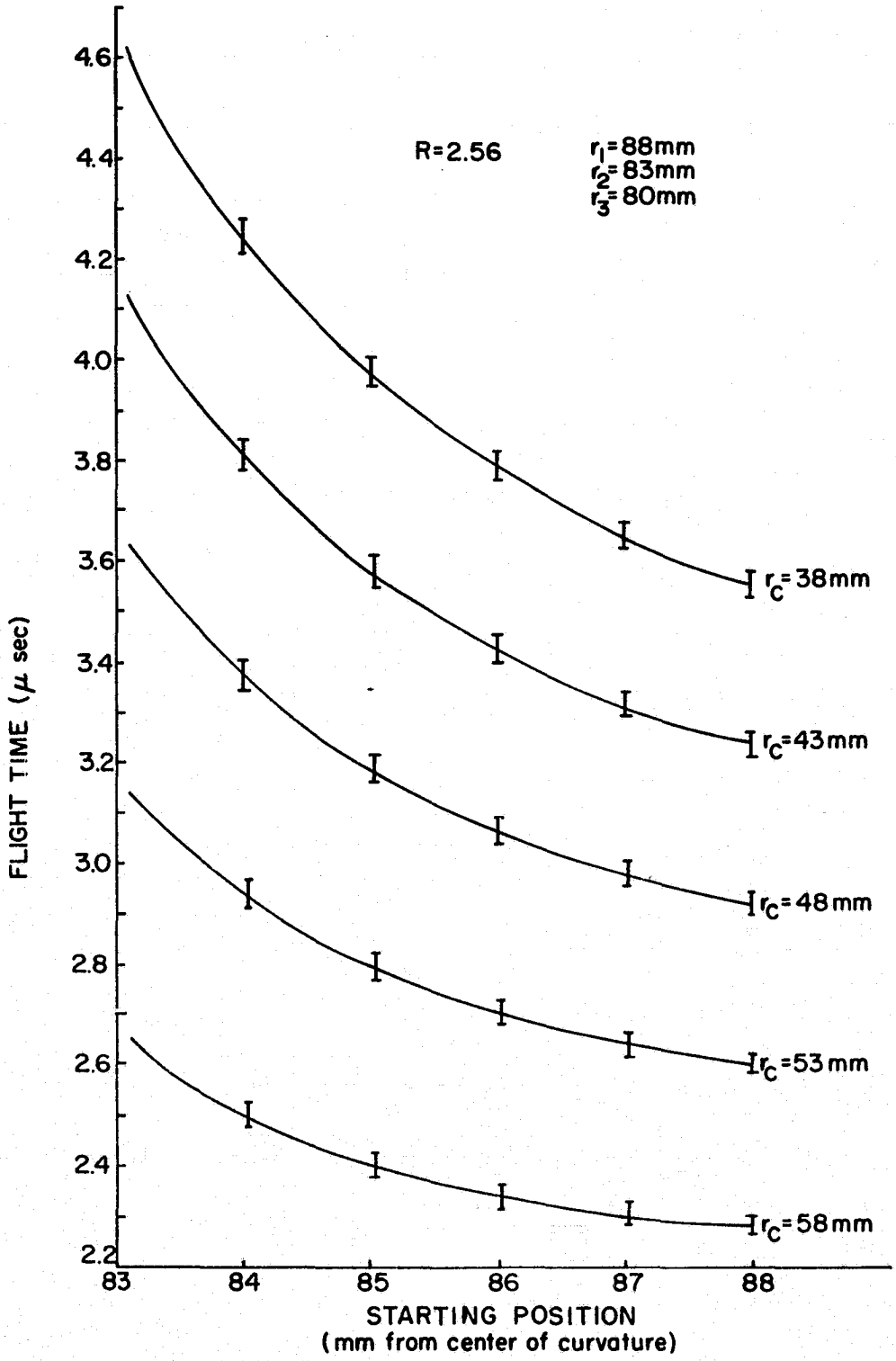

Figure 2.15 Computer Generated Space Focusing Characteristics for a Cylindrical-Electrode TOFMS Having r_1 = 88 mm, r_2 = 83 mm, r_3 = 80 mm, R = 2.56, an Ion Mass of 133 amu, and Ion Initial Energy of 4 eV (Directed Toward the Collector), While r_c was Varied. The Bars Represent an Initial Ion Energy Spread of ± 1 eV.

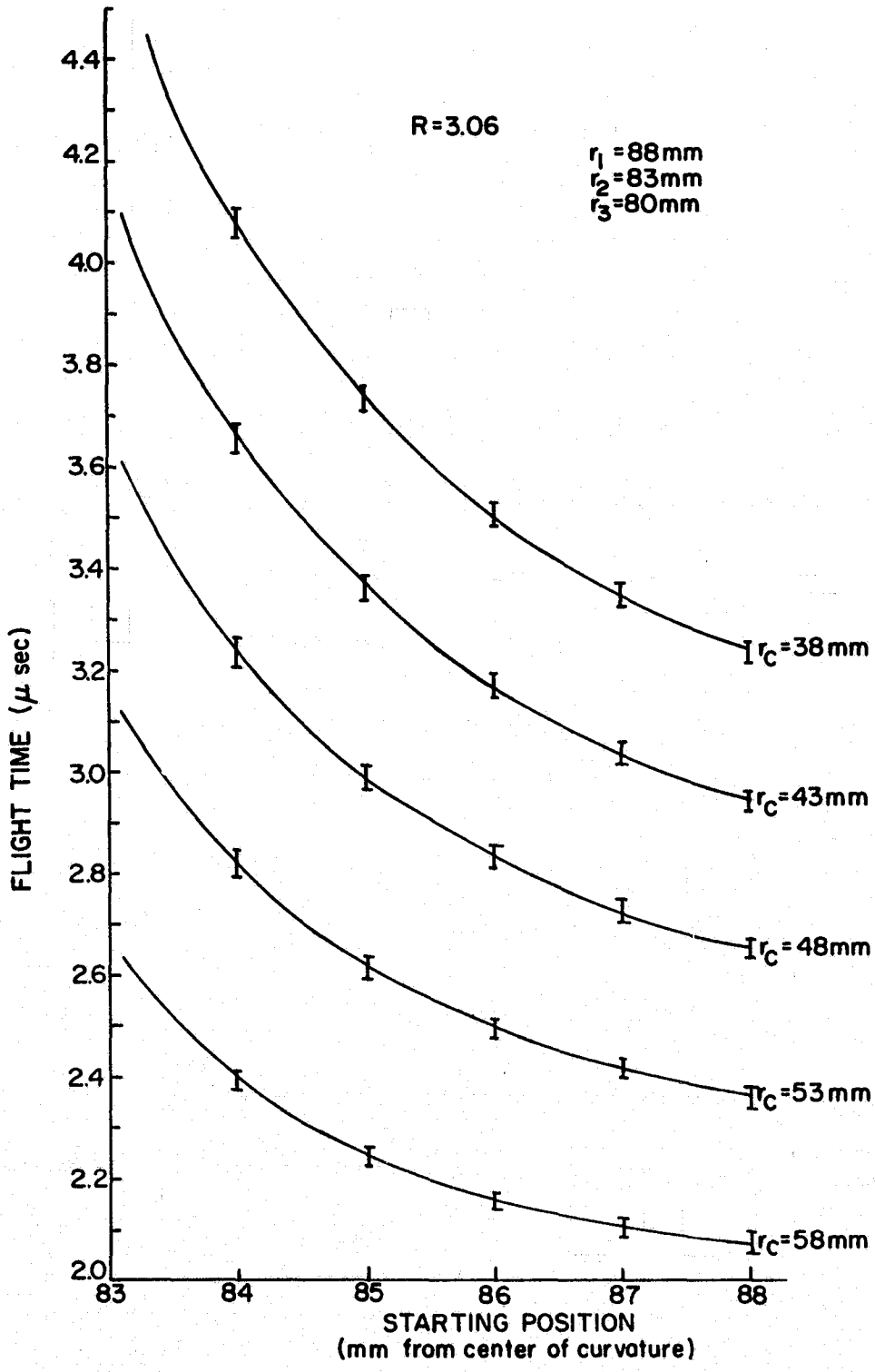

Figure 2.16 Computer Generated Space Focusing Characteristics for a Cylindrical-Electrode TOFMS Having r_1 = 88 mm, r_2 = 83 mm, r_3 = 80 mm, R = 3.06, an Ion Mass of 133 amu, and an Ion Initial Energy of 4 eV (Directed Toward the Collector), While r_c was Varied. The Bars Represent an Initial Ion Energy Spread of ± 1 eV.

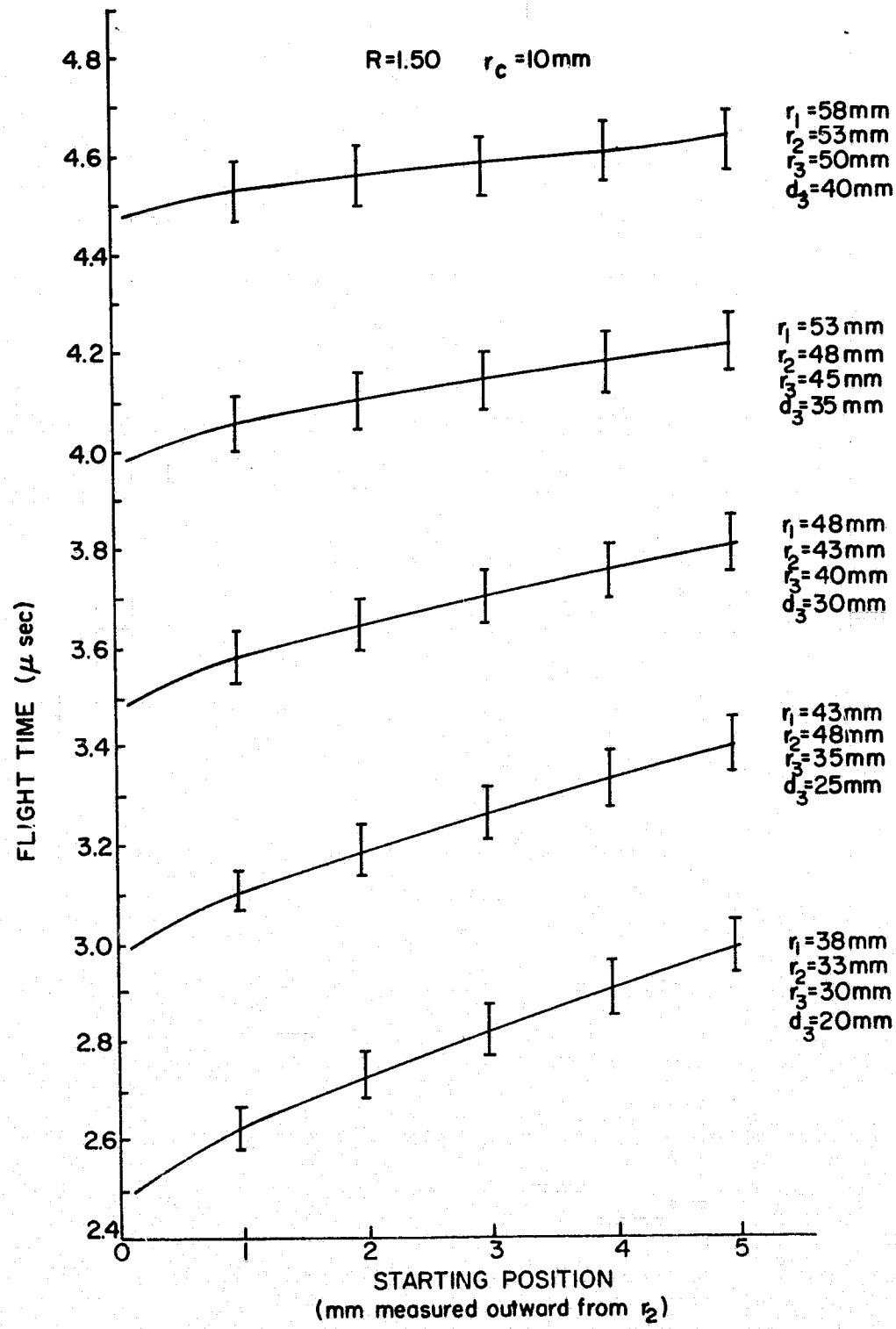

Figure 2.17 Computer Generated Space Focusing Characteristics for a Cylindrical-Electrode TOFMS Having R = 1.50, r_c = 10 mm, an Ion Mass of 133 amu, and an Ion Initial Energy of 4 eV (Directed Toward the Collector), While r_1, r_2, r_3, and the Drift Region Length (d_3) Were Varied. The Spacings Between r_1 and r_2 and Between r_2 and r_3 Were Kept Constant. The Bars Represent an Initial Ion Energy Spread of ± 1 eV.

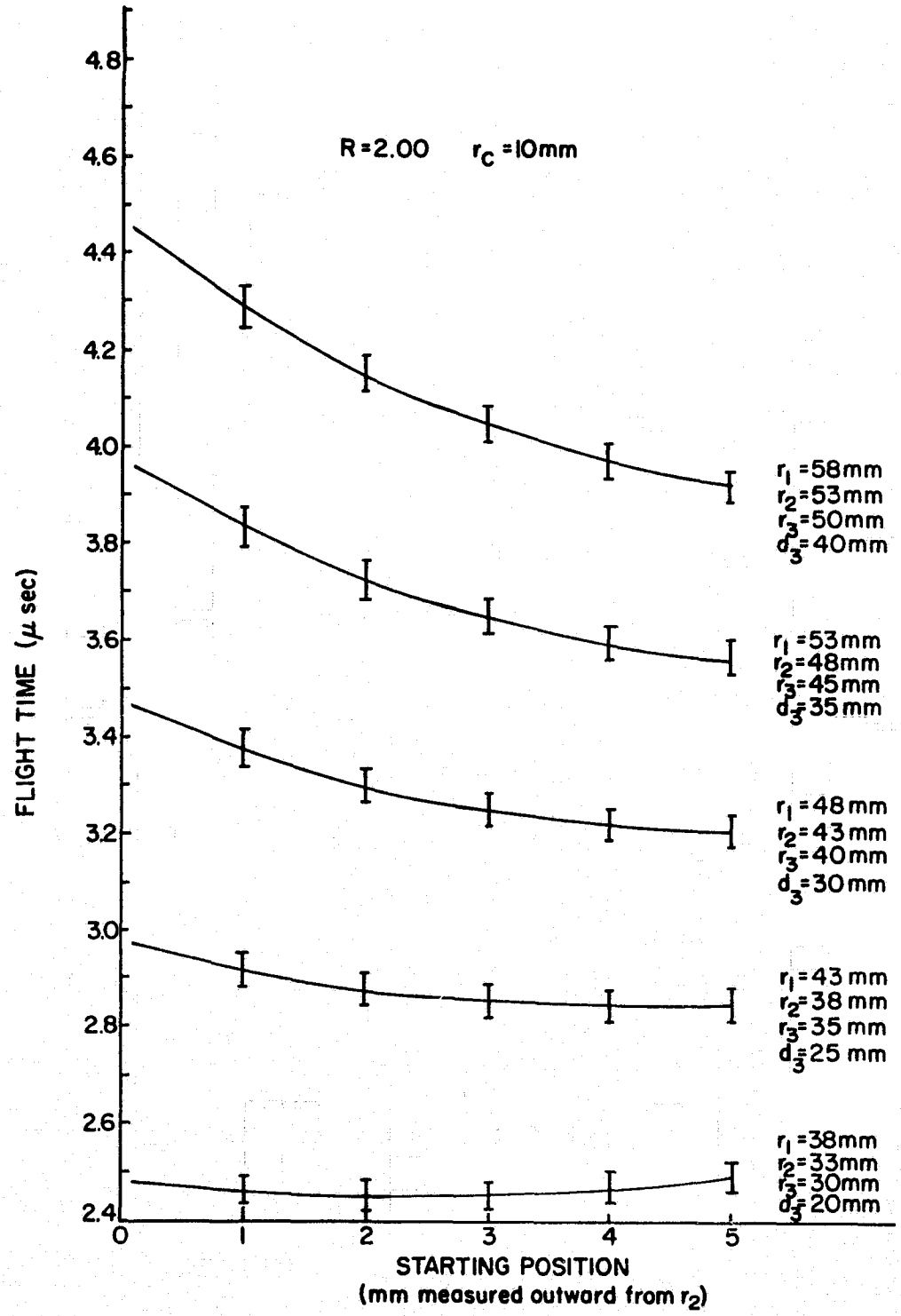

Figure 2.18 Computer Generated Space Focusing Characteristics for a Cylindrical-Electrode TOFMS Having R = 2.00, r_c = 10 mm, an Ion Mass of 133 amu, and an Ion Initial Energy of 4 eV (Directed Toward the Collector), While r_1, r_2, r_3, and the Drift Region Length (d_3) Were Varied. The Spacings Between r_1 and r_2 and Between r_2 and r_3 Were Kept Constant. The Bars Represent an Initial Ion Energy Spread of ± 1 eV.

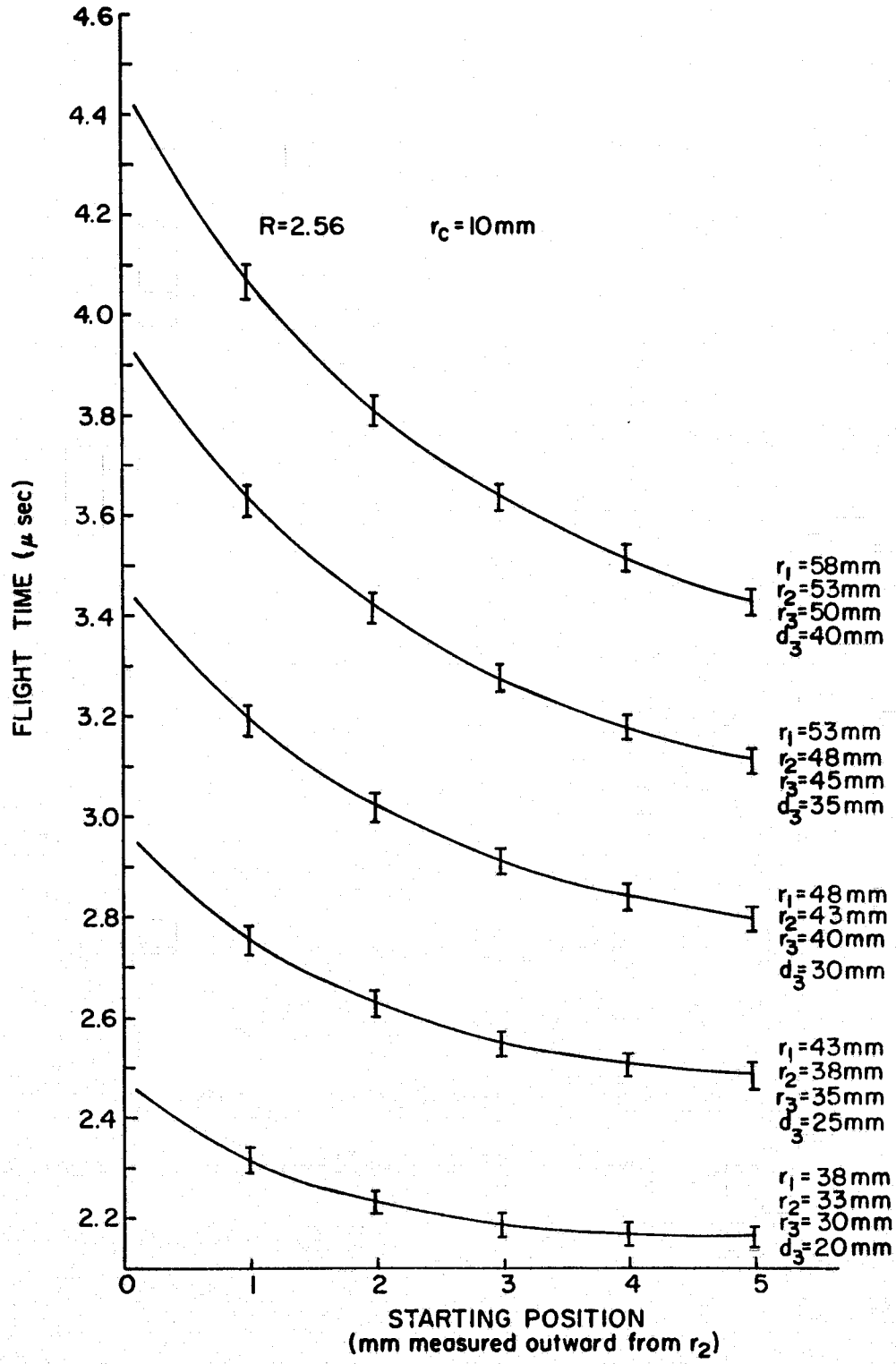

Figure 2.19 Computer Generated Space Focusing Characteristics for a Cylindrical-Electrode TOFMS Having R =2.56, r_c = 10 mm, an Ion Mass of 133 amu, and an Ion Initial Energy of 4 eV (Directed Toward the Collector), While r_1, r_2, r_3, and the Drift Region Length (d_3) Were Varied. The Spacings Between r_1 and r_2 and Between r_2 and r_3 Were Kept Constant. The Bars Represent an Initial Ion Energy Spread of ± 1 eV.

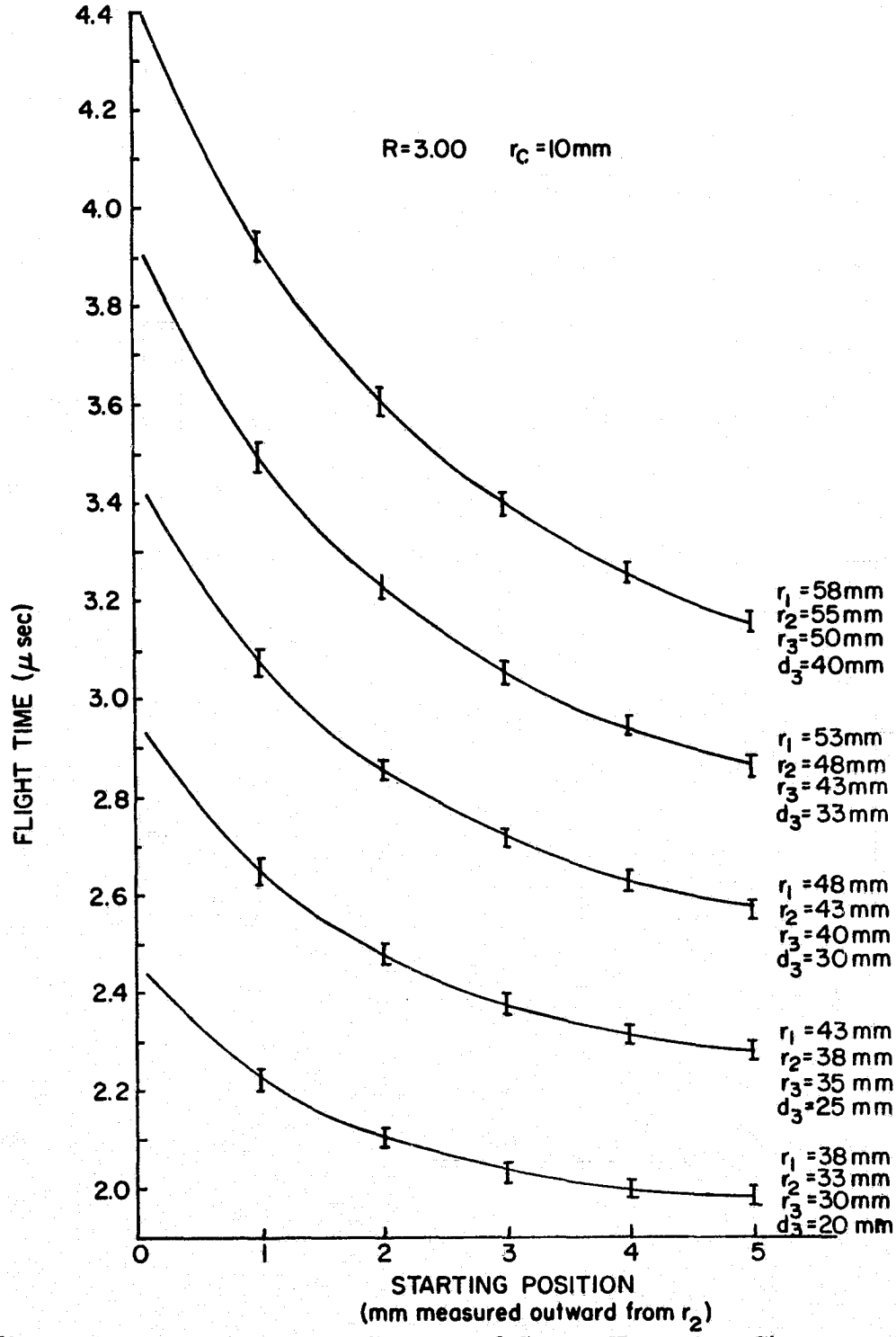

Figure 2.20 Computer Generated Space Focusing Characteristics for a Cylindrical-Electrode TOFMS Having R = 3.00, r_c = 10 mm, an Ion Mass of 133 amu, and an Ion Initial Energy of 4 eV (Directed Toward the Collector), While r_1, r_2, r_3, and the Drift Region Length (d_3) Were Varied. The Spacings Between r_1 and r_2 and Between r_2 and r_3 Were Kept Constant. The Bars Represent an Initial Ion Energy Spread of ± 1 eV.

spaced cylindrical-electrodes are less than 23 mm and 28 mm. A useful area for future study would be to examine the flight time characteristics of cylindrical and spherical TOFMS with an outer source electrode radius of less than 30 mm.

The Figures presented in this section confirm a number of observations made by previous researchers. First, inferior mass peak shapes would result if the operating voltages of a TOFMS were adjusted to allow ions starting at the inner and outer source region electrodes to arrive at the collector simultaneously (i.e. be space focused). Second, the optimum space focusing voltage ratios for a planar, cylindrical or spherical TOFMS are very nearly identical. Third, the spread in ion initial energies (velocities) is the cause for the poor resolving power at good space focusing voltage ratios in a TOFMS. Fourth, the velocity focusing characteristics can be improved by increasing the voltage ratio at the cost of degrading the space focusing if the ion initial energies and the grid spacings are not altered. Fifth, varying the drift region length is equivalent to varying the voltage ratio, as far as space focusing is concerned. Sixth, the fact that a mass peak produced by a voltage ratio near the optimum space focusing value, with no initial velocity spread, is extremely narrow with respect to the mass peak which is produced when an initial energy spread greater than about .5 eV is considered. At the optimum space focusing voltage ratio in a cylindrical TOFMS, the flight time spread, due to an initial energy spread of .5 eV, (for a specific initial energy) is about 10 times the full width at half height of a mass peak produced only by space focusing.

Since the true mass peak is a convolution of the space and velocity contributions to the flight time spread, it should be possible to deduce significant information on an unknown initial ion energy spread. For large initial energy spreads (>.5 eV), the initial energy distribution can be deduced from direct observation of the resulting mass peak shape. This is because the space focused contribution to the mass peak is similar to a delta function (for optimum voltage ratios) and the convolution of the flight time spread due to the initial energy spread and a delta function will reproduce the flight time spread directly due to the initial energy spread. It should still be possible to deduce the initial energy distribution for smaller energy spreads (<.5 eV) through deconvolution, since the space focusing flight time distribution can be easily calculated, with great accuracy, from computer programs. This last observation was originally made by Ferguson et al., (1965) and has been used, with great success, to calculate the translational energy of ions in TOFMS by Franklin et al., (1967) and by Hadley and Franklin (1975).

There are also two observations which can be made that have not been mentioned by previous researchers. The first is that the velocity focusing characteristics in a TOFMS are almost entirely determined in the source and acceleration regions since varying the drift region length has little effect on velocity focusing while having a large effect on space focusing.

The second observation was suggested by Figure (2.12). This Figure showed that it was possible to simulate a change in voltage ratio by changing the initial ion velocity distribution in the source

region. Although Figure (2.12) illustrates flight times for a low voltage ratio where there was a large flight time spread, it seems entirely possible to apply this effect to high voltage ratios. This would greatly improve the velocity focusing characteristics. The ions closest to the collector, in the source, arrive at the collector last, while ions farthest from the collector arrive there first (see Figures (2.8) and (2.9) for example). If ion initial velocities (before the buncher pulse turns on) can be produced, which are greater closer to the collector than in the outer portion of the source region, it should be possible to reduce the effective space focusing voltage ratio while still keeping good velocity focusing. This should produce greatly improved resolving power. The next two sections will discuss this resolving power improvement and present computer simulations for several examples.

2.9 Resolving Power Improvement; Variable Initial Source Velocity

The resolving power in commercial time-of-flight mass spectrometers has shown an increase over the results by such early workers as Wolff and Stephens (1953), Cameron and Eggers (1948), Katzenstein and Friedland (1955), Ionov and Mamyrin (1953) and Agishev and Ionov (1956). However, the resolving power obtainable in time-of-flight mass spectrometers today (up to about 600) is a mere fraction of the resolving power which could be obtained if, for example, double time focusing could be obtained (see Stein (1974)). Curiously, there has been little reported effort, since the two-field planar TOFMS of Wiley and McLaren (1955), to improve the resolving

power in time-of-flight mass spectrometers. There have been some results reported by Studier (1963) and Marable and Sanzone (1974) who attempted to improve resolving power by decreasing the ion turn around time in the source region. This improvement in velocity focusing was achieved by increasing the initial force on the ions in the source through the use of an initial ion accelerating pulse which was initially a high voltage spike that was quickly reduced to a good space focusing value. Improved resolving power has also been reported by Carrico (1971), Poschenrieder and Oetjen (1972), Bakker (1971, 1973), Oran and Paiss (1973) and Karataev et al., (1974). These workers used equal momentum acceleration, time varying fields, two-dimensional ion motion, ion reflection or a combination of these methods.

Sanzone (1970) has reported theoretical analyses of planar time-of-flight mass spectrometers with a variety of electric field directions and a number of acceleration regions. He concluded that none of the cases he considered showed any significant improvement in the resolving power. One possible arrangement, not considered by Studier, is suggested by the numerical results in the first part of this chapter. The addition of an electric field in the source region, directed toward the collector when the bunching pulse is off, makes it possible to give ions in the source an initial velocity which varies across the source region. This variable initial velocity in the source region can be used to improve resolving power in situations where there is a large energy spread in the ions under study. A large

energy spread requires a large voltage ratio to improve the velocity focusing characteristics of the mass spectrometer. However, when the voltage ratio is increased beyond the optimum space focusing value, the ions closest to the collector, in the source, begin arriving at later times at the collector. The variable initial velocity makes it possible to correct for the poorer space focusing characteristics.

This variable source velocity can be produced by several methods. The most straight forward is to make V_2 more negative than the dc level of the bunching pulse (V_0). This produces ion velocities which increase as the ions approach grid 2. V_1 and V_3 are then altered to produce the desired voltage ratio (and the same source and acceleration region electric fields).

The theoretical description of the variable initial velocity requires only the substitution of $v_0(x_i)$ for v_0 in the sections of the time-of-flight equations referring to the initial velocity. The complete time-of-flight equations can be altered by inspection.

The total time-of-flight for a planar two-field TOFMS with the variable source velocity can be written as

$$t = \left(\frac{m}{2q}\right)^{1/2} \left\{ \frac{2d_1}{(V_1 - V_2)} \left[\left\{ \frac{(V_1 - V_2)}{d_1} d_o + \frac{mv_o^2(x_i)}{2q} \right\}^{1/2} \pm \left\{ \frac{mv_o^2(x_i)}{2q} \right\}^{1/2} \right] + \frac{2d_2}{(V_2 - V_3)} \left[\left\{ V_2 - V_3 + \frac{m\gamma'^2}{2q} \right\}^{1/2} - \left\{ \frac{m\gamma'^2}{2q} \right\}^{1/2} \right] + \frac{d_3}{\left[(V_1 - V_2)\frac{d_o}{d_1} + V_2 - V_3 + \frac{mv_o^2(x_i)}{2q} \right]^{1/2}} \right\} \tag{2.71}$$

where

$$\gamma'^2 = v_o^2(x_i) + \left(\frac{2q}{m}\right)\frac{d_o}{d_1}(V_1 - V_2) \tag{2.72}$$

The total time-of-flight for a cylindrical geometry two-field TOFMS with variable initial velocity is given by

$$t = \left(\frac{m}{2q}\right)^{1/2}\left\{r_o\left(\frac{\pi \ln(r_1/r_2)}{(V_1 - V_2)}\right)^{1/2} e^{C'_{12}}\left[\operatorname{erf}\left\{(\ln(r_0/r_2) + C'_{12})^{1/2}\right\} \pm \operatorname{erf}\left\{C'^{1/2}_{12}\right\}\right] + r_2\left(\frac{\pi \ln(r_2/r_3)}{(V_2 - V_3)}\right)^{1/2} e^{C'_{23}} \cdot \left[\operatorname{erf}\left\{(\ln(r_2/r_3) + C'_{23})^{1/2}\right\} - \operatorname{erf}\left\{C'^{1/2}_{23}\right\}\right] + \frac{r_3 - r_c}{\left\{V_i - V_3 + \frac{mv_o^2(x_i)}{2q}\right\}^{1/2}}\right\} \tag{2.73}$$

where

$$C'_{12} = \left\{\frac{mv_o^2(x_i)}{2q}\right\}\frac{\ln(r_1/r_2)}{(V_1 - V_2)} \tag{2.74}$$

$$C'_{23} = \left\{\frac{m\beta'^2}{2q}\right\}\frac{\ln(r_2/r_3)}{(V_2 - V_3)} \tag{2.75}$$

and

$$\beta'^2 = \left(\frac{2q}{m}\right) \frac{(V_1 - V_2) \ln (r_0/r_2)}{\ln (r_1/r_2)} + v_o^2 (x_i) \qquad (2.76)$$

The total time-of-flight for a spherical-geometry two-field TOFMS with an initial velocity which depends on the source position is given by

$$t = \left(\frac{m}{2q}\right)^{1/2} \left\{ \left(\frac{\alpha'_{12}}{k_{12}}\right)^{1/2} \left[r_2^{1/2} (\alpha'_{12} - r_2)^{1/2} - \alpha'_{12} \cdot \left\{ \sin^{-1} \left\{ \left(\frac{r_2}{\alpha'_{12}}\right)^{1/2} \right\} - \frac{\pi}{2} \right\} \pm \left[r_0^{1/2} (\alpha'_{12} - r_0)^{1/2} - \alpha'_{12} \cdot \left\{ \sin^{-1} \left\{ \left(\frac{r_0}{\alpha'_{12}}\right)^{1/2} \right\} - \frac{\pi}{2} \right\} \right] \right] + \left(\frac{\alpha'_{23}}{k_{23}}\right)^{1/2} \cdot \left[r_3^{1/2} (\alpha'_{23} - r_3)^{1/2} - r_2^{1/2} (\alpha'_{23} - r_2)^{1/2} - \alpha'_{23} \cdot \left\{ \sin^{-1} \left\{ \left(\frac{r_3}{\alpha'_{23}}\right)^{1/2} \right\} - \sin^{-1} \left\{ \left(\frac{r_2}{\alpha'_{23}}\right)^{1/2} \right\} \right\} \right] + \frac{r_3 - r_c}{\left\{ V_i - V_3) + \frac{m v_o^2 (x_i)}{2q} \right\}^{1/2}} \right\} \qquad (2.77)$$

where

$$\alpha'_{12} = \frac{r_0 k_{12}}{k_{12} - r_0 \left(\frac{m v_o^2 (x_i)}{2q} \right)} \tag{2.78}$$

$$\alpha'_{23} = \frac{r_2 k_{23}}{k_{23} - r_2 \left(\frac{m \Delta'^2}{2q} \right)} \tag{2.79}$$

$$\Delta'^2 = \left(\frac{2q}{m} \right) \cdot (V_i - V_2) + v_o^2 (x_i) \tag{2.80}$$

and V_i is defined by equation (2.62).

These revised equations can be studied through the computer models developed for the conventional two-field TOFMS with minor modifications. The computer results are presented in the next section.

2.10 Numerical Studies; Variable Initial Source Velocities

Figure (2.21) presents the computer simulated flight time curves for a planar-electrode TOFMS as V_2 is varied for a constant voltage ratio, R = 2.15. Since V_0 (the potential on electrode 1 when the buncher pulse is off) is held constant at -4V, the ion initial energies will be 4 eV plus a contribution depending on the ion's position in the source region before the buncher pulse turns on. As V_2 is made more negative than V_0, positive ions approaching r_2 will be given larger velocities. Maintaining the same electric field across the source and acceleration region, as well as a constant voltage ratio, requires that V_1 and V_3 be altered as V_2 is varied.

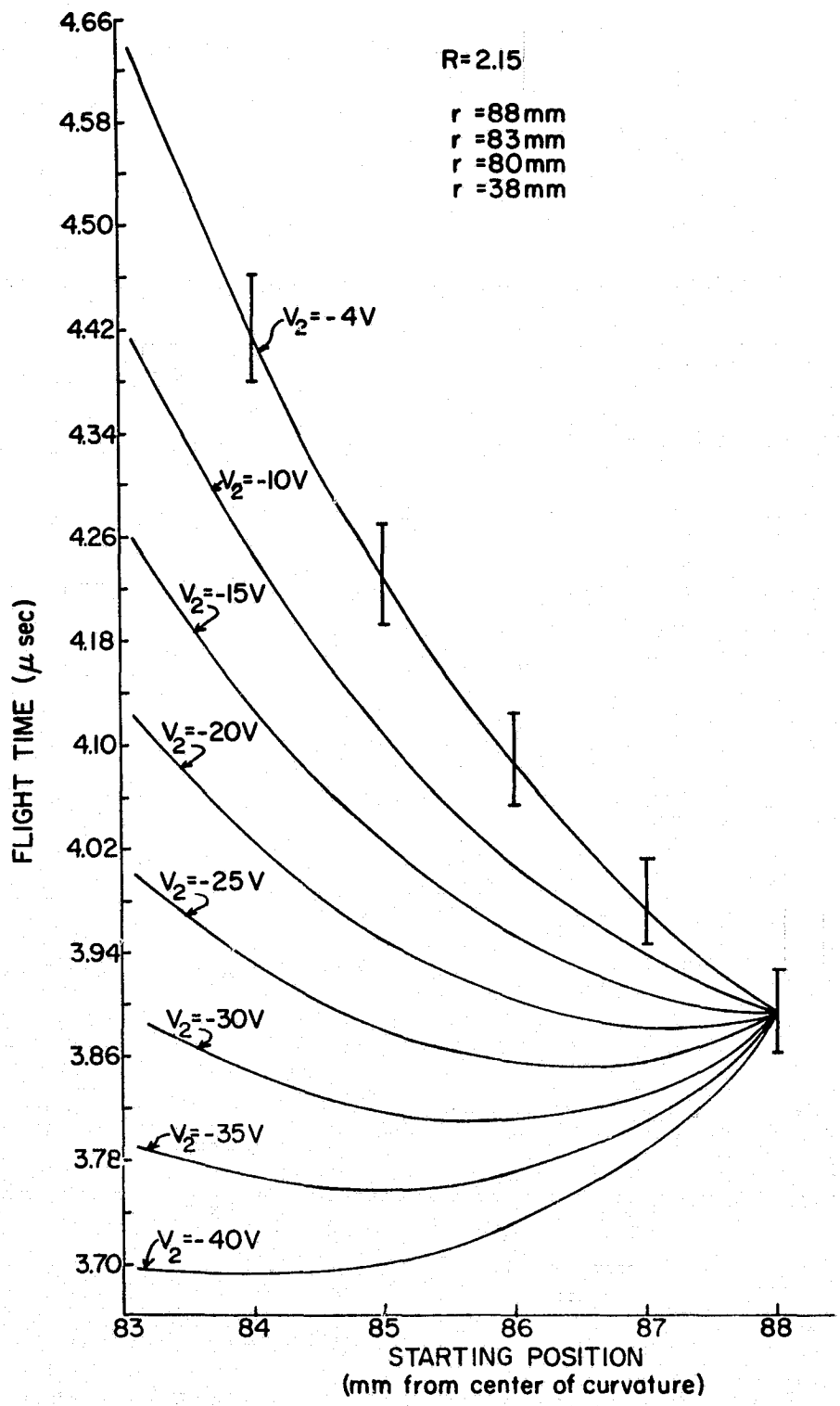

Figure 2.21 Computer Generated Space Focusing Characteristics for a Planar-Electrode TOFMS Having r_1 = 88 mm, r_2 = 83 mm, r_3 = 80 mm, r_c = 38 mm, R = 2.15, and an Ion Mass of 133 amu, While V_2 was Varied. This Produced an Ion Initial Energy Which was Dependent on the Ion Starting Position. The Bars Represent an Initial Ion Energy Spread of ± 1 eV.

A constant voltage ratio does not always produce the same electric fields in the source and acceleration regions. In this thesis, the use of a constant voltage ratio will always mean that the source and acceleration region electric fields will be constant. Remember that the voltage ratio applies to the mass spectrometer when the buncher pulse is turned on. The bars in Figure (2.21) represent an initial energy spread of 2 eV (the bars in all the Figures in this section will represent a 2 eV initial energy spread). The ion initial energy (velocity) should not be confused with initial energy spread. The initial energy spread is ±1 eV regardless of the ion initial energy at any starting position. This stipulation is applied to all the flight time versus starting position curves in this chapter.

The effect of making the ion initial velocities increase as the ion starting positions become closer to the inner electrode of the source region is to lower the effective voltage ratio without increasing the flight time spread due to the initial energy spread. Since the velocity focused flight time spread is held constant while the space focused flight time spread is decreasing, the resolving power should be significantly improved. This resolving power enhancement will be offset slightly by the decreasing overall flight times. There is a point where decreasing V_2 will no longer improve the space focusing characteristics but will start to degrade them. This can be seen in Figure (2.21). The actual point of maximum resolving power could be anywhere from $V_2 = -15$ V to $V_2 = -40$ V since it is the presence of maxima or minima in the space focusing

characteristics curves which produce a narrow mass peak.

Figure (2.22) illustrates the flight time characteristics for a cylindrical-electrode TOFMS with the same operating characteristics as were used to produce Figure (2.21). Figure (2.23) illustrates the flight time characteristics for a spherical-electrode TOFMS with the same operating characteristics as were used to produce Figures (2.21) and (2.22). The differences in the flight time characteristics between Figures (2.21), (2.22) and (2.23) are minimal for the operating conditions considered.

The actual point of maximum resolving power was determined experimentally for a cylindrical-electrode TOFMS with operating conditions near those used to produce Figure (2.22). The value of V_2 obtained was about -25 V and the maximum resolving power was about 17 for an ion mass of 133 amu (Cs^+). The initial energy spread was estimated to be about 1.5 eV. Taking V_2 = -25 V as our example, we can calculate the theoretical resolving power from Figure (2.22) for a cylindrical-electrode TOFMS. The theoretical space focused resolving power is about 960. When a 2 eV initial energy spread is considered, the theoretical resolving power drops to about 34. This means the actual resolving power is about half of the predicted resolving power. The presence of an ion gate in the laboratory cylindrical-electrode TOFMS and finite rise and fall times on the buncher and gate voltage pulses can explain the lower actual resolving power (see Chapters III and IV).

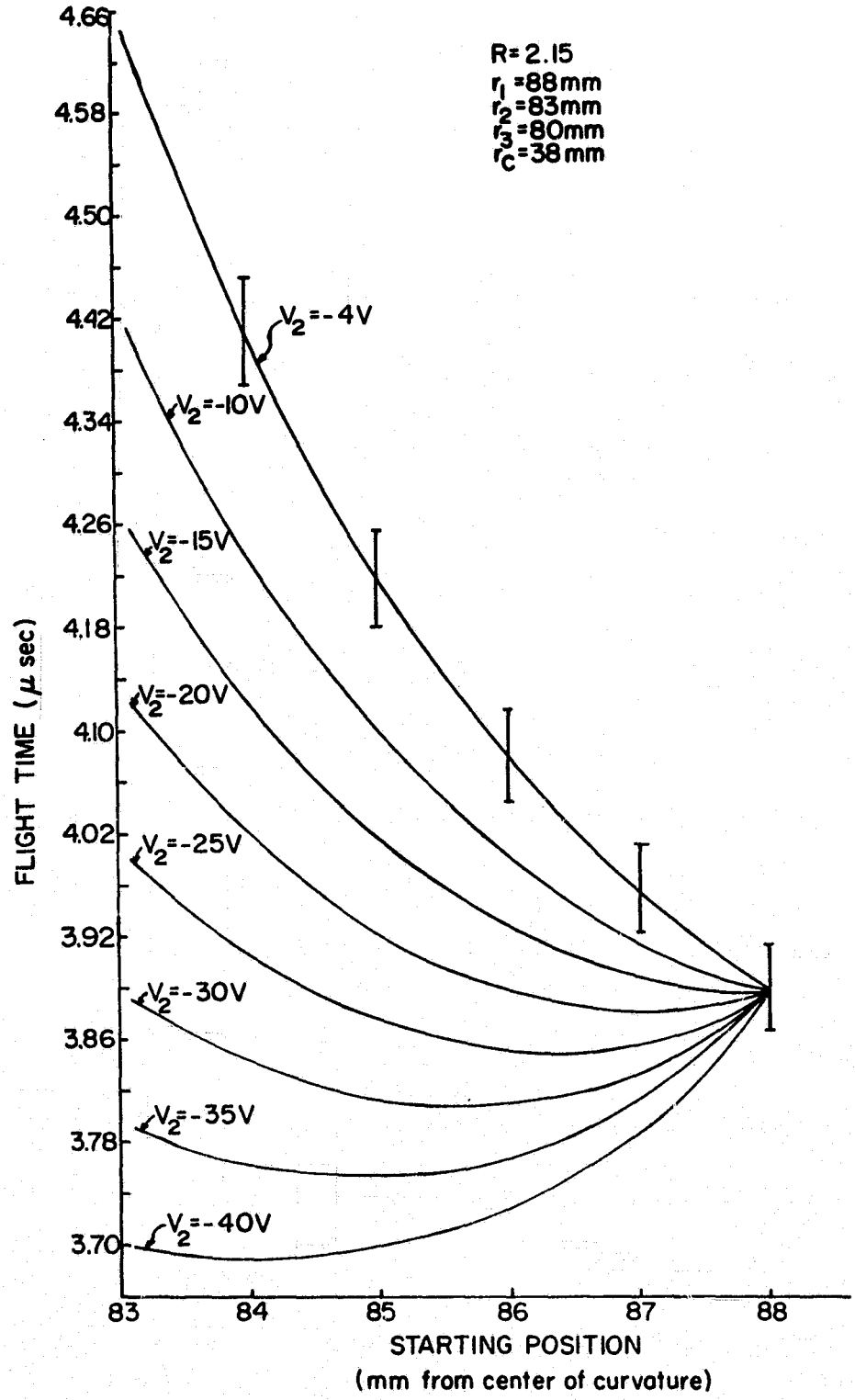

Figure 2.22 Computer Generated Space Focusing Characteristics for a Cylindrical-Electrode TOFMS Having r_1 = 88 mm, r_2 = 83 mm, r_3 = 80 mm, r_c = 38 mm, R = 2.15, and an Ion Mass of 133 amu, While V_2 was Varied. This Produced an Ion Initial Energy Which was Dependent on the Ion Starting Position. The Bars Represent an Initial Ion Energy Spread of ± 1 eV.

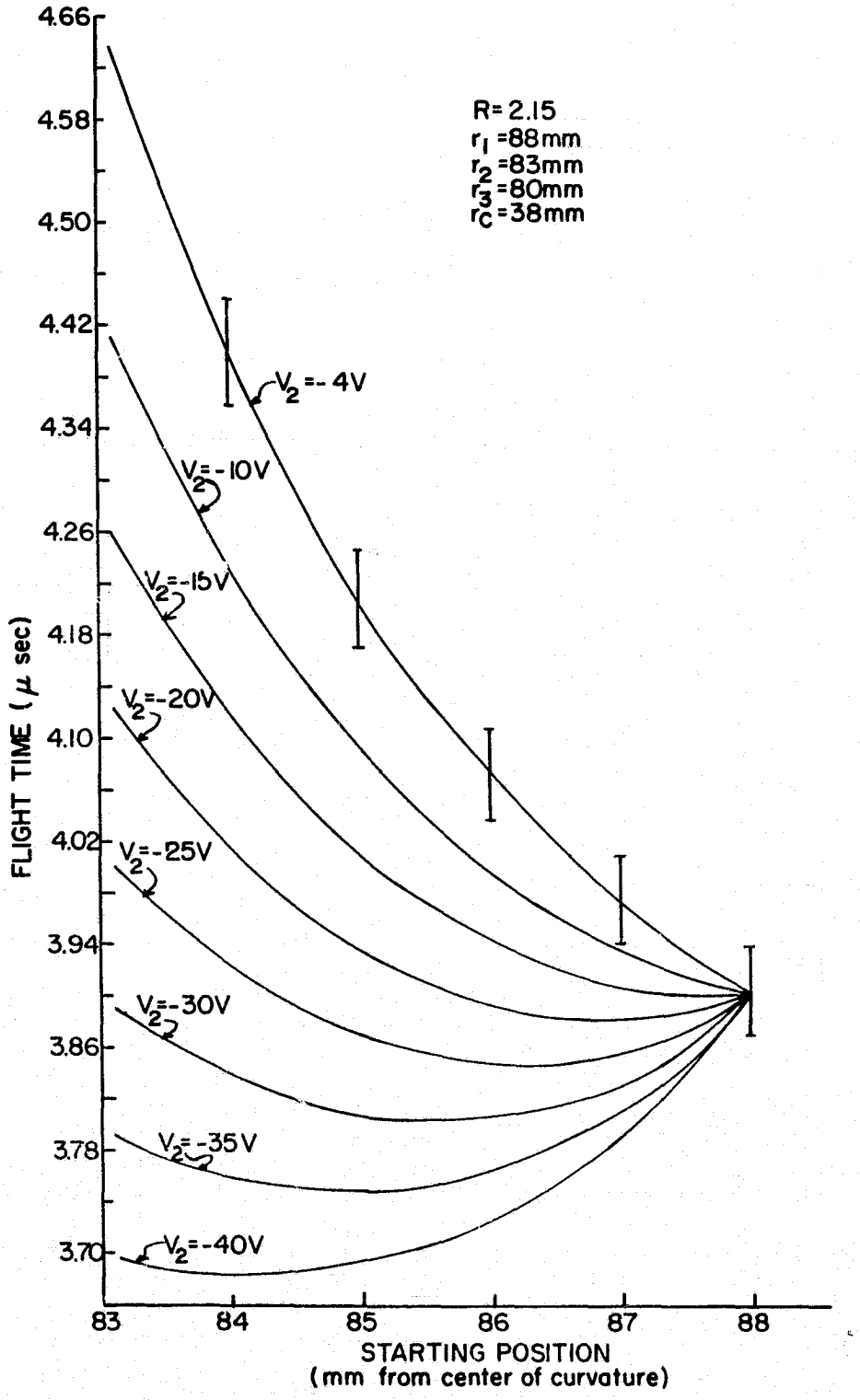

Figure 2.23 Computer Generated Space Focusing Characteristics for a Spherical-Electrode TOFMS Having r_1 = 88 mm, r_2 = 83 mm, r_3 = 80 mm, r_c = 38 mm, R = 2.15, and an Ion Mass of 133 amu, While V_2 was Varied. This Produced an Ion Initial Energy Which was Dependent on the Ion Starting Position. The Bars Represent an Initial Ion Energy Spread of ± 1 eV.

Figure (2.24) represents the flight time characteristics for a cylindrical-electrode TOFMS when a voltage ratio of 6.0 is used. The curves show the effects of varying V_2 while maintaining a constant voltage ratio (by varying V_1 and V_3). V_0 is, again, - 4 V and the electrode spacings are the same as those used in Figures (2.21), (2.22) and (2.23). Making V_2 more negative than V_0 results in a lower effective voltage ratio without significantly altering the velocity focusing characteristics. Notice that the voltage required on electrode 2 is much more negative than the voltage required for R = 2.15. Also notice the dramatically reduced flight time spread due to the 2 eV initial energy spread. A sample calculation of the theoretical resolving power using the V_2 = - 180 V curve from Figure (2.24) shows the space focused resolving power to be about 122. This is greatly reduced from the space focused resolving power for R = 2.15 and V_2 = -25 V calculated from Figure (2.22). This theoretical resolving power is also less than 1/10 the theoretical space focused resolving power for an optimum space focused voltage ratio for a TOFMS with no variable source velocity. But when the 2 eV energy spread is considered, the theoretical resolving power for R = 6.0 and V_2 = - 180 V only drops to about 75. This is more than twice the theoretical resolving power for R = 2.15 and V_2 = -25 V and more than seven times the resolving power of an optimally space focused TOFMS (with no variable source velocity) with an initial energy spread of 2 eV. Figure (2.25) illustrates the flight time characteristics for a spherical-electrode TOFMS with the same operating characteristics as were used to produce Figure (2.24).

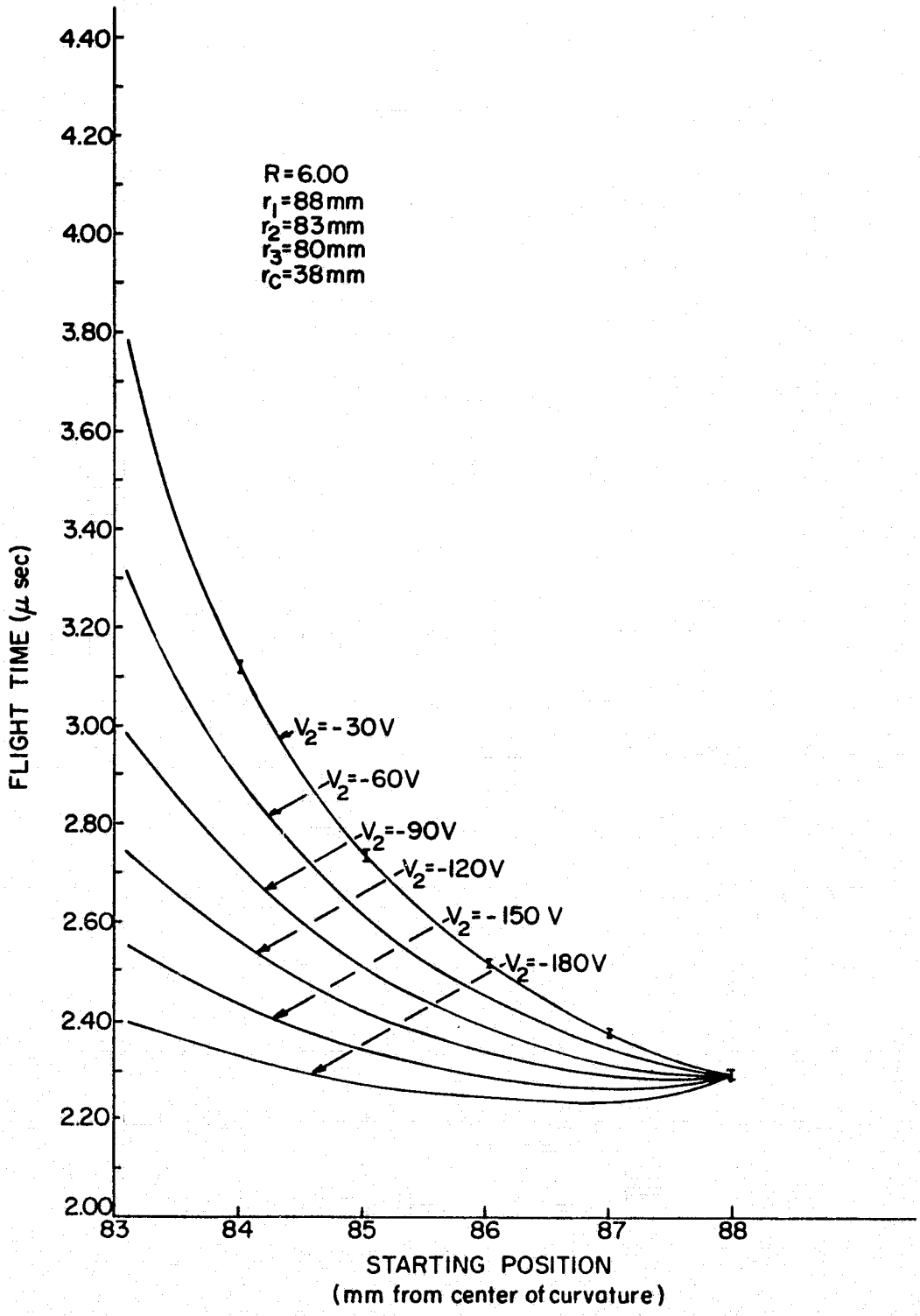

Figure 2.24 Computer Generated Space Focusing Characteristics for a Cylindrical-Electrode TOFMS Having r_1 = 88 mm, r_2 = 83 mm, r_3 = 80 mm, r_c = 38 mm, R = 6.00, and an Ion Mass of 133 amu, While V_2 was Varied. This Produced an Ion Initial Energy Which was Dependent on the Ion Starting Position. The Bars Represent an Initial Ion Energy Spread of ± 1 eV.

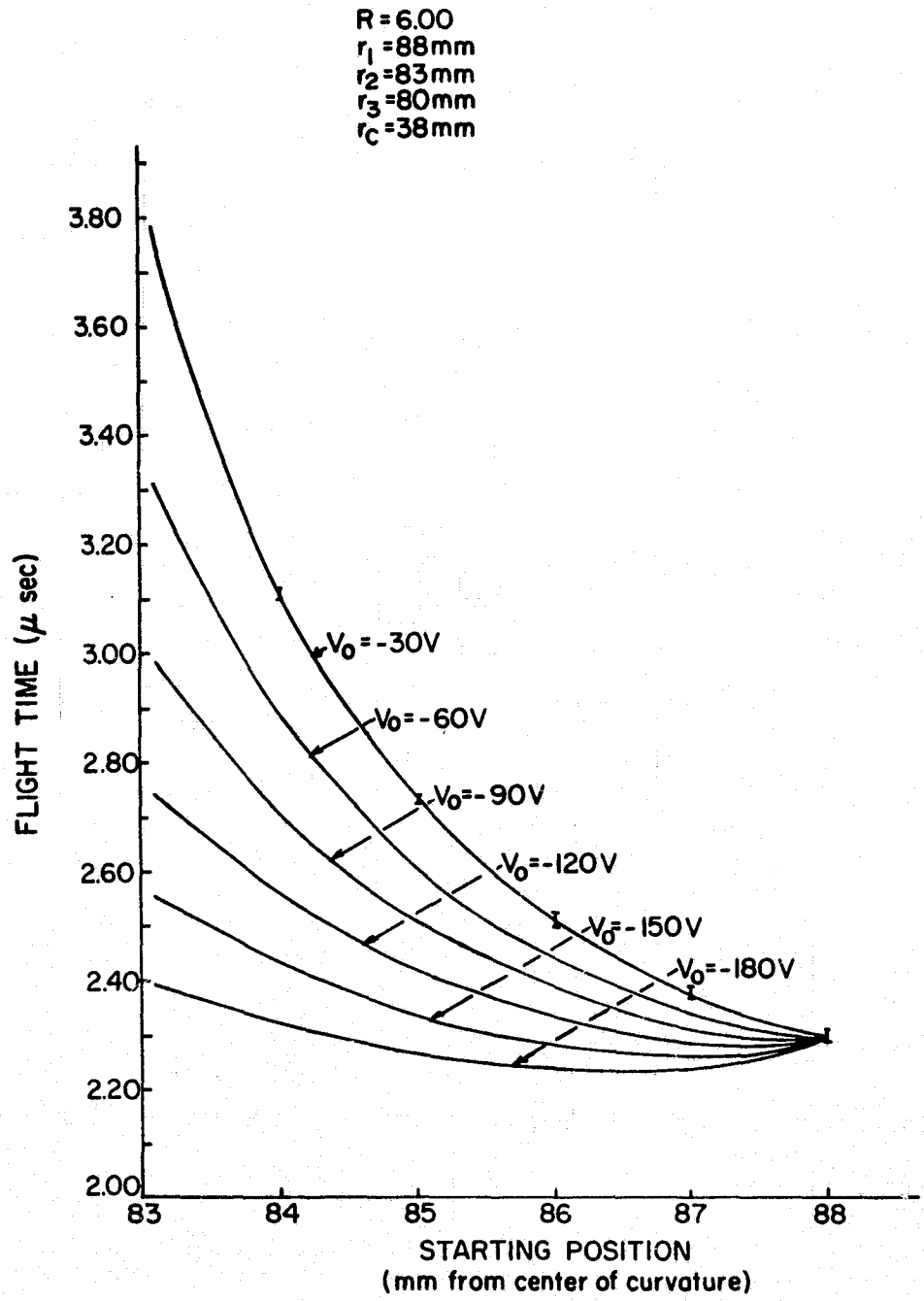

Figure 2.25 Computer Generated Space Focusing Characteristics for a Spherical-Electrode TOFMS Having r_1 = 88 mm, r_2 = 83 mm, r_3 = 80 mm, r_c = 38 mm, R = 6.00, and and Ion Mass of 133 amu, While V_2 was Varied. This Produced an Ion Initial Energy Which was Dependent on the Ion Starting Position. The Bars Represent an Initial Ion Energy Spread of ± 1 eV.

There will be a decrease in the sensitivity of a TOFMS operated with variable source velocities because of the increased velocities in the source region. This means there will be fewer ions in the source region for each mass spectrum. However, this sensitivity loss will be offset, to some extent, by the fact that more ions will be arriving in a shorter period of time at the collector. Experimental measurements at $R \cong 2.15$ with a cylindrical-electrode TOFMS showed no significant decrease in sensitivity which could be attributed to operation in the resolving power enhancement mode. Experimental confirmation of the resolving power enhancement produced by the variable initial source velocity will be discussed in Chapter IV.

CHAPTER III

ION GATING IN TIME-OF-FLIGHT MASS SPECTROMETERS

3.1 Background

The use of gating systems in time-of-flight mass spectrometers has been present for nearly as long as time-of-flight mass spectrometers. The first reported gating systems were used by Glenn (1952), Ionov and Mamyrin (1953) and Katzenstein and Friedland (1955). Glenn (1952) placed a grid with a dc potential directly in front of the collector. Ions arriving at the appropriate time were given additional energy by the gate pulse and could reach the collector. The gating system of Ionov and Mamyrin (1953) used four grids placed at the end of the ion drift tube, directly in front of the collector. The outer two grids were at the drift tube potential. The inner grid closest to the collector was set at a dc potential corresponding to the ion acceleration voltage plus a small ΔV. The other inner grid had a positive pulse which gave ions arriving at the proper time enough energy to spill over the potential barrier. In this instrument, varying the gate pulse time and varying the ion acceleration voltage produced equivalent results. Katzenstein and Friedland (1955) used an arrangement which was very similar to the system of Glenn (1952). The systems of Glenn (1952) and Katzenstein and Friedland (1955) were similar to the varied gate pulse delay time mode of Ionov and Mamyrin (1953). The grid arrangement of Katzenstein and Friedland (1955) is shown in Figure (3.1b). Other gating systems have been

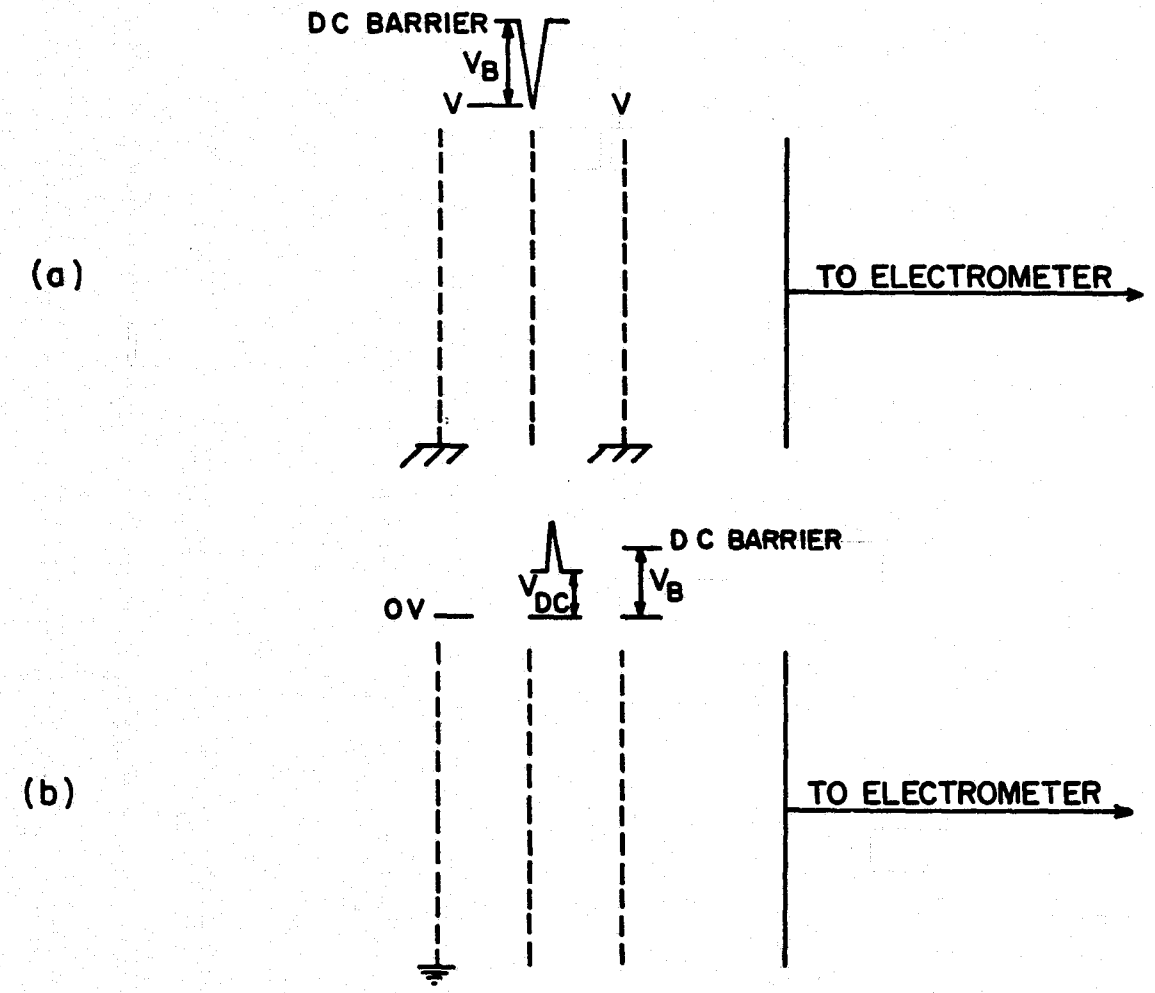

Figure 3.1 a. The Gating Arrangement Used for the Computer Simulations in Chapter III and in the Laboratory Version of the Cylindrical-Electrode TOFMS.

b. The Gating Arrangement Used by Katzenstein and Friedland (1955).

described by Wager (1960), Narcisi et al., (1966), Diem (1967) and Zabielski (1970). These systems will be described below.

Glenn (1952) used his gating system to insure that ions which did not have the appropriate flight times did not reach the collector. Ionov and Mamyrin (1953) used their gating system in order to produce enough current at the collector to be measured with the electrometers in use at that time. The gate was also used to eliminate the need for an electrometer with a high frequency response. With their gating system a dc electrometer could be used. The gating system of Katzenstein and Friedland (1955) was developed to eliminate excessive capacitive coupling to the collector plate. This improved the signal-to-noise ratio of the mass spectrum. The gating systems reported by Wager (1960), Narcisi et al., (1966), Diem (1967) and Zabielski (1970) were used in instruments carried on balloon and sounding rocket flights. The fact that time-of-flight mass spectrometers produce a spectrum in a very short time (μsec) results in two major problems when used in atmospheric applications. The first problem is the need for an electrometer which can satisfy the severe environmental constraints imposed by a sounding rocket or balloon flight and still have a sufficiently high frequency response. The second problem is the low-bandwidth constraint imposed by the telemetry systems in use. Even if an electrometer could be developed to handle the output of a TOFMS directly, the telemetry system could not handle the electrometer output.

These problems can be solved by "slowing down" the mass spectra, without losing any of the significant features, through the

use of gating. Wager (1960) developed the necessary electronics to sample a mass spectrum after amplification and to reproduce the spectrum at a suitably slowed down time. However, a high performance (with respect to frequency response) electrometer was still required. Narcisi et al., (1966), Diem (1967) and Zabielski (1970) described gating systems which were used to sample a mass spectrum before the ions reached the collector and so introduced a slowed down spectrum to the electrometer. This second gating method greatly reduced the frequency response requirements of the electrometer and allowed a much greater electrometer sensitivity. It also satisfied telemetry constraints. The electronics used in the gating systems used by Zabielski (1970) and Diem (1967) were described by Hazelton (1968) and Barnes (1971).

The gating systems of Katzenstein and Friedland (1955) and Wager (1960) produced a significant increase in the mass spectrum signal-to-noise ratio. A partial analysis by Zabielski (1970) showed all the gating systems discussed here produce a slight decrease in sensitivity (in this thesis, sensitivity refers to the number of ions collected in mass peaks in relation to the number of ions entering the spectrometer) and no marked decrease in resolving power. The sensitivity decrease was also mass dependent. It was also mentioned by Zabielski (1970) that the gate pulse shape would have a direct bearing on the mass peak shape. Unfortunately, no further studies were made.

The difficulty in producing a gate pulse which had a variable width and was compatible with the other spectrometer electronics

prevented most direct experimental studies of the effects of gating on mass spectrometer operation in this laboratory. It is possible to study a number of gate pulse shapes, used in the gating configuration shown in Figure (3.1a), by using computer simulations. Ion transit times through the gate region can be interpreted to give the effects on sensitivity and resolving power by the gate pulse shape for any number of TOFMS operating conditions.

3.2 Computer Simulation

A typical gate pulse shape is shown in Figure (3.2). It can be approximated closely by a triangular pulse shape. The ideal gate pulse is a square pulse with infinitely fast rise and fall times. Both a triangular gate pulse shape and a square gate pulse shape can be studied with relative ease using computer models.

The important parameters in the study of a gate pulse are the gate voltages, the ion energy as it enters the gate region, the ion mass, the time the gate starts with respect to the ion arrival in the gate region, and in the case of a triangular pulse, the rise and fall times. The computer programs used for these analyses followed the path of one ion at a time through the gate region and calculated the time for the ion to pass the electrode with the gate pulse.

The flight times for ions traveling a distance corresponding to the width of the gate region are shown in Figure (3.3). The calculations carried out for this Figure and the Figures that follow were carried out by using planar electrodes for greater simplicity.

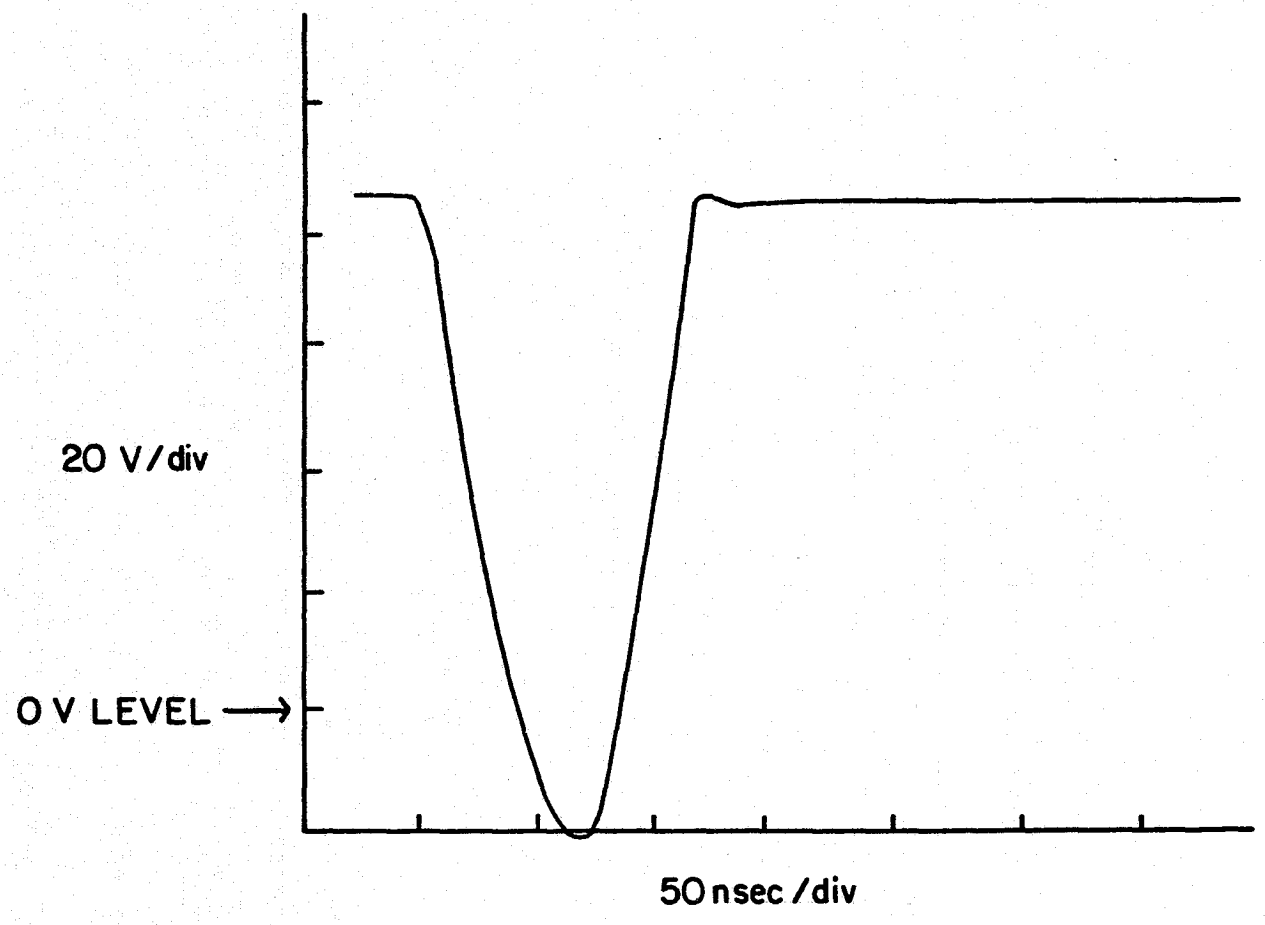

Figure 3.2 A Typical Gate Pulse Used in a Cylindrical-Electrode TOFMS with the Gating Arrangement Shown in Figure 3.1a.

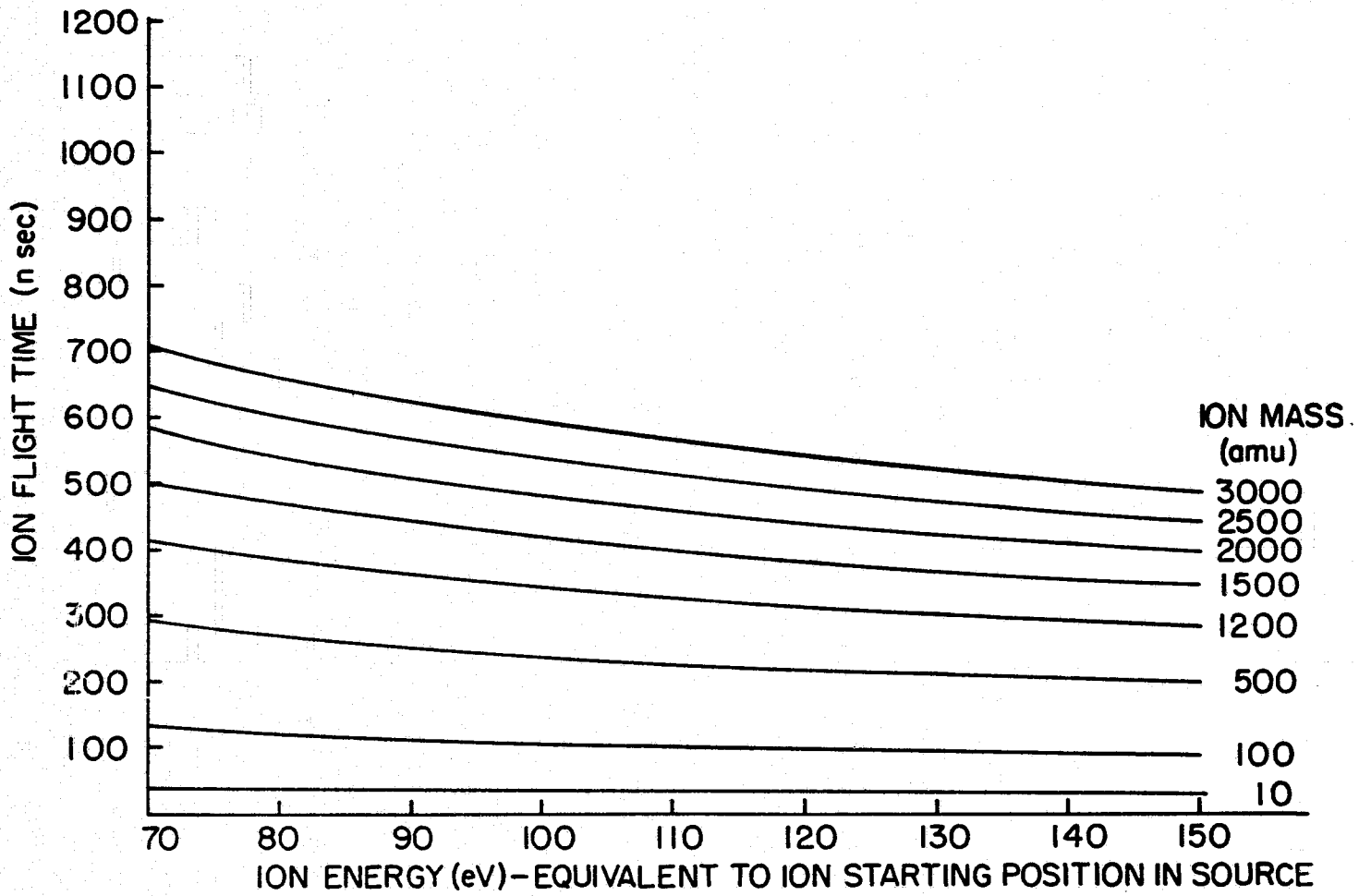

Figure 3.3 Computer Generated Ion Flight Times for the Gating Arrangement in Figure 3.1a (Width = 1.5 mm) with No Gate Pulse Present.

The ion energies considered are typical for the mass spectrometers under study. Figure (3.3) can be used as a reference for ion flight times when a gate pulse is present.

The ion flight times for a triangular gate pulse closely approximating an actual gate pulse shape (see Figure (3.2)) are shown in Figure (3.4). The flight times discussed in this chapter are only the transit times through the gate region and should not be confused with the total ion flight times in a spectrometer. The rise and fall times for the pulse were 50 nsec, the barrier potential was 155 V, the pulse amplitude was 100 V, and the gate pulse was started just as the ions entered the gate region. This Figure illustrates several interesting effects. The first effect of the gate is to produce a mass discrimination against the heavier ion masses. This should result in a sensitivity decrease as the mass of ions under study increases. For the operating conditions under study, this discrimination is not easily noticeable at masses less than 100 amu. A sensitivity decrease for K^+ (39, 41) and Cs^+ (133) was observed experimentally by Zabielski (1970) when the barrier potential was increased (which is also similar to narrowing the gate pulse). The results of Zabielski's measurements are reproduced in Figure (3.5). The presence of this sensitivity decrease at higher masses has been confirmed in measurements made by me, although exact sensitivity values were not obtained. The second effect of the gate pulse was not expected. The gate pulse also discriminated against certain ion starting positions in the source. In a typical operational cylindrical-electrode time-of-flight

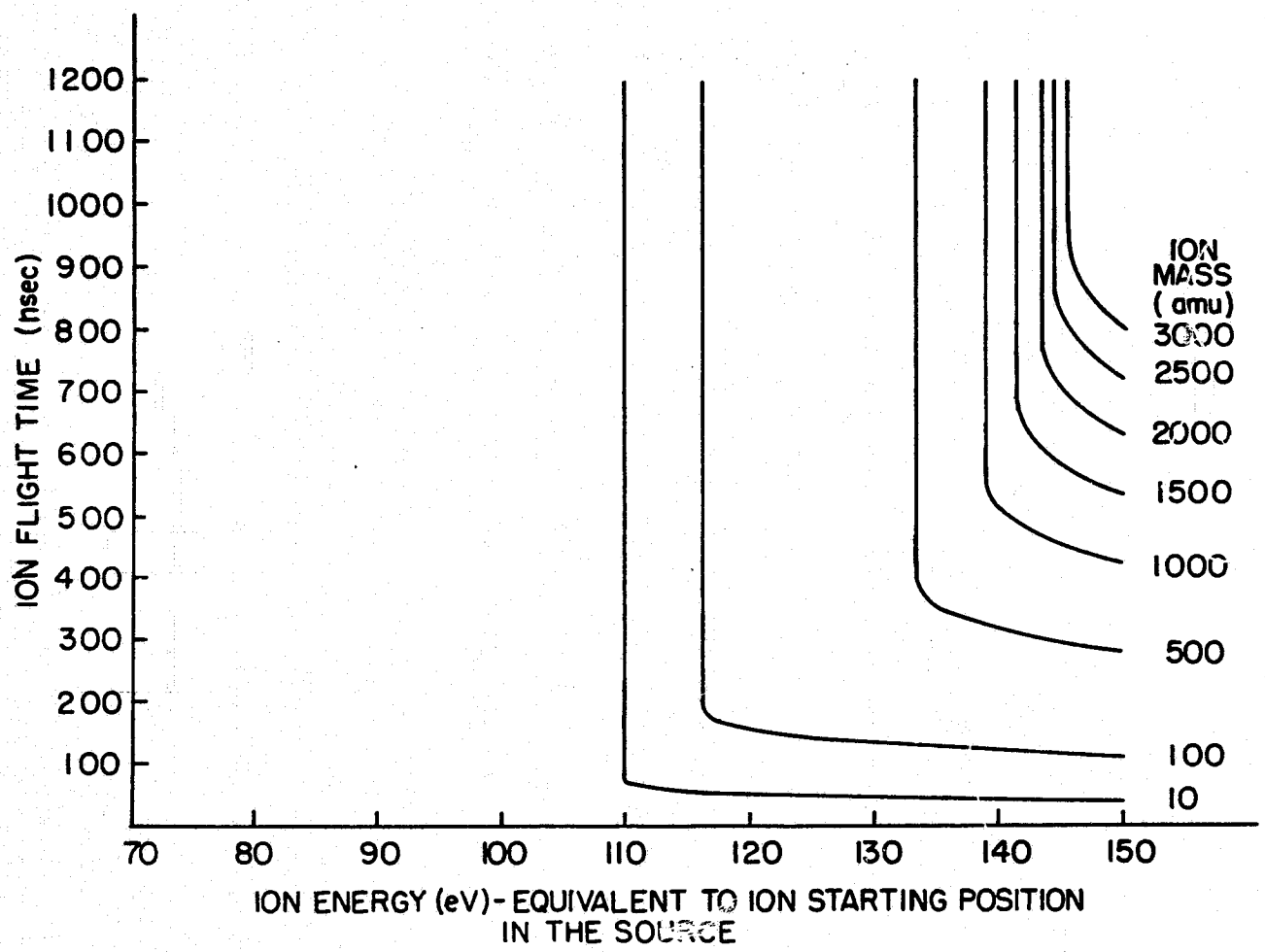

Figure 3.4 Computer Generated Ion Flight Times for a Triangular Gate Pulse. The Pulse Amplitude was 100 V, the Gate Barrier Potential was 155 V, and the Pulse Base Width was 100 nsec. The Gate Pulse was Turned on Just as Each Ion Entered the Gate Region.

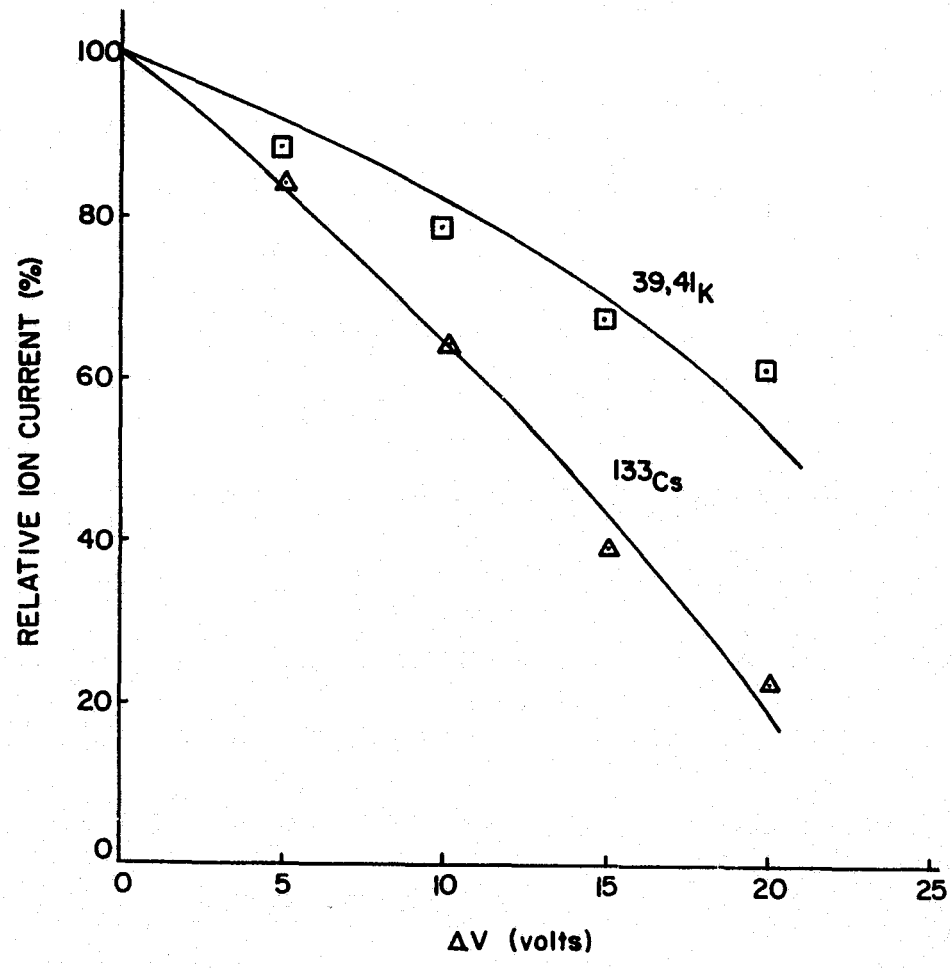

Figure 3.5 Experimentally Determined Sensitivity Decrease as the Gate Barrier Potential was Raised Above an 'Optimum Value'. (Reference: Zabielski (1970)).

mass spectrometer developed at Penn State, the various starting positions in the source produce ions with energies between 78 eV and 150 eV when they reach the gate. The lower energies correspond to a starting position closer to the collector while the higher energies correspond to ion starting positions away from the collector. As Figure (3.4) indicates, for an ion mass of 100 amu, only about 50 per cent of the ions will be collected. The 100 amu ions that are collected will only be from starting positions in the half of the source farthest from the collector.

The ion flight times in Figure (3.4) are for only one gate starting time with respect to the ion arrival in the gate region. When a number of gate starting times are considered, the three dimensional figures illustrated in Figures (3.6) and (3.7) are the result. The minimum ion flight times through the gate region can be seen to be very near or at a gate starting time coincident with the ion arrival in the gate region. Ions entering before or after the gate starting time corresponding to the minimum ion flight times travel through the gate region more slowly. There is a significant time spread introduced for ions of the same mass which enter the gate region as little as 30 nsec apart. Also notice the distinct asymmetry of the ion flight times referenced to the gate start time corresponding to the ion arrival in the gate region.

The effect of raising the gate barrier potential to 175 V (keeping the other operating conditions the same as for Figure (3.4)) on the ion flight times can be seen in Figure (3.8). The decrease in sensitivity for Cs^+ (133) and K^+ (39, 41), when compared to the

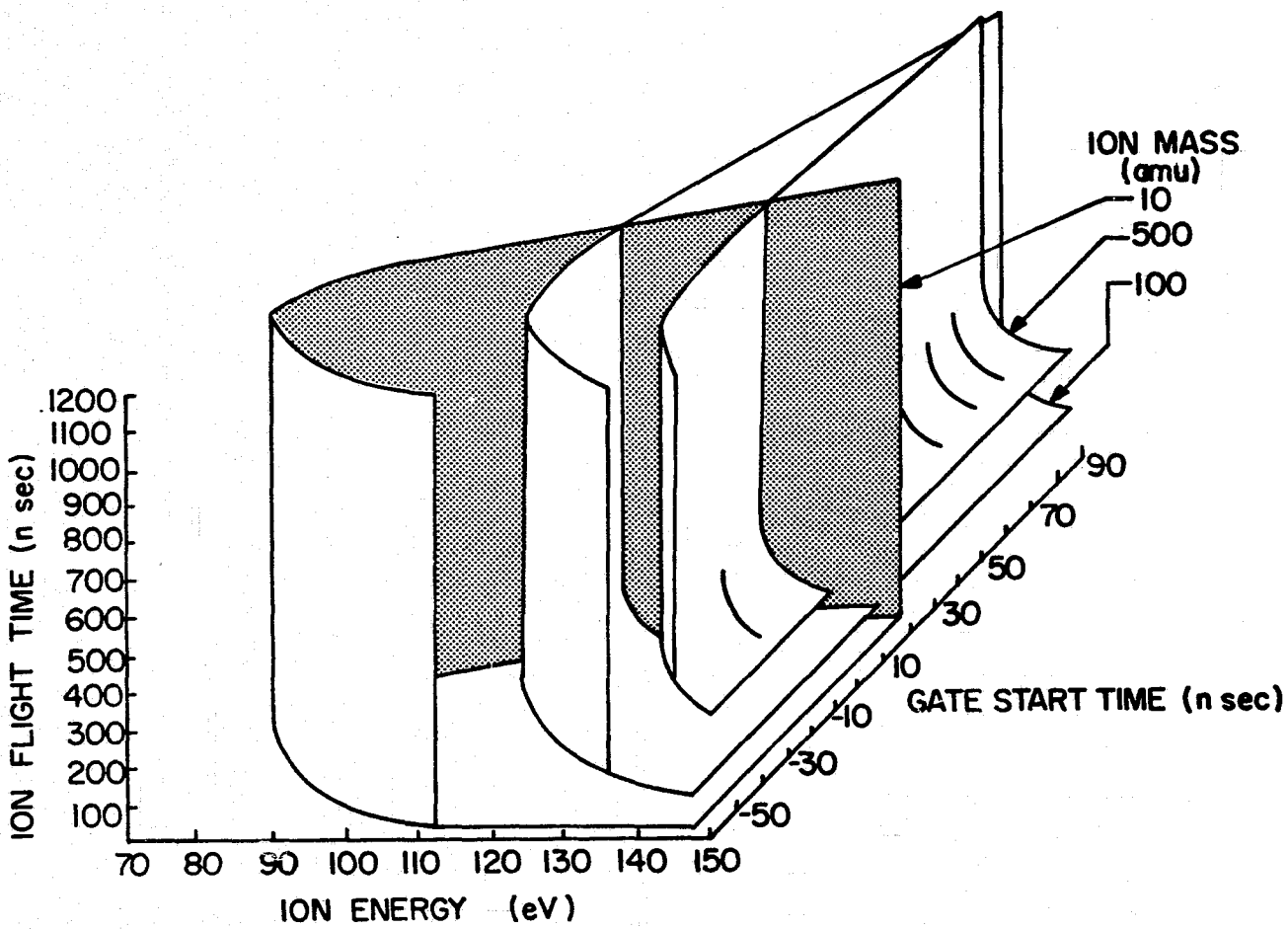

Figure 3.6 Computer Generated Ion Flight Times for a Triangular Gate Pulse, as the Gate Starting Time was Varied, for Ion Masses of 10, 100 and 500 amu. The Pulse Amplitude was 100 V, the Gate Barrier Potential was 155 V, and the Pulse Base Width was 100 nsec. A Positive Gate Start Time Means the Gate Turned on Before the Ion Entered the Gate Region and a Negative Gate Start Time Means the Gate Turned on After the Ion Entered the Gate Region.

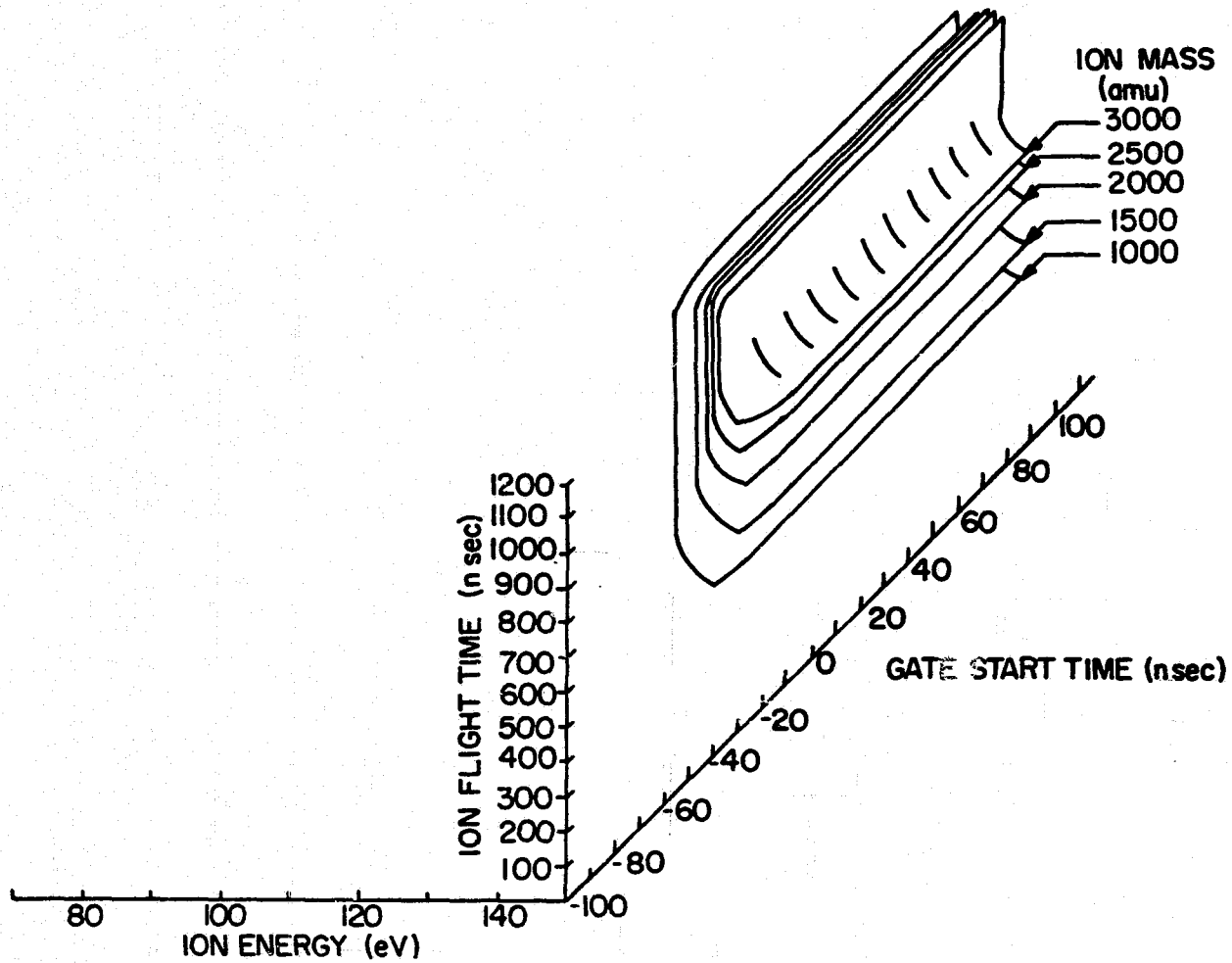

Figure 3.7 Computer Generated Ion Flight Times for a Triangular Gate Pulse, as the Gate Starting Time was Varied, for Ion Masses of 1000, 1500, 2000, 2500 and 3000 amu. The Pulse Amplitude was 100 V, the Gate Barrier Potential was 155 V, and the Pulse Base Width was 100 nsec. A Positive Gate Start Time Means the Gate Turned on Before the Ion Entered the Gate Region and a Negative Gate Start Time Means the Gate Turned on After the Ion Entered the Gate Region.

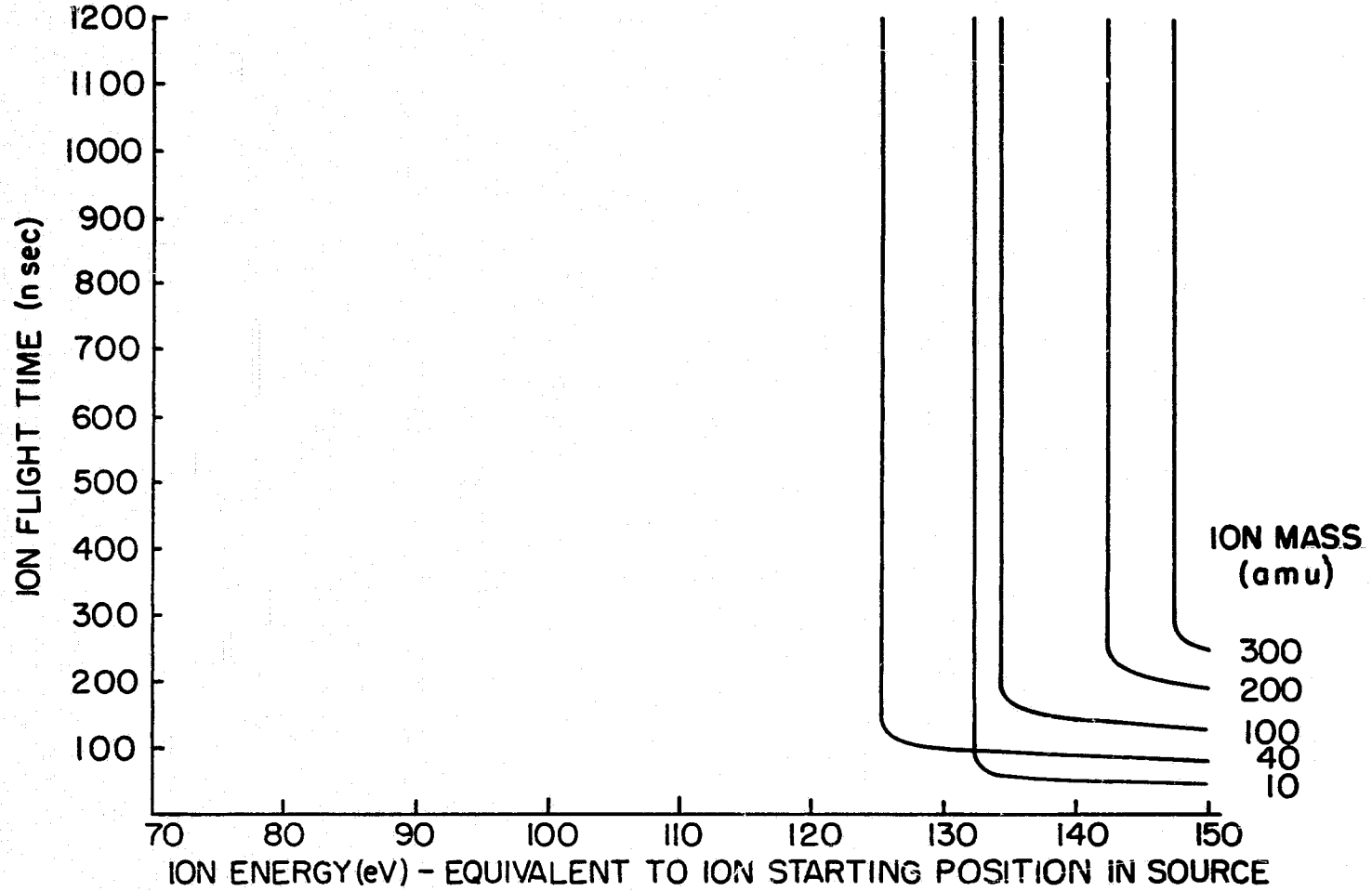

Figure 3.8 Computer Generated Ion Flight Times for a Triangular Gate Pulse with a Raised Barrier Potential. The Pulse Amplitude was 100 V, the Gate Barrier Potential was 175 V, and the Pulse Base Width was 100 nsec. The Gate Pulse was Turned on Just as Each Ion Entered the Gate Region.

results in Figure (3.4), can be calculated to be approximately 60 per cent and 40 per cent respectively. The experimental results of Zabielski (1970) show the sensitivity decrease to be approximately 75 per cent for Cs^+ (133) and 40 per cent for K^+ (39, 41). The computer simulation results agree fairly well with the experimental measurements. It must be remembered that the computer results are for only one gate start time. A completely correct result would require an integration over all gate start times. There is also a larger sensitivity decrease for very light ions than for ions of mass 40 amu to 100 amu. This is due to the fact that the lighter ions turn around and leave the gate region before the gate reaches a sufficiently low voltage to let the lighter ions through the gate. Ion masses greater than about 350 amu do not get through the gate at all.

Increasing the triangular gate pulse width to 200 nsec (rise time and fall times equal to 100 nsec each) while keeping the barrier potential at 155 V and the pulse amplitude at 100 V produces the ion flight times shown in Figure (3.9). Again, the gate start time is coincident with the ion arrival in the gate region. This produces several interesting effects. Ion masses near 100 amu traverse the gate region in approximately the same times and with the same sensitivity as for the 100 nsec wide triangular gate pulse (see Figure (3.4)). The lighter masses are severely discriminated against in this case. This is, again, because these ions turn around and leave the gate region before the gate pulse is fully turned on. The heavier mass ($m > 200$ amu) ions travel through

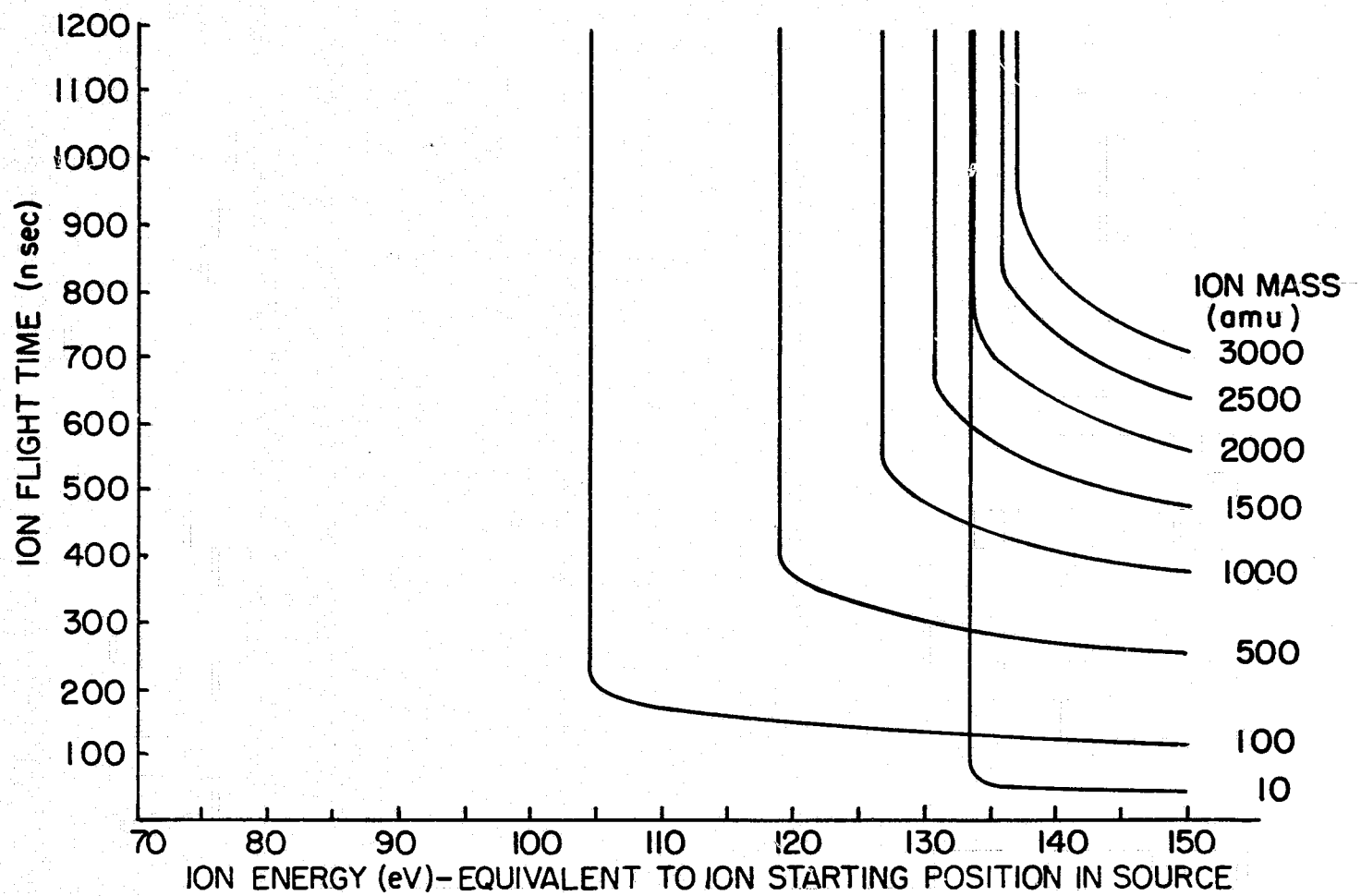

Figure 3.9 Computer Generated Ion Flight Times for a Triangular Gate Pulse with an Increased Pulse Width. The Pulse Amplitude was 100 V, the Gate Barrier Potential was 155 V, and the Pulse Base Width was 200 nsec. The Gate Pulse was Turned on Just as Each Ion Entered the Gate Region.

the gate region in faster times and with less sensitivity loss. For example, about three times as many 3000 amu ions pass through the gating region as for a 100 nsec wide triangular gate pulse.

When a square gate pulse is used, with a pulse amplitude of 100 V, a potential barrier of 155 V and a pulse width of 100 nsec, the ion flight times through the gate region for a gate starting time coincident with the ion arrival in the gate region are shown in Figure (3.10). It can be seen that there is no sensitivity loss for the lighter ions ($m < 100$ amu) but the sensitivity falls off for higher masses. The mass discrimination effects are still present but are not as serious as for a triangular gate pulse. This Figure can be compared usefully to Figures (3.3) and (3.4).

If a number of gate starting times are considered for the square gate pulse described in the preceeding paragraph, the ion flight times in Figures (3.11) and (3.12) are the result. An interesting feature of Figure (3.11) is the distinct asymmetry of the lighter masses (< 500 amu) and especially for ion masses less than 100 amu. The minimum flight times for $m = 10$ amu occur at a gate start time before the ion arrival in the gate region. For masses greater than 100 amu, the minimum flight times are for a gate start time very near the ion arrival time in the gate region.

The ion flight times for a 100 V square gate pulse, a 100 nsec pulse width, a 175 V barrier, and a gate start time coincident with the ion arrival time in the gate region are shown in Figure (3.13). Because of the infinitely fast rise time of the pulse, there is no discrimination against the very light ions ($m \cong 10$ amu) as there is

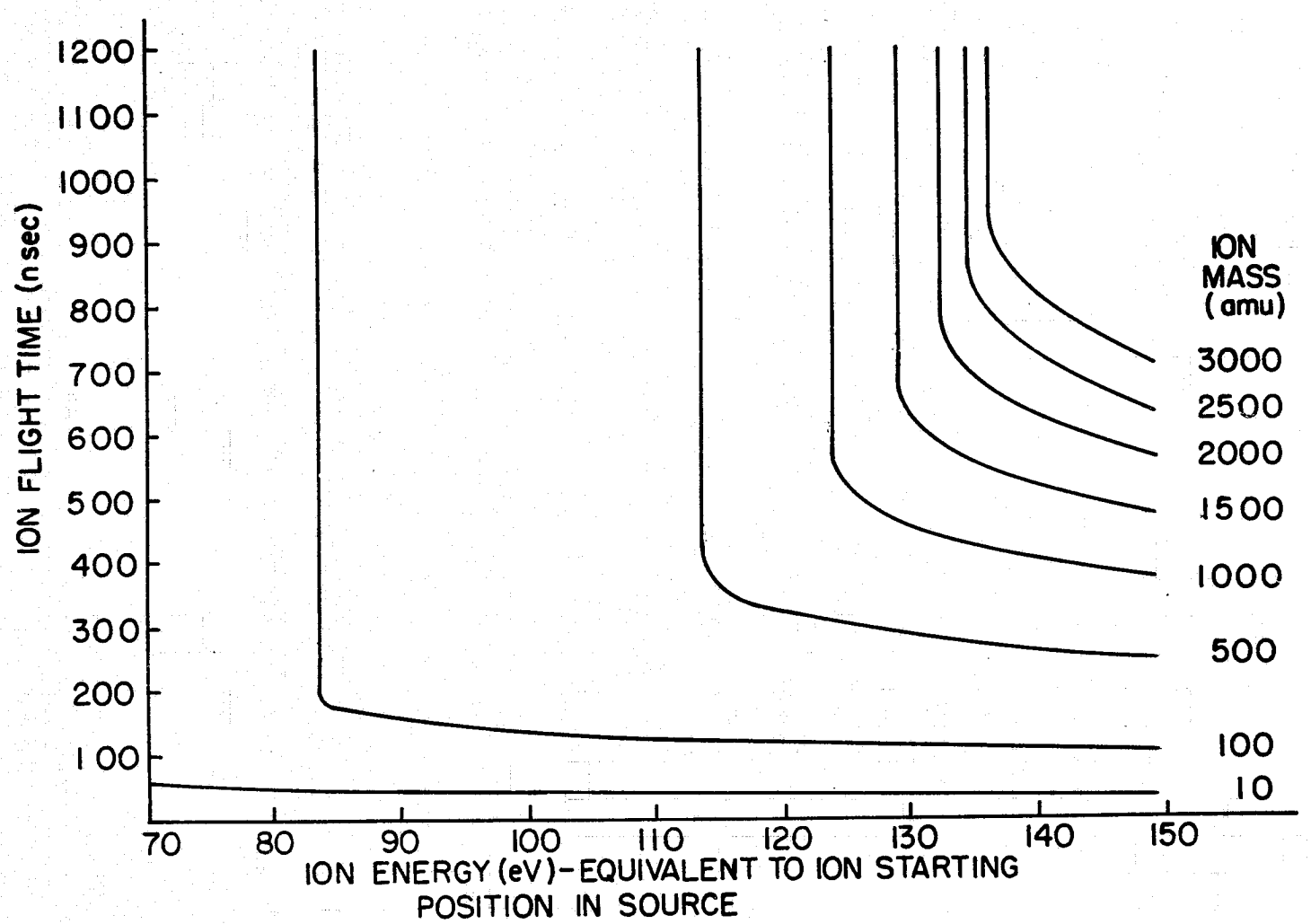

Figure 3.10 Computer Generated Ion Flight Times for a Square Gate Pulse. The Pulse Amplitude was 100 V, the Gate Barrier Potential was 155 V, and the Pulse Width was 100 nsec. The Gate Pulse was Turned on Just as Each Ion Entered the Gate Region.

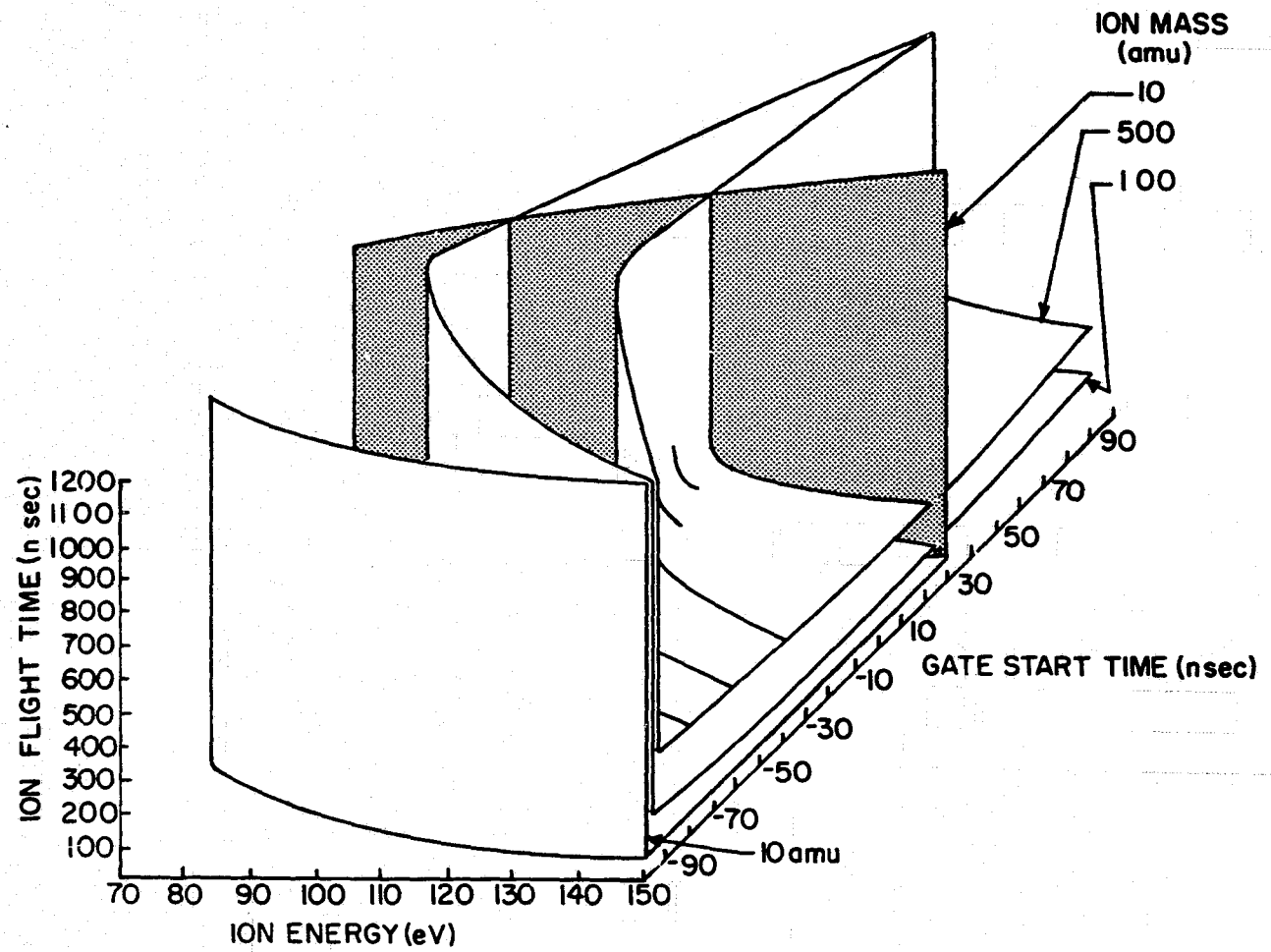

Figure 3.11 Computer Generated Ion Flight Times for a Square Gate Pulse, as the Gate Starting Time was Varied, for Ion Masses of 10, 100 and 500 amu. The Pulse Amplitude was 100 V, the Gate Barrier Potential was 155 V, and the Pulse Width was 100 nsec. A Positive Gate Start Time Means the Gate Turned on Before the Ion Entered the Gate Region and a Negative Gate Start Time Means the Gate Turned on After the Ion Entered the Gate Region.

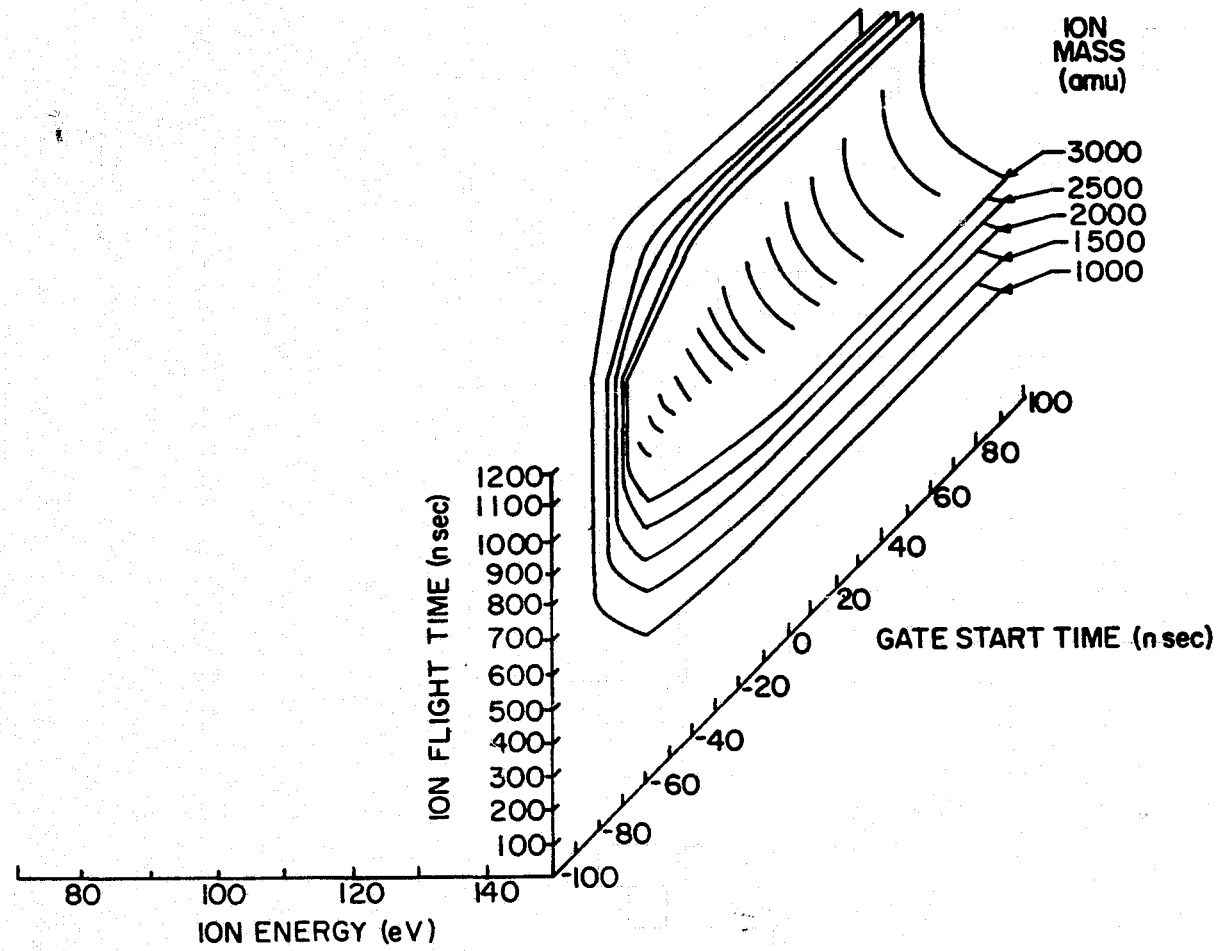

Figure 3.12 Computer Generated Ion Flight Times for a Square Gate Pulse, as the Gate Starting Time was Varied, for Ion Masses of 1000, 1500, 2000, 2500 and 3000 amu. The Pulse Amplitude was 100 V, the Gate Barrier Potential was 155 V, and the Pulse Width was 100 nsec. A Positive Gate Start Time Means the Gate Turned on Before the Ion Entered the Gate Region and a Negative Gate Start Time Means the Gate Turned on After the Ion Entered the Gate Region.

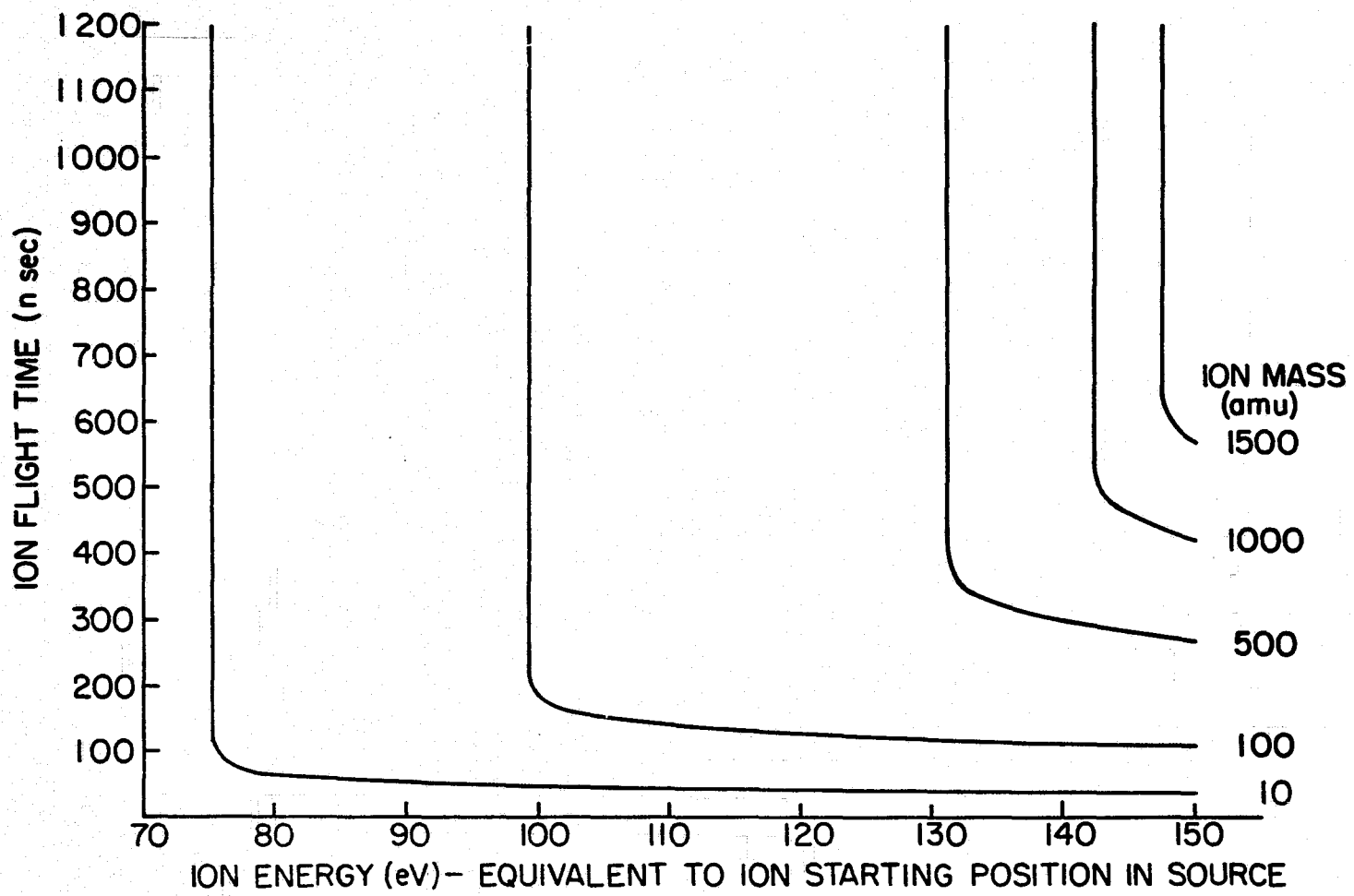

Figure 3.13 Computer Generated Ion Flight Times for a Square Gate Pulse with a Raised Barrier Potential. The Pulse Amplitude was 100 V, the Barrier Potential was 175 V, and the Pulse Width was 100 nsec. The Gate Pulse was Turned on Just as Each Ion Entered the Gate Region.

for a triangular gate pulse with a raised potential barrier (see Figure (3.7)). The sensitivity at higher masses does not fall off as rapidly for the square gate. However, there is a mass cut off at $m \cong 1600$ amu.

If the width of the 100 V gate pulse is increased to 200 nsec while the potential barrier is set at 155 V, the ion flight times that are the result are shown in Figure (3.14). The sensitivity is significantly improved at all masses compared to the triangular gate flight times (see Figure (3.9)). The most significant improvement is at the very light masses ($m \cong 10$ amu) where there is no slow pulse turn on to affect the ions' trajectory through the gate region.

Care must be taken in the evaluation of the flight time curves in this chapter and their effect on resolving power. Except for Figures (3.6), (3.7), (3.11) and (3.12), only one gate start time has been considered. In order to gain a complete understanding of the gate pulse effects, it is necessary to consider all gate starting times.

3.3 Ion Background Current

The presence of a dc potential barrier with a superimposed gate pulse in a time-of-flight mass spectrometer allows ions with a selected flight time (corresponding to a selected mass) to reach the collector. However, this gating technique produces the discrimination effect described in the previous section. It also produces a uniform background current. This background current

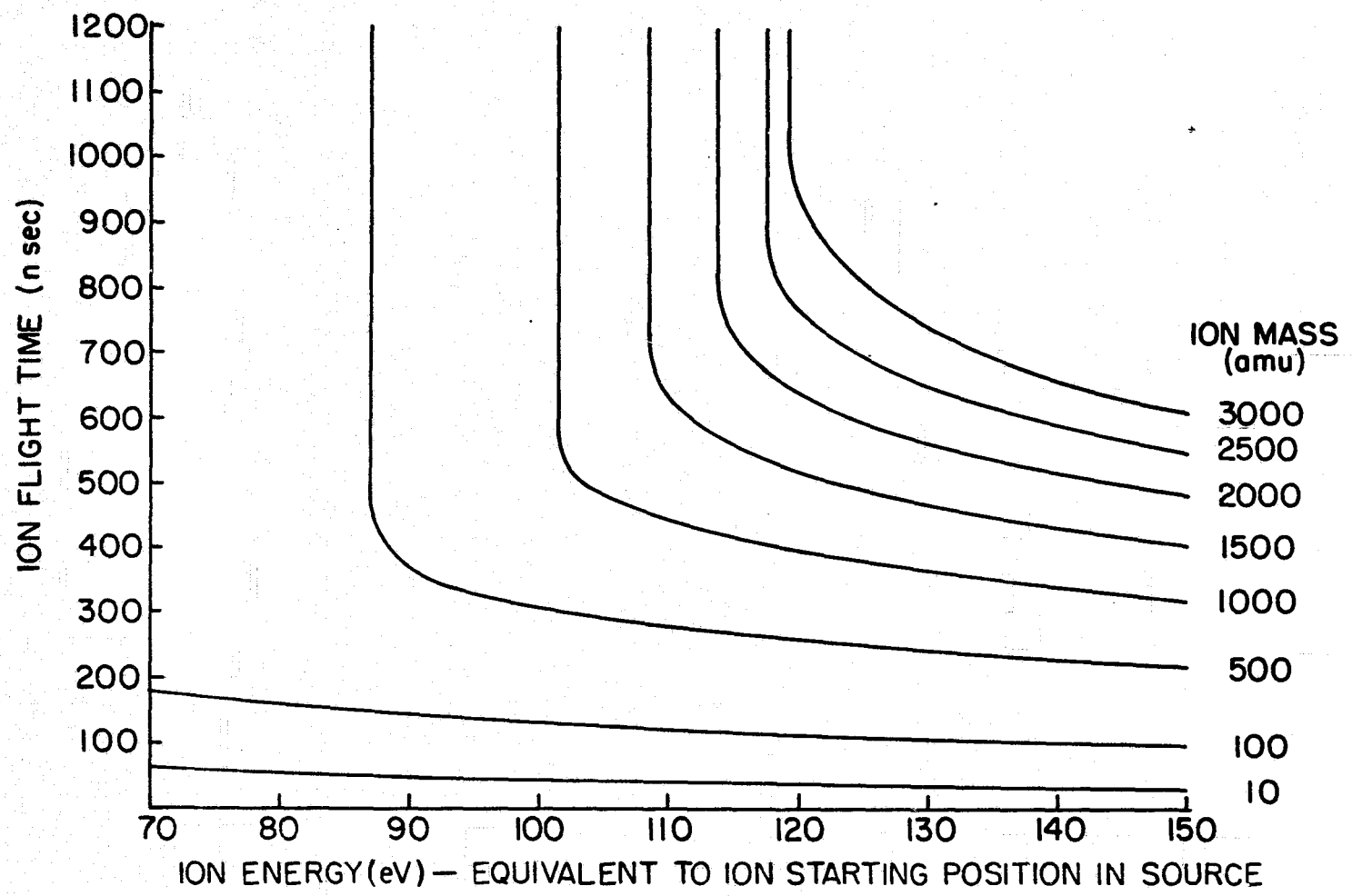

Figure 3.14 Computer Generated Ion Flight Times for a Square Gate Pulse with an Increased Pulse Width. The Pulse Amplitude was 100 V, the Gate Barrier Potential was 155 V, and the Pulse Width was 200 nsec. The Gate Pulse was Turned on Just as Each Ion Entered the Gate Region.

was subject to study to try to find the answers to several questions. These questions were whether the background current was proportional, in a simple manner, to the ambient plasma density; what was the background current dependence on the mass spectrometer operating conditions and what are the sources of the components of the background current.

The production of the background current was originally thought to come from three sources. The first was ions which enter the mass spectrometer after the bunching pulse has turned off. These ions would then gain enough energy to pass through the gate if they arrive at the right time. The second source was thought to be ions which had undergone one or more collisions and therefore had their flight times (and energy) altered enough to still pass through the gate but too much to arrive in the proper ion peak. The third source was supposed to be the alteration to the ion flight times by the action of the gate.

The flight times illustrated in Figures (3.6) and (3.7) for a typical triangular gate pulse show that it would be impossible for ions not receiving energy from the buncher pulse to get past the gate potential barrier. The energy of ions entering the mass spectrometer after the buncher pulse has turned off would be 78 eV at the most.

The dependence of the background current on the operating voltages of the mass spectrometer is illustrated in Figure (3.15). The background current ratio is defined as the total ion current in

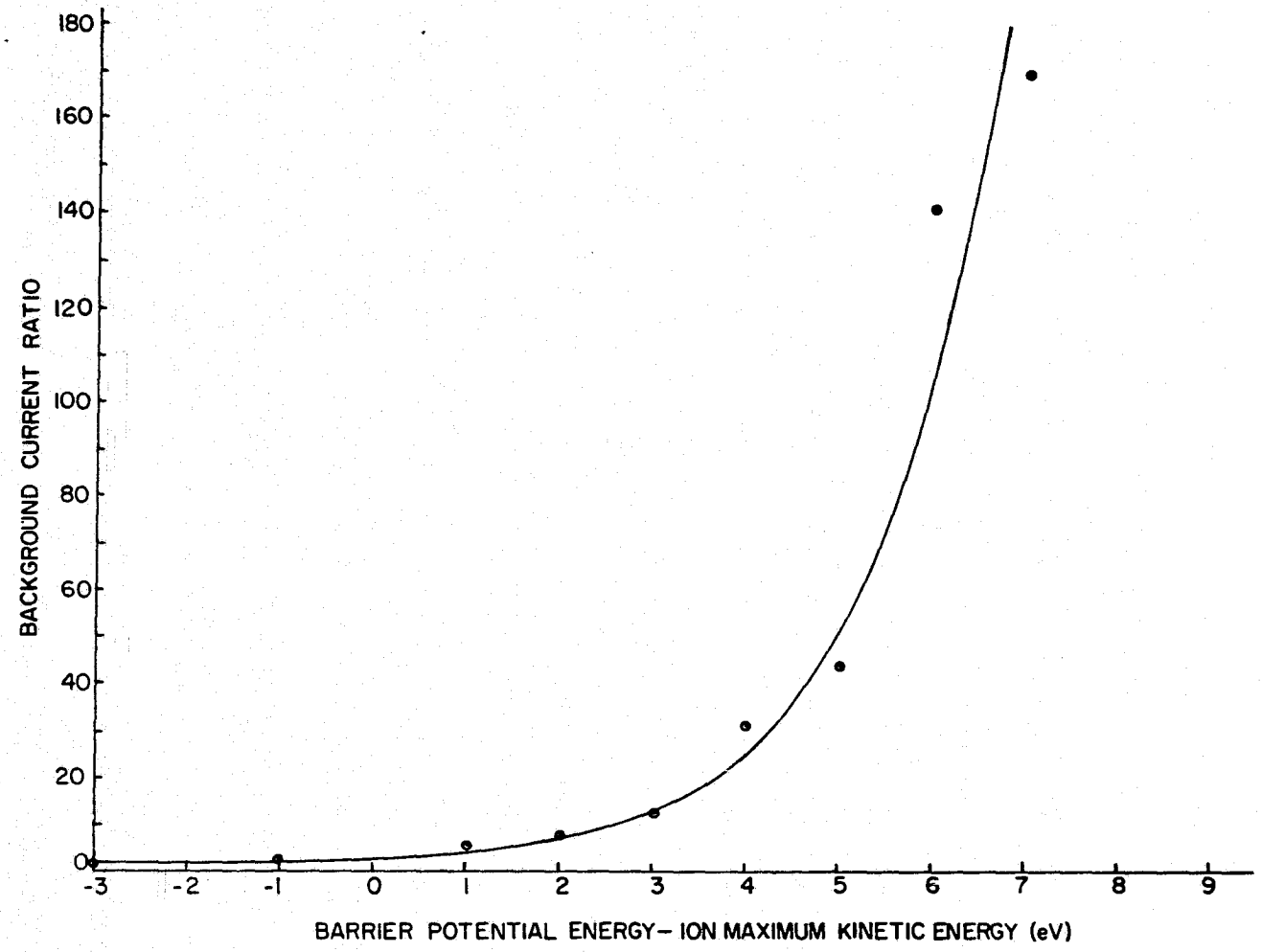

Figure 3.15 Experimentally Measured Background Current Ratio, as a Function of the Difference Between the Gate Barrier Potential Energy and the Maximum Ion Kinetic Energy, for a Cylindrical-Electrode TOFMS.

the mass spectrum ion peaks divided by the background current. The voltage difference is the difference between the barrier potential and the maximum ion energy in one bunch of ions. The typical barrier potential was 155 V while the maximum ion energy was 150 V. Since the background current is greatly reduced by raising the barrier potential, the time spread introduced by the gate itself can not be a major source of the background current.

The contribution to the background current due to collisional effects was studied by measuring the background current while raising the pressure in the mass spectrometer. The results are shown in Figure (3.16). The results were surprising in that the background current ratio was not a constant at all pressures as simple theory would predict, but increased as the pressure increased. No satisfactory explanation for the variation of the background current ratio due to changes in the pressure has been found to this date.

A contribution to the background current which could not be studied in the laboratory is the presence of a shock wave in the mass spectrometer flight region (as could easily occur in a sounding rocket flight). The presence of a shock wave makes the breakup of heavy cluster ions a distinct possibility. A study of the breakup of heavy cluster ions in a shock wave has been made by Narcisi and Roth (1970). In a time-of-flight mass spectrometer with no potential barrier gating, there would be no problem since the charged ion fragment would arrive at the proper time at the collector (at a time corresponding to the flight time of the heavy ion) as long as there were no energy losses. When a gating system

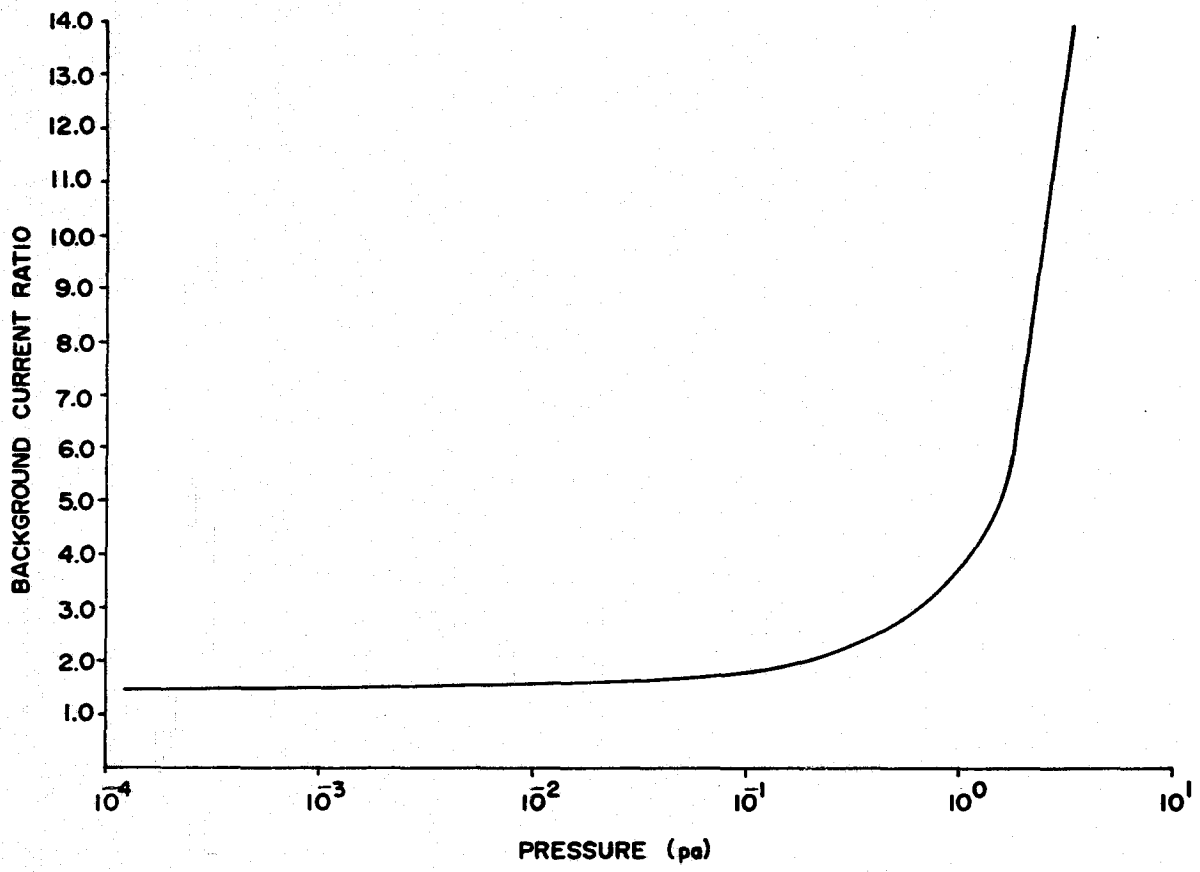

Figure 3.16 Experimentally Measured Background Current Ratio, as a Function of Pressure, for a Cylindrical-Electrode TOFMS. The Maximum Ion Kinetic Energy was Equal to the Gate Barrier Potential Energy.

is used there is a time difference in the flight times of heavy and light ions traversing the gate region (see Figure (3.4) for example). Therefore, the ion fragments would contribute to the wings of a mass peak. With the possibility of the presence of very heavy ions in the D-region ionosphere (see Cuirle (1976), Farrokh (1975) or Chesworth (1974)), this might be a source of the background current in D-region ionosphere measurements.

In summary, at low pressures, gate spillover and time spreads introduced by the gate are probably the dominant contributions to the background current. Ion spillover can be reduced by raising the barrier potential at the cost of significant sensitivity loss. At higher pressures collisional effects become important to the background current ratio, contrary to simple theory. It was also found that the background current did have a simple relationship to the ion density entering the mass spectrometer in the laboratory if care was taken to apply the proper pressure correction. However, the ion flight times through the gate region presented in this chapter show complicated discrimination effects which would make the relationship between background current and total ion density difficult, but not impossible, to deduce in the presence of very heavy ions (>500 amu).

CHAPTER IV

LABORATORY MEASUREMENTS WITH CYLINDRICAL AND HEMISPHERICAL-ELECTRODE TIME-OF-FLIGHT MASS SPECTROMETERS

4.1 Vacuum System and Ion Source

The primary motivation for the study of the cylindrical-electrode and the hemispherical-electrode time-of-flight mass spectrometers (TOFMS) was the need to understand the operation of these instruments for use in the D-region ionosphere. In order to simulate the vacuum environment of the D-region, the vacuum system illustrated in Figure (4.1) was used. This vacuum system included a gas inlet system and a zero pressure reference system for a diaphragm manometer. The ion source used in all the laboratory measurements was a surface ionization source identical to the one described by Diem (1967) and Zabielski (1970). The ion source and the associated electronics are shown in Figure (4.2).

4.2 Cylindrical-Electrode Two-Field TOFMS

4.2.1 Operating Voltages and Electronics

The results in these sections extend the experimental work reported by Diem (1967), Zabielski, Diem and Kendall (1970) and Zabielski (1970). The cylindrical-electrode two-field TOFMS used for laboratory analysis is shown, completely assembled, in Figure (4.3). A cross-sectional view of the spectrometer is shown in Figure (4.4) with the grid labeling and interelectrode spacings. The operating voltages are designed for positive ion collection. The voltage applied to the outermost grid, V_0, is used to draw ions into the

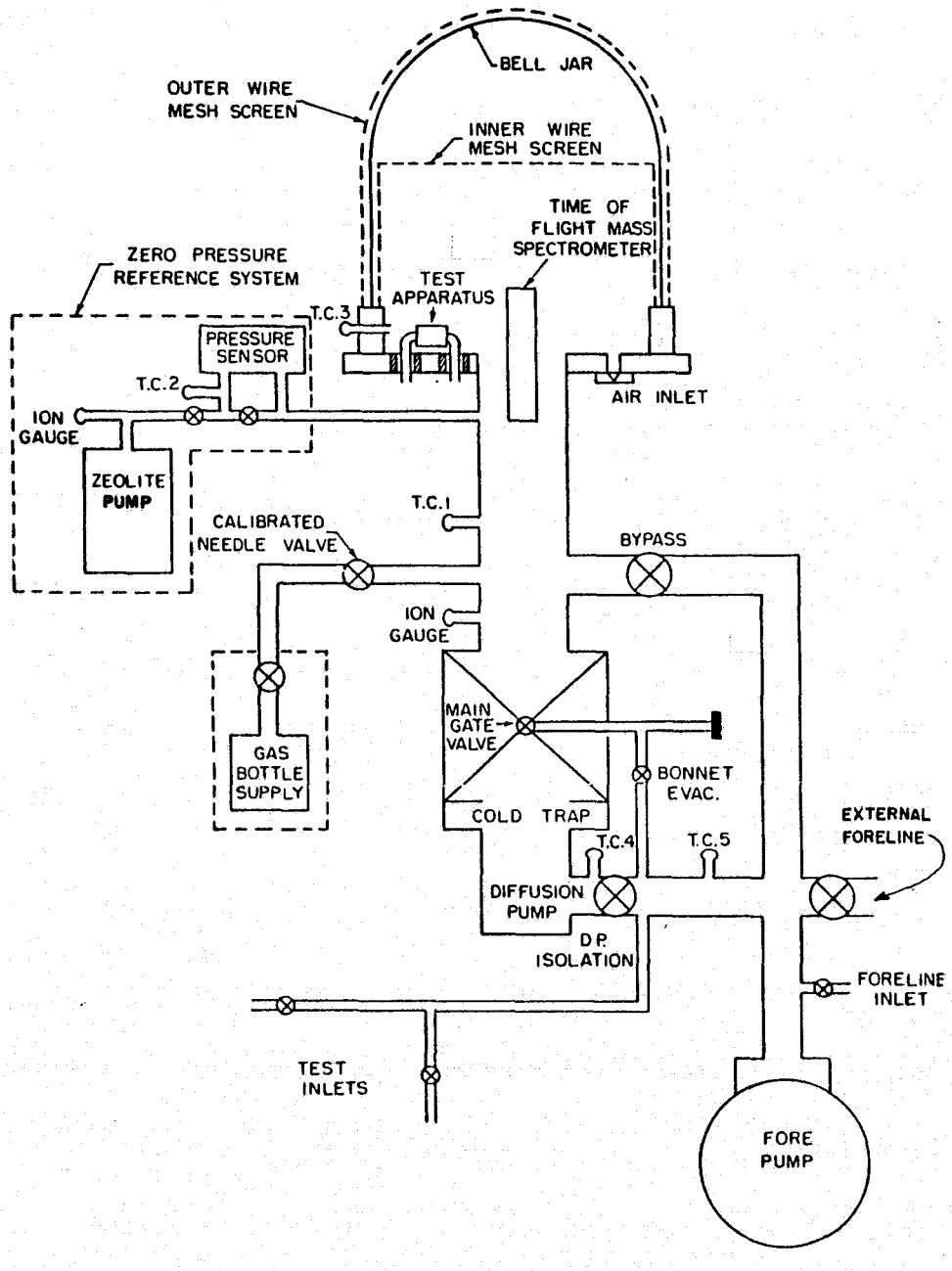

Figure 4.1 Vacuum System Used for Laboratory Studies of Cylindrical and Hemispherical TOFMS.

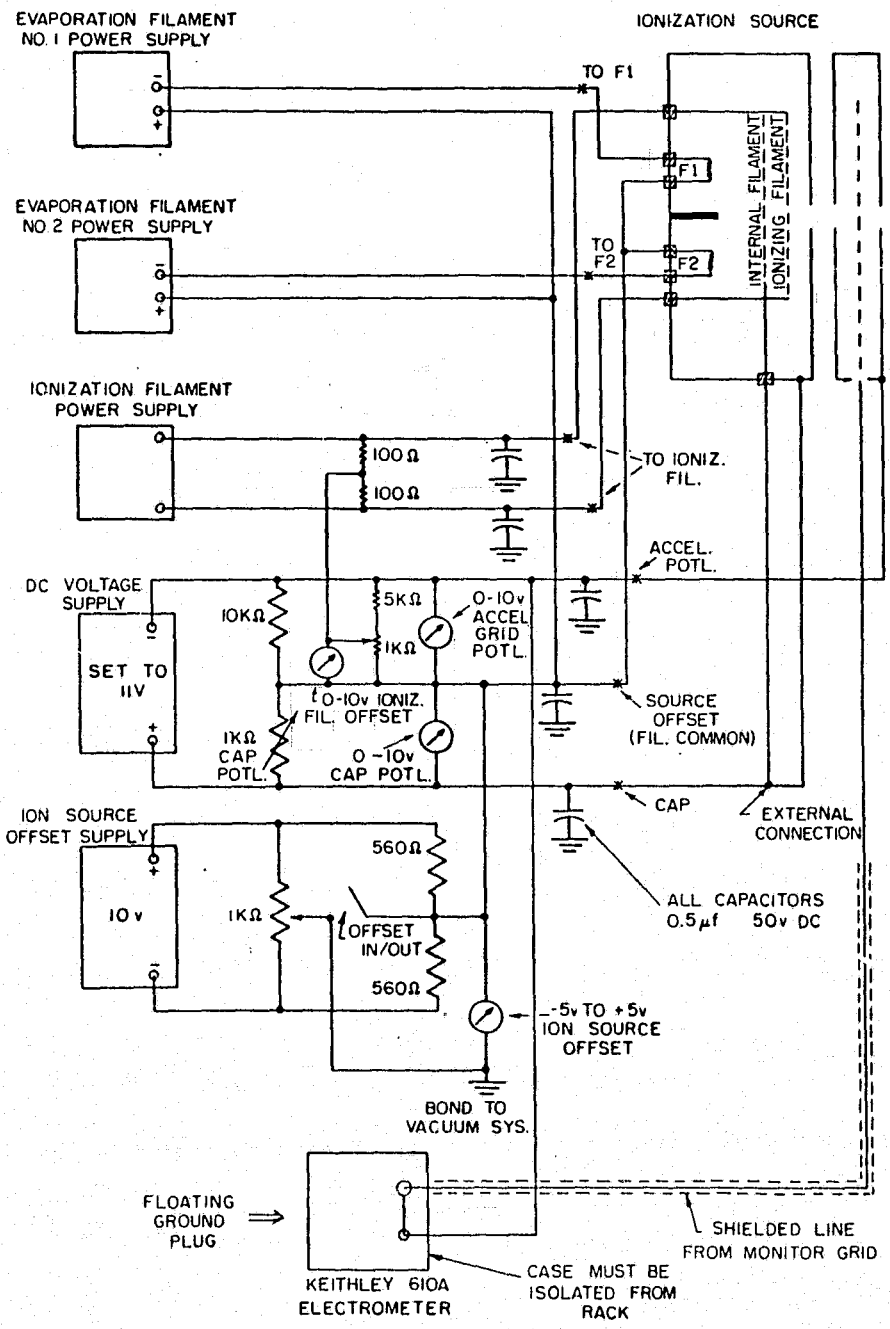

Figure 4.2 Surface Ionization Ion Source and Associated Electronics.

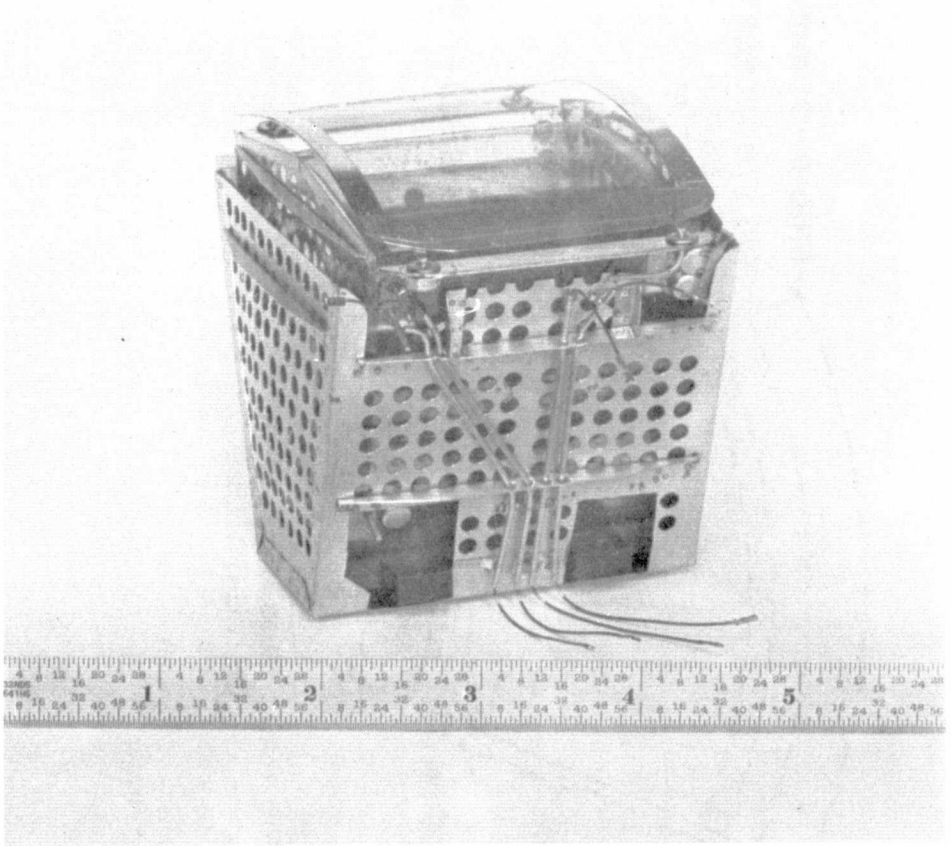

Figure 4.3 Cylindrical-Electrode TOFMS Used for Laboratory Studies.

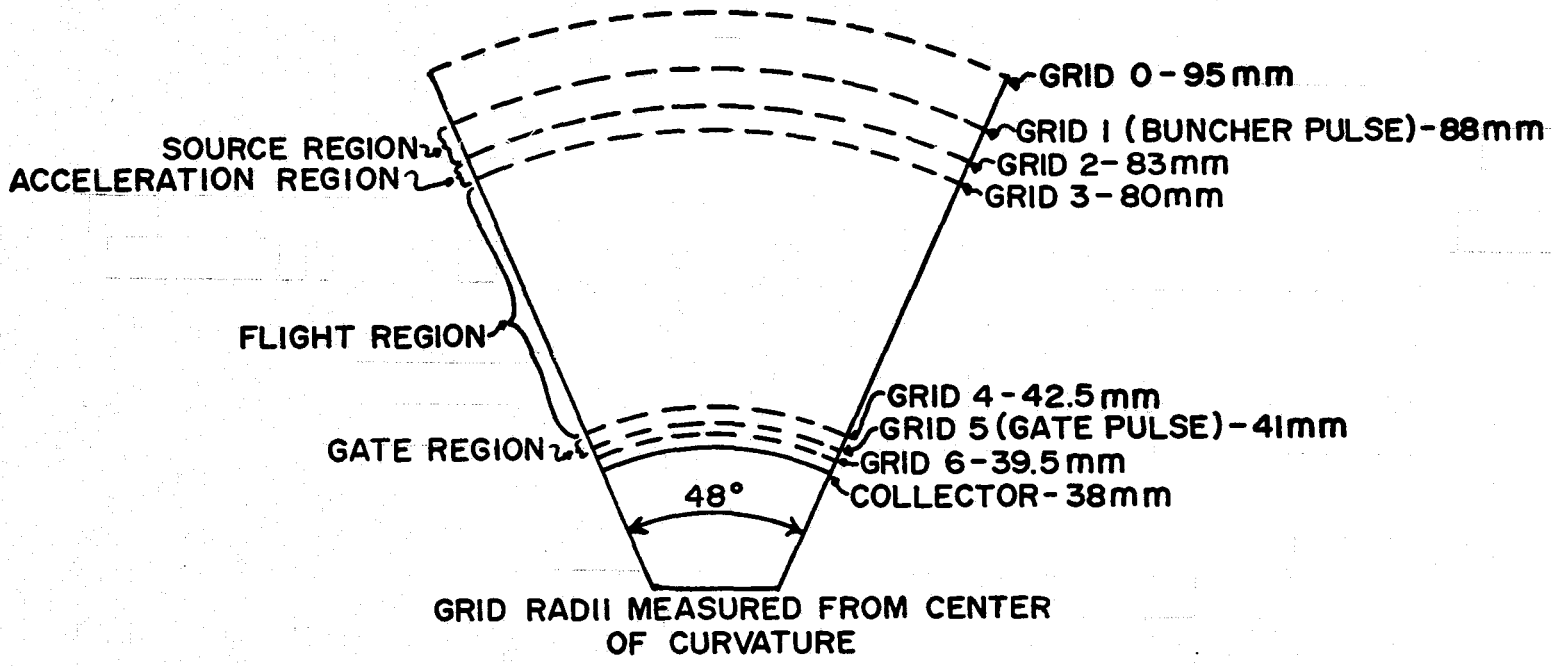

Figure 4.4 Cross-Sectional View of the Laboratory Version of the Gated Cylindrical-Electrode TOFMS.

spectrometer and to isolate the surrounding medium from the voltage pulses inside the mass spectrometer. The bunching pulse, with positive amplitude V_1, is applied to grid 1. The dc potential applied to grid 1 is usually V_0 (the same as the potential on grid 0). A dc potential, V_2, is applied to grid 2. Grid 3 carries the ion acceleration voltage, V_3. Grids 4 and 6 are also set at V_3. Grid 5 carries the dc barrier potential, V_5, and the gate pulse. The collector is also at V_3. All potentials can be varied independently. The interelectrode spacings are fixed. The electrodes were made from nickel wire mesh with 80 lines per inch and individual wire diameters of 1 mil. The grid transparency was about 89 per cent.

The electronics for the production of the voltages for this mass spectrometer were contained in a single controller built to the specifications of Dr. B. R. F. Kendall by the Electronic Services Group of the Electrical Engineering Department of The Pennsylvania State University. The controller was based on the designs of Hazelton (1968), Barnes (1971) and Zabielski (1970). Modifications were made on the controller by myself at a later date. The buncher pulse and gate pulse widths were fixed by the original controller design. A typical buncher pulse is shown in Figure (4.5). A typical gate pulse has already been illustrated in Chapter III. The gate pulse delay time could be varied at fixed scan rates of 20 Hz, .5 Hz, and .1 Hz. A manual scan was also possible.

Several electrometers were used during the study of this mass spectrometer. The first was a linear electrometer with four gain settings based on a Keithly 302 commercial electrometer. This

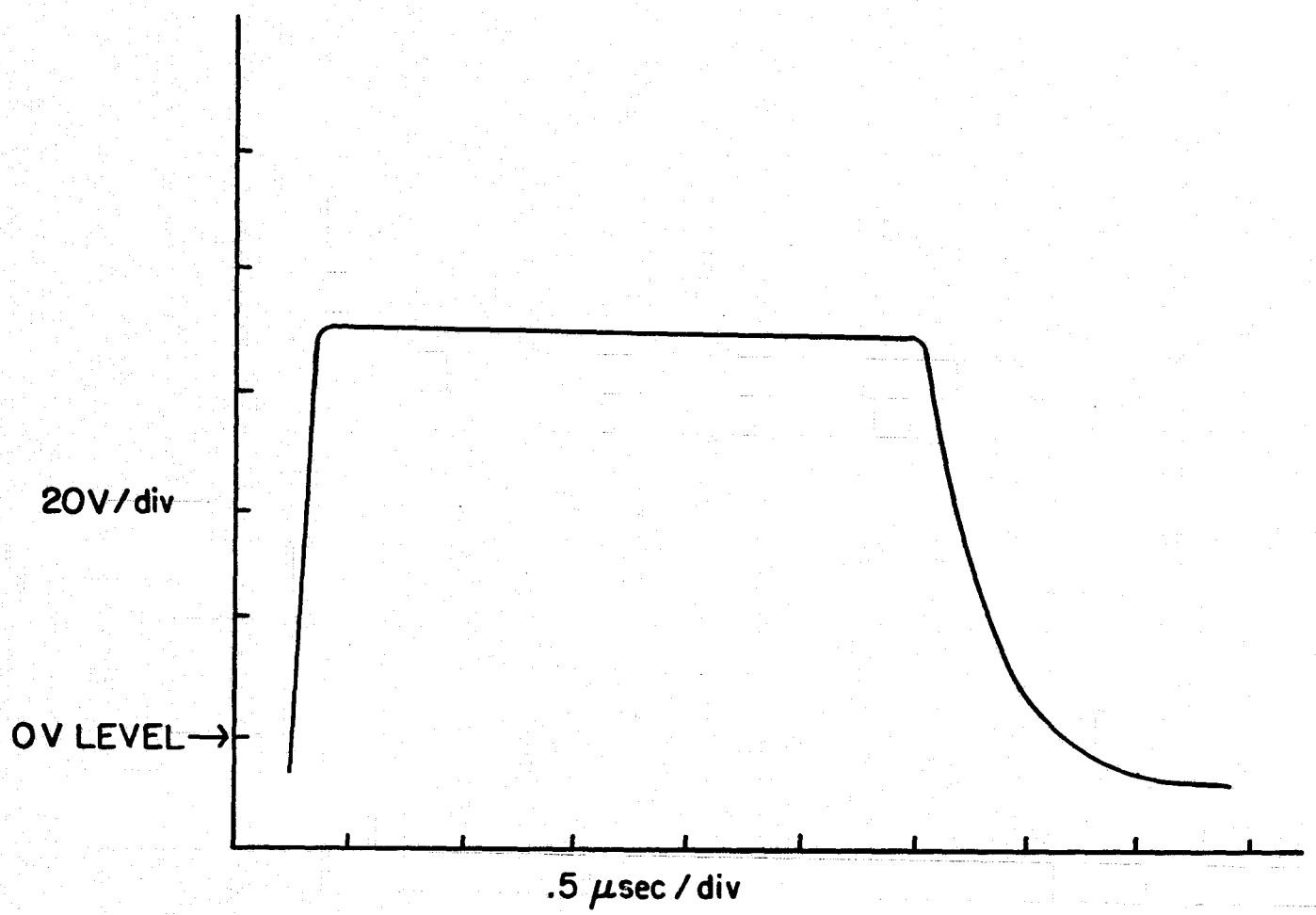

Figure 4.5 A Typical Buncher Pulse Used in the Cylindrical-Electrode TOFMS.

electrometer circuit is shown in Figure (4.6). The frequency response of this electrometer was about 100 Hz at the lowest gain setting. The second electrometer was a logarithmic electrometer, based on an Intersil 8500A commercial electrometer, designed by Locus, Inc. of State College, Pennsylvania. The frequency response of this electrometer was better than 1 kHz at the currents of interest. The third electrometer was a Keithley 610B vacuum tube electrometer. This electrometer could only be used with the manual gate sweep because of its extremely low frequency response (less than 1 Hz). Extraneous microphonic noise caused by pump vibration was a constant problem in making noise-free current measurements. The vacuum system backing pump could be shut down for short periods and a liquid nitrogen cooled zeolite pump used in its place. When this method was inconvenient, a signal averager (a Princeton Applied Research Waveform Eductor) was used. Care was needed when using the logarithmic electrometer with the signal averager since amplitude measurements could be misleading in this situation.

4.2.2 Ion Flight Times and Mass Spectrum Characteristics

Experimental flight time calibrations were obtained for a number of mass spectrometer operating conditions. A representative example is shown in Figure (4.7). The mass spectrometer operating voltages can be deduced from the buncher pulse positive amplitude, V_1, and the voltage ratio, $R = V_1 - V_3/V_2 - V_3$. The gate barrier was 155 V (V_5 = 85 V and V_3 = -70 V) and the gate pulse amplitude was typically 100 V. The $m^{1/2}$ dependence of the flight times can be seen easily. A typical mass spectrum obtained by using the

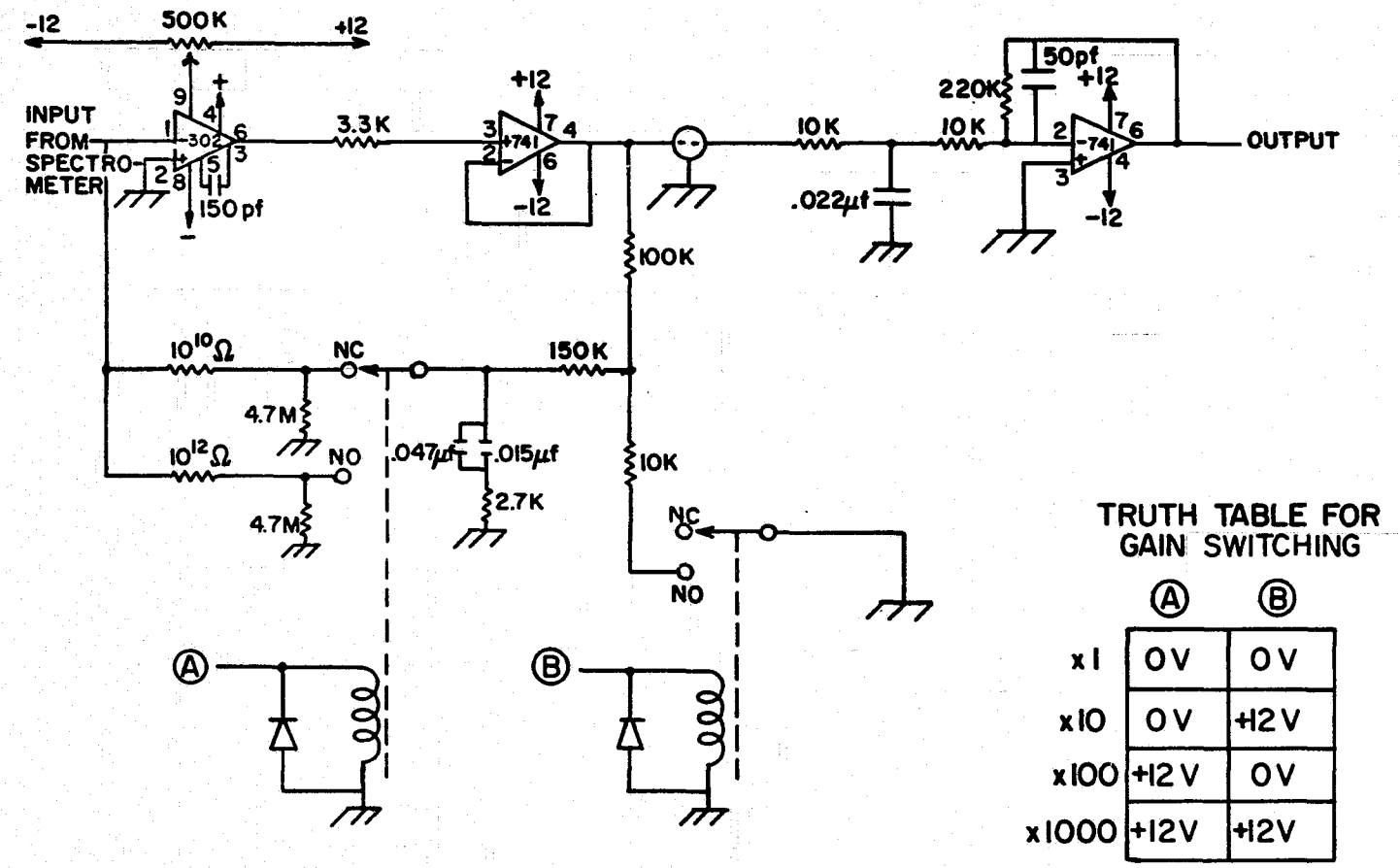

TRUTH TABLE FOR GAIN SWITCHING

	A	B
x1	0V	0V
x10	0V	+12V
x100	+12V	0V
x1000	+12V	+12V

Figure 4.6 Linear Electrometer Circuit Based on a Keithley 302 Commercial Electrometer.

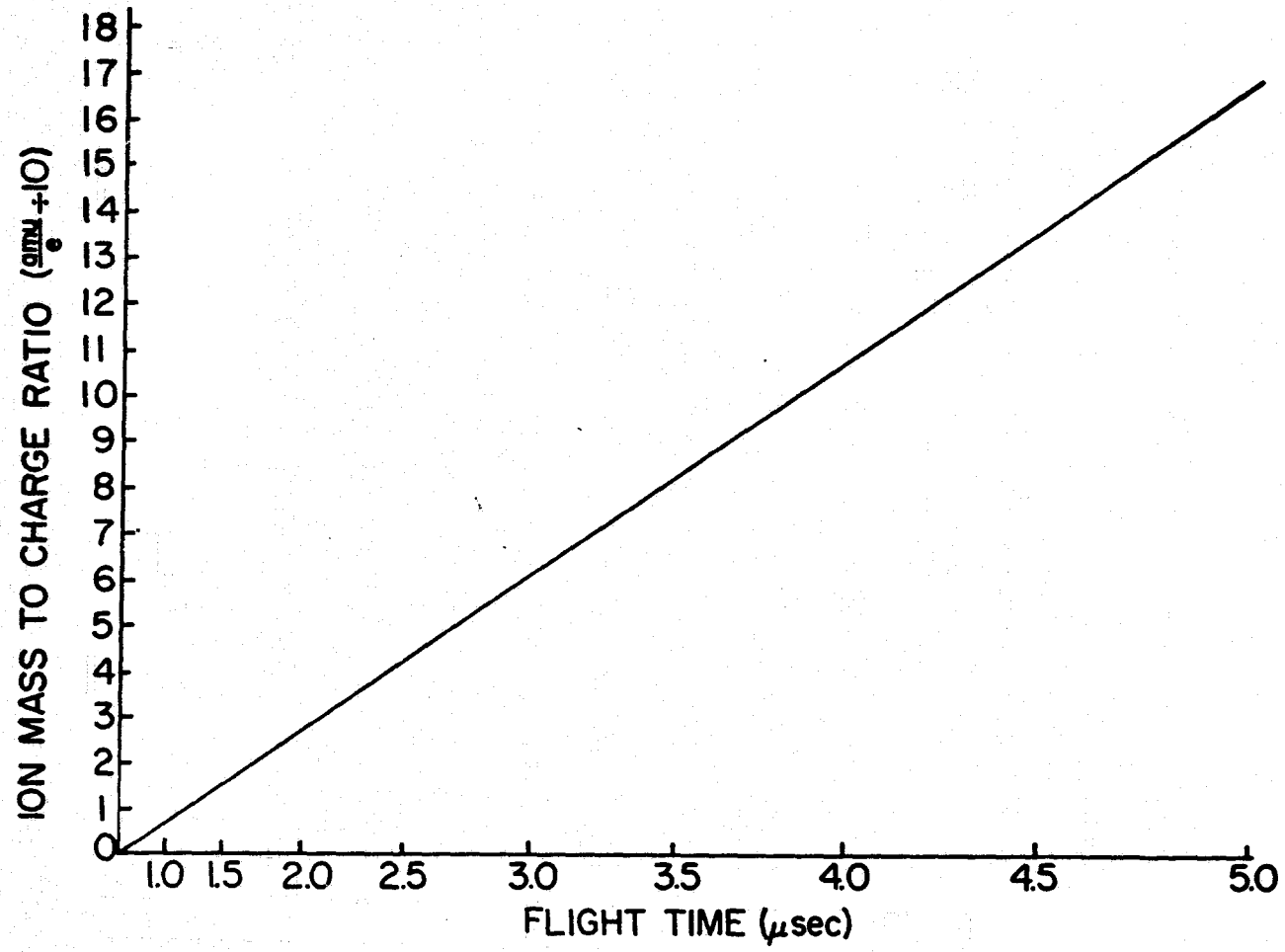

Figure 4.7 Experimental Ion Flight Time as a Function of Ion Mass-to-Charge Ratio.

surface ionization source is shown in Figure (4.8). The resolving power ($m/\Delta m = t/2\Delta t$) was 5.9 at Na^+ (23), 6.5 at K^+ (39, 41) and 9.4 at Cs^+ (133). The voltage ratio was 2.30. This voltage ratio was higher than the theoretical ratio for optimum space focusing to offset the effect of the initial ion energy spread. The variation in resolving power with mass is thought to be due to the operation of the gate and to the finite rise time of the buncher pulse. The improvement in resolving power over the results reported by Zabielski is due to improved electrometer frequency response and buncher pulse rise time characteristics (typically 10 nsec).

4.2.3 High Pressure Operation

Measurements of the mass spectrometer sensitivity at high pressure have been reported by both Diem (1967) and Zabielski (1970). However, these measurements were taken using a thermocouple pressure gauge to measure the pressure from 6.67×10^{-2} pa to 6.67 pa. A thermocouple gauge is not particularly accurate over this pressure range and requires constant calibration. The addition of a diaphragm manometer to the vacuum system used for these measurements made it possible to make extremely accurate pressure readings for sensitivity measurements. Because of this improvement in pressure accuracy, the sensitivity measurements for the cylindrical TOFMS were repeated in conjunction with the measurements of the background current ratio reported in Chapter III. The relative sensitivity as a function of pressure is shown in Figure (4.9). The sensitivity has been corrected for the distance the ions have to travel before entering the mass spectrometer. An important

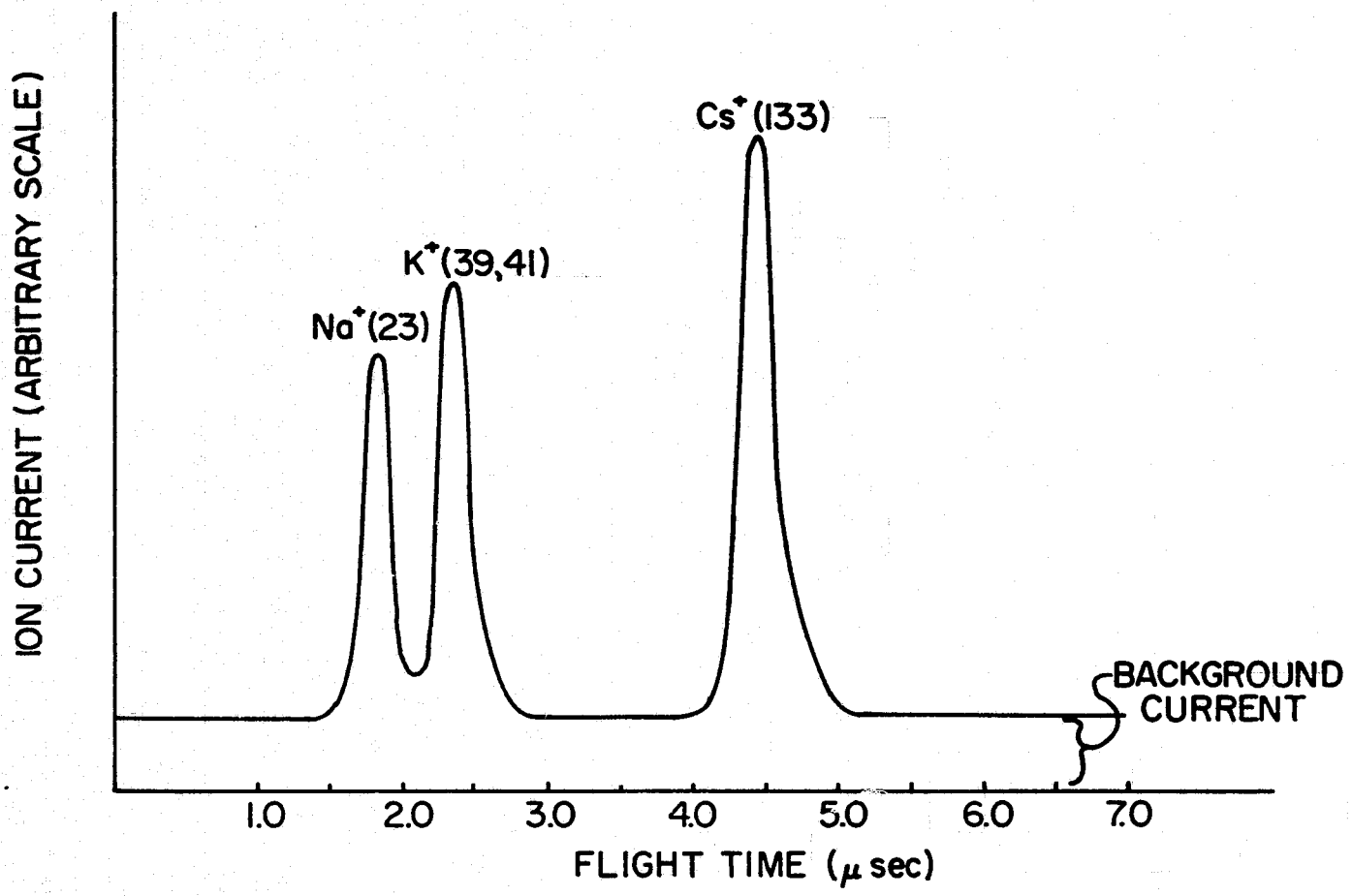

Figure 4.8 A Typical Mass Spectrum Taken with a Gated Cylindrical-Electrode TOFMS.

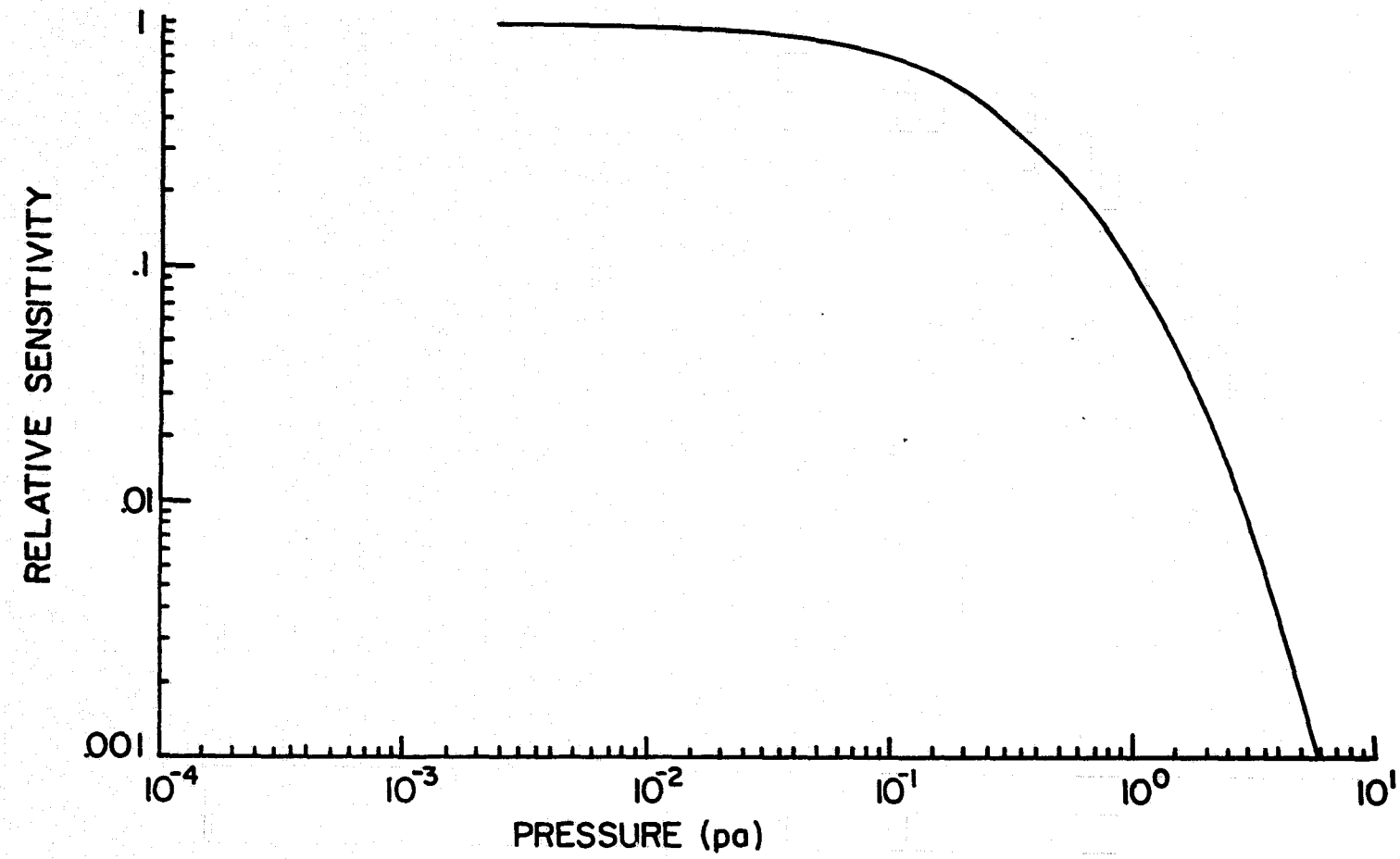

Figure 4.9 Experimentally Measured Relative Sensitivity Versus Pressure for a Gated Cylindrical-Electrode TOFMS.

observation, also reported by Zabielski (1970), was that there was no degradation in the resolving power at pressures up to 5.33 pa. This is due to the way in which a time-of-flight mass spectrometer operates. Once an ion has left the very narrow source and acceleration regions, it enters the drift region. Any ion which has its flight time altered in the drift region (due to collisions) will usually not get through the gate. Those which do undergo collisions and get through the gate will contribute to the background current instead of the proper mass peak. Therefore, it is only collisions in the source and acceleration regions which can degrade the resolving power. Above 5.33 pa the ion mean free paths become shorter than the width of the source and acceleration regions. The extremely high sensitivity of this spectrometer and the lack of resolving power degradation at high pressures makes it an excellent instrument for D-region ionosphere measurements.

4.2.4 Resolving Power Improvements; Variable Source Velocity

The numerical studies in Chapter II showed the possibility of improving the resolving power in time-of-flight mass spectrometers. A cylindrical-electrode TOFMS was used to test these studies experimentally. The principle was to make the ion velocities in the source proportional to their distance from the collector before the buncher pulse turns on. While operating in a high voltage ratio mode these ion initial velocities should make it possible to correct for the poor space focusing characteristics inherent in the high voltage ratio mode. The new ion initial velocities were produced by making

$V_2 < V_0$ while altering the other operating conditions to produce the desired voltage ratio. The results of these measurements are illustrated in Figure (4.10). The voltage difference across the source region is plotted horizontally as $\Delta V = V_0 - V_2$. The resolving power is plotted vertically. For these measurements R = 2.30 was used. The resolving power maximum occurred at a ΔV which was within the range of ΔV's predicted in Chapter II for a voltage ratio of 2.15. The difference in the voltage ratios between the computer studies in Chapter II (see Figure (2.22)) and the ratio used in this section will not make a significant difference in this discussion. The effect in Figure (4.10) which does not agree with computer results in Chapter II is the immediate decrease in the resolving power for ΔV's greater than the ΔV corresponding to the maximum resolving power. There should be a broad range of ΔV's, from $\Delta V \cong 25$ V to $\Delta V \cong 35$ V, where the resolving power is maximized. The resolving power decrease for $\Delta V > 25$ V can be easily explained when computer studies of gating in TOFMS in Chapter III are considered (see Figure (3.4)). Only ions starting in the outer half (approximately) of the source when the buncher pulse is turned on are collected for Cs^+ (133). Therefore, when the minimum in the flight time curves (Figure (2.22)) moves inward toward r_2 (as V_2 is made more negative) and passes the center of the source region, the resolving power should decrease rapidly. The behavior of the K^+ (39, 41) resolving power curve should exhibit a broader resolving power maximum and a slower resolving power decrease above the optimum ΔV values because gating will discriminate

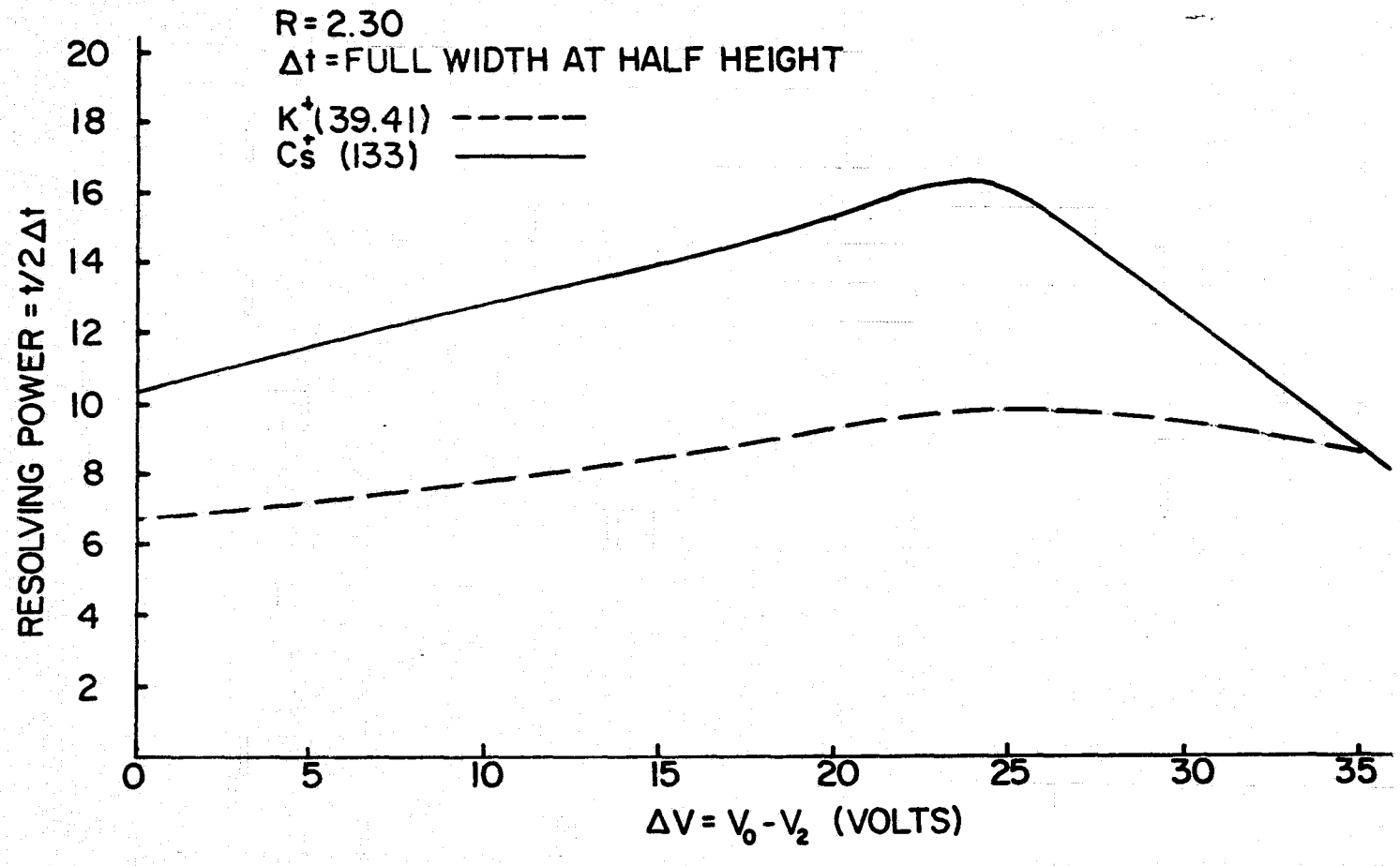

Figure 4.10 Experimentally Measured Resolving Power Versus the Voltage Difference Across the Source Region for a Gated Cylindrical-Electrode TOFMS.

against only the innermost source starting positions. This is, in fact, the behavior which is observed in Figure (4.10). This discussion shows that the computer simulations of Chapter II and Chapter III can be combined to accurately explain the experimental measurements with a gated cylindrical-electrode TOFMS.

A resolving power maximum of 21 for Cs^+ (133) had been obtained at a slightly lower voltage ratio (R = 2.03) in other studies using source position dependent initial ion velocities.

4.3 Hemispherical-Electrode Two-Field TOFMS

4.3.1 Instrument Dimensions and Electronics

The theoretical calculations carried out in Chapter II were for a spherical-electrode TOFMS. In order to experimentally test the results of Zabielski (1970), Zabielski, Stein and Kendall (1972/1973), Stein (1974) and myself, it was decided to use a TOFMS constructed with hemispherical electrodes because the construction of hemispherical electrodes was thought to be simpler (than spherical electrodes) and could be accomplished quickly. It also simplified the proper spacing of the electrodes. The hemispherical TOFMS used for these measurements is shown in Figure (4.11). The effects of fringing fields were bypassed by taking care that ions entered the spectrometer at the center of the outer electrode. This was accomplished by injecting the ions through a cover which had a hole at the center. This cover was maintained at the same potential as the outermost spectrometer grid before the buncher pulse was applied. Ion detection was made using a 16 stage venetian blind

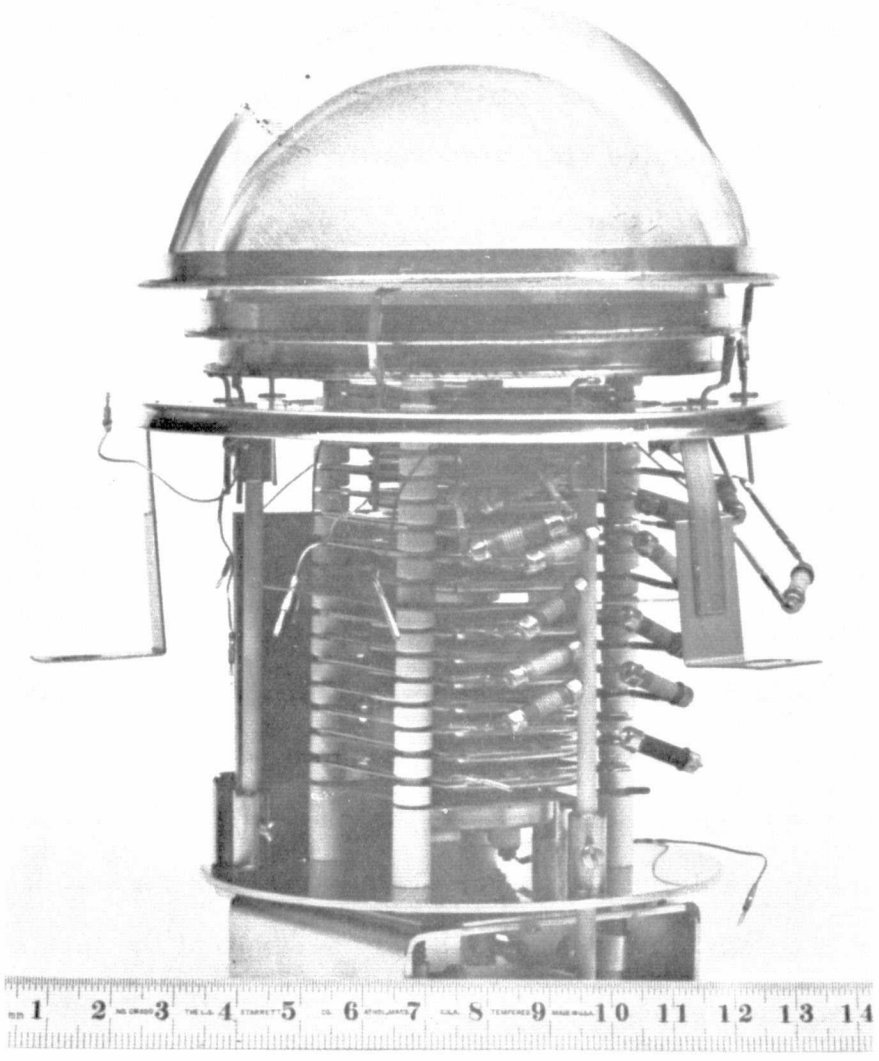

Figure 4.11 Hemispherical-Electrode TOFMS. A 16 Stage Electron Multiplier Used for Ion Detection is Shown.

electron multiplier with unactivated Be-Cu dynodes. The spectrometer cover also performed the same task as grid 0 did for the cylindrical TOFMS. The associated electronics and spectrometer grid spacings are shown in Figure (4.12). The hemispherical TOFMS did not use any form of gating. Because a commercial pulse generator was used for these studies, the buncher pulse rise time was considerably longer than the cylindrical TOFMS buncher pulse rise time. The buncher pulse rise time was typically 150 nsec in the hemispherical TOFMS studies.

4.3.2 Ion Flight Times and Mass Spectrum Characteristics

A composite mass spectrum is shown in Figure (4.13). This mass spectrum illustrates a number of characteristics which might not be visible on any one mass spectrum. The ion mass peaks represent Na^+ (23), K^+ (39, 41) and Cs^+ (133). The resolving power at these particular mass peaks are 8.2 at Na^+ (23), 9.2 at K^+ (39, 41) and 10.1 at Cs^+ (133). The significantly lower resolving power at the lower ion masses is thought to be due to the relatively long rise time of the buncher pulse. Another important observation is the smaller resolving power variation with mass than in the cylindrical TOFMS. This is undoubtedly because of the lack of gating in the hemispherical device. It is obvious that the use of gating does have a significant effect on resolving power. Also notice the overall improvement in the resolving power at all masses over the cylindrical TOFMS operating with normal voltages as reported in this thesis and by previous researchers. Some of this improvement must be due to the lack of gating. The extremely high

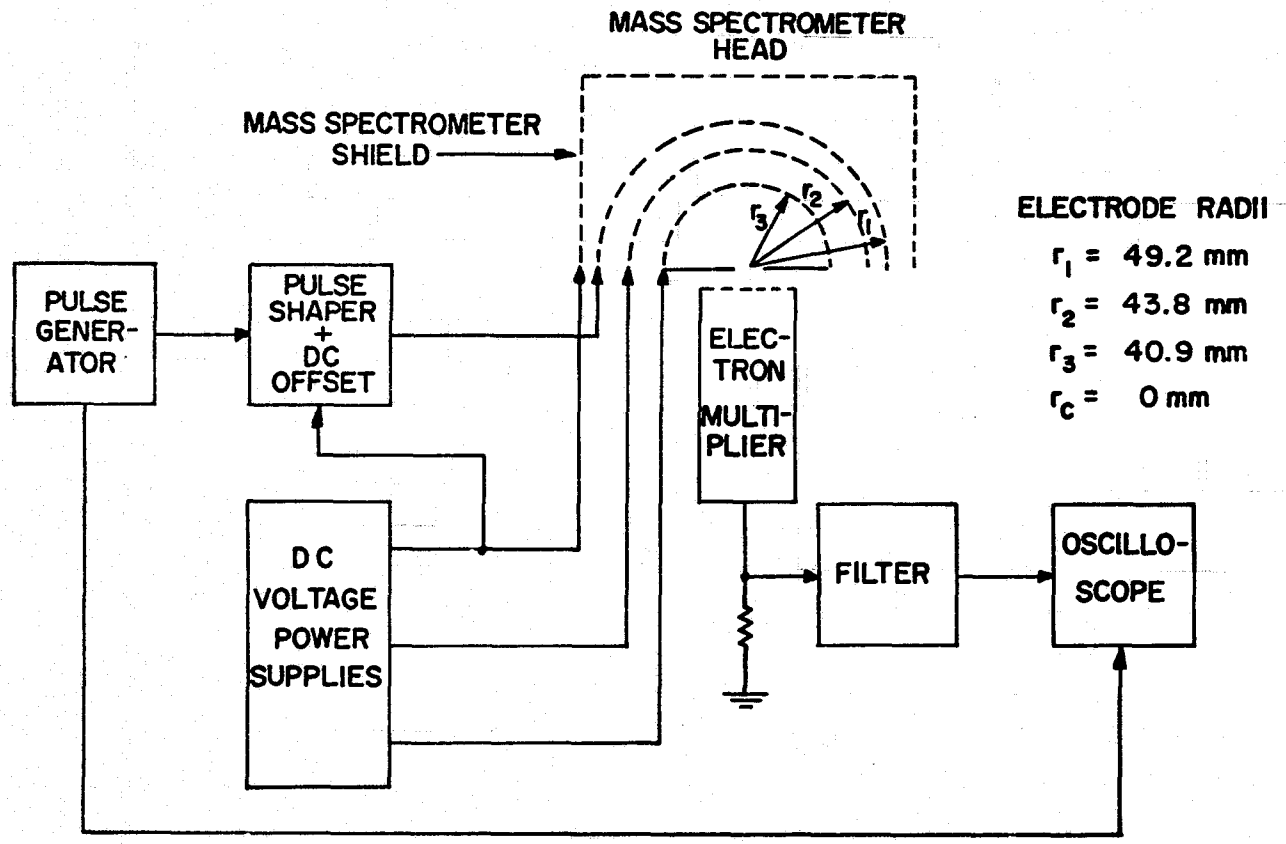

Figure 4.12 Hemispherical-Electrode TOFMS Electrode Radii and Associated Electronics.

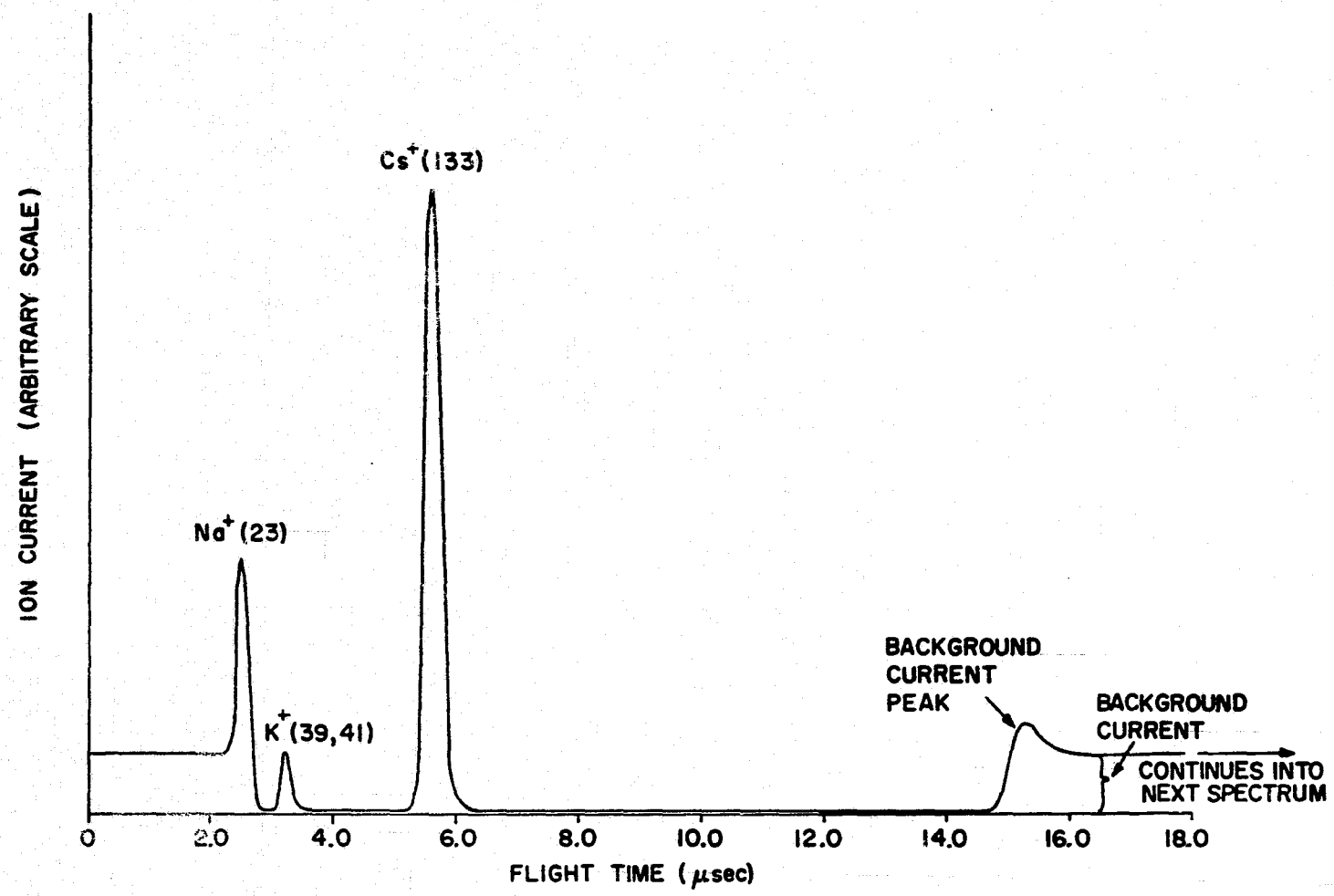

Figure 4.13 Composite Mass Spectrum for the Hemispherical-Electrode TOFMS.

frequency response of the electron multiplier might also contribute to this resolving power improvement. The finite depth of the conversion dynode of the electron multiplier could produce an ion flight time spread corresponding to as much as 17 per cent of the observed Cs^+ (133) mass peak (and a correspondingly larger amount for the lighter ion mass peaks) if the ions were not properly focused at the collector. This lack of proper focusing could easily result if the hemispherical TOFMS electrodes were improperly centered or if the electron multiplier conversion dynode was not placed in the correct position. In actual fact, an examination of the conversion dynode showed the ions had been focused onto a spot which covered only about 25 per cent of the depth of the conversion dynode.

The background current starting to the right of the Cs^+ (133) mass peak is produced by ions entering the mass spectrometer after the buncher pulse turns off. These ions pass through the source region before the next buncher pulse starts and are eventually collected. The lack of background current up to this point is due to the buncher pulse repelling ions about to enter the source. This explanation for the background current was verified by varying the width of the buncher pulse, which caused a corresponding change in the starting flight time for the background current, and by varying the spectrometer potentials, which again caused a corresponding variation in the background current starting time. One feature of the background which could not be explained immediately was the small current peak at the beginning of the background current. It was concluded that this small peak was caused by ions which were

just at the turn around point outside the spectrometer as the buncher pulse turns off. Since the current density of the ion beam from the ion source is conserved, the ion density (charge density) at the turn around point is enhanced and produces the small peak when they are eventually collected.

A best resolving power of about 13 was obtained with the hemispherical TOFMS at Cs^+ (133) with a voltage ratio of 2.46. This is the best resolving power obtained with a hemispherical spectrometer operating with the normal operating voltages. The resolving power improvement method using a variable initial source velocity has not been attempted with the hemispherical TOFMS to this date. The high voltage ratio required for best resolving power is probably due to the slightly larger source region width and the shorter drift region length combined with the large initial energy spread (see the discussion of high initial energy spreads in Stein (1974)). The smaller radii of curvature of the hemispherical-electrode TOFMS used for these studies will not make a significant difference in the resolving power compared to the cylindrical-electrode TOFMS (see the discussion of radius of curvature in Chapter II). Some of the results presented in this chapter have been previously reported by Reiter and Kendall (1974), Kendall and Reiter (1975) or were used as examples in Stein (1974).

CHAPTER V

SOUNDING ROCKET EXPERIMENT PACKAGE AND VEHICLE

5.1 Mechanical

5.1.1 Vehicle

In 1969 the initial plans for a second generation sounding rocket experiment package were discussed by Dr. Kendall, members of our research group and NASA personnel. It was decided to fly this package on a Nike-Apache two-stage sounding rocket. The mechanical configuration of the experiment package was then designed by Electronic Services (a special projects group associated with the Electrical Engineering Department of The Pennsylvania State University).

5.1.2 Experiment Package

The actual experiment package was a combination of two sections. One half of the package was made at Penn State University and contained the electronics for the instruments carried by the package. These instruments were to be a cylindrical-electrode time-of-flight mass spectrometer, three ion probes of various geometries, a thermocouple vacuum gauge and two thermistors for temperature measurement. The mass spectrometer and two of the probes were forward facing. The remaining probe and the thermocouple gauge inlet ports were facing to the side. One temperature thermistor was placed in contact with the inside of the experiment package skin while the second thermistor was placed in contact with the hottest part of

the electronics inside the experiment package. The other half of the package was made at Wallops Island, Virginia by NASA personnel. This second half of the package contained telemetry equipment, batteries, a magnetometer, solar sensors and thermistors. When both sections were combined, the complete experiment package was hermetically sealed. This was considered essential for two reasons. First, outgassing from the interior of the package would be a serious source of contamination to the measurements contemplated in the ionosphere. A discussion of this effect can be found in Kendall and Weeks (1974). Secondly, the loss of convective dissipation of heat that would be a result of a reduction in pressure around the electronic components could cause component failure. The exterior of the complete experiment package was also gold plated to reduce both outgassing effects and photoelectron emission. Figures (5.1), (5.2) and (5.3) show photographs of the Penn State portion of the experiment package.

5.1.3 Mass Spectrometer Vacuum Cap

A vacuum cap made of bare aluminum was designed to be placed over the front end of the experiment package, covering the mass spectrometer, the two forward facing ion probes and the inlet ports to the thermocouple gauge. The purpose of this cap was to keep the enclosed instruments, and the front end of the package in general, under partial vacuum until the payload (the complete experiment package will be called the payload) was ejected into the ionosphere and began taking measurements. The volume under this cap was to

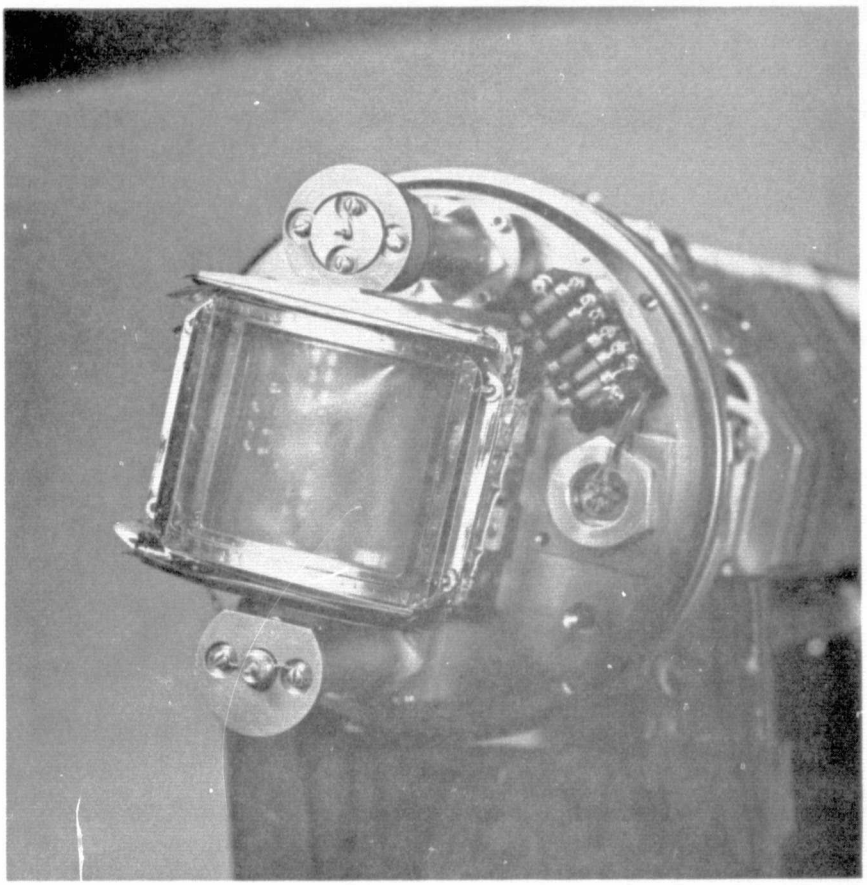

Figure 5.1 Front View of the Nike-Apache Experiment Package Showing the Cylindrical-Electrode TOFMS and Two Ion Probes.

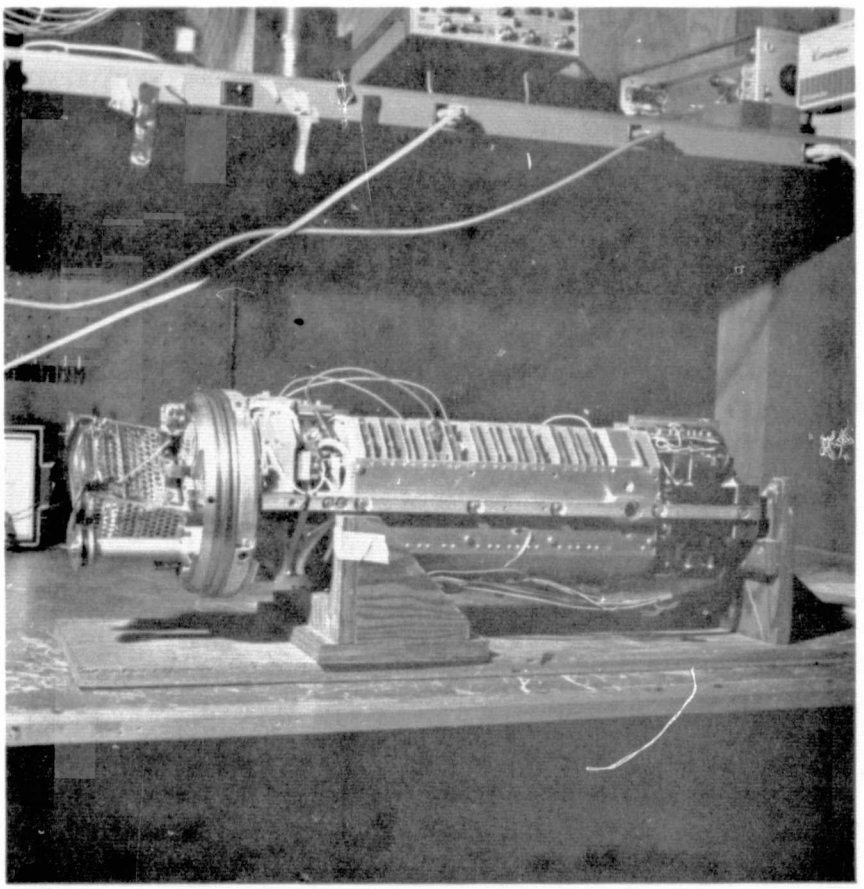

Figure 5.2 Side View of the Nike-Apache Experiment Package Showing the Arrangement of the Electronics.

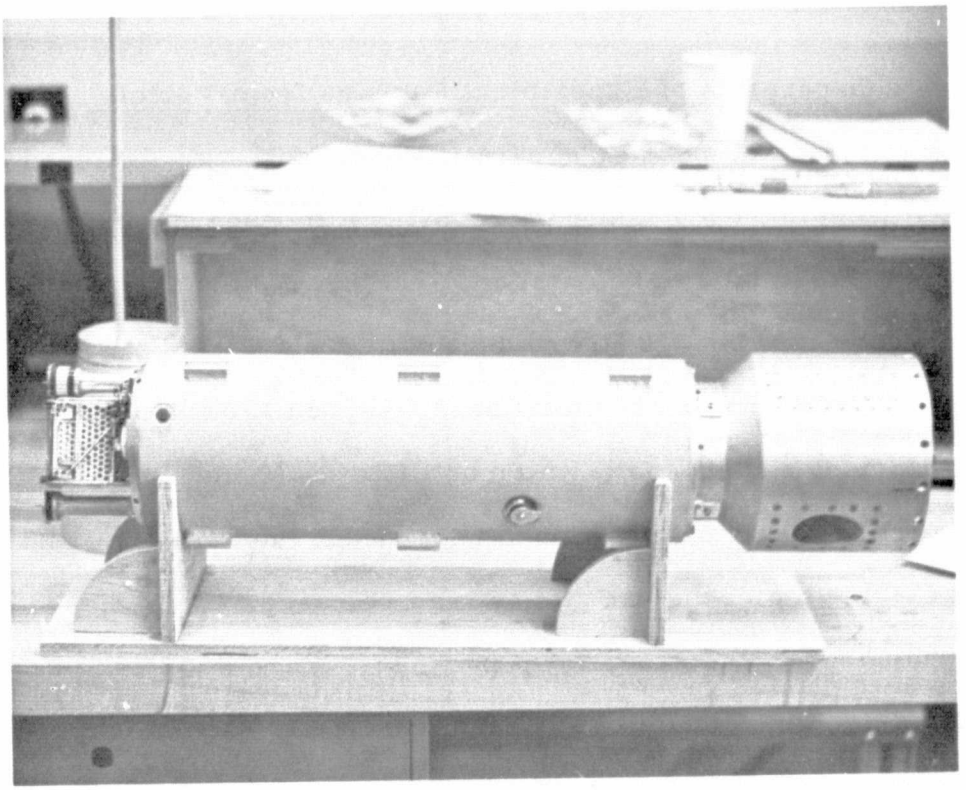

Figure 5.3 Side View of the Nike-Apache Experiment Package in the Outer Skin Showing the Side Probe Connector. An Adapter for Shake Testing is Shown Attached to the Bottom of the Experiment Package.

be pumped for approximately 24 hours and then backfilled to near atmospheric pressure with dry Nitrogen. A pressure valve was added to the cap to keep the pressure differential to about 1.38×10^4 pa during the rocket ascent.

5.1.4 Separation of Experiment Package from Vehicle

The experiment package separation procedure was designed for minimum contamination of the surrounding atmosphere. The separation takes place in two stages. The first stage starts when a sealed pyrotechnic charge fires a bolt cutter which cuts a bolt holding a V-band (a flexible metal band wrapped around a joint and held in place by a metal bolt) which holds the nose cone. The V-band flies away and a spring, positioned underneath the nose cone and attached to the top of the vacuum cap, is released. This pushes the nose cone ahead of the experiment package. When the spring reaches full extension, the vacuum cap is also jerked off. All the experiment package instruments are exposed at this time. However, the package is still resting in a short sleeve attached to the second stage motor. After the first stage of the payload ejection, the experiment package is no longer directly attached to the rocket motor. The second stage of the payload ejection takes place at this time. A second sealed pyrotechnic charge fires a second bolt cutter. This releases an air spring, located beneath the experiment package, which has been pumped out and then backfilled to about 1.03×10^5 pa with dry Nitrogen. The piston of the spring then pushes the experiment package out of the sleeve on Teflon skids. A strap is attached to the

piston to keep it from escaping. The experiment package is then completely separated from the rocket motor and nose cone and follows its own trajectory. See Figure (5.4) for a diagram of the ejection sequence.

The pyrotechnic charges were designed to be completely sealed when the charge is fired. Three versions of the charges were tested in the vacuum laboratory at The Pennsylvania State University by Dr. B. R. F. Kendall and John O. Weeks. The final version was found to have a satisfactory leak rate. The initial leakage from the successful charge was 2.00×10^{-3} pa-liters at firing and 4.44×10^{-6} pa-liters/sec thereafter.

An important design parameter was the altitude at which separation was to take place. This altitude needed to be high enough so that the dynamic forces which the mass spectrometer grids are subjected to would not tear the grids. Studies, using high speed films, were made by Dr. B. R. F. Kendall and J. O. Weeks of the reaction of the mass spectrometer grids to sudden decompression. Static pressure tests made by myself were also made. Results of these studies showed the minimum ejection altitude to be about 65 km. An ejection altitude of 70 km was decided on to include a safety factor..

5.2 Environmental Testing

5.2.1 Shake Testing

In order to qualify for launch on the Nike-Apache sounding rocket, the experiment package had to undergo several shake tests. The first shake test was with just the Penn State section of

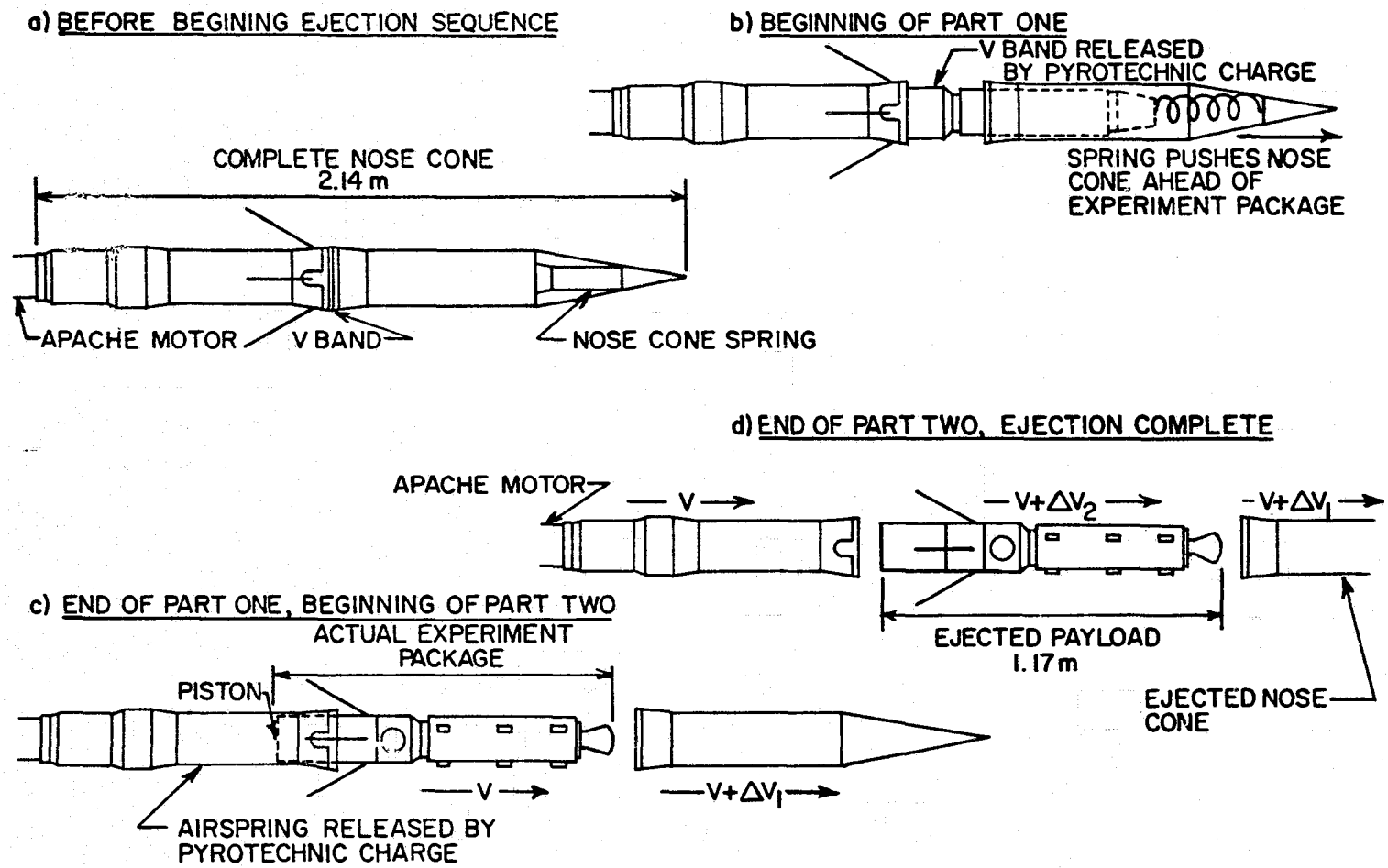

Figure 5.4 Experiment Package Ejection Sequence.

the payload. The second test was with the complete payload installed inside the nose cone. The shake tests were conducted at the Wallops Island, NASA, facility. These tests were conducted on the three axes of the payload, the thrust axis (z-z axis) and the two axes perpendicular to the thrust axis (the x-x axis and the y-y axis). The thrust axis shake tests included a low level sine-wave shake test, a simulated flight level shake test, a random noise shake test, and a transient shake test (to simulate the shock of a Nike booster ignition). The shake tests for the other axes included a low level sine-wave shake test, a simulated flight level shake test, and a random noise shake test. The details of the simulated flight level shake tests are shown in Table (5.1).

The experiment package electronics and telemetry were run during all the shake tests to monitor the behavior of the payload instruments. The electrometer outputs showed severe microphonic effects during the actual shake tests but this was not considered important to the operation of the electronics after payload ejection.

5.2.2 Payload Weight, Center of Gravity, Pitch and Roll Moments

In order to accurately determine the altitude to be attained by the payload and the precise trajectory to be followed by the payload and the nose cone after ejection, the weight and center of gravity of the complete payload had to be determined. The payload weight of the complete experiment package was 23 kg. The center of gravity was found to be 50.3 cm from the rear of the combined experiment package (the total package length was about 117 cm).

Table 5.1: Shake Test Parameters for the Nike-Apache Experiment Package

Axis	Frequency	g Level or Displacement	Sweep Rate
Z-Z (Thrust)	10-120 Hz	3g	4 octaves/min
	120-200 Hz	10g	
	200-350 Hz	20g	
	350-2000 Hz	5g	
X-X and Y-Y (Lateral)	7-11 Hz	1.02 mm	4 octaves / min
	11-20 Hz	0.508 mm	
	20-30 Hz	0.203 mm	
	30-40 Hz	0.408 mm	
	40-120 Hz	0.06 mm	
	120-200 Hz	0.0187 mm	

note: Lateral g levels were limited to 30g's at the center of gravity.

Two other important parameters to the payload trajectory are the pitch and roll moments of the payload. These were measured at the same time as the center of gravity.

5.2.3 Spin Test

A dynamic spin test of the experiment package and the complete payload and nose cone assembly was carried out to determine the dynamic stability. The stability was found to be such that it would produce a 2^{o} - 3^{o} coning angle for the experiment package from after payload ejection until the payload reaches about 70 km on the downleg.

The behavior of the experiment package electronics were monitored during the spin test to determine the effect of the projected spin rate. The outputs of the electronics showed severe microphonic effects. This was considered more important than the microphonics caused by the shake tests since the experiment package would be spinning throughout the flight.

After a careful analysis for possible reasons for the severity of the microphonics, it was found to be caused by the slight instability of the experiment package acting through the fixed base of the spin table to cause vibration. Since the base of the experiment package would not be fixed after it was ejected from the rocket motor, this effect would not be important. However, it was decided to apply a potting compound to the sensitive electronics in any future experiment packages. Microphonic noise was found to be negligible during the actual flight after the second stage rocket motor stopped

firing. It decreased even further once the atmospheric pressure had decreased to the point where the experiment package trajectory was ballistic.

5.2.4 Outgassing and Ion Collection Tests

A special vacuum chamber which could hold the entire experiment package was built to study the outgassing from the surface of the package and any leakage from the interior of the package. A surface ionization ion source was included so to be able to check ion collection of the mass spectrometer and ion probes.

The results of several measurements show the outgas/leak rate of the clean, complete experiment package to range between 5.2×10^{-2} pa-liters/sec and 1.6×10^{-1} pa-liters/sec. The spread in the outgas/leak rate is due to the cleaning and handling methods for the experiment package.

Ion collection by the mass spectrometer and the ion probes was confirmed by using the ion source in this vacuum chamber. The telemetry operation was tested at this time to compare the data outputs with previous results hard wired out of the experiment package.

5.3 Experiment Package Electronics

5.3.1 Determination of Mass Spectrometer Repetition Frequency and Electrometer Requirements

The volume of the pulsing region of the flight version of the cylindrical-electrode mass spectrometer is 16.34 cm^3. The fill time of this pulsing region is dependent on the ion draw-in potential, the

vehicle velocity and the experiment package angle-of-attack (defined as the angle between the package velocity vector and the package spin axis). The fill time for the minimum vehicle speed ($\sim$300 m/sec), smallest draw-in voltage (-5 V) and maximum angle of attack is about 5 μ sec for 500 amu ions (this is the worst possible case and would never be found in flight). To analyze heavy ions up to 500 amu in this mass spectrometer, a sufficiently long initial pulse width needs to be selected. A pulse width of 3 μ sec was calculated to be more than sufficient. The total mass sweep time would then be 8 μ seconds. A repetition frequency of 90 kHz was selected for the sounding rocket flight.

The dominant fill mechanism for up to 500 amu ions will be the draw-in potential at all times after payload ejection until the experiment package reaches about 50 km on the downleg. At the lowest draw-in potential (-5 V) the radially directed ion velocity due to the draw-in potential will be at least twice the thermal and ram filling velocity contributions at altitudes above 70 km.

Calculations of the total ion concentration for any measured ion peak can be made, assuming the source region is completely filled. If we define the sensitivity correction for the increased pressure behind the vehicle shock wave as S, the correction for grid transparency as T, and t_s as the length, in time, of each mass spectrum then for a measured ion current, in a mass peak, I;

$$n = \frac{S \times T \times I \times t_s}{(16.34 \text{ cm}^3)(1.6 \times 10^{-19} \text{ coul/ion})} \qquad (5.1)$$

S and T are dimensionless constants, I is in amperes, and t_s is in seconds. Singly charged ions are assumed.

For example, suppose the peak ion current for NO^+ at 85 km is measured to be 3.0×10^{-11} a and t_s is 11.1×10^{-6} seconds. S can be found from the pressure vs. sensitivity curve discussed earlier in this thesis. At 85 km the ambient pressure is about .333 pa. The pressure behind a normal detached shock wave calculated for this experiment package will be 6.19 pa (see Cuirle (1976)). This corresponds to $S \cong 75$, where S is the inverse of the relative sensitivity. For 90 per cent transparency grids T = 1.69, where T is the inverse of the transmission fraction for the spectrometer when all the grids are considered. Substituting these values into equation (5.1) yields $n = 1.61 \times 10^4$ ions/cm^3.

The minimum detectable current for the mass spectrometer electrometer was originally set for 1×10^{-13} a. However, because of difficulties with oscillations, the minimum detectable current was altered to 3×10^{-13} a. The original calculations of Zabielski showed that a current of 3×10^{-13} a would give a sensitivity of about 150 ions/cm^3 at 75 km and 6 ions/cm^3 at 90 km for an 8.9 cm diameter blunt nosed cylinder travelling at Mach 1.5. Recently revised pressure enhancement calculations by Cuirle (1976) for a 15 cm diameter blunt nosed payload travelling at about Mach 3 show that 3×10^{-13} a would correspond to a sensitivity of about 215 ions/cm^3 for NO^+ at 90 km. The revised sensitivity versus pressure data will be discussed in greater detail in the next chapter.

5.3.2 Mass Spectrometer Stepping Ground

In order to study the effect of a varied potential gradient used to draw ions into the mass spectrometer, the ground to which all the mass spectrometer voltages were referenced was stepped from +3 V to +1 V to -1 V to -3 V. The mass spectrometer was run at each offset level for one second before shifting to the next offset level. Hopefully, the study of the effects of these various offset levels superimposed on the dc draw-in potential on the pulse terminator grid will shed some light on chemical reactions that might be induced by the draw-in potential.

5.3.3 Potential on the Pulse Terminator Grid

The dc potential on this grid shields the surrounding plasma from the pulses inside the mass spectrometer and acts as the ion draw-in grid. This grid is called grid 0 because it is not essential to the mass spectrometer operation. The potential was set at -8 V with respect to the mass spectrometer offset ground. With respect to the payload skin, this voltage will step from -5 V to -11 V.

5.3.4 Potential on the Pulsed Grid and Grid 2

The dc potential of the pulsed grid, which will be called grid 1, was set at -7 V with respect to the mass spectrometer ground. This potential produces a nearly field-free region between grid 0, grid 1 and grid 2 when the pulse is not applied to grid 1. This reduces the possibility of electric field induced chemical events occurring in this region. The dc potential of the third grid, called grid 2, was set at -8 V.

The performance of the mass spectrometer is very dependent on the energy spread of the ions in the source region. The -8 V dc potential on grid 2 can produce an ion energy spread in the source up to 5eV to 11eV (depending on the mass spectrometer offset ground). This initial energy spread requires the operating voltages of the spectrometer be set for better velocity focusing. This means a larger pulse voltage will be required than for optimum space focusing. A positive pulse amplitude, applied to grid 1, of 72 V with respect to the offset ground (from now on all mass spectrometer voltages will be referenced to the offset ground) was decided on as the optimum voltage. The energy spread in the source region could be lowered by lowering the dc potentials on grids 0, 1 and 2. There were two reasons for choosing the dc potentials that were actually used. First, the effect of larger draw-in potentials was of interest and this required draw-in voltages of -10 V or larger (more negative). Secondly, there was a possibility of the payload skin swinging positive with respect to the surrounding plasma. This necessitated a draw-in potential at least several volts negative. As a compromise between these two requirements, the flight voltages were decided on.

5.3.5 Remaining DC Potentials and the Gate Pulse Height and Width

The potential of the fourth grid, called grid 3, was set at -70 V. This voltage was a result of the need to produce the proper velocity focusing characteristics and to give ions a reasonably fast flight time in order to measure ions up to 500 amu. Grid 4 (the fifth

actual grid) defines the beginning of the gate region. The potential on this grid is common to the sides of the drift region (between grids 3 and 4) and grid 3. Grid 4 shields the drift region from the gate pulse. The gate dc potential was set to + 85 V (grid 5) with gate pulse amplitude at about 100 V. The base width of the gate pulse was set at about 110 nsec. The grid terminating the gate region (grid 6) was common with the sides of the mass spectrometer inner shield and was at -70 V. In future experiment packages this grid will be set at a slightly more negative potential and isolated from the sides of the wedge in order to suppress secondary electron emission from the collector. Finally, the collector was set at -70 V. The collector was gold plated to reduce possible photoemission effects.

The gate pulse was swept from .8 μsec to 8.7 μsec which sweeps over a mass range of 7 amu to 500 amu. This scan occurred twice in a one second interval. One scan was over a .95 sec interval and a fast retrace occurred in .05 sec. The slower sweep was from light to heavier ions; the fast retrace was from heavier to lighter ions.

5.3.6 Spectrometer Shields

A shield was placed around the mass spectrometer in order to prevent the spectrometer sides and bottom from being exposed to the plasma. This shield was held at the mass spectrometer offset ground (it steps from +3 V to -3 V with respect to the payload skin). This outer shield had a number of holes cut in it to allow the ambient atmosphere to flow through part of the mass spectrometer.

An inner shield at -70 V with respect to the offset ground was placed inside the shield at the offset ground. This inner shield covered the mass spectrometer from grid 3 to the collector.

5.3.7 Summary of Flight Mass Spectrometer Voltages

A listing of the flight voltages is shown in Figure (5.5).

5.3.8 Payload Electronics

Figure (5.6) shows a block diagram of the mass spectrometer electronics. The portion of Figure (5.6) showing the dc voltage buss is self-explanatory and the voltages have been discussed in the previous sections. The buncher pulse production begins by putting the output of the 1.11 MHz clock through the $\div$ 10 multivibrator. The output of this multivibrator is then used to trigger the buncher multivibrator after passing through a delay window. The delay window produces a trigger every 11.1 μsec. The buncher multivibrator is set to produce a pulse width of 3 μsec. This pulse is then amplified and biased to the proper level and applied to grid 1. The gate pulse is produced by putting the fast and slow sweep generator outputs into a comparator. This produces a trigger pulse which occurs at varying intervals after the buncher pulse starts. This trigger pulse then triggers the gate multivibrator. The gate multivibrator produces a negative pulse with a width of about 110 nsec. This pulse is amplified by the gate pulse amplifier and biased to the proper voltage level. The pulse is then applied to grid 5.

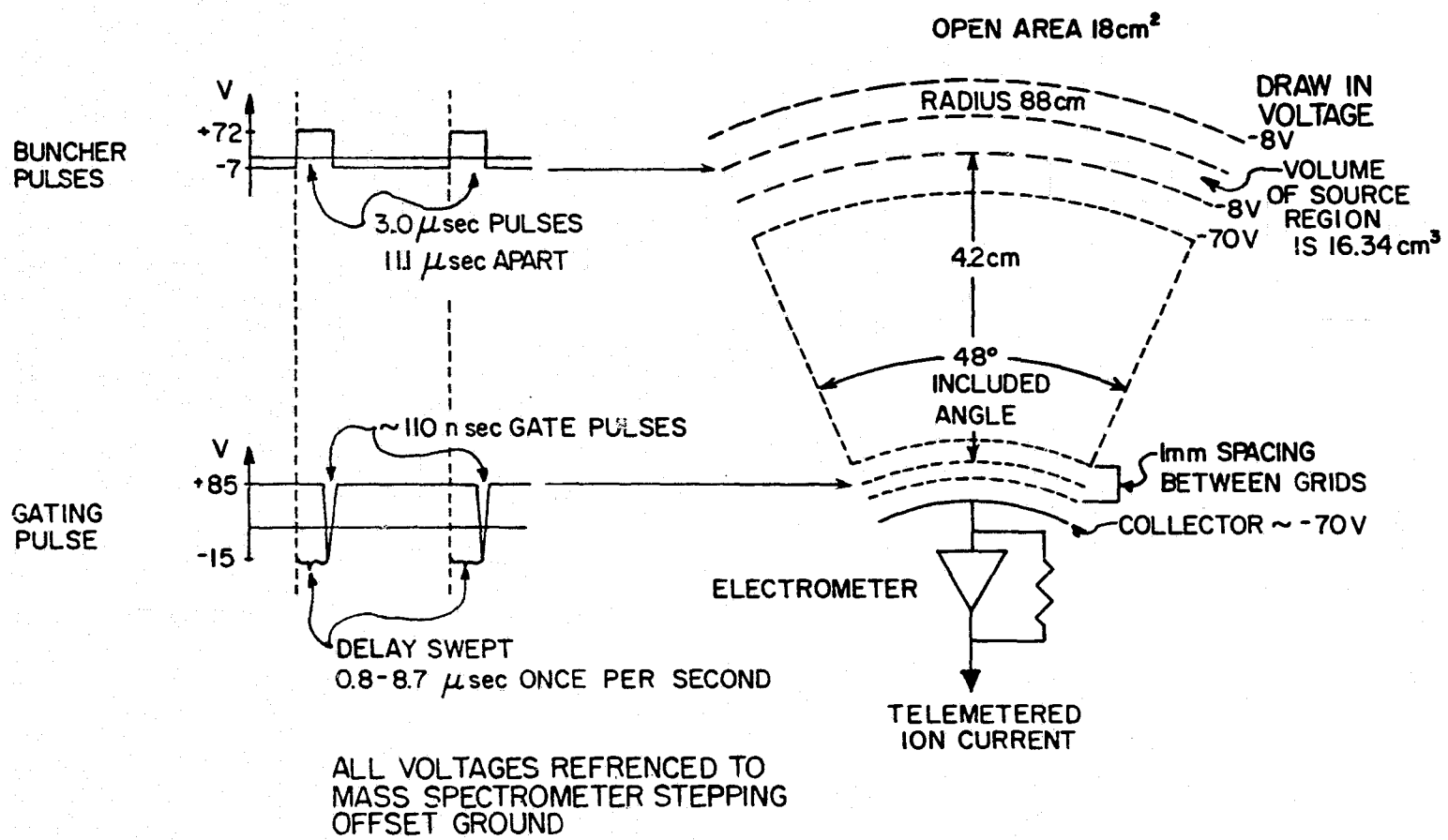

Figure 5.5 Operating Voltages for the Cylindrical-Electrode TOFMS Carried on the Experiment Package.

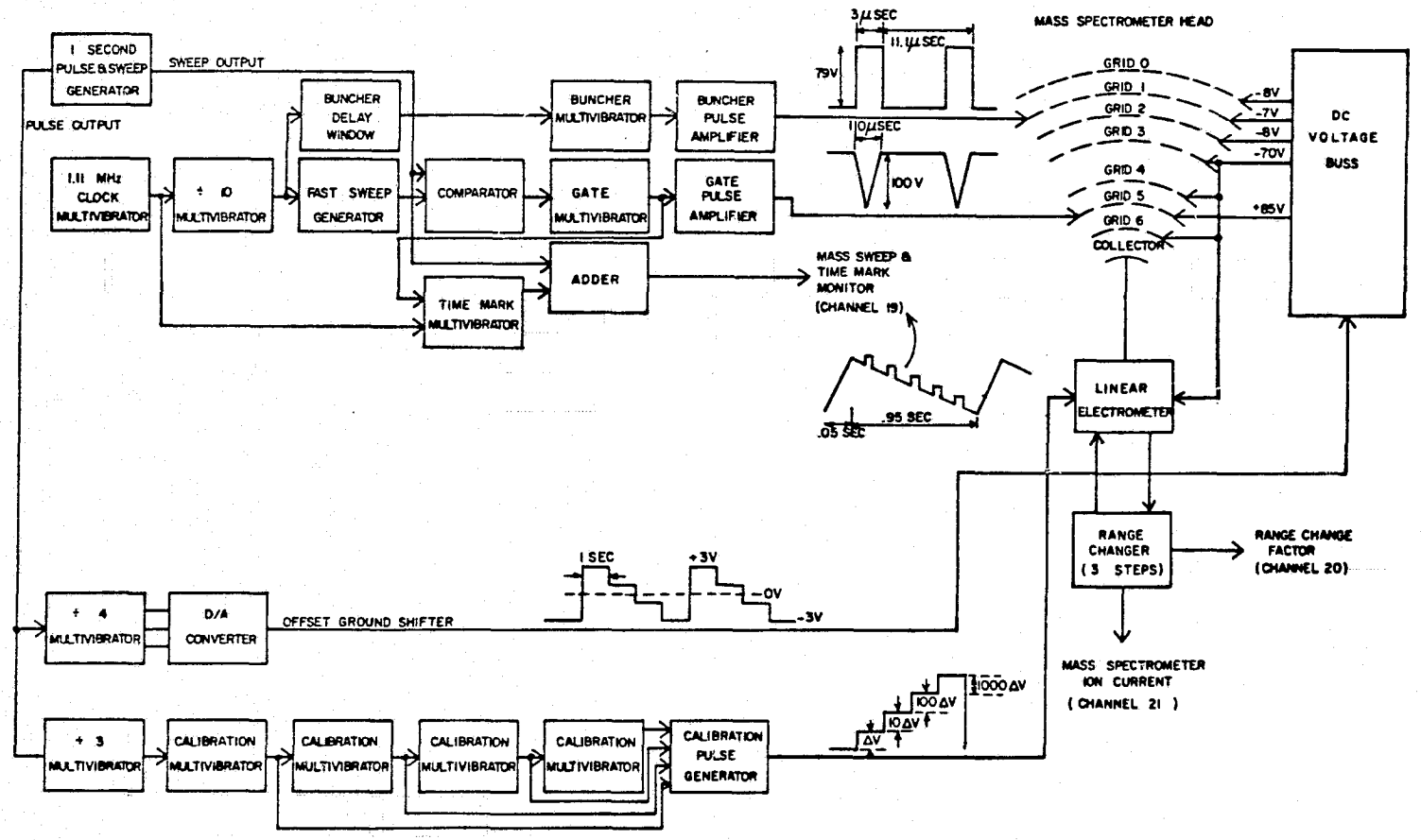

Figure 5.6 Block Diagram of the Nike-Apache Experiment Package Electronics for the Cylindrical-Electrode TOFMS.

There are a number of additional functions illustrated in Figure (5.6) which are not directly related to the mass spectrometer voltages. The first of these is the production of a signal which contains mass sweep information and timing marks for the calculation of ion flight times. The output of the slow sweep generator is a fast increasing ramp and a slow decreasing ramp. The fast ramp corresponds to the fast flyback and the slow ramp to the normal mass spectrum. The time mark multivibrator, when triggered by the 1.11 MHz clock, generates positive pulses which represent ion flight times measured from the beginning of the buncher pulse. The first time mark represents an ion flight time of 1.85 μ sec. Each succeeding time mark represents an additional flight time of .925 μ sec. The ramps and the time marks are combined in an adder.

The second function is the production of the mass spectrometer offset ground. The pulse output of the 1 second pulse generator triggers the $\div$ 4 multivibrator. The outputs of this multivibrator are combined in the D/A converter. This produces the 4 step offset ground which is then used to bias the mass spectrometer voltages and the electrometer ground.

The third function is a calibration signal which was originally designed to make it possible to determine the relationship between the electrometer output voltage and the collector current. Every third sweep the calibration signal is added to the collector current. The calibration signal was deliberately out of step with the 4 step offset ground so that the signal would not appear during mass sweeps with the same offset ground voltage throughout the flight. This

method of calibrating the electrometer was found to be inadequate because of the difficulty in determining absolute current values. However, the calibration signal was left in operation as a general check on the operation of the electrometer. The revised calibration procedure will be discussed in the Mass Spectrometer Calibration section.

The last function is the presence of an automatic gain changer which determines the gain to be applied to the electrometer signal. When the spectrometer current exceeds certain levels, the signal gain is decreased. Similarly, when the current falls below certain levels, the gain is increased. The switching levels had a hysteresis built in to prevent oscillations from occurring during a gain change (referred to as a range change). The original design was for a linear electrometer which had four range levels. However, the most sensitive range level had to be eliminated because of excessive electrometer noise. The electrometer used was a Keithley 302 commercial electrometer.

5.3.9 Telemetry

The telemetry system used for this payload was designed and installed by NASA personnel at Wallops Station, Virginia. The carrier frequency was 240.2 MHz. This is a standard P-band carrier frequency. The total telemetry system was a PAM/FM/FM system. Analog signals from the payload electronics drive voltage controlled oscillators (VCO's) which then are used to frequency modulate the carrier. The subcarrier channel assignments and

frequencies are listed in Table (5.2). IRIG* channel 21 carried the mass spectrometer ion current. IRIG channel 20 carried the mass spectrometer electrometer gain indicator. Channel 19 carried the slow sweep or fast retrace indicator and ion flight time timing marks. IRIG channels 13 and 14 carried both the Penn State monitor lines and the NASA monitor lines. The Penn State monitor lines are listed in Table (5.3). These two telemetry channels were commutated channels with 30 segments, each sampled at 5 times/sec. The payload antennas were 4 Vega bent spikes phased 90° apart.

5.3.10 Mass Spectrometer Calibration

Ion flight times were calibrated against ion mass-to-charge ratios for the experiment package on several occasions. Calibrations were done with the Penn State portion of the payload run off an external power supply. They were also done with complete payload run off external power. As a final check the calibrations were repeated with the complete payload run off battery (internal) power. The mass spectrometer outputs were measured while hard wired out of the vacuum test chamber and then measured using the telemetry equipment. The results of these calibrations were consistent.

The mass spectrometer electrometer output could not be properly equated with a collector current by using calibration signals described in the Payload Electronics section because of the difficulty in determining absolute current values. An alternative method for calibrating the electrometer was developed. Artificial ion currents were fed directly onto the collector through a connector in the side of the mass spectrometer. The artificial currents were produced

*IRIG: Interrange Instrumentation Group

Table 5.2: Telemetry Channel Assignments for the Sounding Rocket Flight

IRIG CHANNEL	CHANNEL OUTPUT	SUBCARRIER FREQ.	LOW PASS FILTER CUTOFF
21	MASS SPECTROMETER CURRENT	165 KHz	3720 Hz
20	MASS SPECTROMETER RANGE FACTOR	124 KHz	3720 Hz
19	MASS SWEEP AND TIME MARK MONITOR	93 KHz	1395 Hz
18	PROBE 1 ION CURRENT	70 KHz	1200 Hz
17	PROBE 1 RANGE FACTOR	52.5 KHz	1200 Hz
16	SOLAR SENSORS 1 + 2	40 KHz	790 Hz
15	PROBE 2 ION CURRENT	30 KHz	600 Hz
14	COMMUTATED CHANNEL #1	22 KHz	330 Hz
13	COMMUTATED CHANNEL #2	14.5 KHz	330 Hz
12	PROBE 2 RANGE FACTOR	10.5 KHz	220 Hz
11	PROBE 3 ION CURRENT	7.35 KHz	110 Hz
10	PROBE 3 RANGE FACTOR	5.4 KHz	110 Hz
9	CALIBRATE SEQUENCE	3.9 KHz	110 Hz
8	ACCELEROMETER	3.0 KHz	110 Hz
7	MAGNETOMETER ROLL	2.3 KHz	35 Hz
6	MAGNETOMETER PITCH	1.7 KHz	25 Hz
5	SOLAR SENSOR #2	1.3 KHz	20 Hz

Table 5.3: Monitor Outputs on the Commutated Channels

GRID 0 DC VOLTAGE

GRID 1 BUNCHER PULSE

GRID 1 BUNCHER DC VOLTAGE

GRID 2 DC VOLTAGE

GRIDS 3,4&6 DC VOLTAGE

GRID 5 GATE PULSE

GRID 5 GATE DC VOLTAGE

GATE PULSE LOGIC

BUNCHER PULSE LOGIC

FAST SWEEP INPUT

1-SEC PULSE GENERATOR

CALIBRATION SEQUENCE

15A POWER SUPPLY

15B POWER SUPPLY

15C POWER SUPPLY

15D POWER SUPPLY

15E POWER SUPPLY

90 VOLT POWER SUPPLY

MASS SPECTROMETER OFFSET GROUND

PROBE OFFSET GROUND

THERMOCOUPLE HEAD CURRENT

THERMOCOUPLE OUTPUT

SKIN TEMPERATURE

POWER SUPPLY TEMPERATURE

MAIN CURRENT SUPPLY

MAIN VOLTAGE SUPPLY

by picking a voltage off a battery through a potentiometer and putting the voltage through high valued resistors chosen to simulate ion currents. The battery and potentiometer were placed in a grounded box. A coaxial cable carried the voltage to the high value resistor. The resistor was shielded by a specially designed grounded sheath. In addition, the entire procedure was carried out in a grounded wire mesh cage.

CHAPTER VI

SOUNDING ROCKET DATA REDUCTION

6.1 Sounding Rocket Flight Conditions

6.1.1 Launch Conditions

The experiment package described in Chapter V was launched on a Nike-Apache two-stage sounding rocket on May 15, 1974 at 21:37 GMT. The launch site was Wallops Island, Virginia (latitude -37.85°N, longitude -75.47°W). The NASA identification number for the flight was 14.482 and the experiment package will be referred to by this number. May 15, 1974 was classified as a disturbed day according to the Kp index (Journal of Geophysical Research, 76, 3886, 1974). The Kp index at near the launch time was 4.3, the Ap index was 30 and the Ca^{II} index was 8.7. The sunspot number was 24. Electron densities for May 15, 1974, for near the 14.482 launch time, were calculated from an ionogram taken by the Wallops station facility and are shown in Figure (6.1). The ionogram was reduced using the Ionosphere Research Laboratory reduction program. Electron densities calculated by Dr. H. S. Lee from wave interaction data, taken at State College, Pennsylvania on May 15, 1974 are shown in Figure (6.2).

6.1.2 Sounding Rocket Flight

The 14.482 sounding rocket had a number of difficulties during the flight. The output transistor of the NASA transmitter failed about three seconds into the flight, corresponding to the end of the Nike booster burn. The transmitter operated at six per cent of its

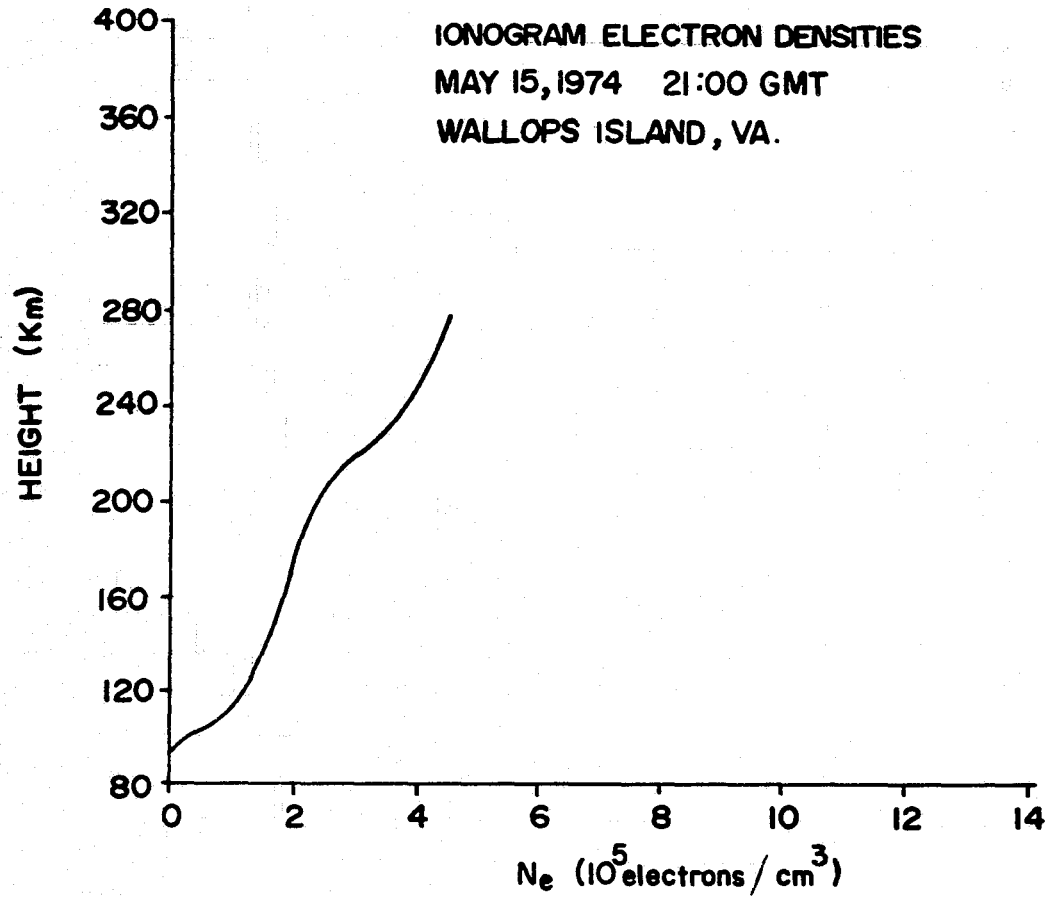

Figure 6.1 Electron Densities at Wallops Island, Virginia Taken from an Ionogram Made at 21:00 GMT on May 15, 1974.

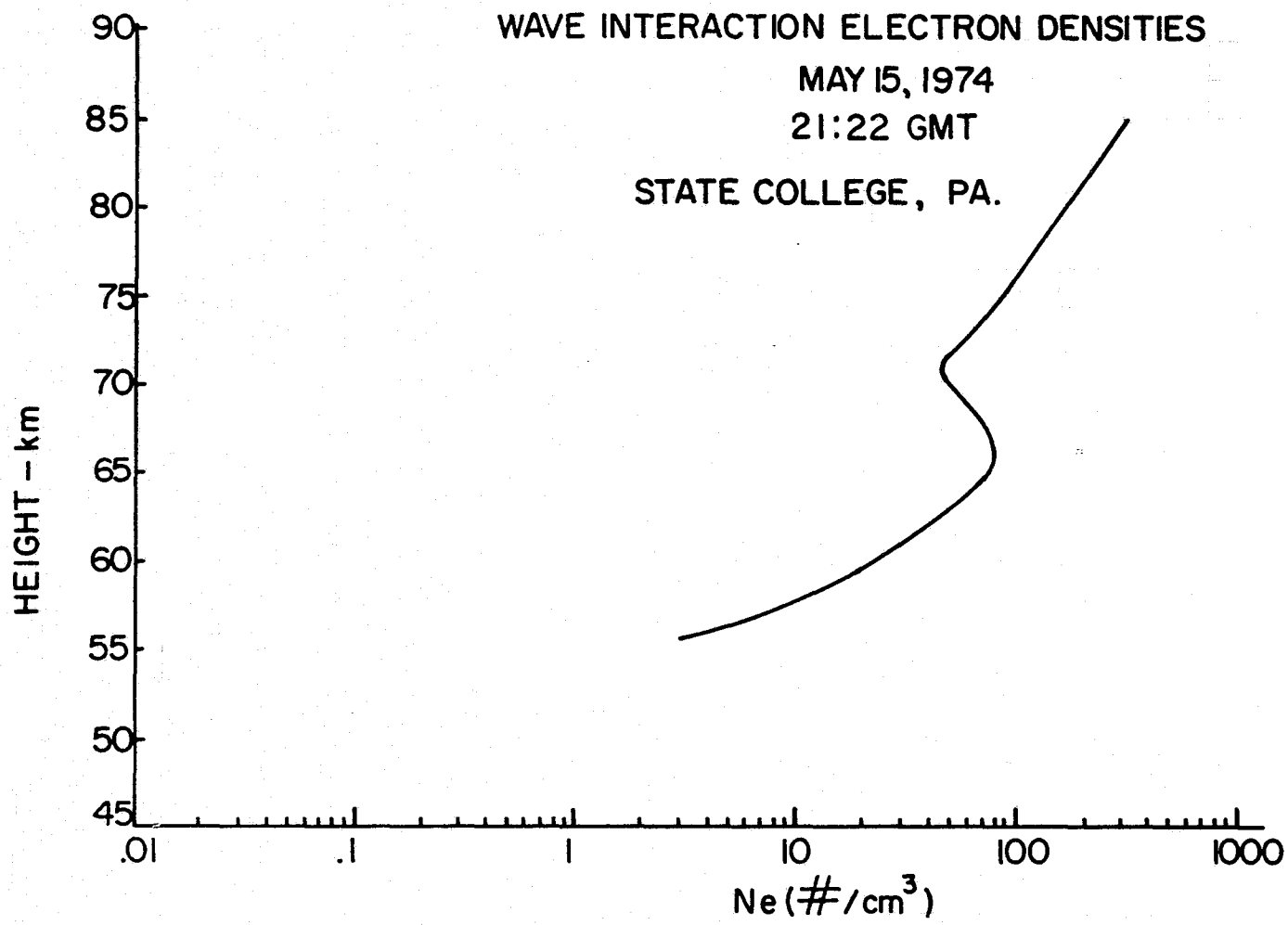

Figure 6.2 Wave Interaction Electron Densities Measured at State College, Pennsylvania at 21:22 GMT on May 15, 1974.

normal power output for the remainder of the flight. This reduced power output was still sufficient for telemetry reception with only small portions of data loss due to telemetry dropout. It has been suggested by Wayne Powell (1976) of the Computer Science Corporation that this failure might have been caused by the discharge of a large potential, on the rocket, through the pointed telemetry antennas. The antennas on the 14.482 package were capacitively coupled to the transmitter and the failure of the coupling capacitor would allow excess current to flow through the transmitter output transistor. The large potential on the rocket could be the result of charged particles being carried away from the rocket during the firing of the Nike booster. Such charging effects have been observed on jet airplanes (Nanevicz (1974)) and rockets (Nanevicz (1972)). There have been eight transmitter failures on recent NASA sounding rocket flights with pointed, capacitively coupled, antennas. Since switching to inductively coupled antennas, no transmitter failures have been observed due to this charging problem.

The second stage (Apache) burn was uneventful. The nose cone ejection occurred at the proper time (about 65 seconds after launch) and all the 14.482 experiment package instruments were exposed. However, the experiment package failed to separate from the second stage motor. This was probably caused by the failure of the bolt cutting mechanism which was supposed to release the air spring ejection mechanism (see the explanation of the experiment package ejection sequence in Chapter V). This problem did not directly

affect the data collection by the 14.482 instruments. However, it could have provided a serious source of contamination for any large angle-of-attack; the angle between the experiment package spin axis and the experiment package velocity vector.

Data was collected by all the experiment package instruments from nose cone ejection at about 70 km on the upleg, to about 70 km on the downleg. One of the ion probes operated down to about 40 km.

A typical portion of the 14.482 time-of-flight mass spectrometer (TOFMS) raw data is shown in Figure (6.3). A portion of the slow mass sweep, lasting about 950 msec, is shown. The slow mass sweep is from low mass-to-charge ratios to high mass-to-charge ratios. The fast mass sweep, called the flyback, is not shown in Figure (6.3). One mass peak is visible at the mass of 30 amu, assuming singly charged ions. This spectrum was taken at an altitude of 138.6 km. Also shown in Figure (6.3) are the timing marks for ion flight time calculations and the gain multiplier for the mass spectrometer electrometer.

The experiment package altitude versus time after launch, also called flight time but not to be confused with the ion flight time in the mass spectrometer, is shown in Figure (6.4). The experiment package apogee occurred at 138.7 km. The experiment package angle-of-attack versus altitude for the 14.482 flight is shown in Figure (6.5).

Two thermistors were carried in the 14.482 experiment package to monitor the temperatures inside the experiment package. One

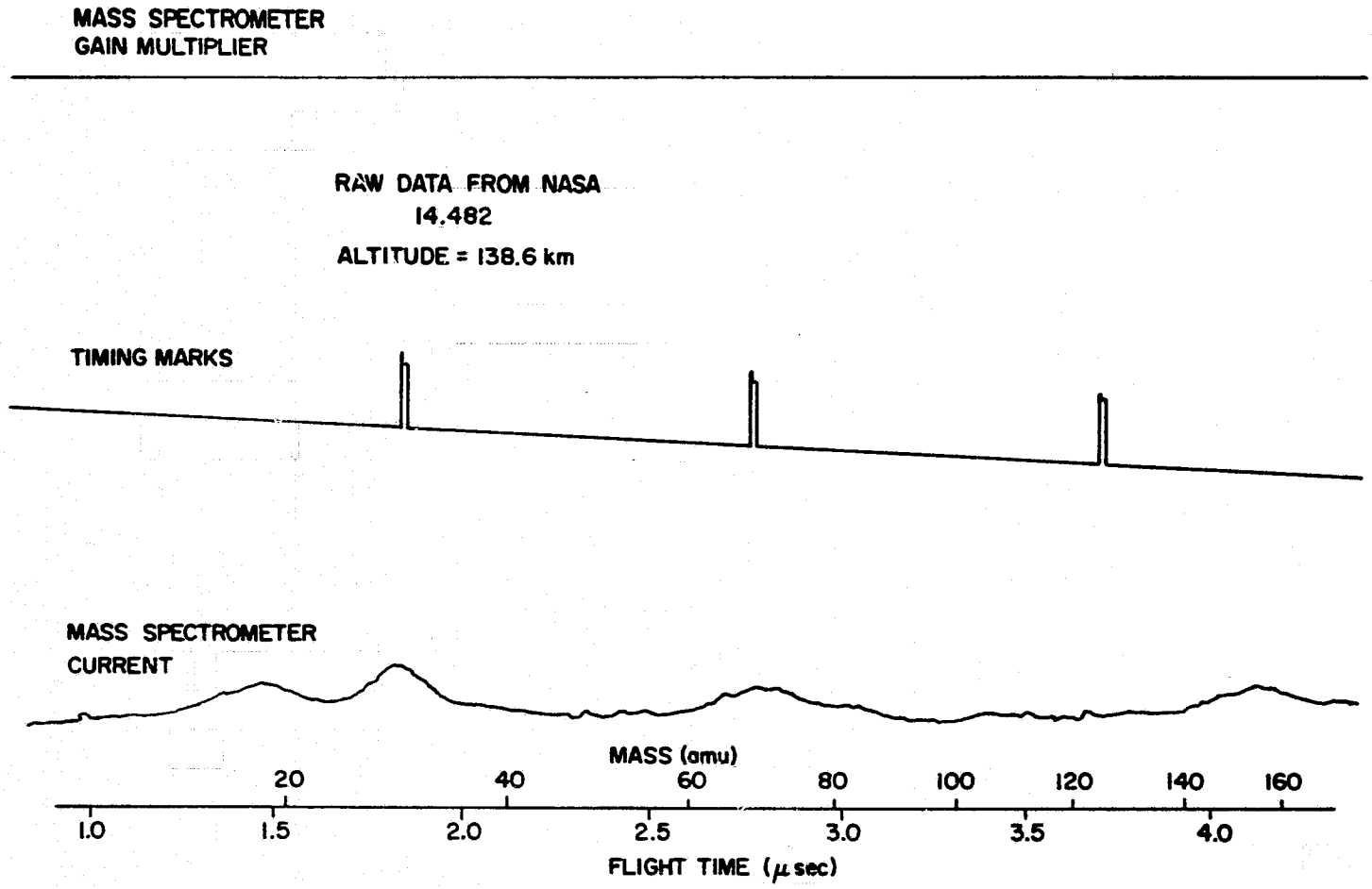

Figure 6.3 Typical Portion of 14.482 Mass Spectrometer Raw Data.

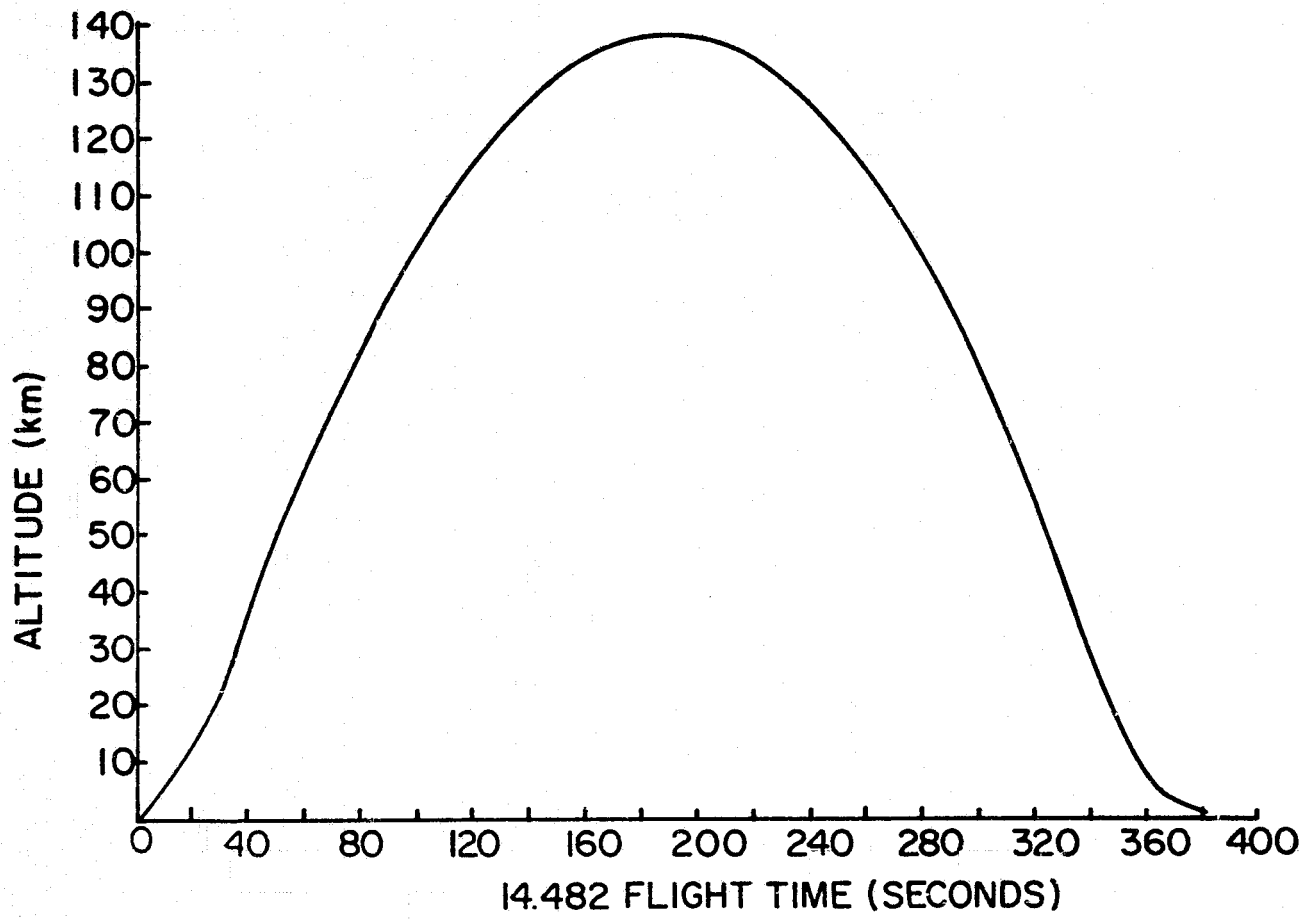

Figure 6.4 Experiment Package Altitude Versus Time for the 14.482 Flight.

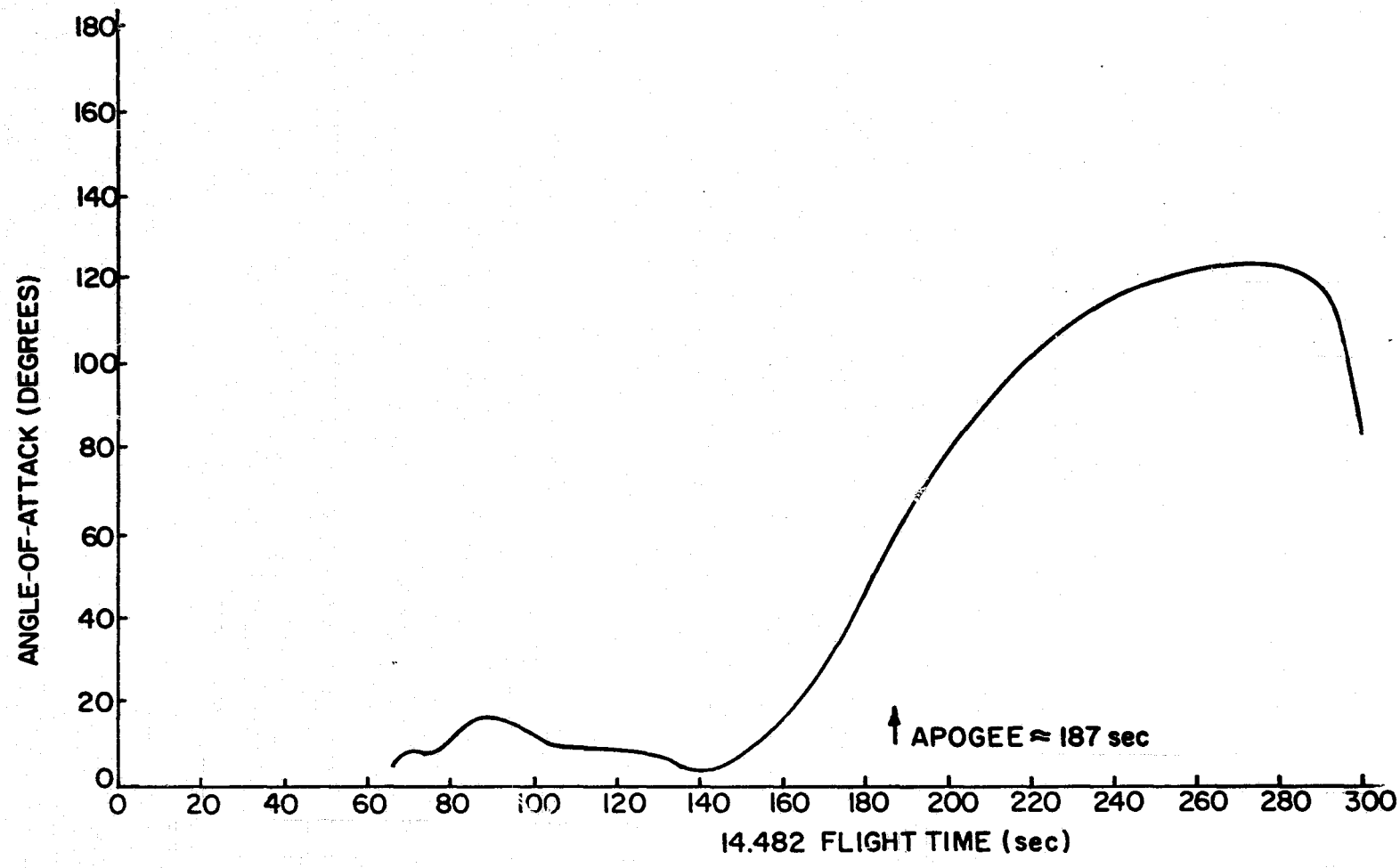

Figure 6.5 14.482 Experiment Package Angle-of-Attack Versus Flight Time.

thermistor was in contact with the experiment package skin. The other thermistor was in the power supply section of the experiment package to monitor the largest source of heat inside the package. The results of the thermistor measurements during the 14.482 flight are shown in Figure (6.6). The skin temperature was nearly constant until re-entry heating occurred and then the skin temperature increased rapidly until impact. The experiment package power supply temperature showed a small but steady increase during the flight. The internal temperature of the package stayed well within permissible levels, for proper operation of the package electronics, during the flight.

The data from the three ion probes and the thermocouple gauge will be presented in Cuirle (1976).

6.2 Calibrations and Calculation of Detached Shock Wave Parameters

6.2.1 14.482 Mass Spectrometer Calibrations

The ion flight times versus mass-to-charge ratio calibration curves for the cylindrical-electrode TOFMS carried on the sounding rocket experiment package are shown in Figure (6.7). Since the mass spectrometer offset ground steps with respect to the experiment package ground and with respect to the surrounding plasma, there is a calibration curve for each of the four resulting ion draw-in potentials. The measurements of the ion flight times for these curves were made using the surface ionization ion source described in Chapter IV. The vacuum system described in Chapter IV was modified so that the entire experiment package could be placed in a vacuum.

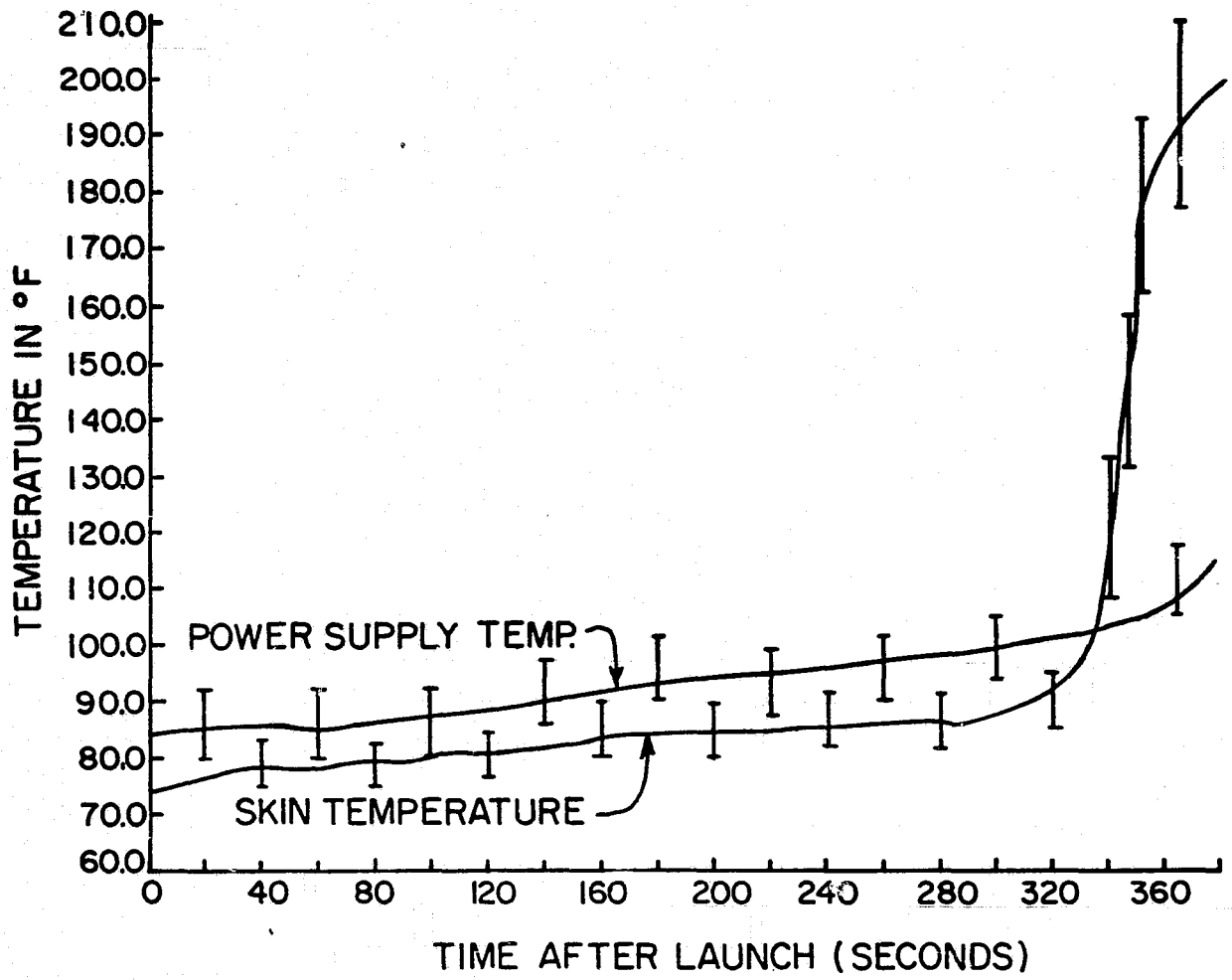

Figure 6.6 Temperatures in the 14.482 Experiment Package During the Flight.

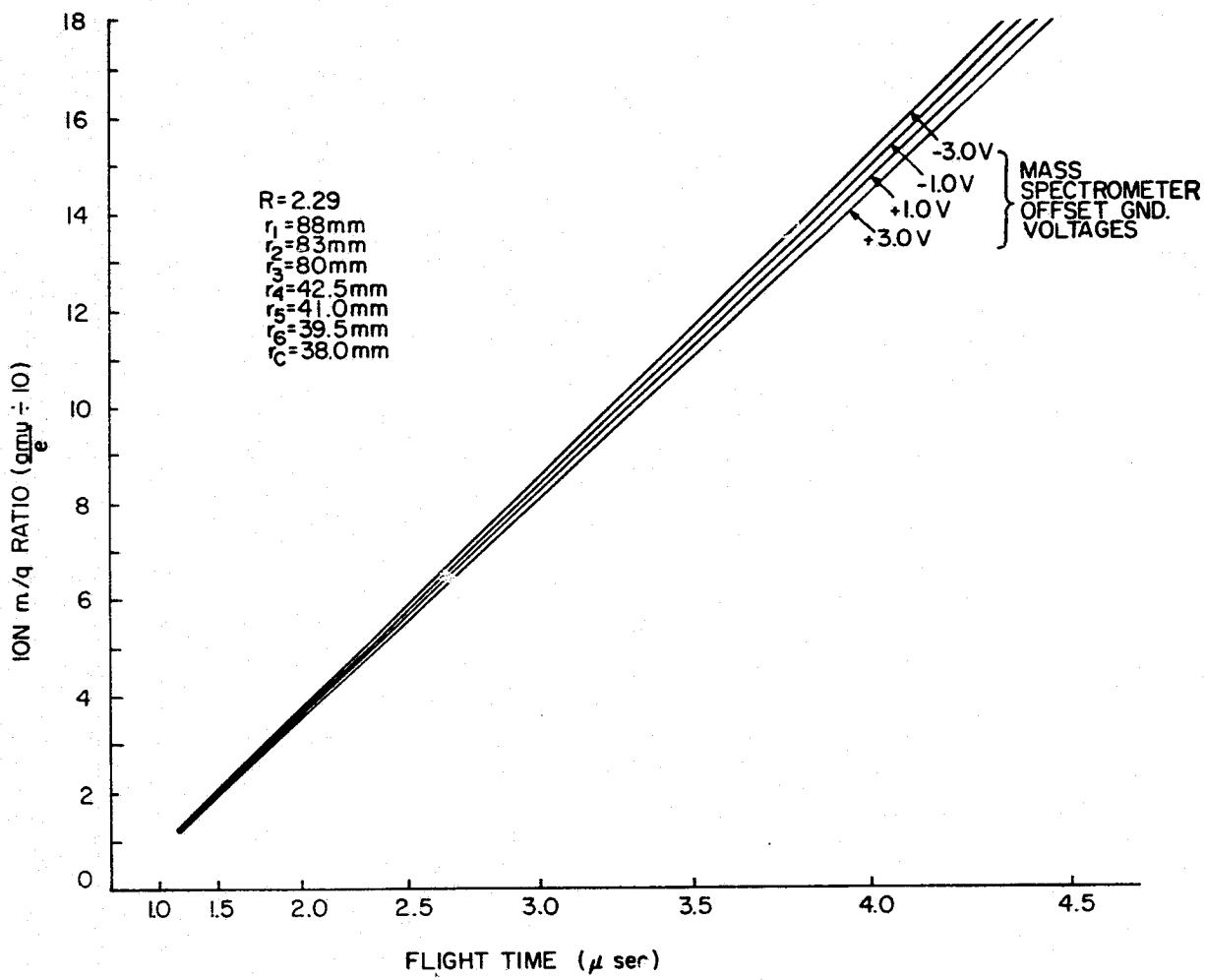

Figure 6.7 Ion Flight Times Versus Mass-to-Charge Ratios for the 14.482 Cylindrical-Electrode TOFMS.

The mass spectrometer electrometer calibration curves for ion current versus telemetry voltage are shown in Figure (6.8). The curves in Figure (6.8) can be grouped in four sets of three straight line segments. Each straight line segment describes the electrometer output for one gain setting. Each set of line segments represent one of the four offset ground voltages. The method used to produce these calibration curves was described in Chapter V.

6.2.2 Detached Shock Wave

A detached shock wave was generated in front of the 14.482 experiment package while moving at supersonic speeds. The important shock wave parameters are the shock wave detachment distance, the stagnation point pressure and the pressure enhancement profile between the shock wave and the stagnation point. The shock wave behavior has been studied by Cuirle (1976) for the 14.482 experiment package and the discussion of the shock wave parameters here represents a summary of his work.

Using elementary continuum theory based on Liepmann and Roshko (1957), the shock wave parameters can be calculated if the payload angle-of-attack is small. The 14.482 experiment package was in the continuum flow regime only below 60 km. Calculations of the Reynolds numbers and the Knudson numbers show the 14.482 experiment package was in the transition flow regime from 60 km to about 100 km on the upleg and in the free molecular flow regime from 100 km to apogee. The same flow regimes apply to the downleg. However, some of the continuum

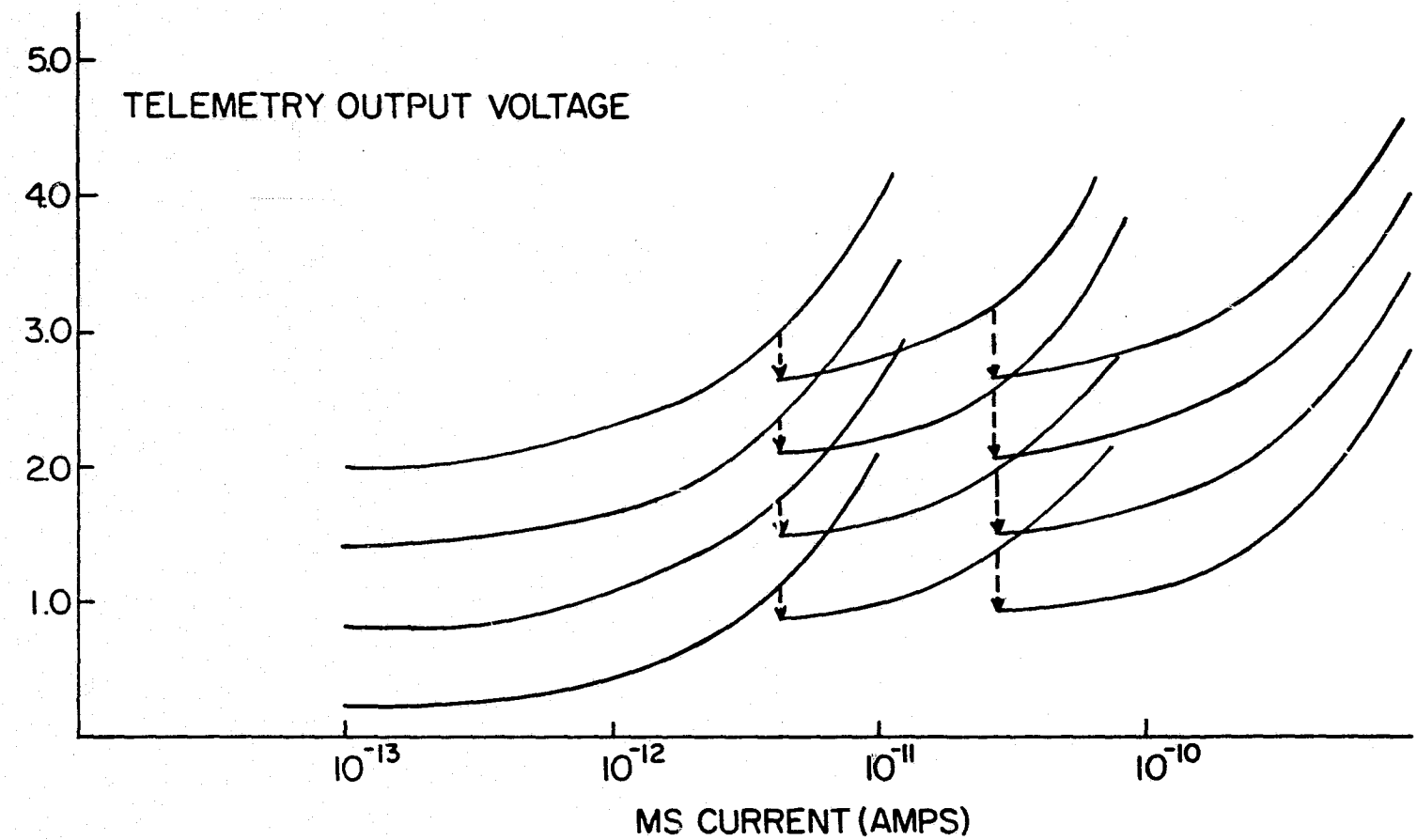

Figure 6.8 Telemetry Voltage Versus Mass Spectrometer Current for the 14.482 Cylindrical-Electrode TOFMS.

flow regime results can still be applied to the transition flow regime since the various flow regimes are distinguished mainly by the boundary conditions used tor transverse flow calculations. The stagnation pressure, at least, is a phenomenon considered relatively independent of flow effects. Also, neutral pressure calculations by Cuirle (1976) from the 14.482 thermocouple gauge, using continuum flow theory, are extremely close to accepted values (CIRA 1972) up to about 95 km. This indicates that continuum flow theory can be extended at least for the 14.482 experiment package, to the transition flow regime. In the free molecular flow regime there will be no pressure enhancement behind the shock wave and the ambient atmospheric pressure can be used for calculations.

It has been calculated by Cuirle (1976) that the elementary continuum flow theory of shock wave production can be rigorously applied only for angles-of-attack near 0^{o} (axial flow) and 90^{o} (transverse flow). The precise angles-of-attack for the 14.482 experiment package which can be justified in the theory are 0^{o} to 4.5^{o} and 85.5^{o} to 90^{o}. The theory can be extended to include 4.5^{o} to 7.5^{o} and 82.5^{o} to 85.5^{o} with less confidence in the results. The use of continuum theory to calculate the shock wave parameters for angles-of-attack from 7.5^{o} to 82.5^{o} can not be justified. This is because the stagnation point was near, or went over, the edge of the forward bulkhead of the 14.482 experiment package.

The upleg angles-of-attack for the 14.482 package, while it was in the transition flow regime, varied between 5^{o} and 18^{o}. However, the angle-of-attack was greater than 7.5^{o} from 70 km to

to 100 km. This means the exact shock wave parameters can not be calculated but it is possible to place limits on the shock wave parameter values and to make an educated guess about the precise values.

The 14.482 experiment package had an angle-of-attack greater than 90^{o} during the downleg portion of the flight through the transition flow regime altitudes. This means the stagnation point was somewhere on the side, or rear, of the experiment package. Since the second stage motor was still attached to the experiment package, there are significant unknowns in the calculations. It also means that continuum flow theory can not be used to calculate the stagnation point pressure because the flow is primarily transverse.

6.3 Mass Spectrometer Data Reduction

6.3.1 Gross Features of Mass Spectra

Figure (6.3) showed a typical portion of the 14.482 TOFMS raw data. The significant features of the mass spectrometer data, other than any mass peaks, are the presence of a uniform background current and the periodic modulation of the mass spectrometer current. The presence of the uniform background current in the mass spectra of a gated cylindrical-electrode TOFMS has been discussed in Chapters III and IV. The background current represents a fraction of the total ion current entering the mass spectrometer.

The periodic modulation of the mass spectrometer ion current corresponds to the spin rate, or multiples of the spin rate, of the experiment package. This spin modulation had at least two causes.

The first was the effect of the two forward facing ion probes, situated on posts on opposite sides of the spectrometer (see Figure (5.1)), passing between the mass spectrometer and the direction of the gas flow into, or past, the spectrometer. The ion probes can interfere physically with the gas flow or the region affected by the ion probe draw-in potentials can affect the entry of ions into the spectrometer. The second cause of the modulation was the interference of the sides of the spectrometer with the ion collection at the collector.

The observed spin modulation of the ion current had more fine structure than should have beer the result of the two causes mentioned above. However, the general behavior is explained very well by the two causes for the entire flight.

The background current which appeared in the 14.482 mass spectra was much larger than the background current expected on the basis of pre-flight calibrations. A change in the background current would be caused by a shift in the experiment package potential with respect to the surrounding plasma. The 14.482 experiment package potential was calculated by me from the ion probe data. The results are shown in Figure (6.9) for the upleg portion of the flight. The experiment package did, in fact, shift its potential with respect to the surrounding plasma. The experiment package either had a positive potential of about +2V or immediately took on that potential when nose cone ejection occurred. The potential then went negative to about -3V within 15 seconds. The potential then slowly became less negative until it reached -1 V at apogee. The slow oscillation in the package potential corresponds to the period of the coning of the

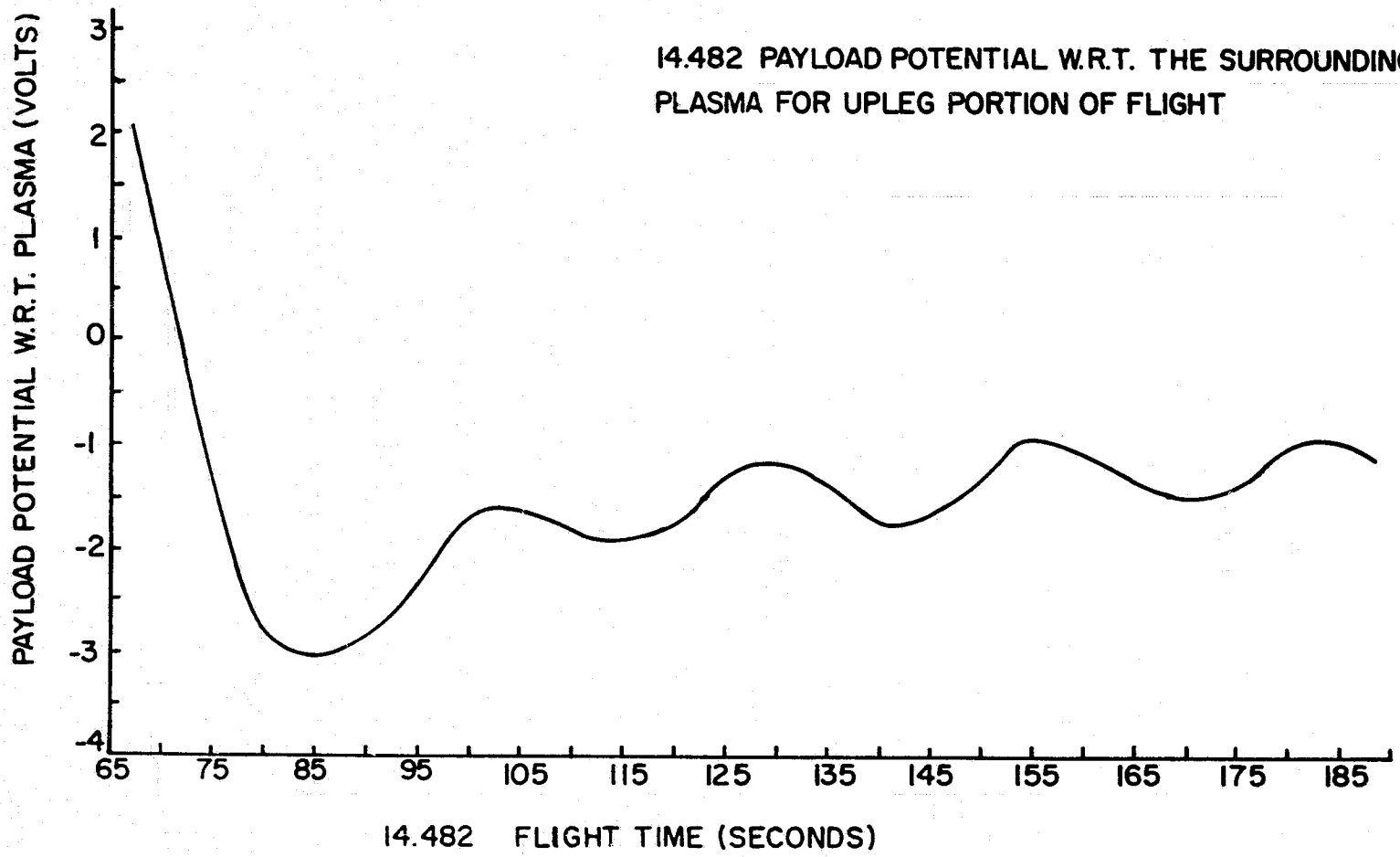

Figure 6.9 The 14.482 Experiment Package Potential with Respect to the Surrounding Plasma for the Upleg Portion of the Flight.

experiment package with a coning half-angle of about 3.5^{o}. The payload potential during the downleg portion of the flight was remarkably similar to the potential during the upleg. The potential went more negative until an altitude of 85 km was reached. The potential then shifted from negative to positive and it reached about +2 V at 70 km. This shift in the experiment package potential was not enough to completely explain the high background currents. Therefore, there must have been a drop in the gate dc barrier potential which occurred after launch. A small drop of several volts in the gate barrier potential could not be confirmed by studying the appropriate telemetry monitor output. This is because the monitors were used to detect gross changes in any of the payload potentials. A change of only a few volts in the gate barrier potential would be undetectable.

Because of the probable drop in the gate barrier potential, the mass spectra near apogee were used to recalibrate the background current ratio for each of the four draw-in potentials on the mass spectrometer. An additional correction was then applied for the change in the payload potential with respect to the plasma.

6.3.2 Analysis of Mass Spectrometer Data

The proper examination of the mass spectra from the 14.482 flight required the removal of the spin modulation. This was accomplished by using autocorrelation to normalize the spin modulation. One spin modulation period near the end of each mass spectrum was used to normalize that mass spectrum. Since the spin modulation varied from one mass spectrum to the next, due to the

changing draw-in voltages on the spectrometer, the normalization needed to be done for each individual mass spectrum. Care was taken to make sure there were no mass peaks in the spin modulation periods used for the normalization. The complete normalization procedure was to digitize each mass spectrum, convert telemetry voltage to ion current (using the calibration curves shown in Figure (6.8)), average the digitized current data using a three point average, and then use autocorrelation to remove the spin modulation. These calculations were done partly by hand, partly at the Hybrid Computer facility of The Pennsylvania State University and partly on an IBM 360/175. Brad Kuhn was primarily responsible for the hybrid computer programming.

All the mass spectrometer data from the 14.482 flight have been digitized and converted to ion current. However, only small portions of the mass spectrometer data have actually been normalized. The normalization procedure has not been computerized and, therefore, has been done by hand. This thesis will concentrate on the portion of the mass spectrometer data which has been completely reduced.

The concentrations of ions with mass-to-charge ratios greater than 500 can be deduced from the background current collected by the 14.482 cylindrical-electrode TOFMS. The relationship between the background current and the mass spectrometer operating voltages is well understood. The behavior of the background current at various pressures inside the spectrometer is known empirically. A more convenient quantity for comparison with previous researchers is the percentage of ions with mass-to-charge

ratios greater than 500. These ions will be referred to as heavy ions.

The background current ratio has been defined (Chapter III) as the total current collected in the mass peaks present in a mass spectrum divided by the background current. Therefore, if we define B_I as the background current ratio with heavy ions present and B_L as the background current ratio with no heavy ions present, the percentage of heavy ions, H, is given by

$$H = 100 \left(1 - \frac{B_I}{B_L}\right) \tag{6.1}$$

Care must be taken to use the value of B_L for the pressure at which the B_I measurement is taken. B_L contains the corrections for the experiment package potential variation and for the drop in the gate barrier potential. The mass discrimination effects due to ion gating have not been included in equation (6.1). Because the discrimination is more severe against larger mass-to-charge ratios, H is the minimum percentage for singly charged heavy ions.

It is necessary to have some knowledge of the pressure inside the 14.482 spectrometer during the flight in order to calculate B_L and, therefore, H. The difficulties in calculating the shock wave parameters and, therefore, the pressure inside the mass spectrometer have been discussed. The precise values for the pressure inside the spectrometer can not be calculated. However, it is possible to calculate the limits on the spectrometer pressure. One of the

limits for the upleg portion of the flight is to assume that there was no pressure enhancement in the mass spectrometer (i.e. there was no shock wave) and use the ambient atmospheric pressure for data reduction. This will provide a lower limit on the pressure inside the mass spectrometer. The other limit is to assume an angle-of-attack of 0^{o}, and a shock wave detachment distance equal to the distance grid 0, of the mass spectrometer, was in front of the forward bulkhead of the experiment package. Emphasis is placed on a 0^{o} angle-of-attack because it should provide the highest average pressure inside the spectrometer. Also, an angle-of-attack of 0^{o} is the closest angle-of-attack to the 14.482 upleg attack angles to which the continuum flow shock wave theory applies rigorously. The average pressure inside the 14.482 TOFMS is shown in Table (6.1), as a function of altitude, for the two limiting cases. These cases will be referred to as the ambient pressure case and the total immersion case for simplicity. Also tabulated in Table (6.1) is the pressure multiplication factor which represents the ratio of the mass spectrometer pressure for the total immersion case to the mass spectrometer pressure for the ambient pressure case. The altitudes considered in Table (6.1) are altitudes of interest in heavy ion calculations. Table (6.1) was calculated using parameters calculated by Cuirle (1976) and mach numbers calculated from

$$M = v \sqrt{\frac{W}{\gamma RT}} \qquad (6.2)$$

Table 6.1: Average Pressure in the 14.482 Mass Spectrometer During the Upleg Portion of the Flight for the Ambient Pressure Case and for the Total Immersion Case

FLIGHT TIME AFTER LAUNCH (seconds)	APPROXIMATE ALTITUDE (km)	AMBIENT PRESSURE (pa)	AV. ENHANCED PRESSURE (pa)	MULTIPLICATION FACTOR [enhanced pressure / ambient pressure]
80	85	.424	14.5	34.1
81	86	.355	9.96	28.1
82	87	.293	8.05	27.5
83	88	.247	6.43	26.1
84	89	.213	5.36	25.1
85	90	.185	4.41	23.8
86	91	.157	3.55	22.5
87	92	.130	2.72	20.9
88	93	.108	2.15	19.9
89	94	.091	1.69	18.6
90	95	.077	1.33	17.2
91	96	.065	1.05	16.1
92	97	.056	.845	15.1
93	98	.048	.688	14.5
94	99	.041	.532	13.1
95	100	.035	.428	12.3
96	101	.029	.317	11.0

ANGLE-OF-ATTACK = 0°
CONTINUUM FLOW BEHAVIOR ASSUMED
SHOCKWAVE DETACHMENT DISTANCE
IS ASSUMED TO BE 76mm

where v = the total payload velocity (m/sec), W = the mean molecular weight of the neutral atmosphere (kg/mole), γ = the ratio of specific heats, R = the gas constant and T = the neutral temperature (^{o}K). The temperature values used were the CIRA 1972 mean values. The mach number profile, for the portion of the 14.482 flight referred to in Table (6.1), is shown in Figure (6.10).

Only the upleg mass spectrometer data will be considered, in detail, in this thesis. This is because of the difficulty in even estimating the limits on the pressure inside the mass spectrometer on the downleg, the possibility of contamination due to the second stage motor and problems with the normalization procedure when there was a large angle-of-attack and the resulting extreme spin modulation.

6.3.3 Effects on Mass Spectra of Sampling Through a Detached Shock Wave

If the detached shock wave was in the TOFMS drift region during the upleg (85 km to 105 km) portion of the flight this could have important implications for the heavy ion calculations. The drift region of a TOFMS is field free. Therefore, any breakup of cluster ions in the drift region, due to the shock wave will not significantly affect the measured flight times of the cluster ions. This is because a charged fragment from a fragmented cluster ion will be collected at approximately the flight time corresponding to the mass-to-charge ratio of the original cluster ion. The ion gate will slightly affect the flight time of the charged ion fragments. For example, if we assume a singly charged cluster ion of mass $\sim$500

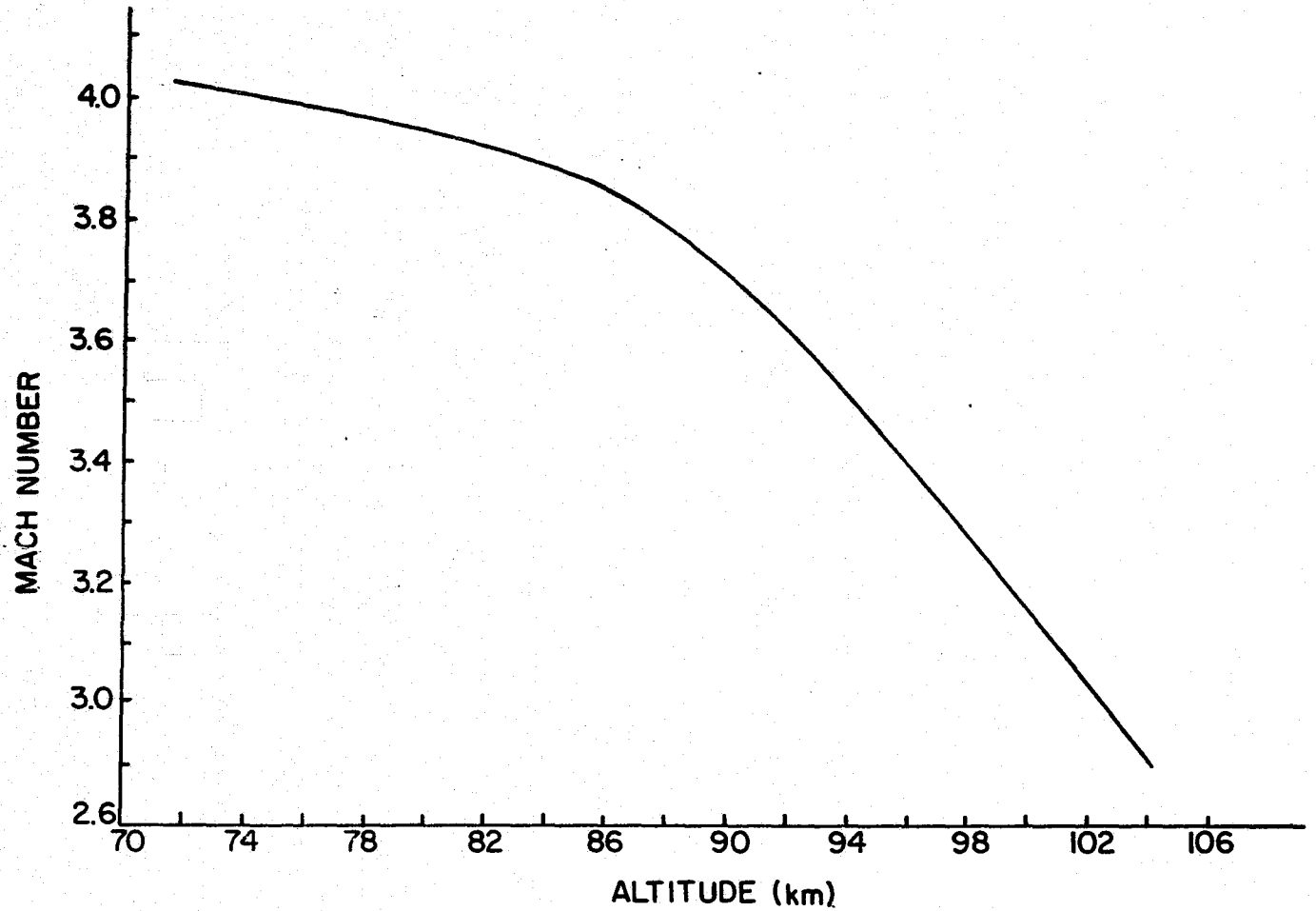

Figure 6.10 Mach Number Versus Altitude for the 14.482 Experiment Package from 72 km to 104 km.

amu exists and has been fragmented into one H_3O^+ (19) ion and a number of neutral fragments, the H_3O^+ (19) transit time through the gate will be about 60 nsec. The gate region transit time for the original 500 amu cluster ion would have been about 300 nsec. This will change the apparent flight time of the 500 amu ion by only 2.5 per cent. If the shock wave was outside the drift region, the fragmentation of any cluster ions should occur before the ions enter the drift region. The charged fragments will then appear at the collector at flight times corresponding to their own mass-to-charge ratios.

CHAPTER VII

MASS SPECTROMETER MEASUREMENTS, IMPLICATIONS AND COMPARISONS WITH PREVIOUS MEASUREMENTS

7.1 Results of 14.482 Mass Spectrometer Measurements

7.1.1 Altitude Profile of Major Positive Ion Species

A portion of a 14.482 time-of-flight mass spectrometer (TOFMS) mass spectrum with the spin modulation and background current removed is shown in Figure (7.1). This mass spectrum was taken at about 95 km on the upleg. The mass peaks present are at mass-to-charge ratios of about 30 and 56. The mass peak at m/e = 30 is presumably NO^+ (30) and O_2^+ (32). The resolving power of the spectrometer was insufficient to separate these two peaks. The peak at m/e = 56 is probably Fe^+ (56) based on the results of other researchers.

The altitude profiles of the positive ions detected during the upleg portion of the 14.482 flight are shown in Figure (7.2). The positive ion densities were calculated assuming ambient atmospheric pressure inside the 14.482 mass spectrometer. The relative ion densities at any particular altitude are accurate. However, since only a fraction of the ions in any bunching cycle will actually be collected (Glenn (1952)) the cylindrical-electrode TOFMS should not be used to calculate absolute ion densities. The 14.482 spectrometer, as well as other types of mass spectrometers, are only accurate in relative ion density measurements. The minimum sensitivity, translated to ions/cm^3, is indicated by the dashed line in Figure (7.2) as a function of altitude.

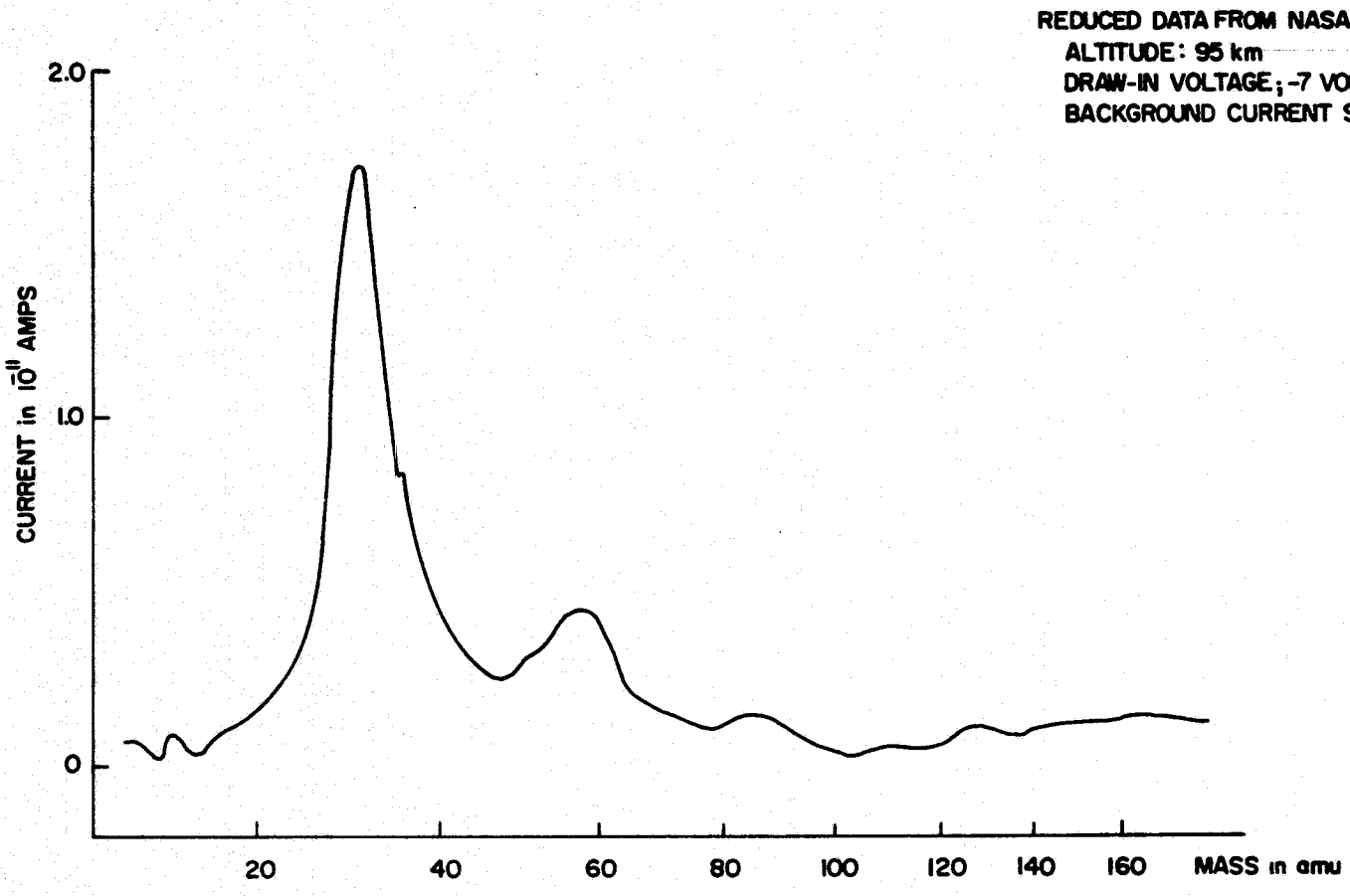

Figure 7.1 Portion of the 14.482 TOFMS Data with the Spin Modulation and Background Current Removed. This Mass Spectrum was Taken at 95 km on the Upleg.

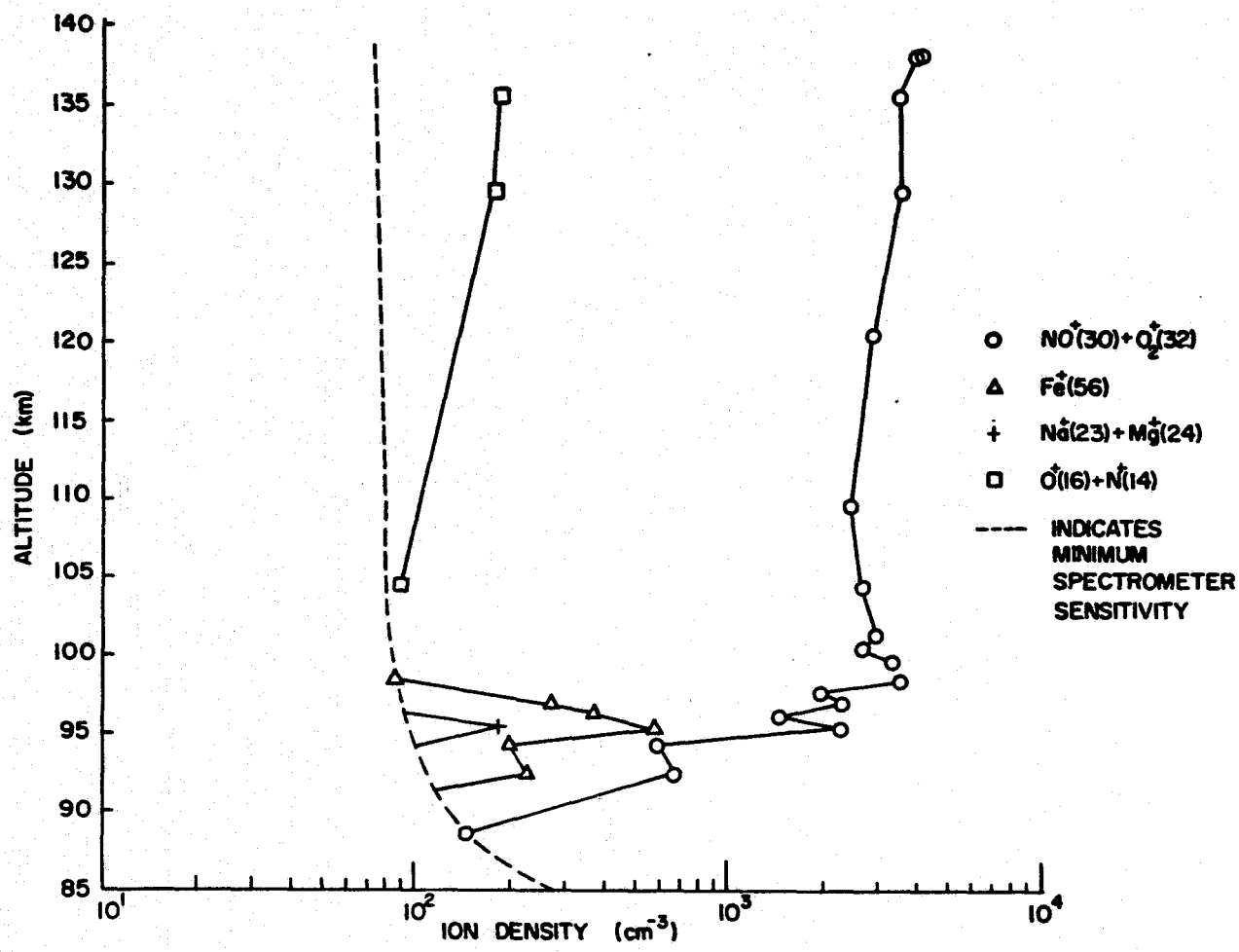

Figure 7.2 Major Positive Ion Species Detected During the Upleg of the 14.482 Flight.

A significant feature of Figure (7.2) is the lack of any clearly defined peaks corresponding to hydrated ions of the form $H_3O^+ \cdot (H_2O)_n$ with m/e ratios less than 500. This statement is subject to the constraint of lower than expected sensitivity due to the larger than expected background current. In the small portions of the downleg data which have been normalized there was a similar lack of hydrated ions with m/e ratios less than 500.

A metallic ion layer was observed at about 95 km which was made up of Fe^+ (56). Mg^+ (24) (or Na^+ (23)) was observed in one spectrum at about 96 km. These observations correspond to the results of numerous investigators (for example, see Krankowsky et al., (1972c)). The metallic ion layer at about 115 km reported by some investigators was not seen.

It is possible to obtain a more precise determination of the ion densities by normalizing to the ion densities measured by the 14.482 experiment package ion probes. The results of the probe measurements are to be presented in Cuirle (1976) but have not yet been calculated.

7.1.2 Heavy Ion (m/e > 500) Altitude Profile

The lack of hydrated ions was a rather surprising result in light of the measurements of previous researchers. However, when the background current was used to discover the presence of ions with mass-to-charge ratios greater than about 500, a possible explanation was found for the lack of hydrated ions with m/e ratios less than about 500.

The heavy ion percentage for the ambient pressure case and the total immersion case, both defined in Chapter VI, are shown in Figure (7.3). These heavy ion percentages were calculated assuming singly charged ions. A more exact definition for the heavy ion percentage might be the amount of positive charge carried on positive charge carriers with m/e ratios greater than 500 in relation to the total amount of positive charge on all positive charge carriers.

The differences in the heavy ion altitude profiles in Figure (7.3) are not especially large. The two cases provide the lower (ambient pressure case) and the upper (total immersion case) limits on the variation of the heavy ion percentage as a function of altitude. Assuming an angle-of-attack of 0°, a more realistic shock wave detachment distance can be calculated as well as the other shock wave parameters. The exact shock wave detachment distances and their spatial relationships to the 14.482 TOFMS for a 0° angle-of-attack, and for upleg altitudes from 85 km to 105 km, are shown in Figure (7.4). The shock wave detachment distances can be seen to be inside the mass spectrometer drift region. The altitude profile for the heavy ion percentage for this case, called the continuum flow pressure case, is shown in Figure (7.5). The heavy ion percentage altitude profiles for the total immersion and ambient pressure cases are included in Figure (7.5) for comparison. It can be seen that the altitude profile for the heavy ion percentage for the continuum flow pressure case is almost identical to the profile for the total immersion case. Again, singly charged ions were assumed.

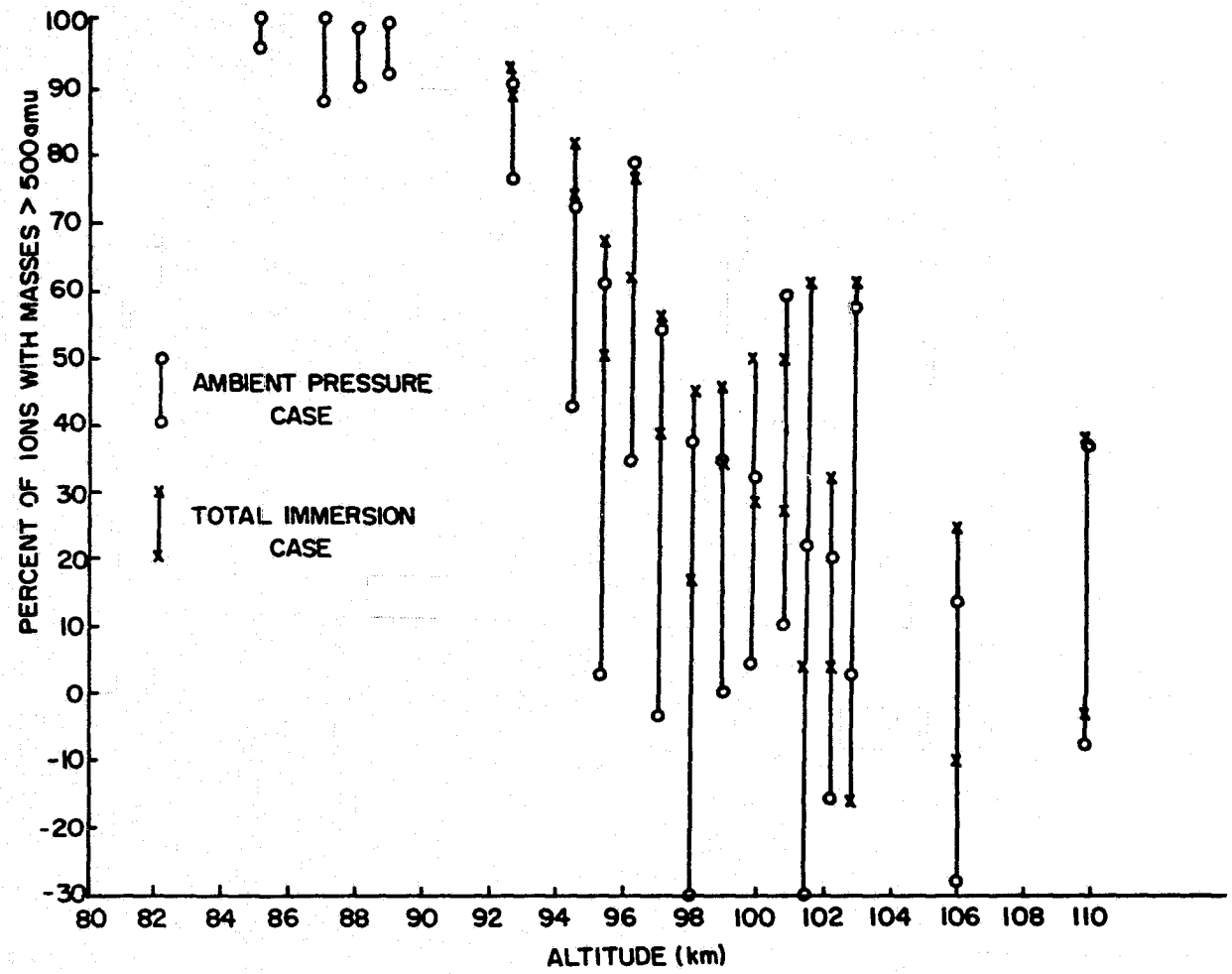

Figure 7.3 Heavy Ion Percentage Variation with Altitude for the Ambient Pressure Case and for the Total Immersion Case. Singly Charged Ions are Assumed.

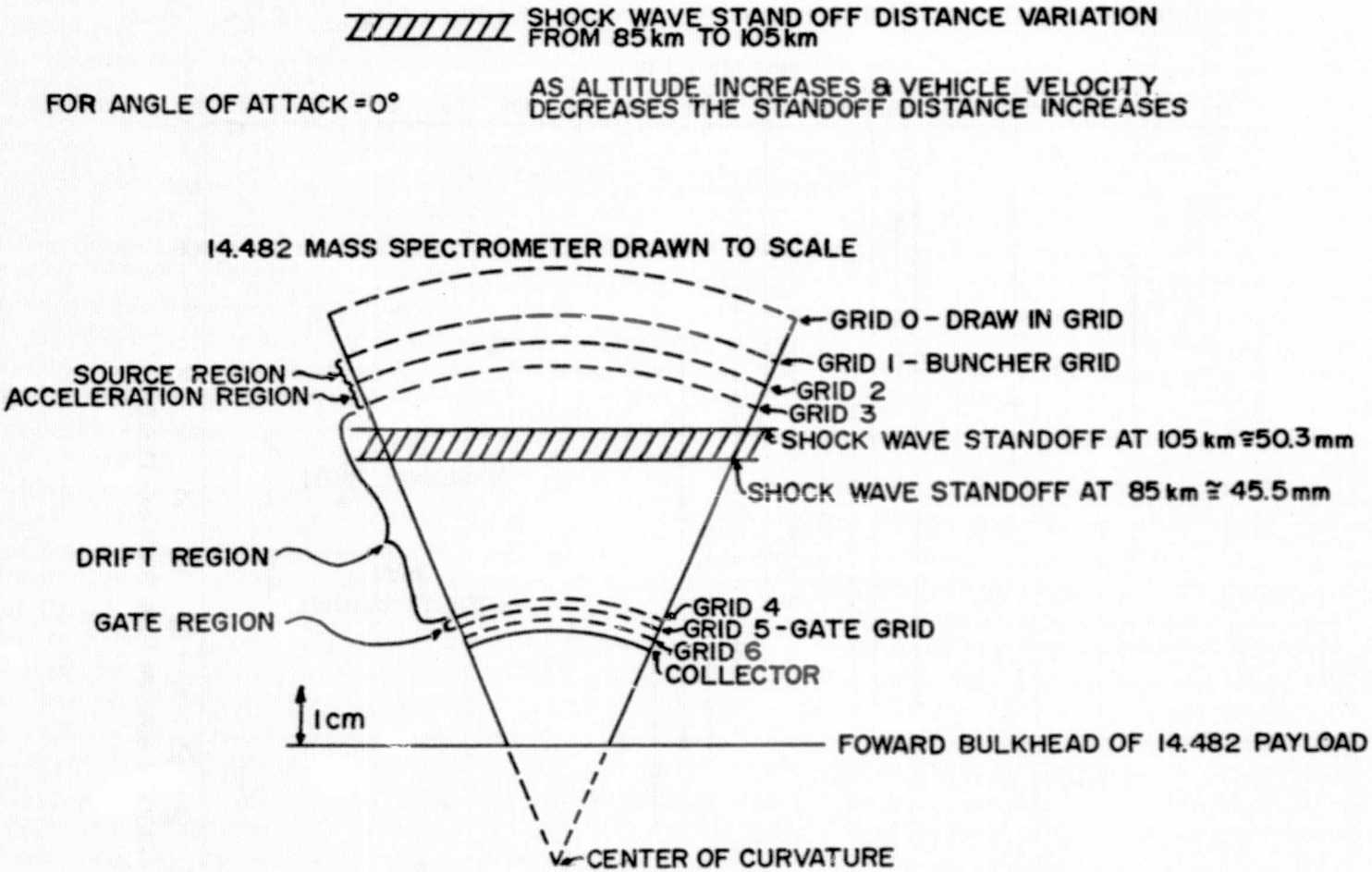

Figure 7.4 Shock Wave Detachment Distance for the Continuum Flow Pressure Case. An Angle-of-Attack of 0^{o} is Assumed. The Altitude Range from 85 km to 105 km is Considered.

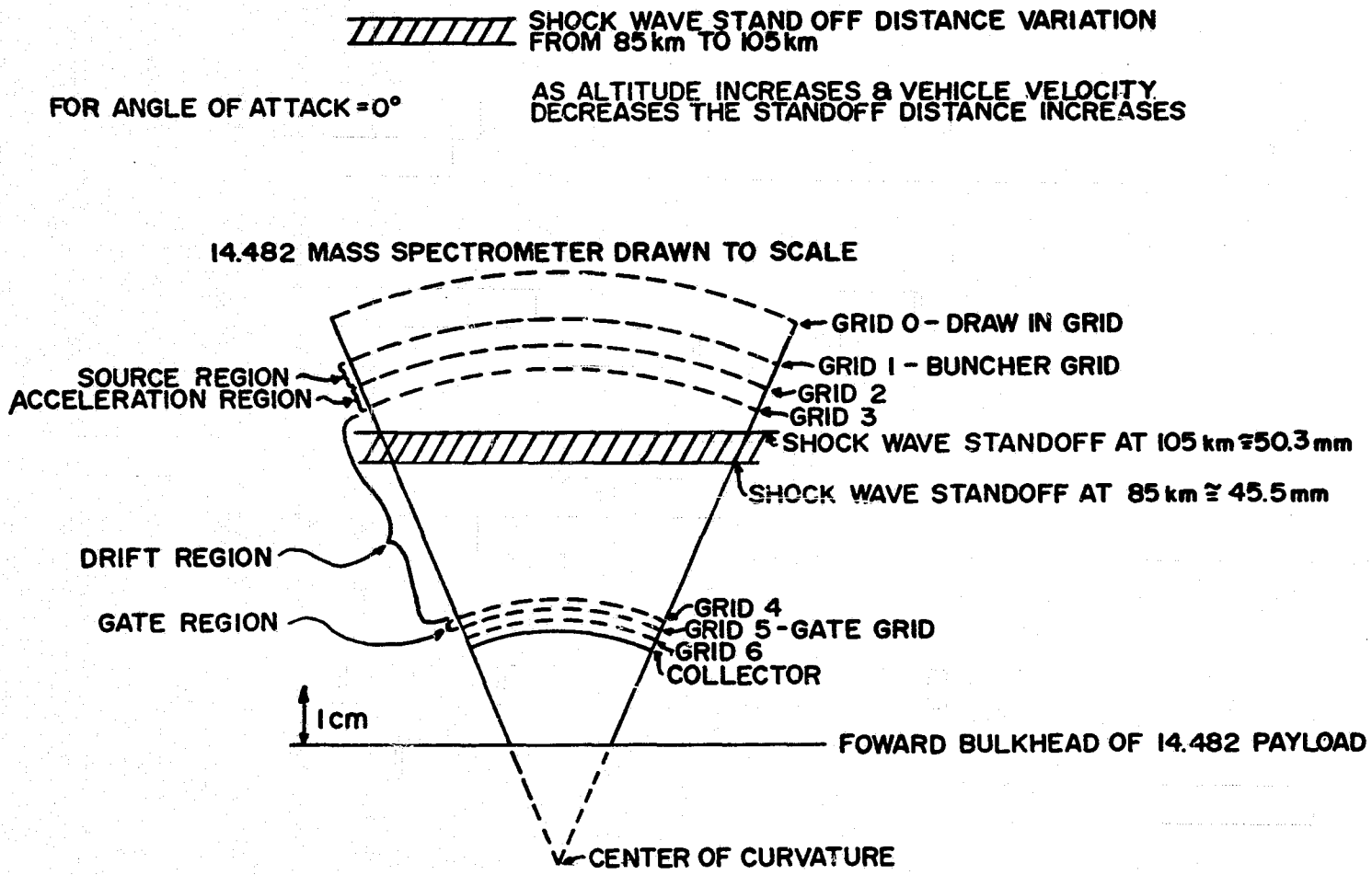

Figure 7.4 Shock Wave Detachment Distance for the Continuum Flow Pressure Case. An Angle-of-Attack of 0^{o} is Assumed. The Altitude Range from 85 km to 105 km is Considered.

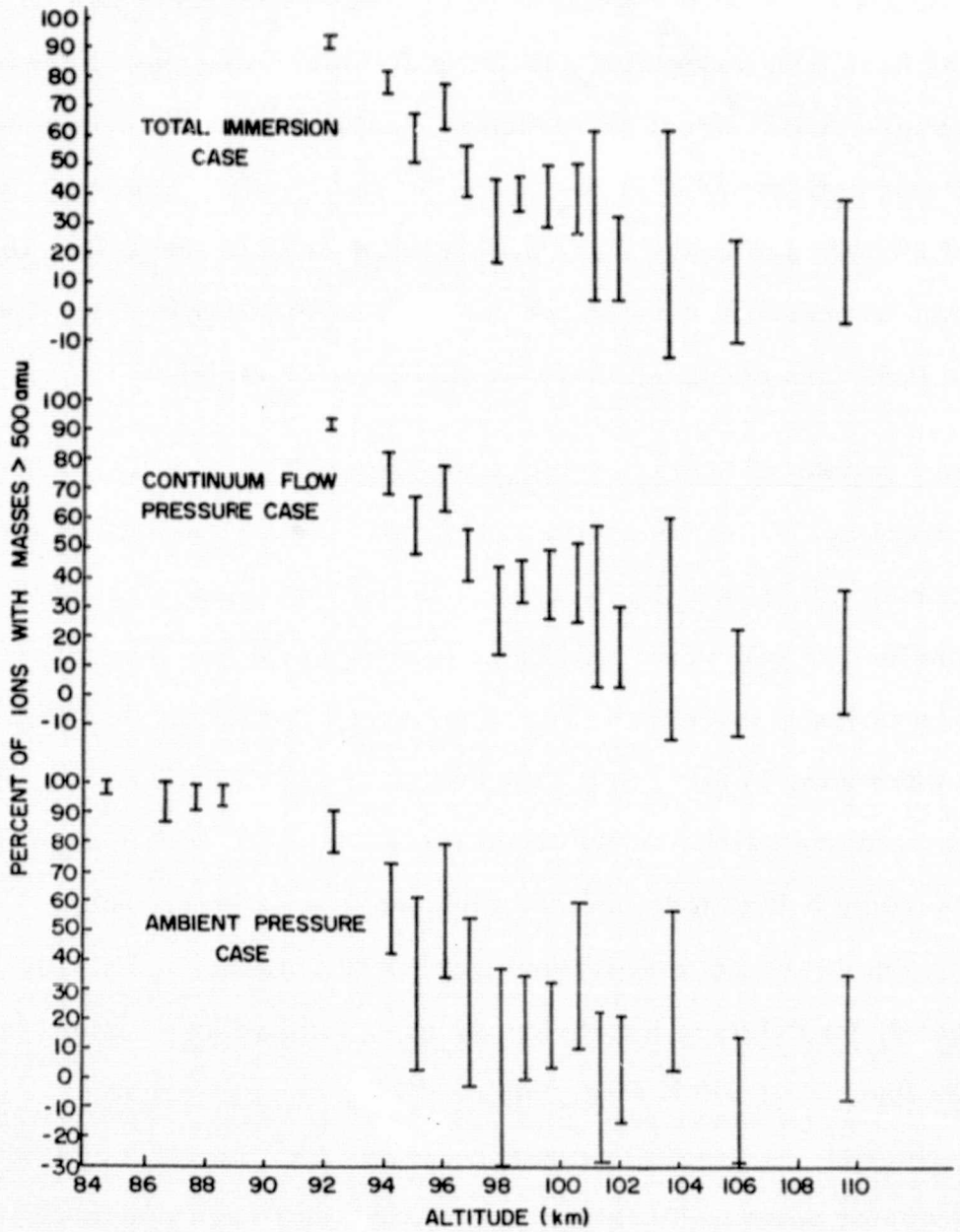

Figure 7.5 Heavy Ion Percentage Variation with Altitude for the Total Immersion Case, the Ambient Pressure Case and the Continuum Flow Pressure Case. Singly Charged Ions are Assumed.

Calculations of the heavy ion percentages on the downleg portion of the 14.482 flight are significantly more difficult than for the upleg. This is because of the difficulties discussed in Chapter VI. A few points of the altitude profile of the heavy ion percentage on the downleg have been calculated assuming ambient atmospheric pressure, no pressure enhancement or reduction, inside the mass spectrometer. These calculations indicate the heavy ion cutoff point, where 50 per cent of all ions are heavy ions, occurred about 2 km lower than for the ambient pressure case on the upleg. The changeover from heavy ions to light ions occurred more quickly on the downleg.

7.2 Implications of Mass Spectrometer Data

Since no cluster ions with m/e ratios less than about 500 were seen during the 14.482 flight, subject to the constraint on sensitivity, two conclusions can be made. The first is that all the cluster ions had m/e ratios greater than 500. The second is that the detached shock wave was, in fact, in the mass spectrometer drift region during the upleg portion of the flight below 100 km. A discussion of the reasoning behind these two conclusions was given in section 6.3.3. The heavy ion measurements showed that essentially 100 per cent of the detected ions below about 92 km had m/e ratios greater than about 500 if singly charged ions were assumed.

Although the heavy ion measurements from the 14.482 mass spectrometer seem to be rather surprising, there are a number of possibilities which could make the results more consistent with previous measurements. First, the quadrupole mass filters and the

magnetic sector mass spectrometer used by previous researchers for D-region and lower E-region measurements required a low pressure, much lower than the ambient pressure in the D-region especially, for proper operation. This means ions are sampled through an orifice into the differentially pumped mass spectrometers. If these mass spectrometers were moving supersonically all the sampled ions must pass through a shock wave. Any composition changes which occur in the shock wave will be indistinguishable from the true ion composition. However, the cylindrical-electrode TOFMS flown on the 14.482 experiment package was specifically designed for high pressure operation with a large, open, ion collection area and no differential pumping. Since the shock wave for the upleg portion of the 14.482 flight was probably in the mass spectrometer drift region, the ion composition measurements are more likely to reflect the correct ion composition, even if ion fragmentation occurred.

Second, the quadrupole mass filters and the magnetic sector mass spectrometer flown on previous sounding rocket flights are extremely sensitive to the experiment package angle-of-attack in their detection of massive ions. This is because of the fairly long distances ions have to travel from the sampling orifice to the actual spectrometer (see especially Zbinden et al., (1975) or Johannessen and Krankowsky (1972)). Another difficulty in coping with large angles-of-attack, in the collection of massive ions, occurs in quadrupole mass filters. These instruments are unable to cope with large transverse velocities and the massive ions are more likely to collide

with the rods (Brubaker (1975)). Therefore, even if massive ions survive passing through the shock wave and the sampling orifice, they are much less likely to be collected in quadrupole or magnetic sector mass spectrometers on sounding rockets. The cylindrical-electrode TOFMS is relatively insensitive to transverse velocities because of the large ion acceptance area and the short ion flight path.

Third, the possibility of greatly decreased sensitivity at large ion masses ($m > 150$ amu) in quadrupole mass filters (Dawson (1975)) makes measurements using the quadrupole high pass mode very doubtful. The 14.482 cylindrical-electrode TOFMS does have discrimination effects, mainly from the ion gate, which will decrease the sensitivity of the spectrometer at larger ion masses. However, the sensitivity decrease is much slower, as the ion mass increases, compared to the quadrupole mass filter. It has also been calculated by Dr. B. R. F. Kendall and me that extremely heavy ions, with m/e ratios of 10^4 or more, will be collected by the cylindrical TOFMS if the experiment package angle-of-attack is less than 25°. These particles will have a large enough equivalent energy due to ram filling that they will pass through the ion gate and contribute to the background current.

Fourth, essentially all the previous D-region mass spectrometer experiments used some form of electron multiplier for ion detection. Electron multipliers have discrimination effects which are not well understood. This is because the operation of an electron multiplier

depends on the relationship between the collisions of various ions with the multiplier conversion dynode and the subsequent emission of secondary electrons. The emission of secondary electrons following an ion collision with a multiplier surface depends on the material the multiplier surface is made of, the type of ion, the mass of the ion, the energy of the ion and the angle at which the collision occurs. The cylindrical-electrode TOFMS used an electrometer for ion current measurements and was free of those discrimination effects.

The detection of heavy ions during the 14.482 flight does not really contradict the actual measurements of previous researchers. The lack of ion measurements for ion masses greater than 77 amu using the magnetic sector mass spectrometer (Zbinden et al., (1975)) and the doubtful results of the quadrupole mass filter in the high pass mode make it entirely possible that the presence of heavy ions in the D-region and the lower E-region ionosphere would not have been detected.

7.3 Comparison of 14.482 Heavy Ion Measurements with Results of Previous Investigators

A range of possible values for the heavy ion percentage from the 14.482 flight is shown in Figure (7.6). The measurements of water cluster ions of a number of previous investigators are shown for comparison. Narcisi and Bailey (1965), Goldberg and Aikin (1971), Narcisi et al., (1972b) and Johannessen and Krankowsky (1972, 1974) used differentially pumped quadrupole mass filters. Zbinden et al., (1975) used a magnetic sector mass spectrometer. The results from

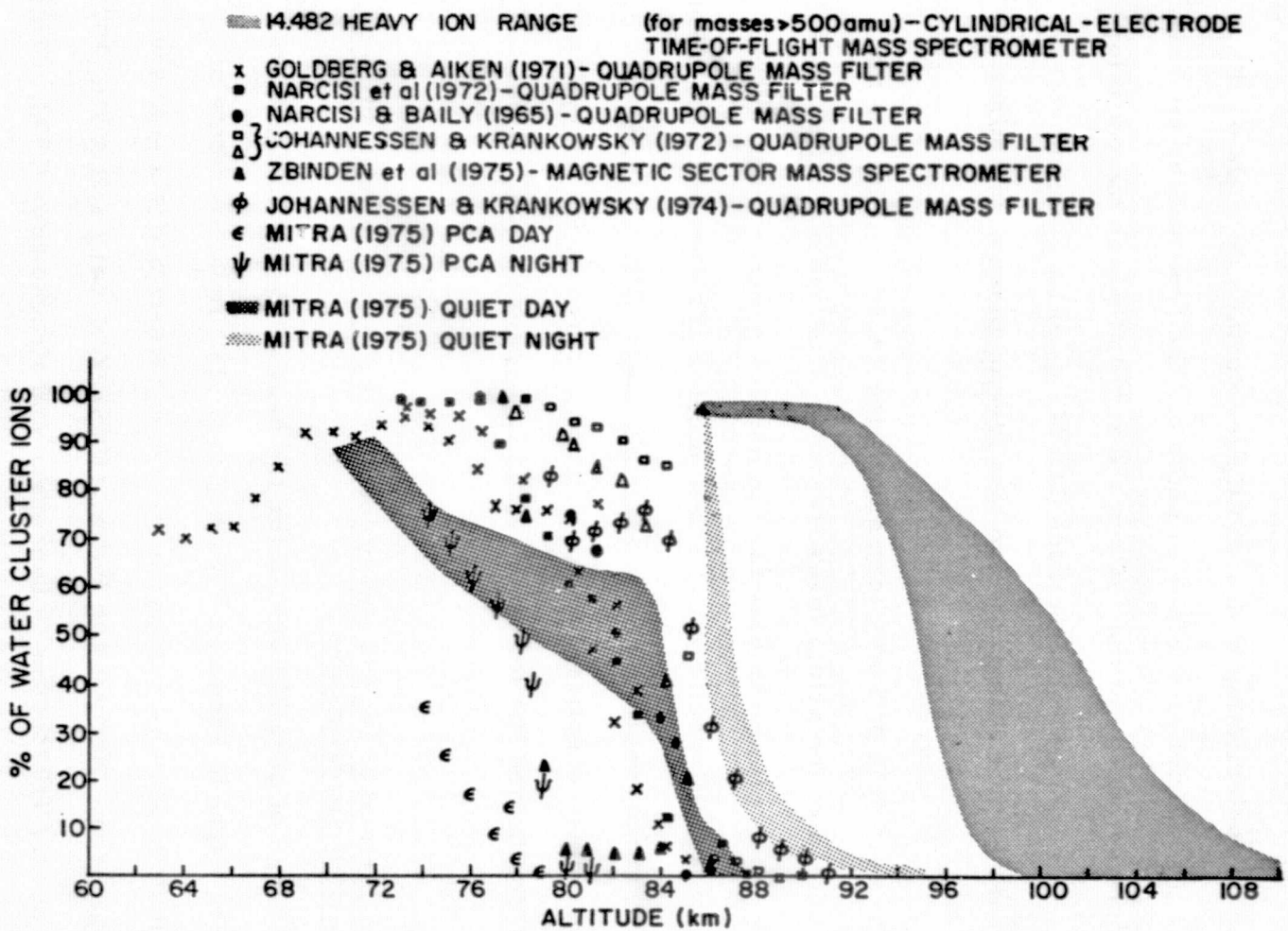

Figure 7.6 Comparison of the 14.482 Heavy Ion Profile with the Water Cluster Measurements of Previous Researchers. Singly Charged Ions are Assumed.

Mitra (1975) are a generalization of previous mass spectrometer data. The heavy ion altitude range for the 14.482 flight was obtained by taking, as limits, the minimum and maximum possible values of the heavy ion percentage from Figure (7.3) (while being consistent with aerodynamic constraints). At altitudes below 100 km, the experiment package was still definitely in the transition flow regime and the heavy ion altitude values were probably close to the maximum values of the 14.482 heavy ion percentage values shown in Figure (7.3) for the total immersion case. Near 100 km the experiment package was moving into the free molecular flow regime and the heavy ion percentage values profile approached the heavy ion profile representing the ambient pressure case shown in Figure (7.3). Singly charged ions were assumed for the 14.482 heavy ion range shown in Figure (7.6).

The altitude where the 14.482 measurements show the heavy ion cutoff point is at least 10 km higher than most of the measurements of water cluster ions. However, the slope of the 14.482 heavy ion cutoff is similar to some of the previous water cluster measurements. Also, a 10 km variation in the water cluster ion cutoff altitude has been seen under varying conditions.

The existence of hydrated ions of the form $H_3O^+ \cdot (H_2O)_n$ in the D-region was first reported by Narcisi and Bailey (1965). Many experimenters have since reported that the detection of $H_3O^+ \cdot (H_2O)_n$ ions (Goldberg and Blumle (1970), Goldberg and Aikin (1971), Johannessen and Krankowsky (1972, 1974), Krankowsky et al., (1972a, b) and Zbinden et al., (1975)). It has been shown that the

measured concentrations of $H_3O^+ \cdot (H_2O)_n$ ions vary considerably depending on draw-in potentials, vehicle velocities, vehicle attitudes and launch sites. Some general tendencies in the D-region hydrated ion measurements are an increase in the value of n at high latitudes, with slower vehicle velocities (reduced shock wave sampling effects) and with lower draw-in potentials. Significant variations of n are seen at different times of the year and with different ionosphere conditions.

The presence of hydrated ions with masses greater than 150 amu was detected by a quadrupole mass filter flown on a slowly moving experiment package (Aikin (1976)). Data from a previous cylindrical-electrode TOFMS flight has been examined by Kendall (1975) and showed that at least 75 per cent of the ions at 80 km had m/e ratios greater than 275. A sounding rocket ion composition measurement reported by Boyd et al., (1974) showed some interesting results. The instrument flown on this sounding rocket flight was a modified version of the Rogers-Boyd rf mass spectrometer (Rogers and Boyd (1966)). Because of the extremely small size of this spectrometer, and its position with respect to the sounding rocket, it was relatively free of shock wave effects. Unfortunately, the spectrometer was oriented so that it was parallel to the gas flow and ion collection might have been affected by the transverse velocities of the ions. The Rogers-Boyd instrument measured H_3O^+ (19) ions in significant quantities up to, and slightly above, 100 km. It also showed a sharp cutoff of NO^+ (30) and O_2^+ (32) ions just below 100 km. The mass

range of the instrument only extended to 60 amu. The sharp cutoff of the NO^+ (30) and O_2^+ (32) ions at higher altitudes than usually reported tends to support the 14.482 measurements.

It is significant that the investigators who delibrately altered the operating conditions of their quadrupole mass filter to increase the sensitivity at larger ion masses (> 100 amu), saw the most massive positive cluster ion to be reported to date (Johannessen and Krankowsky (1972)).

Observations of several other types of positive cluster ions in the D-region have also been made. These ions are $NO^+ \cdot (H_2O)_n$, $Na^+ \cdot (H_2O)_n$ and $Fe^+ \cdot (H_2O)_n$. At room temperature in uncontaminated atmospheres, at a pressure of one atmosphere, containing H_2O, CO_2, Ar, O_2 and N_2, the reported values for n for the hydrates $O_2^+ \cdot (H_2O)_n$, $H_3O^+ \cdot (H_2O)_n$ and $NO^+ \cdot (H_2O)_n$ usually do not exceed 6 (Siksna (1973)). However, under certain conditions larger values of n have been observed. Lin (1973) has observed $H_3O^+ \cdot (H_2O)_n$ cluster ions with n values up to 179 in studies of supersonic water jets. He used a quadrupole mass filter with a radio frequency of 650 kHz. This was a low frequency compared to the frequency used in quadrupole mass filters carried on sounding rockets. Searcy and Fenn (1974) have observed $H_3O^+ \cdot (H_2O)_n$ cluster ions with n up to 27 in studies of free jet expansion. Both Lin (1973) and Searcy and Fenn (1974) reported an unusual stability of the $H_3O^+ \cdot (H_2O)_{20}$ ion. A study of water clathrates by Siksna (1973) has suggested a possible mechanism for the stability of massive cluster ions. This stability is accomplished by the formation of a clathrate cage around an alien molecule

or ion. The original study of clathrates was made by Powell (1948). The role of clathrates as prenucleation bases for condensation of water vapor has been studied by Bolander et al., (1969), Allen and Kassner (1969), and Loeb (1971). A significant prediction of these studies of clathrates was the existence of the unusual stability of clathrates with 20, 24, 26, 57, 70, 72, etc. water molecules. The stable clathrate with 20 water molecules corresponds exactly to the reported stability of $H_3O^+ \cdot (H_2O)_{20}$ ions in the laboratory.

The existence of particulates in the mesosphere has been proposed by a number of researchers (for example, Narcisi et al., (1972b) and Hunt (1969)). The attachment of ions and electrons to these particulates has been suggested as a possible mechanism for the production of massive ions by Chesworth and Hale (1974). The measurements of some Gerdien condensers have indicated the existence of ions with possible m/e ratios of several thousand (Bourdeau et al., (1959), Pederson (1963), Widdel et al., (1971), Rose and Widdel (1972) and Farrokh (1975)). Exact calculations of ion m/e ratios from Gerdien condenser measurements is difficult because of the lack of knowledge about the relationship between ion mobility and ion m/e ratios. Also, Gerdien condenser measurements above 70 km are difficult to obtain because of the large size of the condenser which would be required.

The existence of noctilucent clouds is a well documented phenomenon of the D-region. These noctilucent clouds are thought to be particulates, possibly composed mostly of water vapor. These clouds have been observed at altitudes up to 92 km. A

summary of the knowledge about noctilucent clouds was given by Hummel (1973).

The presence of noctilucent clouds, the possibility of the existence of massive cluster ions, the existence of clathrates and the possible existence of massive charged particulates tend to support the measurements of the 14.482 mass spectrometer. Because of the problems involved in D region and lower E-region ion measurements with quadrupole mass filters and magnetic sector mass spectrometers, the measurements of previous researchers using these instruments do not really contradict the 14.482 measurements. The results of the 14.482 flight indicate that, if singly charged ions were assumed, heavy ions with m/e ratios greater than about 500 dominated the upper D-region and probably extended up beyond 95 km on the 14.482 launch date.

The cylindrical-electrode TOFMS can not tell us which type of massive ion produced the background currents observed during the flight. It is entirely possible that the heavy ions which produced the background current were of several different types. It should also be pointed out that singly charged ions are not the only possible type of ion. A relatively small number of multiply charged massive ions could produce the observed currents. In this case the heavy ion percentages, calculated assuming singly charged ions, would vary considerably. It would then be more accurate to say that the amount of charge carried on positive charge carriers was carried predominantly on charge carriers with m/e ratios greater than about 500 up to 95 km. It is because of the possibility of multiply charged ions that number densities for the 14.482 heavy ions have not been calculated. However, for reference, the number of singly charged

heavy ions in the upper D-region, calculated from the 14.482 measurements, would be about 5×10^3 ions/cm^3.

In summary, the 14.482 heavy ion measurements are worthy of being considered. The use of an open ion source, a spectrometer which operated at ambient D-region pressures, the completely different operation of the 14.482 spectrometer, a shock wave detachment distance which probably did not affect ion composition measurements, different mass discrimination effects and the reasonable results from the 14.482 spectrometer with respect to the metallic ion layer and the ion composition above 100 km should make the 14.482 measurements an important check on previous D-region ion composition measurements using quadrupole mass filters and magnetic sector mass spectrometers. Adequate explanations for the dominance of the charge on heavy ions to a relatively high altitude and the evident lack of lighter cluster ions have not yet been discovered. The flight of a nearly identical sounding rocket package in the near future is expected to help find the answers to these questions.

CHAPTER VIII

SUMMARY, CONCLUSIONS AND SUGGESTED ADDITIONAL INQUIRIES

8.1 Summary

8.1.1 Ion Dynamics in TOFMS

The results of the studies of miniature time-of-flight mass spectrometers (TOFMS), in order to better understand their operation in a lower ionospheric environment, are summarized below.

A cylindrical-electrode two-field TOFMS was analyzed theoretically. Computer programs were developed to study the space focusing and velocity focusing characteristics for a variety of operating voltages, electrode radii, electrode spacings and non-zero initial ion velocities. A spherical-electrode two-field TOFMS was also analyzed theoretically and computer programs were developed to study the space focusing and velocity focusing characteristics. A number of observations were made which confirm the results of previous investigators. They are:

1. Cylindrical-electrode TOFMS, spherical-electrode TOFMS and planar TOFMS had almost identical space focusing and velocity focusing characteristics, if similar electrode spacings and operating voltages were used, for an outer electrode radius as small as 38 mm.
2. Inferior mass peak shapes would result if the operating voltages of a TOFMS were adjusted to allow ions starting at the inner and outer source region electrodes to arrive at the collector simultaneously (i.e. be space focused).

3. The spread in ion initial energies was the cause for the poor observed resolving power at good space focusing operating voltages in a TOFMS.
4. The velocity focusing characteristics can be improved by increasing the voltage ratio, at the cost of degrading the space focusing, if the ion initial energies and electrode spacings are not altered.
5. Varying the drift region length was equivalent to varying the voltage ratio as far as space focusing was concerned.
6. It was possible to deduce the ion initial energy distribution, in the radial direction. by studying the mass peak produced by operating with good space focusing voltages.
7. The velocity focusing characteristics of a TOFMS were almost entirely determined in the source and acceleration regions.

The possibility of enhancing the resolving power of a TOFMS by using initial ion velocities which depended on the ion positions in the source region was suggested by computer studies. This resolving power enhancement method was studied theoretically and using computer programs. These studies suggested a significant improvement in resolving power was possible up to a factor of 7.5 for certain operating conditions.

Computer programs were developed to study the effects of gating in a TOFMS on resolving power and sensitivity and to examine any mass discrimination effects. It was found that, theoretically,

gating will decrease the spectrometer sensitivity for all ion masses. The amount of sensitivity decrease depended on the gate pulse width and height and the height of the gate barrier potential. It was also found that the gating arrangement studied in this thesis discriminated against heavier ion masses and against ions with lower kinetic energies. The discrimination against lower ion energies was equivalent to discrimination against certain starting positions in the source region. For typical cylindrical-electrode TOFMS operating voltages, only ions starting in the outer half of the source region, corresponding to the ions receiving the largest kinetic energies, will get through the gate. The operation of the gate usually degraded the spectrometer resolving power but under certain conditions had no effect on the resolving power, or even slightly improved the resolving power, because of the discrimination against some of the ion starting positions.

An attempt was made to study the effect of the gate pulse starting time on the ion flight times through the gate region. The gate pulse starting time was measured with respect to an ions arrival in the gate region. This study showed that it should be possible to use the computer results to determine the exact effect of gating on an ion mass peak by integrating over all gate starting times.

Both cylindrical and hemispherical-electrode TOFMS have been experimentally investigated. The cylindrical-electrode TOFMS studied was a gated version with a drift region length of 4.2 cm. A maximum resolving power of about 10 was obtained, with improvements in the associated electronics, while operating without the

variable initial source velocity method of resolving power enhancement. Operation in the resolving power enhancement mode has produced a maximum resolving power of 21 to date. A decrease in sensitivity was expected in the enhanced resolving power mode because of the higher average velocities in the source region. However, no significant decrease in sensitivity was observed in the preliminary measurements. The operation of a cylindrical-electrode TOFMS at pressures up to about 7 pa was re-examined because of improvements in pressure measuring methods. The results were consistent with previous measurements and showed the usefullness of the cylindrical TOFMS at pressures which are found in the D-region of the ionosphere. A hemispherical-electrode TOFMS with a drift region length of 4.02 cm, and without gating or the resolving power enhancement method, produced a maximum resolving power of 13. Hemispherical electrodes were used in the laboratory instrument because of greater simplicity in construction and handling.

8.1.2 Ionospheric Measurements

An experiment package carrying a cylindrical-electrode TOFMS and three ion probes was described. This package was developed for sounding rocket positive ion composition measurements in the D-region and E-region ionosphere. The spectrometer calibration methods and a description of the environmental testing of the experiment package were given.

A successful sounding rocket experiment package was launched on May 15, 1974 from Wallops Island, Virginia. The sounding rocket

launch conditions and the actual flight were described. The presence of a detached shock wave in front of the experiment package was discussed and the method for calculating the shock wave parameters, based on Cuirle (1976), was presented. The method for reducing the mass spectrometer data was also discussed. There were two major difficulties in reducing the mass spectrometer data. First, the spin modulation had to be removed. This was done by auto-correlation. Second, the background current was much larger than expected. A drop in the gate barrier potential and a shift in the payload potential with respect to the surrounding plasma explained a portion of this large background current. The background current at apogee was used to recalibrate the mass spectrometer background current ratios. The expected effects, on the mass spectra, due to sampling through a shock wave were discussed. Because of the difficulties in the data reduction and because the experiment package did not separate from the second stage motor only the upleg portion of the mass spectrometer data was considered in detail.

The TOFMS data from the sounding rocket flight will give the correct ratio of the ion densities for ions with different mass-to-charge ratios observed at any one altitude. The mass spectrometer data indicated the presence of what was probably NO^+ (30), O_2^+ (32) and O^+ (16) in the upper E-region ionosphere. A metallic ion layer at about 95 km, probably consisting of Fe^+ (56) and Mg^+ (24) or Na^+ (23), was also observed. The absolute ion densities for these ions could not be calculated. This was because the TOFMS was

never intended to measure ion densities, but rather just the ion composition. The mass spectrometer current can be normalized to give correct ion densities if another instrument, such as one of the ion probes on the experiment package, was used to calculate the total ion density. Unfortunately, the 14.482 ion probe data has not been completely reduced and no other accurate source of total ion density for the 14.482 flight was available.

When the background current from the 14.482 mass spectrometer data was examined, it was calculated that ions with mass-to-charge ratios greater than about 500 dominated the upper D-region and at least up to 95 km when singly charged ions were assumed. If the presence of multiply charged ions was assumed, the 14.482 data could be interpreted to indicate that the positive charge carried on charge carriers with m/e ratios greater than about 500 was greater than 50 per cent of the total positive charge carried on all positive charge carriers below about 95 km.

8.2 Conclusions and Implications

The use of a TOFMS with an open source which operated at D-region pressures with no differential pumping, the completely different operation of the 14.482 TOFMS, shock wave sampling effects which probably did not affect the ion composition measurements, and completely different mass discrimination effects indicated the usefullness of the 14.482 results as a check on previous ion composition measurements.

The reasonable ion composition detected by the 14.482 mass spectrometer in the upper E-region indicated the proper operation of the mass spectrometer. However, the presence of ions with m/e ratios greater than 500, detected by the 14.482 mass spectrometer in the upper D-region and the lower E-region, has not been observed in the past. The possible types of ions which could have m/e ratios greater than 500 are massive cluster ions, charged clathrates or charged particulates. The more likely contributors to the background current measured by the 14.482 mass spectrometer are charged particulates and charged clathrates. The massive ions detected during the sounding rocket flight probably were multiply charged. In this case, the results of the 14.482 flight indicate the dominance of the charge on massive charge carriers with m/e ratios greater than about 500 up to an altitude of about 95 km.

These massive ions, with m/e ratios greater than 500, would not have been observed by the quadrupole mass filters and the magnetic sector mass spectrometer flown by previous investigators for a number of reasons. They are:

1. The sampling through an orifice, behind any shock wave, into the differentially pumped quadrupole mass filters and the magnetic sector mass spectrometer flown on previous sounding rocket flights allows composition changes before ions enter the actual spectrometer.
2. The sensitivity of previously flown mass spectrometers to angle-of-attack, because of the relatively long distances between the orifice and the spectrometer in these flights,

makes the collection of massive ions less likely in these instruments.

3. The inability of the quadrupole mass filter to cope with large transverse velocities makes the collection of massive ions less likely.
4. The mass range of the magnetic sector mass spectrometer flown by Zbinden et al., (1975) extended only to 77 amu.
5. The rapid sensitivity decrease of the quadrupole mass filter at large m/e ratios (greater than about 150) makes the quadrupole high pass mode measurements very doubtful.
6. The use of electron multipliers as current detectors on previous quadrupole mass filter and magnetic sector mass spectrometer flights introduced serious mass discrimination effects against massive ions.

The implications of the 14.482 results are important. The presence of massive positive ions would require a new appraisal of the chemistry of the D and lower E-regions of the ionosphere to properly account for their presence.

The data reduction of the 14.482 data required the assumptions that continuum flow theory could be used in the transition flow regime for the 14.482 flight and the experiment package had an angle-of-attack of 0°. It was also assumed that there were no massive ions at the 14.482 experiment package apogee ($\sim$ 138 km) in order to calculate the background current ratios used for data reduction.

8.3 Suggested Additional Inquiries; Ion Dynamics

For continued studies of the time-of-flight mass spectrometers discussed in this thesis it would be useful to carry out the following projects.

1. Study the changes in the focusing characteristics in cylindrical or hemispherical TOFMS when the outer spectrometer electrode radius is reduced to less than 30 mm. This should emphasize the variations from the electric field between planar electrodes and might improve space focusing.
2. Apply deconvolution methods in order to increase the resolving power of the TOFMS beyond the factor of 7.5 mentioned in this thesis. Computer deconvolution methods have been described by Zabielski (1966) and Rarick (1969) which could produce an effective increase in resolving power up to a factor of 8 under optimum conditions (no noise). Commonly used Fourier deconvolution methods can produce effective increases in resolving power up to a factor of 2.5. Using Fourier deconvolution methods, an effective resolving power of 180 is entirely possible for the instruments discussed in this thesis.
3. Use the gate simulation computer programs with the computer programs for calculating ion flight times in a TOFMS to deduce the exact mass peak shapes. The

most effective use of the computer programs developed for the work in this thesis would be an interactive (with the programmer) study of TOFMS operating conditions on a hybrid computer. Some work in this direction has been started by Steve Rossnagel of the Physics Department of The Pennsylvania State University.

4. Study the operation of the hemispherical-electrode TOFMS using the resolving power enhancement method introduced in this thesis.

8.4 Suggested Additional Inquiries; D-Region Measurements

A follow-up sounding rocket flight scheduled for the near future should provide more data on the D-region ion composition. This flight will have an apogee at about 85 km and will be flown with a parachute. This should allow the examination of D-region under supersonic and subsonic sampling conditions. It should also produce data for an angle-of-attack which is varying (before parachute deployment) and for a constant angle-of-attack (after parachute deployment). Of special interest will be an attempt to find why no light water cluster ions (with m/e ratios less than 500) were observed during the 14.482 flight.

It is suggested that a revealing experiment would be to simultaneously fly a time-of-flight mass spectrometer, a quadrupole mass filter and a charge detector (such as a faraday cup) through a noctilucent cloud. This would allow a comparison of these instruments under conditions where massive particles are known to exist.

The resolution enhancement method presented in this thesis should be incorporated in future TOFMS sounding rocket experiment flights as soon as it is feasible. This will provide a resolving power for the cylindrical-electrode TOFMS which is comparable to the resolving power of other types of mass spectrometers used in lower ionosphere measurements. It is also suggested that a flyable version of the hemispherical-electrode TOFMS be constructed and tested for possible use on future sounding rocket flights. The superior sensitivity of the hemispherical TOFMS should be very useful in lower ionosphere measurements.

REFERENCES

Agishev, E. I. and N. I. Ionov, The pulsed mass spectroscope, Sov. Phys.-Tech. Phys., 1, 201, 1956 (translated from Zh. Tekh. Fiz., 26, 203, 1956).

Aikin, A. C. and R. A. Goldberg, Metallic ions in the equatorial ionosphere, J. Geophys. Res., 78, 734, 1973.

Aikin, A. C., Private communication, 1976.

Allen, L. B. and J. L. Kassner, Jr., The nucleation of water vapor in the absence of particulate matter and ions, J. Colloid. Interface Sci., 30, 81, 1969.

Arnold, F., W. Berthold, B. Betz, P. Lammerzahl and J. Zahringer, Mass spectrometer measurements of positive ions and neutral gas between 100 and 223 km above Andoya, Norway, Space Res. IX (Ed. K. S. W. Champion, P. A. Smith and R. L. Smith-Rose), North-Holland, Amsterdam, 256, 1969.

Arnold, F., J. Kissel, D. Krankowsky, H. Wieder and J. Zahringer, Negative ions in the lower ionosphere: A mass-spectrometric measurement, J. Atmos. Terres. Phys., 33, 1169, 1971.

Arnold, F., K. H. Marien and D. Krankowsky, New aspects in lower ionosphere positive cluster ion composition: Results from an improved mass spectrometer probe experiment, Abstract in Methods of Measurements and Results of Lower Ionosphere Structure (Ed. K. Rawer), Akademie-Verlag, Berlin, 239, 1974.

Arnold, F. and D. Krankowsky, Measurements of $H_2O_2^+$ in the D-region and implications for mesospheric H_2O_2, Geophys. Res. Lett., 1, 243, 1974.

Bakker, J. M. B., The time-focusing principle: A double-focusing design for time-of-flight mass spectrometers, Int. J. Mass Spectrom. Ion Phys., 6, 291, 1971.

Bakker, J. M. B., A beam modulated time-of-flight mass spectrometer. Part I: Theoretical considerations, J. Phys. E, 6, 785, 1973.

Barnes, E. E., Electronics for the operation of a rocket borne wedge time of flight mass spectrometer, PSU-IRL-SCI-379(E), The Pennsylvania State University, University Park, Pennsylvania, 1971.

Bennett, W. H., Radiofrequency mass spectrometry, J. Appl. Phys., 21, 143, 1950.

Bolander, R. W., L. B. Allen and J. L. Kassner, Jr., A molecular theory for the nucleation of water vapor, Proceedings 7th International Conference on Condensation and Ice Nuclei, Prague and Vienna, 64, 1969.

Bourdeau, R. E., E. C. Whipple, Jr. and J. F. Clark, Analytic and experimental conductivity between the stratosphere and the ionosphere, J. Geophys. Res., 64, 1363, 1959.

Bowen, P. J., R. L. F. Boyd, W. J. Raitt and A. P. Willmore, Ion composition of the upper F-region, Proc. R. Sco. (London), A281, 504, 1964.

Boyd, R. L. F. and D. Morris, A radiofrequency probe for the mass-spectrometric analysis of ion concentrations, Proc. Phys. Soc., A68, 1, 1955.

Boyd, R. L. F., Some techniques of physical measurement, Proc. R. Soc. (London), A253, 513, 1959.

Boyd, R. L. F., Space science, Nature, 186, 749, 1960.

Boyd, R. L. F., E. B. Dorling, K. Norman and L. J. C. Woolliscroft, Ion mass spectrometry of the lower ionosphere, 1 May 1967 - 15 February 1974, Final Scientific Report AFCRL-TR-74-0503, European Office of Aerospace Research Contract F 61052-67-C-0078, 1974.

Brinton, H. C., L. C. Scott, M. W. Pharo, III and J. T. Coulson, The Bennett ion-mass spectrometer on Atmosphere Explorer-C and -E, Radio Science, 8, 323, 1973.

Brubaker, W. M., Private communication, 1975.

Cameron, A. E. and D. F. Eggers, An ion 'velocitron', Rev. Sci. Instrum., 19, 605, 1948.

Carrico, J. P., Inhomogeneous oscillatory electric field time-of-flight mass spectrometer, Dynamic Mass Spectrometry (ed. P. Price), 2, Heyden and Son, Ltd., London, 161, 1971.

Chapman, S., The absorption and dissociative or ionizing effect of monochromatic radiation in an atmosphere on a rotating earth, Proc. Phys. Soc. (London), 43, 26, 1931a.

Chapman, S., The absorption and dissociative or ionizing effect of monochromatic radiation in an atmosphere on a rotating earth, II. Grazing incidence, Proc. Phys. Soc. (London), 43, 483, 1931b.

Chesworth, E. T. and L. C. Hale, Ice particulates in the mesosphere, Geophys. Res. Lett., 1, 347, 1974.

CIRA 1972, COSPAR International Reference Atmosphere, Akademie-Verlag, Berlin, 1972.

Cuirle, W., Masters thesis in Physics, to be published, 1976.

Dawson, P. H., The acceptance of the quadrople mass filter, Int. J. Mass Spectrom. Ion Phys., 17, 423, 1975.

Diem, H. T., A time-of-flight mass spectrometer suitable for ionospheric composition investigations, PSU-IRL-SCI-309, The Pennsylvania State University, University Park, Pennsylvania, 1967.

Farrokh, H., Design of a simple Gerdien condenser for ionosphere D-region charged particle density and mobility measurements, PSU-IRL-SCI-433, The Pennsylvania State University, University Park, Pennsylvania, 1975.

Ferguson, R. E., K. E. McKulloh and H. M. Rosenstock, Observation of the products of ionic collision processes and ion decomposition in a linear pulsed time-of-flight mass spectrometer, J. Chem. Phys., 42, 100, 1965.

Franklin, J. L., P. M. Hierl and D. H. Whan, Measurement of the translational energy of ions with a time-of-flight mass spectrometer, J. Chem. Phys., 47, 3148, 1967.

Glenn, W. E., Jr., A time-of-flight mass spectrograph, AECD Report No. 3337 (UCRL-1628), 1952.

Goldberg, R. A. and A. C. Aikin, Studies of positive ion composition in the equatorial D-region ionosphere, J. Geophys. Res., 76, 8352, 1971.

Goldberg, R. A. and A. C. Aikin, Comet Enke: Meteor metallic ion identification by mass spectrometer, Science, 180, 294, 1973.

Goldberg, R. A. and L. J. Blumle, Positive ion composition from a rocket borne mass spectrometer, J. Geophys. Res., 75, 133, 1970.

Goldberg, R. A., Silicon ions below 100 km: A case for SiO_2^+, Radio Science, 10, 329, 1975.

Hadley, F. J. and J. L. Franklin, Iterative deconvolution of time-of-flight mass peaks for the determination of translational energy of ions, Int. J. Mass Spectrom. Ion Phys., 18, 249, 1975.

Hazelton, R. B., Pulse circuitry for a flyable time-of-flight mass spectrometer, PSU-IRL-SCI-329(E), The Pennsylvania State University, University Park, Pennsylvania, 1968.

Heaviside, O., Telegraphy. I, Theory, Encycl. Brittanica (10th ed.), 33, 213, 1902.

Hoffman, J. H., Composition measurements of the topside ionosphere, Science, 155, 322, 1967.

Hoffman, J. H., Ion mass spectrometer on Explorer XXXI satellite, Proc. IEEE, 57, 1063, 1969.

Hoffman, J. H., Studies of the composition of the ionosphere with a magnetic deflection mass spectrometer, Int. J. Mass Spectrom. Ion Phys., 4, 315, 1970.

Hoffman, J. H., W. B. Hanson, C. R. Lippincott and E. E. Ferguson, The magnetic ion-mass spectrometer on Atmosphere Explorer, Radio Science, 8, 315, 1973.

Hulbert, E. O., Ionization in the upper atmosphere of the earth, Phys. Rev., 31, 1018, 1928.

Hummel, J. R., A survey of noctilucent cloud phenomenon, PSU-IRL-IR-28, The Pennsylvania State University, University Park, Pennsylvania, 1973.

Hunt, W. W., Jr., Water conglomerates in the D-region, Aeronomy Report No. 32, University of Illinois, Urbana, 311, 1969.

Ionov, N. I. and B. A. Mamyrin, Mass spectrometer with a pulsed ion source, Zh. Tekh. Fiz., 23, 2101, 1953.

Istomin, V. G., Investigation of the ion composition of the earth's atmosphere on geophysical rockets 1957-1959, Planet. Space Sci., 9, 179, 1962.

Istomin, V. G. and A. A. Pokhunkov, Mass-spectrometer measurements of atmospheric composition in the USSR, Space Res. III (Ed. W. Priester), North-Holland, Amsterdam, 117, 1963.

Johannessen A. and D. Krankowsky, Positive-ion composition measurement in the upper mesosphere and lower thermosphere at a high latitude during summer, J. Geophys. Res., 77, 2888, 1972.

Johannessen, A. and D. Krankowsky, Daytime positive ion composition measurement in the altitude range 73-137 km above Sardinia, J. Atmos. Terres. Phys., 36, 1233, 1974.

Johannessen, A., D. Krankowsky, F. Arnold, W. Riedler, M. Friedrich, K. Folkstad, G. Skovli, E. V. Thrane and J. Troim, Detection of water cluster ions at the high latitude summer mesopause, Nature, 235, 215, 1972.

Johnson, C. Y. and J. P. Heppner, Night-time measurement of positive and negative ion composition to 120 km by rocket-borne spectrometer, J. Geophys. Res., 60, 533, 1955.

Johnson, C. Y. and J. P. Heppner, Daytime measurement of positive and negative ion composition to 131 km by rocket-borne spectrometer, J. Geophys. Res., 61, 575, 1956.

Johnson, C. Y. and E. B. Meadows, First investigation of ambient positive-ion composition to 219 km by rocket-borne spectrometer, J. Geophys. Res., 60, 193, 1955.

Karataev, V. I., B. A. Mamyrin and D. V. Shmikk, New method for focusing ion bunches in time-of-flight mass spectrometers, Sov. Phys.-Tech. Phys., 16, 1177, 1972 (translated from Zh. Tekh. Fiz, 41, 1498, 1971).

Katzenstein, H. S. and S. S. Friedland, New time-of-flight mass spectrometer, Rev. Sci. Instrum., 26, 324, 1955.

Keller, R., Spectre de masses obtenu par mesure du temps de vol, Helv. Phys. Acta, 22, 386, 1949.

Kendall, B. R. F., Private communication, 1975.

Kendall, B. R. F. and J. O. Weeks, Transient desorption of water vapor: A potential source of error in upper atmosphere rocket experiments, J. Geophys. Res., 79, 1582, 1974.

Kendall, B. R. F. and R. F. Reiter, Miniature time-of-flight mass spectrometer for ion composition measurements in the lower ionosphere, presented at the 23rd Annual Conference on Mass Spectrometry and Allied Topics, Houston, Texas, May 25-30, 1975.

Kennelly, A. E., On the elevation of the electrically conducting strata of the earth's atmosphere, Elec. World and Eng., 39, 473, 1902.

Krankowsky, D., F. Arnold and H. Wieder, Recent positive and negative ion composition measurements in the lower ionosphere by means of mass spectrometers, in Magnetosphere-Ionosphere Interactions (Ed. K. Folkestad), Oslo University Press, Oslo, Norway, 1972a.

Krankowsky, D., F. Arnold, H. Wieder, J. Kissel and J. Zahringer, Positive ion composition in the lower ionosphere, Radio Science, 7, 93, 1972b.

Krankowsky, D., F. Arnold, H. Wieder and J. Kissel, The elemental and isotopic abundance of metallic ions in the lower E-region as measured by a cryogenically pumped quadrupole mass spectrometer, Int. J. Mass Spectrom. Ion Phys., 8, 379, 1972c.

Liepmann, H. W. and A. Roshko, Elements of Gas Dynamics, Wiley and Sons, New York, 1957.

Lin, Sin-Shong, Detection of large water clusters by a low rf quadrupole mass filter, Rev. Sci. Instrum., 44, 516, 1973.

Lincoln, K. A., A velocity-modulation mass spectrometer, Doctoral dissertation, Stanford University, 1957, University Microfilms, Ann Arbor, Michigan, Publication No. 23204, 88 pp.

Loeb, L. B., On the appearance and mechanisms of formation of Langevin-type ions and related nuclei, Aerosol Science, 2, 133, 1971.

MacKenzie, E. C., The investigation of ionospheric electron density and ion composition using rocket-borne probes, Doctoral dissertation, Electron Physics Department, University of Birmingham, London, 1964.

Marable, N. L. and G. Sanzone, High resolution time-of-flight mass spectrometry, theory of the impulse-focused time-of-flight mass spectrometer, Int. J. Mass Spectrom. Ion Phys., 13, 185, 1974.

Mitra, A. P., D-region in disturbed conditions, including flares and energetic particles, J. Atmos. Terres. Phys., 37, 895, 1975.

Nanevicz, J. E., Results of Titan III flight electrostatic experiments, AFAL-TR-72-325, Lightning and Static Electricity Conference Papers 12-15 December 1972, Las Vegas, Nevada, AFAL AFSC, WPAFB, Ohio, 1972.

Nanevicz, J. E., Flight-test studies of static electrification on a supersonic aircraft, Final Report, Contract F33615-68-C-1359, SRI Project 6091, Stanford Research Institute, Menlo Park, California, 1974.

Narcisi, R. S., Ion composition measurements and related ionospheric processes in the D and lower E-region, Ann. Geophys., 22, 224, 1966.

Narcisi, R. S., Ion composition in the mesosphere, Space Res. VII (Ed. L. Smith-Rose), North-Holland, Amsterdam, 186, 1967.

Narcisi, R. S., On water cluster ions in the ionospheric D region, Planetary Electrodynamics (Ed. S. C. Coroniti and J. Hughes), 2, Gordon and Breach, New York, 447, 1969.

Narcisi, R. S., Shock wave and electric field effects in D-region water cluster ion measurements (abstract), Eos. Trans. AGU, 51, 306, 1970.

Narcisi, R. S., Mass spectrometer measurements in the ionosphere, in Physics and Chemistry of Upper Atmospheres (Ed. B. M. McCormac), D. Reidel, Dordrecht, Holland, 171, 1973.

Narcisi, R. S. and A. D. Bailey, Mass spectrometric measurements of positive ions at altitudes from 64 to 112 kilometers, J. Geophys. Res., 70, 3687, 1965.

Narcisi, R. S., R. A. Langley, H. A. Cohen and J. M. Elwell, Balloon-borne mass spectrometer measurements of the constituents of the atmosphere up to 28 kilometers, AFCRL-66-339, Environmental Research Papers, No. 197, 1966.

Narcisi, R. S., A. D. Bailey and L. Della Lucca, The composition of the lower ionosphere during the 1965 Leonid meteor shower, Space Res. VII (Ed. R. L. Smith-Rose), North-Holland, Amsterdam, 446, 1967.

Narcisi, R. S., C. R. Philbrick, A. D. Bailey and L. Della Lucca, Review of daytiime, sunrise and sunset ion composition of the D-region, Aeronomy Report No. 32, University of Illinois, Urbana, 355, 1969a.

Narcisi, R. S., A. D. Bailey and L. Della Lucca, Positive ion composition measurements in the lower ionosphere during the 12 November 1966 solar eclipse, Aeronomy Report No. 32, University of Illinois, Urbana, 450, 1969b.

Narcisi, R. S., A. D. Bailey, L. Della Lucca, C. Sherman and D. M. Thomas, Mass spectrometric measurements of negative ions in the D- and lower E-regions, J. Atmos. Terres. Phys., 33, 1147, 1971.

Narcisi, R. S., C. Sherman, C. R. Philbrick, D. M. Thomas, A. D. Bailey, L. E. Wlodyka, R. A. Wlodyka, D. Baker and G. Federico, Negative ion composition of the D and E regions during a PCA, Proceedings of COSPAR Symposium on Solar Particle Event of November 1969 (Ed. J. C. Ulwick), AFCRL-72-0474, 411, 1972a.

Narcisi, R. S., A. D. Bailey, L. E. Wlodyka and C. R. Philbrick, Ion composition measurements in the lower ionosphere during the November 1966 and March 1970 solar eclipses, J. Atmos. Terres. Phys., 34, 647, 1972b.

Narcisi, R. S., C. R. Philbrick, D. M. Thomas, A. D. Bailey, L. E. Wlodyka, D. Baker, G. Federico, R. Wlodyka and M. E. Gardner, Positive ion composition of the D and E regions during a PCA, Proceedings of COSPAR Symposium on Solar Particle Event of November 1969 (Ed. J. C. Ulwick), AFCRL-72-0474, 421, 1972c.

Narcisi, R. S. and W. Roth, The formation of cluster ions in laboratory sources and in the ionosphere, Advan. Electron. Electron Phys., 29, 79, 1970.

Oran, M. and Y. Paiss, A dynamic mass spectrometer for the study of laser-produced plasmas, Rev. Sci. Instrum., 44, 1293, 1973.

Paul, W. and M. Raether, Das elektrische massenfilter, Z. Physik, 140, 262, 1955.

Pavlenko, V. A., L. N. Ozerov and A. E. Rafal'son, Nonmagnetic time-of-flight mass spectrometers, Sov. Phys.-Tech.-Phys., 13, 431, 1968 (translated from Zh. Tekh. Fiz., 38, 581, 1968).

Pederson, A., Measurement of ion concentration in the D-region of the ionosphere with a Gerdien condenser rocket probe, FOA 3 Report A 607, Research Institute of National Defense, Stockholm, 1963.

Poschenrieder, W. P. and G. H. Oetjen, New directional and energy focusing time-of-flight mass spectrometers for special tasks in vacuum and surface physics, J. Vac. Sci. Tech., 9, 212, 1972.

Powell, H. M., The structure of molecular compounds. IV. Clathrate compounds, J. Chem. Soc. (London), 61, 1948.

Powell, W., Private communication, 1976.

Raitt, W. J., S. Laflin and R. L. F. Boyd, A synoptic view of ionic constitution above the F-layer maximum, Space Res. V (Ed. D. G. King-Hele, P. Muller and G. Righini), North-Holland, Amsterdam, 629, 1965.

Raitt, W. J., J. Blades, T. S. Bowling and A. P. Willmore, A satellite-borne positive ion mass spectrometer, J. Phys. E: Sci. Instrum., 6, 443, 1973.

Rarick, J. P., Deconvolution of physical data, PSU-IRL-SCI-344, The Pennsylvania State University, University Park, Pennsylvania, 1969.

Reiter, R. F. and B. R. F. Kendall, Miniature time-of-flight mass spectrometer with hemispherical electrodes, presented at the 22nd Annual Conference on Mass Spectrometry and Allied Topics, Philadelphia, Pennsylvania, May 19-24, 1974.

Rogers, A. J. and R. L. F. Boyd, A radiofrequency ion mass spectrometer of very small path length, J. Sci. Instrum., 43, 791, 1966.

Rose, G. and H. U. Widdel, Results of concentration and mobility measurements for positively and negatively charged particles taken between 85 km and 22 km in sounding rocket experiments, Radio Science, 7, 81, 1972.

Sanzone, G., Energy resolution of the conventional time-of-flight mass spectrometer, Rev. Sci. Instrum., 41, 741, 1970.

Sayers, J., Self-contained measuring equipment for electron density and ionic mass spectrum, Proc. R. Soc (London), A253, 522, 1959.

Searcy, J. Q. and J. B. Fenn, Clustering of water on hydrated protons in a supersonic free jet expansion, J. Chem. Phys., 61, 5282, 1974.

Siksna, R., Water clathrates as aerosol particles, UURIE:53:73, Uppsala Universitet, Institutet För Högspänningsforskning, 1973.

Smith, C. R., H. C. Brinton, M. W. Phara, III and H. A. Taylor, Jr., Lower E-region ion concentrations measured at a time of declining solar activity, J. Geophys. Res., 72, 2357, 1967.

Stein, R., The limits of time-of-flight mass spectrometry: General time-focusing relations and an analysis of cylindrical and spherical geometries, Doctoral dissertation, The Pennsylvania State University, University Park, Pennsylvania, 1974.

Stephens, W. E., A pulsed mass spectrometer with time dispersion, Phys. Rev., 69, 691, 1946.

Studier, M. H., Continuous ion source for a time-of-flight mass spectrometer, Rev. Sci. Instrum., 34, 1367, 1963.

Takekoshi, H., K. Tsurocka and S. Shimizer, Bull. Inst. Chem. Res., Kyoto University, 27, 52, 1951, as cited in Zabielski, M. F., Time-of-flight mass spectrometry for ionospheric measurements: Theory and experiments, PSU-IRL-SCI-353, The Pennsylvania State University, University Park, Pennsylvania, 1970.

Taylor, H. A., Jr. and H. C. Brinton, Atmospheric ion composition measured above Wallops Island, Virginia, J. Geophys. Res., 66, 2588, 1961.

Taylor, H. A., Jr., H. C. Brinton and C. R. Smith, Positive ion composition in the magnetoionosphere obtained from the OGO-A satellite, J. Geophys. Res., 70, 5769, 1965.

Taylor, H. A., Jr., H. C. Brinton, M. W. Pharo, III and N. K. Rahman, Thermal ions in the exosphere. Evidence of solar and geomagnetic control, J. Geophys. Res., 73, 5521, 1968.

Townsend, J. W., Jr., Radiofrequency mass spectrometer for upper air research, Rev. Sci. Instrum., 23, 538, 1952.

Wager, J. H., Electronic equipment for in-flight processing of rocket-borne mass spectrometer data, J. Electron. Control, 8, 227, 1960.

Watson-Watt, R. A., Weather and wireless, Q. J. Roy. Meteorol. Soc., 55, 273, 1929.

Widdell, H. U., G. Rose and R. Borchers, Results of concentration and mobility measurements of positively and negatively charged particles taken by a rocket-borne parachuted aspiration (Gerdien) probe in the height region from 72 to 39 km, Pure and Applied Geophysics (PAGEOPH), 84, 154, 1971.

Wiley, W. C. and I. H. McLaren, Time-of-flight mass spectrometer with improved resolution, Rev. Sci. Instrum., 26, 1150, 1955.

Wolff, M. M. and W. E. Stephens, A pulsed mass spectrometer with time dispersion, Rev. Sci. Instrum., 24, 616, 1953.

Young, J. M., C. Y. Johnson and J. C. Holmes, Positive ion composition of a temperate latitude sporadic-E layer as observed during a rocket flight, J. Geophys. Res., 72, 1473, 1967.

Zabielski, M. F., Enhancing effective instrument resolution by an analog method, PSU-IRL-SCI-280, The Pennsylvania State University, University Park, Pennsylvania, 1966.

Zabielski, M. F., Time-of-flight mass spectrometry for ionospheric measurements: Theory and experiments, PSU-IRL-SCI-353, The Pennsylvania State University, University Park, Pennsylvania, 1970.

Zabielski, M. F., H. T. Diem and B. R. F. Kendall, Theoretical analysis of a cylindrical time-of-flight mass spectrometer with radial ion paths, Int. J. Mass Spectrom. Ion Phys., 5, 349, 1970.

Zabielski, M. F., R. Stein and B. R. F. Kendall, Theoretical analysis of a time-of-flight mass spectrometer with spherical electrodes and radial ion paths, Int. J. Mass Spectrom. Ion Phys., 10, 109, 1972/1973.

Zbinden, P. A., M. A. Hidalgo, P. Eberhardt and J. Geiss, Mass spectrometer measurements of the positive ion composition in the D- and E-regions of the ionosphere, Planet. Space Sci., 23, 1621, 1975.

Zhlood'ko, A. D., V. N. Lebedinets and V. B. Shushkova, Meteor ions in the polar ionosphere: Rocket mass-spectrometric measurements and theoretical calculations, Space Res. XIV (Ed. M. J. Rycroft and R. D. Reasenberg), Akademie-Verlag, Berlin, 1974.